Neuronal Systems Potentially Involved in Autism Spectrum Disorder

Dissertation

zur

Erlangung des Doktorgrades (Dr. rer. nat.)
der
Mathematisch-Naturwissenschaftlichen Fakultät
der
Rheinischen Friedrich-Wilhelms-Universität Bonn

Vorgelegt von

Christian Liemersdorf
aus
Bonn Bad Godesberg

Bonn, im Mai 2016

Angefertigt mit Genehmigung der Mathematischen-Naturwissenschaftlichen Fakultät
der Rheinischen Friedrich-Wilhelms-Universität Bonn.

1. Gutachter: Prof. Dr. Walter Witke
2. Gutachter: Prof. Dr. Frank Bradke
Tag der Promotion: 12.01.2017
Erscheinungsjahr: 2017

Danksagung

Ich danke zunächst Prof. Dr. Walter Witke, der es mir ermöglicht hat mit diesem überaus interessanten Thema und durch seine freundliche Unterstützung diese Arbeit zu verfassen.
Besonders herzlich möchte ich mich bei meinem Betreuer Dr. Pietro Pilo Boyl bedanken, der sich stets Zeit für meine Fragen nahm und stets offen war für Diskussionen über die Arbeit, die mich auf meinem Weg um Vieles bereichert haben.
Bei allen Mitarbeitern im Institut für Genetik bedanke ich mich ganz herzlich für das äußerst angenehme Arbeitsklima und die Unterstützung während meiner Doktorarbeit. Vielen Dank den Mitarbeitern der AG Witke, im Besonderen Nina Roy, Julia Hecker, Stefanie Hauck, Andree Salz, Michael Marleaux, Ilkin Özer, Andreas Husch, Gerda Hertig, Gabriele Matern, Melanie Jokwitz, Stefan Klein, Gerd Landsberg und Gertrud Dienst.

Natürlich gilt der größte Dank meiner Familie, im Besonderen meiner Frau Michaela und meiner Mutter, u.a. für die tatkräftige Hilfe an langwierigen Analysen für diese Arbeit. Im Laufe der Zeit dieser Arbeit sind nicht wenige Dinge geschehen, die diese Arbeit nicht immer einfach gemacht haben. Verschiedene Krankheiten in der Familie und bei Freunden und im Besonderen der Verlust meines Vaters und meiner Großmutter lassen die vergangene Zeit nicht unberührt, doch gibt es selbstverständlich auch viele positive Ereignisse und Bekanntschaften, die diese Zeit unvergesslich werden ließen.
Alles in Allem war es eine aufregende Zeit, die mich um viele Erfahrungen bereichert hat. Die nächsten Schritte in die Zukunft werden wahrscheinlich nicht weniger aufregend, doch jetzt fühle ich mich bereiter mich neuen Herausforderungen zu stellen.

Leeve Papa, leev Oma, dat he is för üsch…

Table of contents

Abbreviations

°C	Degree Celsius
µg	Microgram
µl	Microliter
µM	Micromolar
µm	Micrometer
UTR	Untranslated region
ABP	Actin binding protein
ACh	Acetylcholine
AcOH	Acetic acid
AD	Alzheimer´s disease
ADP	Adenosine diphosphate
app.	Approximately
APS	Ammoniumpersulfate
ASD	Autism spectrum disorder
ATP	Adenosine triphosphate
BBB	Blood-brain-barrier
bp	Base pair
BP	Band-pass filter
BSA	Bovine serum albumine
C_C	Critical concentration
CNS	Central nervous system
DA	Dopamine
DNA	Deoxyribonucleic acid
E	Embryonic day
e.g.	Example given
ETC	External tufted cell
EtOH	Ethanol
F-actin	Filamentous actin
FXS	Fragile X syndrome
G-actin	Globular actin, monomeric actin
G/+	Heterozygous P2-GFP mouse
G/G	Homozygous P2-GFP mouse
GABA	Gamma-aminobutyric acid
GFP	Green fluorescent protein
h	Hour
HD	Huntington´s disease
HRP	Horseradish peroxidase
i.e.	Id est, in other words
IP	Immunoprecipitation
IPC	Intermediate progenitor cell
kb	Kilobase
kDa	Kilodalton
KO	Knock-out
KI	Knock-in

LTD	Long-term depression
LTP	Long-term potentiation
MeOH	Methanol
min	Minute
ml	Milliliter
mm	Millimeter
MSN	Medium spiny neuron
MW	Molecular weight
nm	Nanometer
NSC	Neural stem cell
nt	Nucleotide
o.n.	Over night
PCR	Polymerase chain reaction
PD	Parkinson´s disease
PFA	Paraformaldehyde
pH	Pondus hydrogenii
PKU	Phenylketonuria
PLP	Poly-L-proline
PNS	Peripheral nervous system
PSD	Post-synaptic density
RNA	Ribonucleic acid
RP	Reserve pool
rpm	Rotations per minute
RRP	Readily releasable pool
RT	Room temperature
sec	Second
SAC	Short axon cells
SV	Synaptic vesicle
TSC	Tuberous sclerosis
UV	Ultraviolet light
V	Volt
wt	Wild type

Abstract

Pfn2 is a brain specific actin binding protein involved in actin dynamics. The Pfn2 knock-out mouse model shows an autistic-like phenotype with all of the features commonly reported in autism patients such as social and communicational impairment, repetitive behavior and epileptic seizures. The role(s) and function(s) of Pfn2 in this striking phenotype are not understood completely. A first step in understanding these roles is investigating the expression pattern of Pfn2 in the brain to shed light on the different neuronal systems that could potentially contribute to the many aspects of the autistic-like and epileptic phenotypes.

A Profilin2-GFP fusion protein knock-in mouse model was used in this thesis to investigate the expression of Pfn2 in neuronal cell subtypes that could possibly contribute to the autistic-like phenotype. Pfn2 has been found expressed in glutamatergic, dopaminergic, serotonergic, adrenergic and cholinergic neurons, both pre- and post-synaptically, while GABAergic neurons showed a complex subtype specific expression pattern dependent on the respective brain area. Pfn2 was missing from all glial cell subtypes. Neural stem cells expressed Pfn2, but stem cell-derived progenitor cells were devoid of Pfn2, but it is re-expressed upon their differentiation into post-mitotic neurons.

The P2-GFP fusion protein is expressed in the knock-in mouse model at reduced levels (app. half) compared to the wt in heterozygous animals. P2-GFP also showed a minor impairment in poly-L-proline binding efficiency (app. 75% of Pfn2), but no changes in G-actin binding efficiency. Nevertheless, P2-GFP was able to bind to nearly all ligands that Pfn2 could interact with including a novel interaction partner, cortactin. The P2-GFP KI mouse model is therefore validated to study Pfn2 trafficking and function *in vivo*.

Finally, comparative analysis of wt and Pfn2 KO primary hippocampal neuron cultures as a model system revealed that Pfn2 also has a role during neuronal development. Pfn2 KO neurons showed an accelerated neuronal development, reaching each developmental stage faster than wt cells, possibly due to altered actin dynamics. The P2-GFP KI model was then employed to produce mature hippocampal neuron cultures and the trafficking of Pfn2 following different stimulation protocols was studied. Upon application of various stimulants, Pfn2 mostly re-localized into post-synaptic terminals, as previously described, but also into pre-synaptic terminals and, to a lesser extent, into axons. The view of Pfn2 and its function possibly involved in actin-dependent mechanisms during neuronal development as well as during induced synaptic activity requires further studies, but a complex role of Pfn2 in these processes has been discovered with the help of the P2-GFP mouse model as a valuable tool.

1. Introduction

1.1 Actin and actin polymerization

Networks of filaments of several kinds can be found in every eukaryotic cell. They are essentially divided into three subtypes: microtubules, intermediate filaments and actin filaments.

Microtubules consist of α- and β-tubulin dimers and can form long filaments of app. 25 nm in diameter. Microtubules provide stability to the cell and are important for e.g. spindle formation during cell division or neurite outgrowth and elongation.

Intermediate filaments are composed of protein that can build filaments up to 10 nm in diameter. Intermediate filaments are involved in several processes ranging from structural support of the cell to anchoring of subcellular structures. Most famous constituents of intermediate filaments are the nuclear envelope lamins, the neuronal proteins nestin and the neurofilaments, the typical astrocytic protein GFAP, which will be described further in this study, as well as the mesenchymal marker protein vimentin.

The smallest filaments in terms of their average diameter, but also the most important for this thesis, are the actin filaments, with app. 7 nm thickness. Actin filaments are constituents of the cytoskeleton of the cell and necessary for a variety of cellular processes including cell movement, cytokinesis, membrane trafficking and many related mechanisms.

Actin filaments consist of actin monomers (G-actin = globular actin) with a molecular weight of 42 kDa that polymerize to form a double helical structure called F-actin (filamentous actin).

Actin is encoded by different highly conserved gene families (α-, β- and γ-actin). Each gene encodes a different isoform of actin, often expressed in distinct tissues.

Three isoforms of α-actin are commonly known (skeletal, cardiac and smooth), primarily expressed in the respective type of muscle cells. Additionally one γ-actin isoform, γ_{smooth}-actin, is expressed in smooth muscle enteric cells. The other γ-actin isoform and the most abundantly found β-actin variant are expressed most prominently in non-muscle cells (Perrin and Ervasti, 2010; Pollard et al., 1994). Actin is also highly conserved among species to a degree that in *in vitro* assays it is interchangeable (Kron et al., 1992; Nefsky and Bretscher, 1992).

The globular and filamentous forms are present in the cell in a reversible equilibrium. Actin filaments can be polymerized *de novo* from a nucleation complex by incorporation of G-actin monomers, loaded with ATP, in a unidirectional elongation process.

F-actin filaments are polar molecules with the elongation process taking place mainly at the so-called “barbed end” (or plus (+) end) of the filament. Actin monomers are in general continuously removed at the so-called “pointed end” (or minus (–) end) (Fig. 1). This happens, because the critical concentration of the actin monomer in order to polymerize is lower at the barbed end (C_c = app. 0.1 µM for purified actin *in vitro*) and much higher at the pointed end of a filament. Monomers can be removed when the intrinsic ATPase activity of actin has catalyzed the slow transition from the bound ATP to ADP, changing the biochemical and binding properties of the filament.

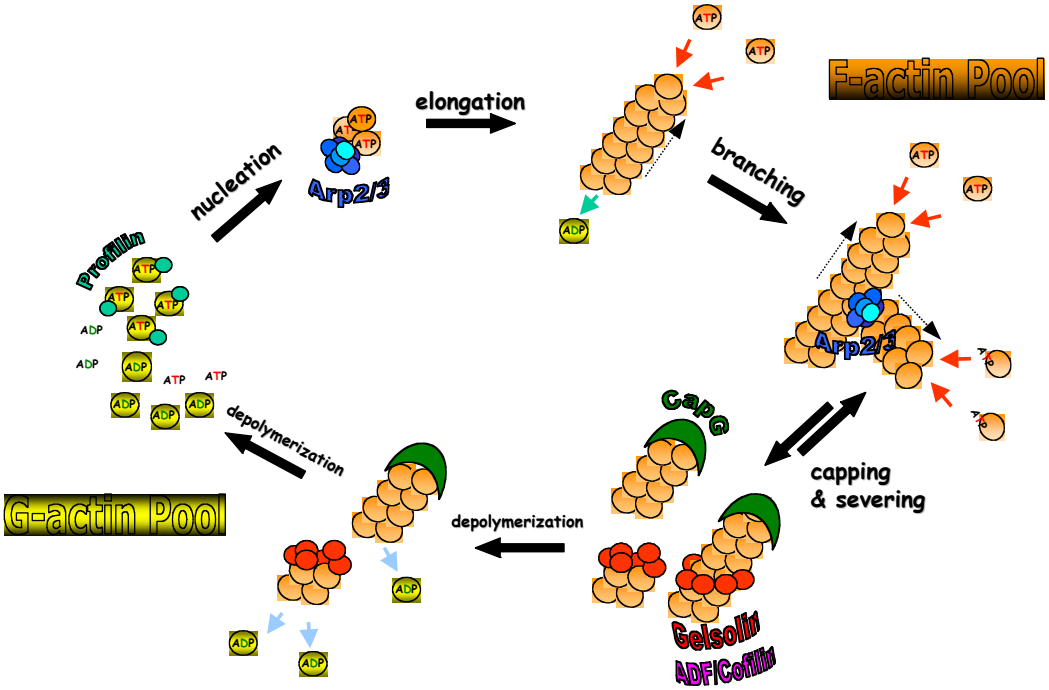

Fig. 1 The actin polymerization cycle

Depicted is the polymerization cycle of actin- filaments. A cell maintains a pool of G-actin bound to profilin, which loads it with ATP. Upon nucleation of app. 3 G-actin monomers with the help of nucleation factors like the Arp2/3 complex an F-actin filament can grow, elongating spontaneously or catalyzed by proteins like formins. Apart from straight elongation, an F-actin filament can also be branched mainly by the action of the Arp2/3 complex. The elongation process can be stopped by capping of an F-actin filament e.g. by binding of CapG to the tip of a filament. F-actin filaments are also frequently severed by proteins like gelsolin or the ADF/cofilin family of proteins, which leads to either depolymerization of the filaments or further elongation from the new ends of the previous filament. After depolymerization of an F-actin filament into G-actin monomers, these are available again in the G-actin pool for the next polymerization cycles.

The circularity depicted in Fig. 1 occurs when the cytosolic concentration of the actin monomer subunit is maintained between the C_c^+ and C_c^- ends with the help of various actin binding proteins. This process is defined as actin treadmilling, in which there is growth at the positive end, and shrinkage at the negative end.

1.2 Actin binding proteins

Actin binding proteins (ABPs) are regulatory proteins that participate in actin dynamics (Winder, 2005) enhancing or inhibiting specific processes during actin polymerization. The proteins functioning as actin nucleators are the Arp2/3 complex, formins and WH2- (WASP-homology-2 also verproline-homology) domain containing actin nucleators (spire, cordon-bleu and leiomodin) (Fig. 2).

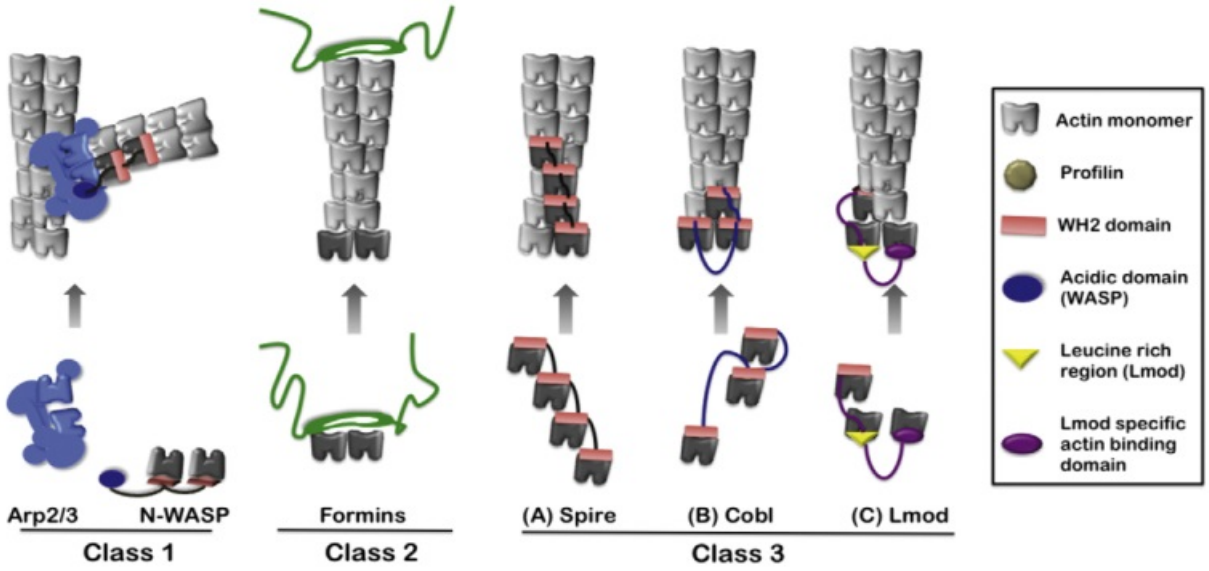

Fig. 2 Actin nucleator classes

Three classes of actin nucleators can be distinguished based on their mode of action.

Class 1 Arp2/3 complexes work in synchrony with a nucleation-promoting factor, such as N-WASP, which provides an actin monomer via its WH2-domain in order to form a trimer of actin and actin-like structures with the actin-related subunits 2 and 3 of the Arp2/3 complex, which serves as a polymerization start point. Formins are class 2 actin nucleators, which are able to stabilize spontaneously occurring actin dimers or even trimers. Upon actin nucleation, formins remain attached to the barbed end of the actin filament further helping to accelerate the elongation process. All three class 3 actin nucleators form actin nuclei stabilized in different modes. Domains of various lengths have a linker function in between the WH2-domains of either Spire, Cobl or Lmod (modified from Chesarone and Goode, 2009).

The function of actin nucleators is to help the G-actin nucleation process, which is needed to initiate the polymerization of an actin filament (Ahuja et al., 2007; Campellone and Welch, 2010; Chesarone and Goode, 2009; Kunda et al., 2003; Quinlan et al., 2005). These proteins help to stabilize or create a nucleus of two to four G- actin monomers from which the filament elongation process can start (Fig. 2). The Arp2/3 complex is the most studied actin nucleator so far (Chesarone and Goode, 2009; Goley and Welch, 2006; Mullins et al., 1997; Welch et al., 1997). It was first purified by its binding capacity to profilin-beads (Machesky et al., 1994) and has since been shown to have a crucial role in the formation of branched actin filament networks during diverse processes. Arp2 and Arp3 are components of this heptameric complex that mimic the structure of an actin monomer. Arp2/3 requires activation from a nucleation promoting factor (NPF) such as WASP, N-WASP and the WAVE complex (Fig. 2).

Another highly conserved class of actin nucleators is named formins (Fig. 2). This protein family consists of over 15 members in mammals (Faix and Grosse, 2006) but is also present in all eukaryotes examined until now. Formins function as homodimers, are inhibited by an autoinhibitory domain and this default inhibition is relieved by RhoA/Cdc42 signaling. They contain one FH2 (formin-homology-2) domain, which stabilizes the first nucleus of two actin monomers, and one FH1 (formin-homology-1) domain, which can bind to profilactin complexes (see 1.3) and deliver the bound G-actin to the barbed end of the growing filament (Paul and Pollard, 2008). Remaining at the barbed end of an actin filament, formins can compete with capping protein binding, resulting in longer actin filaments compared to those generated by Arp2/3, Spire or Cobl (Fig. 2).

Their function of actin nucleators is important not only for stress fiber formation, but also for filopodia and adherent junction formation in mouse and human cell lines, as well as cell polarity and cytokinesis in lower eukaryotes (Chesarone and Goode, 2009; Imamura et al., 1997).

To form e.g. stress fibers, additional proteins are needed to cross-link F-actin filaments and stabilize larger and more complex actin structures. This protein family includes α-actinin, fimbrin, spectrin and dystrophin.

To stop an actin filament from elongating, capping proteins (CapG, CapZ) are needed in the cell, which bind to the barbed end of an actin filament and prevent further monomer attachment.
The disassembly of actin filaments is mediated by actin severing proteins such as gelsolin or the ADF/cofilin family of proteins. These proteins sever actin filaments to generate new endings and nuclei for extended actin polymerization in the cell as well as provide new actin monomers to the G-actin pool.
G-actin monomers are bound by actin sequestering proteins, such as profilin or thymosin-β4. They are highly abundant proteins with opposing roles in the cell of promoting and inhibiting actin polymerization. Profilins are able to sequester ADP-G-actin from the actin monomer pool, on which they can act as an ADP-ATP exchange factor, loading G-actin with ATP and supplying it further to the polymerization cycle. Thymosin-β4 on the other hand sequesters ATP-G-actin away from the polymerizable G-actin pool and therefore inhibits actin polymerization (Safer and Nachmias, 1994).

1.2.1 The WAVE complex

The WAVE (Wasp-family verproline-homologous protein) complex is a hetero-pentameric complex (Eden et al., 2002) that is able to activate the Arp2/3 complex to enhance actin polymerization. In mammals, besides one of the three WAVE isoforms (WAVE 1-3) that have a different tissue expression, the complex contains CyFIP1-2 (cytoplasmic Fragile-X mental retardation protein-interacting protein), Nap1 (Nck-associated protein-1), Abi 1-2 (Abl-Interactor) and HSPC300/Brick (hematopoietic stem cell progenitor protein) (Fig. 3). WAVE1 is highly expressed in brain but at lower levels also in other tissues and various cell lines. WAVE3 is nearly exclusively expressed in brain. WAVE2 is expressed ubiquitously (Takenawa and Miki, 2001). Similarly, CyFIP1 is expressed ubiquitously, while CyFIP2 has a very high expression in brain and a marginal expression in other tissues. Much less is known about the expression pattern of Abi isoforms. This not always overlapping tissue distribution of the components´ isoforms leaves doubts on the effective composition of the WAVE complex *in vivo*.

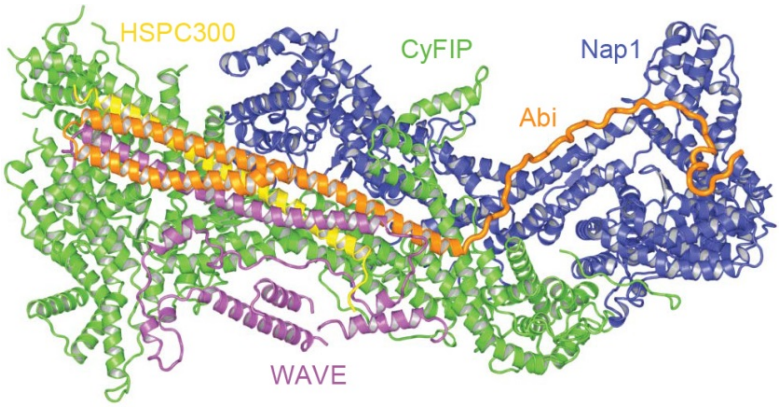

Fig. 3 The WAVE complex
Shown here is a model of the crystal structures of the WAVE complex. The WAVE complex is a heteropentameric complex consisting of one WAVE isoform (WAVE1-3), Nap1, one CyFIP isoform (CyFIP1-2), one Abi isoform (Abi1-3) and HSPC300. CyFIP and Nap1 form a large scaffolding surface to which Abi, WAVE and HSPC300 dock on the side of CyFIP (Chen et al., 2010).

The WAVE complex is activated by Rac1, a small GTPase which induces the exposure of the VCA domain of the WAVE proteins by a transient interaction with CyFIP1 (Chen et al., 2010; Steffen et al., 2004, Fig. 3). The acidic domain of the VCA can bind to and thus activate the Arp2/3 complex, bringing Arp2 and Arp3 in proximity in order to start actin filament polymerization (Egile et al., 2005). The two subunits in turn will bind the G-actin monomer provided by the WH2/verprolin homology domain of WAVE producing the trimeric nucleus essential for actin filament elongation.

1.3 Profilin

An intrinsic ATPse activity of actin is responsible for the hydrolysis of ATP to ADP in actin filaments over time and is also allowing for a preferential binding of ABPs to ATP- or ADP-bound actin.

A very important ABP binding preferentially to ADP-G-actin is profilin, whose study is the subject of this thesis. Profilin is known to bind actin to form a 1:1 complex, from which it was first isolated (profilactin), and to catalyze the exchange of ADP to ATP on the bound G-actin monomer with up to 1000-fold higher efficiency than spontaneous exchange (Goldschmidt-Clermont et al., 1992) before releasing it in response to a membrane signal via PIP_2 (phosphatidylinositol-4,5-bisphosphate). The ATP-loaded G-actin can then be incorporated into the barbed end of a growing actin filament. Profilin can in turn be bound by a variety of proteins including the WAVE

complex, formins and other actin binding proteins, delivering the ATP-G-actin required by profilin ligands for actin polymerization.

The ligand binding cleft of profilin is located opposite to the actin binding site, produced by two juxtaposed N- and C-terminal helices, and specifically binds to poly-L-proline (PLP) stretches (Fig. 4) (Lu and Pollard, 2001; Mahoney et al., 1999).

This PLP-binding site resembles an SH3 (Src-homology-3) domain, common to many other proteins, and can possibly compete with it for poly-L-proline binding. Certain ligands bound to the PLP-binding domain of profilins (e.g. dynamin1) are released together with G-actin, when a phosphoinositide (in particular, phosphatidylinositol-4,5-bisphosphate, PIP_2) binds to its binding site located on the ends of the N- and C-terminal helices, which are also involved in PLP-binding (Gareus et al., 2006; Gieselmann et al., 1995; Lassing and Lindberg, 1985; Machesky et al., 1994) (Fig. 4).

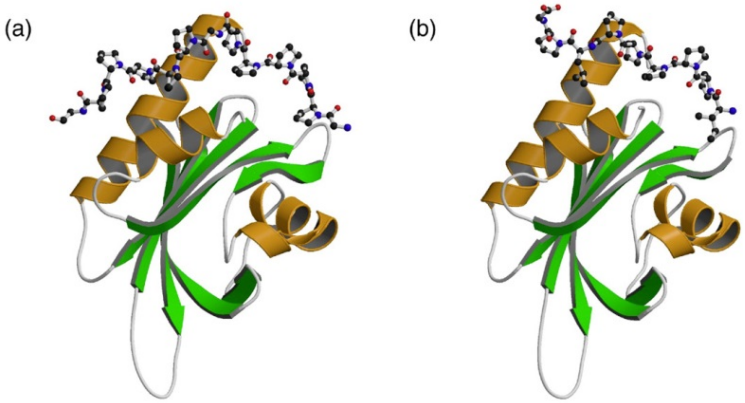

Fig. 4 Crystal structure of Pfn2 with peptides of a) VASP and b) mDia1

The crystal structures of mouse a) Pfn2-VASP and b) Pfn2–mDia1 PLP peptide complexes are shown. Ribbons represent α-helices, flat arrows β-sheets. Peptides are shown as stick and ball structures (modified from Kursula et al., 2008).

It is possible to speculate that profilins are translocated close enough to the membrane by their ligands and there, induced by PIP_2 binding, they release ATP-G-actin to accelerate actin polymerization that is canonically happening in proximity of the cell membrane.

1.3.1 Profilin isoforms

Profilins were mentioned first in 1977 and are one of the earliest ABPs researched on (Carlsson et al., 1977). Profilins are highly expressed in all eukaryotes to a cellular concentration of up to 10 µM (Mogilner and Edelstein-Keshet, 2002) with the exception in certain algae according to a recent study (Aumeier et al., 2015).

The importance of profilins function and therefore their evolutionary conservation can be seen from the list of the many model organisms in which profilin function was already investigated.

Profilins are important in bacterial motility, for example in the actin-based *Listeria* movement within infected cells (Geese et al., 2000; Laurent et al., 1999; Theriot et al., 1994). Knock-out of both profilin isoforms in *Dictyostelium discoideum* results in a decrease of F-actin content with impairments in migration and cytokinesis (Haugwitz et al., 1994). In *Drosophila melanogaster, chickadee*, the orthologue of profilin, controls oogenesis, spermatogenesis, cell migration, bristle and eye formation (Cooley et al., 1992; Verheyen and Cooley, 1994). Pfn1 in Zebrafish (*Danio rerio*) is important for gastrulation (Lai et al., 2008) and XPfn2 (*Xenopus leavis* Pfn2), in addition to gastrulation, is also regulating cell polarization and axial alignment (Khadka et al., 2009). Birds express PFN1 and PFN2 ubiquitously, except for skeletal muscle, and PFN2 plays a role in focal contact formation, cell adhesion and spreading (Murk et al., 2009). Some of the many plant profilin isoforms are also reported to be major pollen allergens (Ruiz-García et al., 2011; Santos and Van Ree, 2011; Smith, 2002; Valenta et al., 1991). Even some types of viruses like Vaccinia virus (Blasco et al., 1991), and all orthopoxviruses (Butler-Cole et al., 2007) as well as certain cyanobacteria (Guljamow et al., 2007) contain profilin homologs.

In humans and mice, the profilin protein family so far consists of 4 distinct profilin isoforms. Pfn1 is ubiquitously expressed in all tissues, except skeletal muscle and heart (Witke, 2004; Witke et al., 1998, 2001). Pfn2 is essentially neuron-specific, although expression in other tissues can be detected at much lower levels (Witke et al., 1998, 2001). Pfn3 and 4 are expressed specifically in mouse and human testis (Behnen et al., 2009; Hu et al., 2001; Obermann et al., 2005).

The amino acid sequence is not very well conserved among the paralogs, for example human PFN1 and PFN2 are only 65% identical and the degree of identity is similar in the mouse. Even greater differences are found in lower eukaryotes (35% homology in Dictyostelium) and in plants (20% homology). Nevertheless, their structural domains and basic functions are well conserved (Gieselmann et al., 1995; Lambrechts et al., 1997).

Both profilin 1 and profilin 2 genes consist of 3 exons with introns of varying lengths in between the coding regions. The exon-intron boundaries are conserved among the isoforms, but the *Pfn2* gene additionally comprises a fourth alternative coding exon in

the 3´UTR in exon3. The alternative exon4 can be included in the ORF of *Pfn2* instead of exon3, leading to two alternative splice variants, Pfn2a and Pfn2b, in mouse and humans (Di Nardo et al., 2000), which differ in their C-terminal structures. In this study I will refer, if not specifically mentioned otherwise, to the splice variant Pfn2a as Pfn2, since it is the isoform involved in actin dynamics and is by far the dominant isoform in terms of expression level in the brain (95% Pfn2a) (Lambrechts et al., 2000; Di Nardo et al., 2000). Pfn2b does not bind actin and the poly-L-proline binding efficiency is reduced in comparison to Pfn2a.

Mouse Pfn2 is predominantly localized to the cytoplasm but has been observed to be able to enter the nucleus. The profilactin complex is specifically transported out of the nucleus by its interaction with Exportin6 (Stüven et al., 2003). It has been observed that Pfn2 trafficking into the nucleus can be NMDA-dependent (Birbach et al., 2006). There is evidence of a nuclear fraction also for Pfn1 (Lederer et al., 2005), which could be recruited to the nucleus by the transcription factor $p42^{POP}$ that also was reported to bind to Pfn2.

Pfn1 and Pfn2 share several ligands, even though with varying binding efficiencies: G-actin for example has a higher binding efficiency for Pfn1, while Mena, VASP and mDia are bound to Pfn2 with a higher efficiency than to Pfn1. But profilin isoforms also have specificity for certain ligands with only Pfn2 binding to dynamin 1, synapsins, ROCK and components of the Wave complex (CyFIP/POP, HEM2/Nap1) (Witke, 2004; Witke et al., 1998). Due to these differences it is still unclear whether Pfn1 and Pfn2 are interchangeable *in vivo*. The KO phenotype of the two profilins in the mouse is indeed very different, with the Pfn1 KO being early embryonic lethal before reaching the blastocyst stage (Witke et al., 2001) while the Pfn2 KO is viable with behavioral abnormalities (Pilo Boyl et al., 2007) (see 1.4.3). The reason for the different impact of Pfn1 and Pfn2 deletion *in vivo* could be rooted in their different embryonic expression patterns, since Pfn1 is expressed throughout embryonic development starting from the gamete stages, while the expression of Pfn2 at the embryonic level appears to begin around embryonic day 10 (E10) with the specification of the neuroectoderm (Witke et al., 2001). Both profilin isoforms could also play different roles, assuming the differences in e.g. binding partners of profilins could account for different functions of the proteins. Certainly these aspects of expression and function of profilins require further investigation.

1.3.2 Profilin 2

The major neuronal profilin isoform is profilin 2 (Pfn2), whose expression in other tissues is several fold less (Witke et al., 1998).
Pfn2 has specific functions that differ from Pfn1, as results from the work of several groups investigating the role of Pfn2 in different organisms and cell lines. A negative role of Pfn2 in neuronal clathrin-mediated vesicle endocytosis through the binding to dynamin 1 was shown in cultured neurons devoid of Pfn2 (Gareus et al., 2006). More recently a repressive role for glutamatergic vesicle exocytosis was also demonstrated in the Pfn2 KO mouse model (Pilo Boyl et al., 2007). An exocytosis impairment of kainate glutamate receptor 2b (GluK2b) was reported in COS-7 cells and Pfn2 knock-out cultured hippocampal neurons transfected with Pfn2, suggesting a specific role of Pfn2 in negatively regulating receptor exocytosis (Mondin et al., 2010).
Pfn2 can be phosphorylated by ROCK2 (Rho-associated coiled-coil kinase 2), but the relevance of Pfn2 phosphorylation has not been extensively investigated so far. A negative regulatory effect of Pfn2 on neuritogenesis, the first step in neuronal differentiation, was shown by inhibiting the ROCK2-dependent phosphorylation of Pfn2 in primary hippocampal neuron cultures (Da Silva et al., 2003).
Importantly, the specific expression pattern of Pfn2 in mouse brain has not been thoroughly investigated yet and needs to be elucidated. Published work has shown the expression and a role in glutamatergic neurons, but other neuronal subtypes were hitherto not investigated and might therefore contribute specific functions in the intricate neuronal network constituting the peripheral and central nervous system.

1.3.3 The Pfn2 knock-out mouse model

A Pfn2 knock-out (KO) mouse was generated by heterologous gene transfer, integrating the lacZ gene fused to the coding region of Pfn2 exon3 by homologous recombination and resulting in a complete loss of Pfn2 expression. Pfn2 KO mice are viable and display a neuronal specific phenotype (Pilo Boyl et al., 2007). They have behavioral impairments such as hyperactivity and hyperexcitability, but no learning deficits (Pilo Boyl et al., 2007). Higher brain functions, such as social behavior and communication, are also impaired leading to an autism-like phenotype (Pilo Boyl,

unpublished). The major physiological defect observed in the Pfn2 KO mouse is a loss of regulation of glutamatergic vesicle exocytosis, possibly due to impaired synaptic fast actin polymerization, accompanied by an increased post-synaptic density (PSD) length. Yet it is unclear if other neuronal systems are also affected by Pfn2 loss and what is their contribution to the phenotype.

1.3.4 The phenotype of Pfn2 KO mice and its implications in autism spectrum disorder

The Pfn2 knock-out mouse shows behavioral abnormalities reminding of autism-like behavior including deficits in social interaction and communication, hyperexcitability, repetitive behavior, coordination impairments and epileptic seizures (Pilo Boyl, unpublished).

Autism is a very complex disorder with many syndromes closely related to it, which are commonly summarized in the term autism spectrum disorder (ASD).

The human autism phenotype has been described first in 1943 by Leo Kanner (Kanner, 1943), who first defined two features that were commonly present in autism spectrum disorders: 1.) “living in your own world” and 2.) “resistance to change”. This “resistance to change” manifests itself very often as stereotypical, repetitive behavior and hyperexcitability upon novel stimuli from the environment. Social and language impairment often associated with mental retardation were later defined as two distinct traits in autism spectrum disorders (Rutter, 1978; Rutter and Schopler, 1987). The incidence of autism is progressively increasing to now 13/10,000 children (in one study of US children even 110/10,000) (Kogan et al., 2009), with the earliest cases reported at only two years of age, while there is still no pharmacological cure or therapy (Chakrabarti and Fombonne, 2005; Fombonne, 2003, 2008; Kim, 2015; Pinto et al., 2010), therefore research on autism is of dire importance.

Autism disorders are highly heritable (app. 90%) and associate frequently with other medical conditions like Fragile X syndrome (FXS), tuberous sclerosis (TSC), Prader-Willi syndrome, Angelman syndrome, phenylketonuria (PKU), Rett´s syndrome and others (Folstein and Rosen-Sheidley, 2001; Tsai, 1999; Veenstra-VanderWeele et al., 2002; Zafeiriou et al., 2007). Moreover, seizures occur in app. 30% of the patients (Gillberg, 2000). An interesting observation is that the incidence of ASD is 3-5 times

higher in males than in females, which would imply a linkage to the X-chromosome, but the results are non-conclusive so far. Chromosome abnormalities in general were observed for several distinct gene loci, but the correlation to the neurodevelopmental phenotype in ASD is not yet fully understood.

Physiologically, alterations in the excitation/inhibition ratio in the brain were observed in patients and mouse models affected by different mutations. Concomitant impairment of different neuronal circuitries, most often in the form of an excess of excitation (shift in the excitation/inhibition ratio) as well as single molecule defects are considered the basic cause of the autistic phenotype.

Concerning the genetic variations implicated in ASD, many gene mutations are known to induce an autistic phenotype. Naturally occurring mutations in the three neurexin and four neuroligin genes (app. 50 known mutations for each gene family) as well as the post-synaptic scaffolding proteins Shank2 and Shank3 can cause forms of ASD (Bang and Owczarek, 2013; Pinto et al., 2010; Tabuchi et al., 2007). The three neurexin genes give rise to α- and β-isoforms with 6 canonical alternative splice sites each, which would yield theoretically app. 2000 splice variants, while the four neuroligin genes are also alternatively spliced without a complete mapping of the resulting isoforms (Bang and Owczarek, 2013; Treutlein et al., 2014). The role of these proteins *in vivo* is to bridge pre- and post-synaptic terminals via trans-synaptic interactions of pre-synaptic neurexins with post-synaptic neuroligins. The neuroligin-3 gain-of-function mutation R451C observed in ASD patients leads to enhanced inhibitory synaptic transmission in mice (Bang and Owczarek, 2013; Tabuchi et al., 2007) causing a mild behavioral deficit in social interactions and enhanced spatial learning. This mutation can serve as an example for the shift in the excitation/ inhibition balance in ASD, which is affected by alterations in either excitatory or inhibitory synaptic transmission (Anderson et al., 2012; Tabuchi et al., 2007). Several mouse models have been generated in recent years to study syndromic autism, for example FMRP (fragile X mental retardation protein) or MeCP2 (methyl CpG binding protein 2) knock-out mice are common models for the autistic phenotype related to Fragile X syndrome (FXS) and Rett syndrome, respectively.

A wide range of mouse models has been described that show only a subset of endophenotypes of ASD and are listed in the autism research database AutDB (http://www.mindspec.org/autdb.html).

Pfn2 is therefore a very promising candidate gene for autism research, since it is involved in synaptic vesicle endo- and exocytosis (Gareus et al., 2006; Mondin et al., 2010; Pilo Boyl et al., 2007) and synaptic plasticity via its function through the interaction with the WAVE complex, several other actin nucleators, gephyrin as well as synapsins. Pfn2 could play a role in a vast number of neuronal systems and circuits leading to the autistic-like phenotype of Pfn2 KO mice. If this specific role of Pfn2, however, is restricted to certain subpopulations of neurons and neuronal circuits, the key impact of the deletion for the autism-like phenotype could be unraveled.

1.4 The nervous system

The brain is the most complex organ imaginable with an immense amount of research trying to understand the underlying mechanisms that regulate the intricate connection circuits of this unique structure.
The nervous system can be subdivided into the central nervous system (CNS), which summarizes the whole brain and spinal cord system. In contrast, the peripheral nervous system (PNS) mainly comprises the different nerve fibers for sensory information and neuromuscular junctions.
Neural tissue is composed of neurons and glial cells. These cells are tightly connected together, with the glial cells supporting the integrity and functionality of the neuronal cells, which are in turn the basis of brain function.

1.4.1 Neurons and synaptic transmission

Neurons are asymmetrical cells, featuring two kinds of processes with different functions (Fig. 5). Neurons extend thin (app. 1-3 µm in diameter), long (app. 100-500 µm) and highly branched processes called dendrites, which differ in their complexity depending on the cell type and neuronal system they belong to. Dendrites are the major recipient of synaptic input to a neuron through post-synaptic terminals that, in case of excitatory synapses, develop into dendritic spines (Fig. 6), small, actin-rich protrusions emerging from the dendritic shaft. The input signals can be relayed and further transmitted to muscles or other neurons via the second kind of process, the

axon, on average even thinner (0.1-0.5 µm) and longer (up to 1 m) than dendrites, extending thousands of pre-synaptic terminals (boutons, Fig. 6) to the target cells (Debanne et al., 2011). When a neuron receives an excitatory input, sodium channels at the plasma membrane open, decreasing the normally negative membrane potential (depolarization), which ultimately leads to a spike of the membrane potential called an action potential.

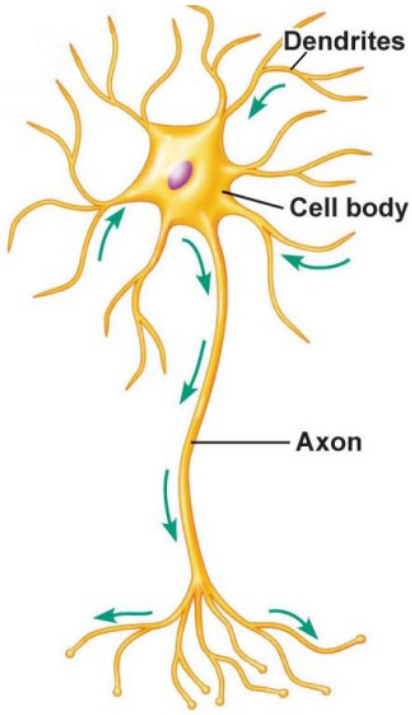

Fig. 5 Neuronal morphology
Neuronal cells show a polar morphology with specialized projections emerging from their cell bodies. Most projections arising from neurons are called dendrites, which feature protrusions called dendritic spines on their shafts (especially excitatory synapses), which receive synaptic signals from contacting neurons. Spines are therefore targeted by the second type of neuronal projections, the axons. Axons also form protrusions on their shafts, so-called boutons, which contact the dendritic spines and transmit information by releasing neurotransmitters via synaptic vesicles exocytosis.

Neurons form these projections upon guidance cues or stimuli during development in a process called neuritogenesis. Neuritogenesis is characterized by breakage of the symmetry of the cell towards finally polarized structures, which emerge from the cell soma as neurites and form the future dendrites and axons (Bradke and Dotti, 1997, 1999; da Silva and Dotti, 2002; Stiess and Bradke, 2010; Tahirovic and Bradke, 2009; Witte and Bradke, 2008).

The ultrastructure of synapses is under growing investigation aiming to understand the basic principles of synaptic function, such as pre-synaptic vesicle exocytosis upon changes in the intracellular ion concentration and resulting changes in the membrane potential of the effector cells. Synaptic vesicles (SV), enveloping the neurotransmitters, are present in pre-synaptic terminals of axonal projections in pools of distinct localization (Fig. 6). SVs are mostly accumulated in the reserve pool (RP), located distally from the site of vesicle exocytosis, which is the active zone and comprises the readily releasable pool (RRP) of SVs. The SVs in the RP are isolated

from the active zone by an actin network, which dynamically regulates the transition of SVs from the RP to the RRP, where SVs are exocytosed and neurotransmitter is released into the synaptic cleft. For an SV to be able to be released it needs to be docked to the synaptic membrane and primed for the fusion process. Priming is dependent on SNARE-complex formation between the SV and the synaptic membrane. The primed vesicles can fuse with the membrane upon action potential/depolarization-dependent Ca^{2+} influx and the released neurotransmitter reaches the post-synaptic site of a synapse of a neighboring neuron. In the case of an excitatory synapse, a dendritic spine protrudes from the shaft, while inhibitory synapses form small enlargements on the dendritic shaft. In spines, neurotransmitter receptors are anchored to an electron-dense, actin-rich structure exactly opposed to the active zone called the post-synaptic density (PSD, Fig. 6).

Binding of the neurotransmitter to these receptors leads to changes in the membrane potential due to the ion influx, as described earlier and can generate an action potential, which can propagate in turn to the pre-synaptic boutons to induce neurotransmitter release to further neurons. Neurons express several kinds of ion channels, such as ligand-gated ionotropic receptors and voltage-gated ion channels, mediating the influx of Na^+, K^+, Cl^- and Ca^{2+} ions (Fig. 7). The most prominent neurotransmitter in the CNS is glutamate, an excitatory neurotransmitter, and its receptors are divided into two classes: ionotropic receptors, such as the NMDA (N-methyl-d-aspartate), AMPA (α-amino-3-hydroxy-5-methyl-4-isoxazole propionic acid) and kainate families of receptors, and metabotropic (mGluR) receptors (Cingolani and Goda, 2008) (Fig. 7). Ionotropic glutamate receptors are ligand-gated ion channels, whereas metabotropic receptor activation leads to a G-protein-coupled second messenger cascade regulating the influx of cations through the ion and receptor channels. Glutamate can be further used to synthesize GABA (γ-aminobutyric acid), which is the primary inhibitory neurotransmitter of the nervous system. GABA receptors are also subdivided in ionotropic ($GABA_A$) and metabotropic ($GABA_B$) receptors (Fig. 7). The many subtypes of the mentioned receptors are differentially expressed in different neuronal systems and even in distinct cell types belonging to the same neuronal system (Biggin, 2002; Cingolani and Goda, 2008; Dutta et al., 2007; Ennis et al., 2001; Greengard et al., 1999; Levey et al., 1993; Lévi et al., 2004; Winters and Bussey, 2005; Xiao et al., 2007).

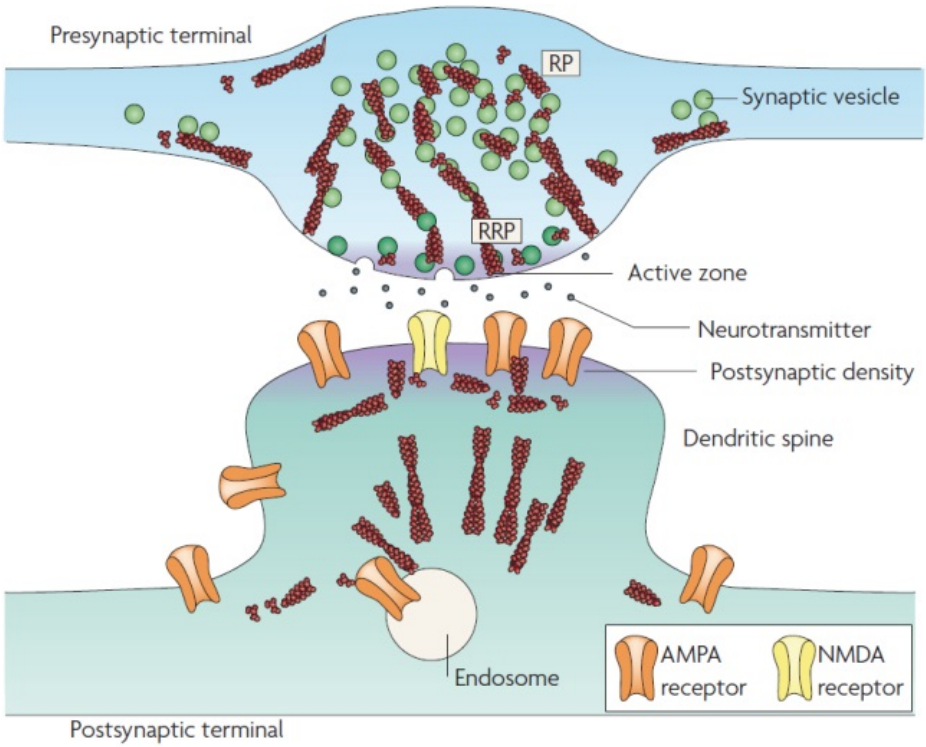

Fig. 6 Schematic overview of an excitatory synapse

Shown here is the schematic view of an excitatory synapse and the distribution of actin filaments (brown helixes), SVs (green circles) and receptors (see in the legend) in its pre- and post-synaptic terminals. Synaptic vesicles of the reserve pool (RP) are held back from the readily releasable pool (RRP) by an actin meshwork. Upon vesicle exocytosis, neurotransmitters are released into the synaptic cleft and are able to bind to post-synaptic receptors anchored to the post-synaptic density (PSD) via different sets of molecules including a dense actin network (from Cingolani and Goda, 2008).

Other neurotransmitters released by neurons of different neuronal systems can have excitatory effects like acetylcholine or noradrenaline or play both excitatory and inhibitory roles depending on the post-synaptic receptor subtype, such as dopamine or serotonin. The flexibility of neuronal transmission is therefore even extended with the same neurotransmitter system also being able to act differently on the post-synaptic target cells depending on their intrinsic molecular composition.

This complexity can also be further emphasized, when neurotransmitter co-expression is taken into account. A few neuronal cell types, in fact, were shown to express two types of neurotransmitters, for example the olfactory short axon cells,

which release dopamine and GABA, or the dopaminergic neurons of the VTA, which co-express small amounts of glutamate.

Neurons often are also associated with the expression of neuromodulatory substances with functions distinct from those of neurotransmitters. The most common neuromodulators are predominantly co-expressed in certain types of GABAergic neurons, such as somatostatin (SOM or SST), substance P (SP), vasoactive intestinal peptide (VIP) or neuropeptide Y (NPY). These neuromodulators often act as peptide hormones mostly with an inhibitory function on their post-synaptic recipient.

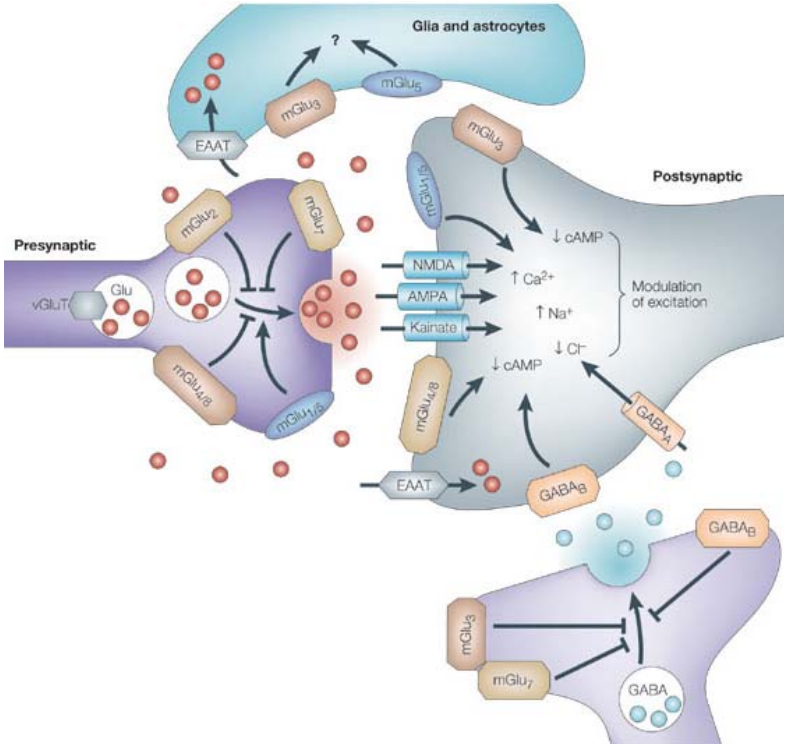

Fig. 7 Schematic representation of the different types of glutamate and GABA receptors localized to distinct synaptic compartments

Glutamate released from synaptic vesicles of the pre-synaptic terminal can bind post-synaptic ionotropic NMDA, AMPA or kainate receptors as well as pre- and post-synaptic metabotropic receptor types (mGluRs). The activation of these receptors induces a change of the post-synaptic potential due to Na^+ and Ca^{2+} influx leading to the excitation of the post-synaptic cell. GABA-mediated inhibition of post-synaptic targets can act through ligand-gated ionotropic $GABA_A$-receptors, by Cl^- influx, or G-protein coupled metabotropic $GABA_B$-receptors,. The concentration of free neurotransmitters in the synaptic cleft is modulated by neurotransmitter transporters, e.g. glutamate transporter (EAAT), especially concentrated on glial cell membranes, and diffusion (modified from Swanson et al., 2005).

All of these excitatory or inhibitory stimuli are acting on synaptic plasticity, inducing changes in synaptic strength and therefore increasing or decreasing performance of individual synapses. Upon repeated high excitatory input, synapses are strengthened

by a process termed long-term potentiation (LTP), in which dendritic spine morphology is altered by enlargement of the spine head and concomitant increase in receptor density leading to enhanced synaptic performance. The opposite alterations (spine shrinkage, reduced synaptic performance) are produced during long-term depression (LTD), when sustained weak inputs are received by post-synaptic terminals (Bellot et al., 2014; Bosch et al., 2014; Chen et al., 2007a; Hering and Sheng, 2001; Dubinsky, 1993; Kim and Lisman, 1999; Krucker et al., 2000; Lee et al., 1998; Oberman and Pascual-Leone, 2013; Shehata et al., 2012; Zhou et al., 2009).

1.4.2 Glial cells

The most abundant type of glial cells in the CNS are astrocytes, who owe their name to the star-shaped appearance *in vivo* (Fig. 8A). Astrocytes are responsible for stabilizing the neurons, providing them with growth factors and nutrients, as well as modulating synaptic transmission (Bergles et al., 2010). Moreover, the clearance of neurotransmitters from the synaptic cleft is highly increased by astrocytes, since excess of neurotransmitters (especially glutamate) in the extracellular matrix can lead to excitotoxic effects. An important function of astrocytes is also the invasion into lesion sites after nervous tissue injury, forming the so called glial scars (Ertürk et al., 2012).

Another type of glial cells are oligodendrocytes, which are important for a fast signal transduction along axons, since they provide the myelin-sheath coating around the axons of neurons in the CNS (Fig. 8B). Impulse transmission is accelerated due to myelination of the axons, since it decreases ion leakage and membrane capacitance. Myelination of axonal projections is not uniform, but leaves small spaces at the nodes of Ranvier to provide a mode of saltatory propagation of action potentials. A loss of oligodendrocytes is associated with diseases like multiple sclerosis and schizophrenia.

The brain is only partially connected to the rest of the body due to the blockage of e.g. cell migration through the blood-brain-barrier (BBB). The brain therefore is in need of an additional defense mechanism against infections, which is provided by the

microglia type of glial cells (Fig. 8C). Microglial cells are responsible for clearing nervous tissue from pathogens and toxic material, while malfunctioning of microglia contributes to neuronal cell death, since inflammatory responses to pathogens from the immune system of the remaining body are not facilitated.

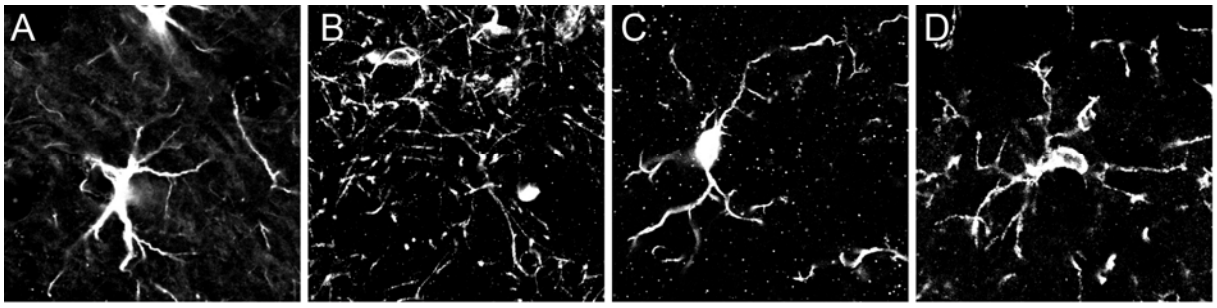

Fig. 8 Types of glial cells in the CNS

The cells supporting the neurons are called glial cells. Four major types of glial cells can be distinguished in the CNS. The role of the respective glial cell type differs profoundly. Astrocytes (**A**, identified by staining for GFAP). are star-shaped cells supporting neurons not only structurally but also by providing nutrients. In addition they are able to clear neurotransmitters from the synaptic cleft to avoid spill over to neighboring synapses and cytotoxic effects on the neurons. Structural support and most importantly insulation of neuronal axons is provided by oligodendrocytes (**B**, identified by staining for CNPase). Synaptic transmission is greatly accelerated by the axonal insulation via myelin-sheaths produced by oligodendrocytes. The brains immune cells are called microglia (**C**, identified by staining for Iba1), permanently scanning for pathogens and clearing the brain from toxic material. The role of the fourth type of glial cells, the NG2 cells (**D**, identified by staining for NG2), is not defined yet, but they are believed to be able to provide lesion sites with newly generated oligodendrocytes, since they were found to act as oligodendrocyte precursor cells (OPCs).

A special type of glial cells are NG2 cells (also called synantocytes or polydendrocytes), which are small, abundant glial cells with an astrocytic appearance and expression of the NG2 surface proteoglycan (Fig. 8D). They are believed to be able to give rise to oligodendrocytes (and possibly astrocytes or even neurons) and are therefore considered oligodendrocyte precursor cells (OPCs), but might also have distinct roles in the CNS (Bergles et al., 2010). These cells receive synaptic input with a low threshold and express AMPA receptors but are devoid of kainate or NMDA receptors. GABAergic signaling in these cells is still under debate as well as their role in other neuronal processes and modulation.

1.4.3 Neuronal circuitry

Neuronal systems are immensely interconnected via distinct types of connections and several different pathways. Compromising one system often leads to alterations and secondary effects in other systems as well.
Understanding the effects of distinct circuits on each other could shed light on neurological phenotypes, which may originate from one system but affect another via the immense interconnectivity of the brain. Pharmacological treatments, for example, are typically targeting individual symptoms of neurological disorders often neglecting the causative source, which could reside in different systems that indirectly modulate the symptoms.

The GABAergic system, for example, features the highest diversity of neuronal cell subtypes. Those subtypes can be distinguished from one another by their distinct location, biochemical characteristics, morphological appearance and electrophysiological properties. Increasing amount of data regarding the specific functions of these cells has led to new insights into synaptic circuits and their properties under various states of stimulation.

Several classical circuitries were part of the investigation in this thesis, but only the key circuits also involved in ASD and/or epilepsy are described further in the following chapters.

1.4.3.1 Hippocampal circuitry

The best studied structure in the rodent brain is the hippocampus. The hippocampal formation is responsible for many higher brain functions such as learning and memory, relaying sensory information from various sources, emotion and several types of behavioral responses.
Several distinct pathways compute information in the hippocampus. The main input comes from the entorhinal cortex (EC) but also several other regions contribute to hippocampal input including the thalamus, hypothalamus, amygdala, deep cerebellar nuclei (glutamatergic systems), the raphe nuclei (serotonergic system), the locus

coeruleus (noradrenergic system) and the substantia nigra and the ventral tegmental area (dopaminergic systems).

The efferents from the entorhinal cortex target mainly dentate gyrus (DG) granular cells and distal dendrites of CA3 pyramidal neurons (perforant path, Fig. 9) leading to weak, mostly sub-threshold excitation (Yu et al., 2010). DG granular neurons send projections (mossy fibers, Fig. 9) to CA3 pyramidal neurons, whose axons target the CA1 neurons (Schaffer collaterals, Grateron et al., 2003, Fig. 9). CA1 pyramidal neurons mediate the output of the hippocampus through the subiculum back to the entorhinal and neocortex. In addition, CA1 pyramidal neurons receive direct input from the entorhinal cortex (layer III) via the temporoammonic pathway (Fig. 9) while DG granule cells receive feed-back from mossy cells and hilar interneurons originating in the dentate gyrus hilus (Deng et al., 2010).

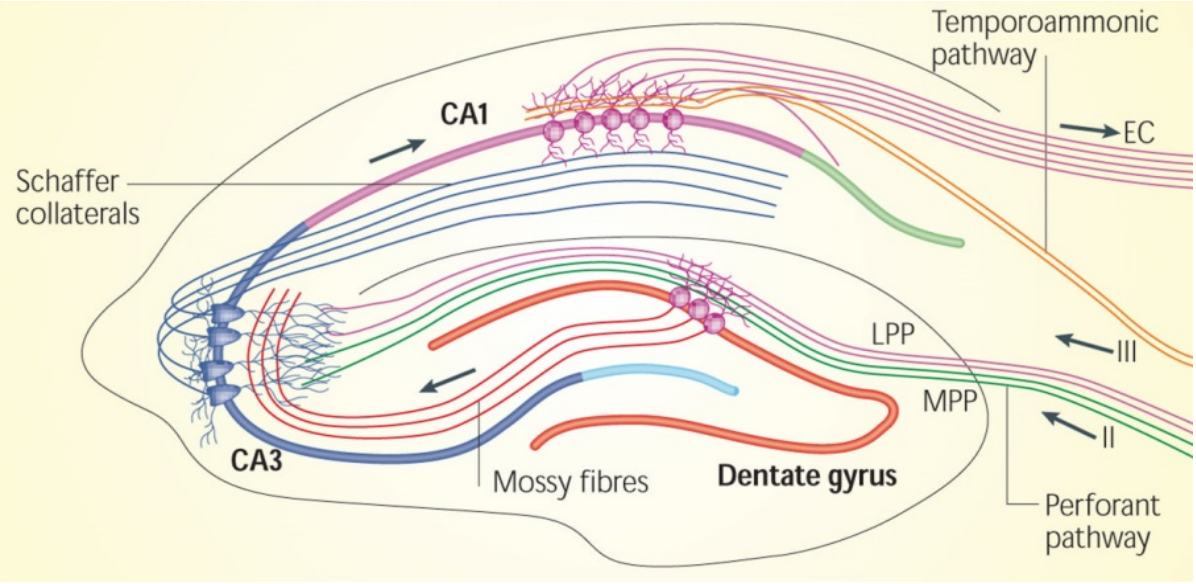

Fig. 9 Hippocampal circuitry

Depicted is a map of the neuronal connectivity of the mouse hippocampus. In brief, dentate gyrus (DG) granular neurons and CA3 pyramidal cells receive input from the entorhinal cortex (EC) via the medial and lateral perforant pathways (MPP, green fibers and LPP, pink fibers). DG granular neurons send mossy fibers to the CA3 pyramidal neurons (red fibers), which in turn target CA1 neurons via Schaffer collaterals (blue fibers), which send efferents back to the entorhinal cortex (EC, pink fibers). CA1 pyramidal cells receive additional input from the entorhinal cortex via the temporoammonic pathway (orange fibers) (modified from Deng et al., 2010)

The effects of LTP and LTD mechanisms upon changes in synaptic activity can typically be observed in pyramidal neurons of the hippocampus. Inhibition in the hippocampus is mediated by GABAergic neurons that mostly form local inhibitory connections, but some form huge networks with several layers.These vast connections lead to a very complex circuitry (Fig. 9) with intrinsic feed-back signaling to efficiently counteract firing/timing/synchrony errors or noise (Kim and Lisman, 1999).

1.4.3.2 Basal ganglia

The basal ganglia system comprises a combination of several interconnected brain areas performing tasks involving movement and cognition in a collaborative fashion. The striatum, consisting of the dorsal caudate putamen (CPu) and the ventral nucleus accumbens (NAc), the subthalamic nucleus (STN), the globus pallidus (GP), the entopeduncular nucleus (EP) and the substantia nigra (SN) together form the basal ganglia nuclei (Prescott et al., 2003).

The key structure in the basal ganglia circuitry is the striatum. Several cell types are present, with app. 98% GABAergic neurons (mostly medium spiny neurons, MSNs, and few interspersed aspiny neurons) and cholinergic interneurons. Excitatory signals are the prevalent input to the striatum originating from the cortex, thalamus, Raphe nuclei, substantia nigra and ventral tegmental area (VTA) (Fig. 11). These input projections can be distinguished not only by the neurotransmitters being released but also by the distinct pathways in which they act. Dopamine is released in the striatum to modulate motor function by different mechanisms. Substantia nigra (especially the pars compacta, SNpc) neurons send efferents to dorsal MSNs through the nigrostriatal pathway, which controls motor function via the direct pathway.

Dopaminergic innervations coming from the VTA, on the other hand, target the ventral striatum MSNs through the mesolimbic pathway, which preferentially modulate motor activity through the indirect pathway (Fig. 11) (Calabresi et al., 2014).

Both direct and indirect pathways act through disinhibition of cortical neurons and therefore activate motor function, but are differentially regulated by dopaminergic input, since dopamine can facilitate neuronal excitability through activation of G-coupled dopamine D1 receptors or repress neuronal excitability via dopamine D2 receptors (Ena et al., 2011; Perreault et al., 2010, 2011; Rubenstein and Merzenich, 2003; Sano et al., 2003; Tan et al., 2003).

Abnormalities in these circuits are associated with movement disorders, schizophrenia as well as neurodegenerative disorders like Parkinson´s and Huntington´s diseases (Galvan et al., 2015; Prescott et al., 2003).

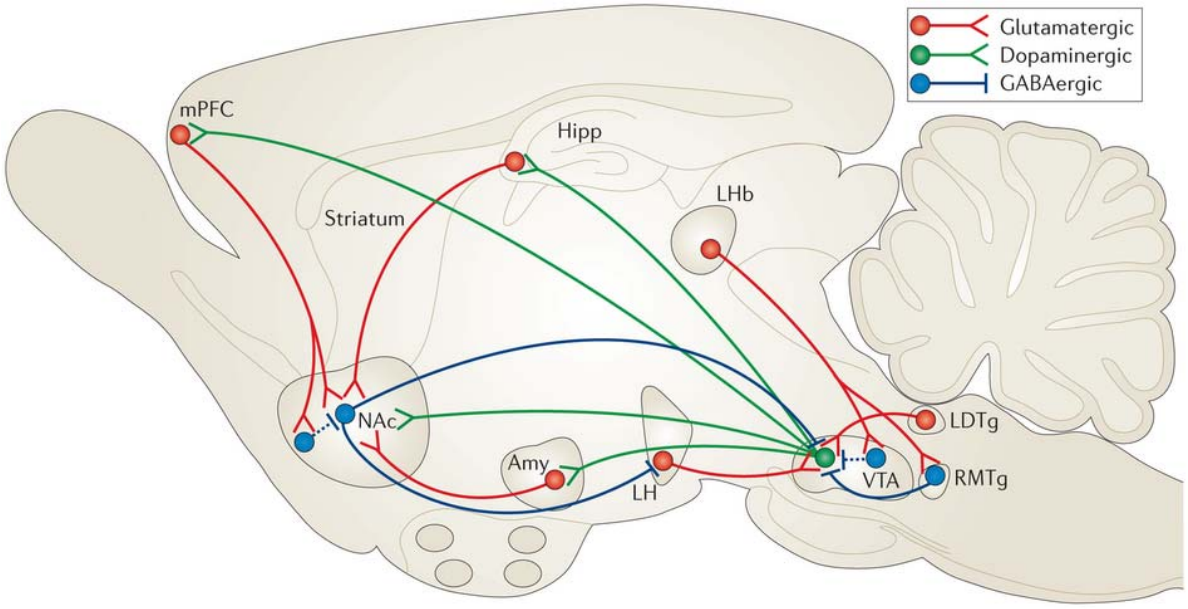

Fig. 11 Schematic overview of the various neurotransmitter systems modulating the basal ganglia pathways

Different neurotransmitter systems mediate the computation of diverse information in two separate striatal pathways. Depicted in the mouse brain scheme (saggital view) is the mesolimbic pathway originating from dopaminergic neurons of the ventral tegmental area (VTA, green fibers) projecting to the ventral striatum (nucleus accumbens, NAc) to regulate motor function. This pathway is additionally modulated by glutamatergic innervations (red fibers) and by feed-back mechanisms through the involvement of GABA (blue fibers) (modified from Russo and Nestler, 2013).

1.4.3.3 Cerebellar circuitry

A conserved structure of the CNS throughout species is the cerebellum. It is located distinct from the cerebrum near the brainstem and is part of the rhombencephalon (hindbrain).

The cerebellum consists of central fibers (white matter), the deep cerebellar nuclei and the cerebellar cortex (grey matter), a three-layered structure consisting of the granular layer, the Purkinje cell layer and the molecular layer (Fig. 12). The functions of the cerebellum are mostly restricted to several aspects of motor control, especially motor coordination, precision, timing and motor learning. Also functions in regulating language as well as fear and pleasure responses have been described for cerebellar signaling computation. Interestingly, the cerebellar circuits are similar across vertebrates with increased mass of the cerebellum compared to the cerebrum in higher organisms (fish, reptiles, birds, mammals).

Sensory information from the spinal cord (motor feed-back, proprioception), the brainstem, the trigeminal nerve (sensation of chewing, biting, etc.), and the visual and auditory systems is processed in the cerebellum.
All major excitatory systems send their axons to the cerebellum (glutamatergic, dopaminergic, cholinergic, serotonergic and adrenergic systems), but two main classes of input fibers can be clearly differentiated, which are the mossy and the climbing fibers. Mossy fibers originating from several brain regions terminate in the granular layer and excite small, densely packed granule cells, which send unmyelinated axons through the Purkinje layer to the molecular layer, where they branch at right angles to form the parallel fibers, which in turn relay the information further to the dendrites of the Purkinje cells (Fig. 12). The Purkinje cells are large, GABAergic neurons featuring vast dendritic arborizations, which receive parallel fiber input but also additional excitatory input from the climbing fibers originating from the inferior olivary nucleus of the brainstem. Purkinje cells transmit the rather weak excitation from parallel and powerful excitation from the climbing fibers further mainly to the deep cerebellar nuclei (DCN), which are located in the center of the cerebellum (Fig. 12).

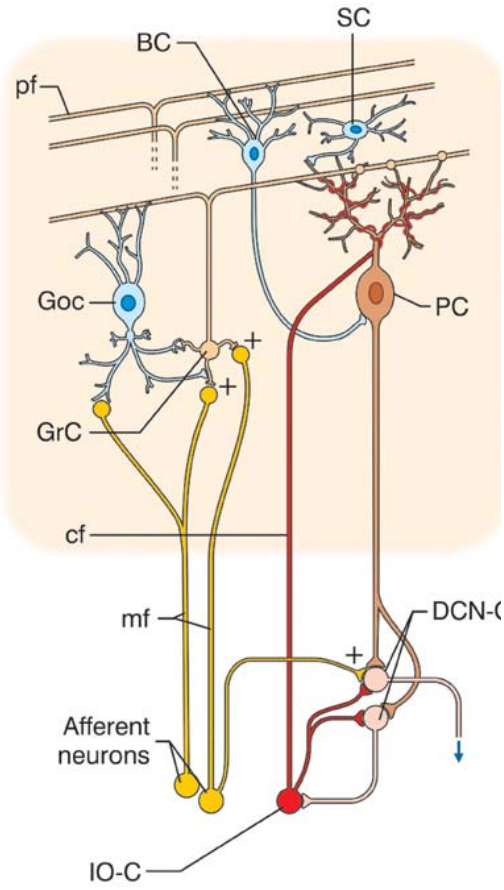

Fig. 12 Schematic view of the cerebellar circuitry
Signal input in the cerebellum begins with innervations by excitatory (+) mossy fibers (mf, yellow) and climbing fibers (cf, red) originating from the inferior olivary nucleus (IO). Mossy fibers mainly target granule cells (GrC, light orange), while climbing fibers mainly innervate Purkinje cells (PC, orange). Granule cells form parallel fiber (pf, light orange) connections with Purkinje cells but also Golgi cells (Goc, blue), basket cells (BC, blue) and stellate cells (SC, blue), which are responsible for local inhibition of granule and Purkinje neurons. Purkinje cells form the sole cerebellar output forming synapses on neurons of the deep cerebellar nuclei (DCN, pink), which further send the signals to the rest of the brain (modified from D'Angelo and Casali, 2012).

The deep cerebellar nuclei are mostly comprised of large glutamatergic projection neurons that spontaneously fire at high frequencies enhanced by mossy and climbing fiber input unless otherwise regulated by the Purkinje cell inhibition (Leto and Rossi, 2011; Uusisaari and Knöpfel, 2012). DCN neurons mediate the sole output from the cerebellum into the rest of the brain.
Purkinje cell activity can furthermore be modified by GABAergic stellate and basket neurons located in the molecular layer of the cerebellar cortex (Fig. 12). Both stellate and basket cells locally inhibit Purkinje cells, while Golgi cells, which can be found sparsely in the granular layer of the cerebellum (Golgi, 1883), relay input from mossy and parallel fibers to locally inhibit the granule cells modifying cerebellar transmission (Sillitoe et al., 2008).

1.4.3.4 Olfactory sensory system circuitry

The sensory systems mediate the environmental input, with stimuli of different kinds (light, odors, tactile sensation, etc.), and their representation in the brain.
Especially the olfactory system is of raising interest in neurological disorders, since odor information is extensively computed in a very conserved structure throughout

species called the olfactory bulb (OB) (Cave and Baker, 2009; Song and Leonard, 2005) and only one single output pathway reaches the main telencephalon.

Odor information from environmental inputs is received by excitatory receptor neurons located in the olfactory epithelium of the nose (Fig. 10), which send their axons to the OB (the most rostral part of the brain) or, more specifically, to spherical structures (app. 50-150 µm in diameter) called glomeruli. In the glomerular layer, the initial information processing is mediated by microcircuits of several cell types surrounding the glomeruli. This glomerular circuitry is signaling to Mitral cells and external tufted cells (ETC) in the Mitral cell and external plexiform layer, which facilitate the sole output of the OB via the lateral olfactory tract (LOT) mainly to the piriform as well as entorhinal cortex and the amygdala (Fig. 10).

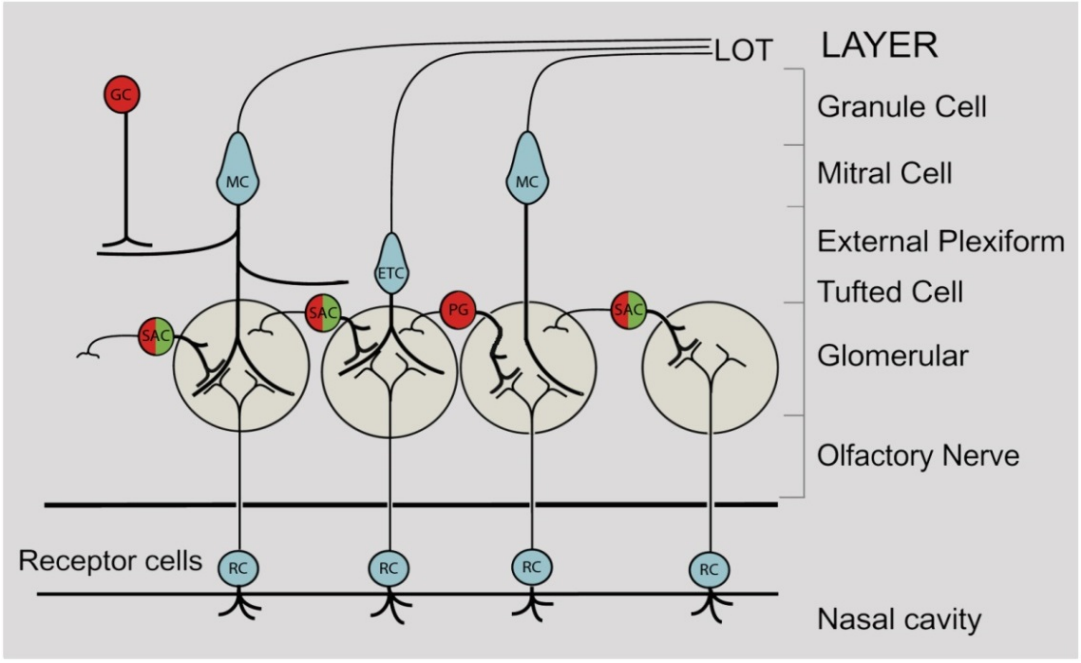

Fig. 10 Schematic representation of the olfactory projection circuitry

Odor recognition is carried out by olfactory receptor neurons (RC) in the nasal cavity, which send efferents to the olfactory bulb and more specifically to the glomeruli. Surrounding the glomeruli three types of cells can be found (short axon cells (SAC), periglomerular cells (PG) and external tufted cells (ETC)), which receive and compute the sensory input and transmit it further to the Mitral cells (MC). ETC and Mitral cells mediate the sole output of the olfactory bulb via the lateral olfactory tract (LOT) and are additionally inhibited by granule cells (GC).

Green= dopamine, red= GABA, blue= glutamate (modified from Cave and Baker, 2009)

The representation and relay of the sensory information in the OB is generated by various cell types in several layers of the OB using several pathways of modulation by feed-back and feed-forward inhibition (Fig. 10).
In the glomerular layer information is processed by three types of neurons surrounding a glomerulus, which are ETCs, short axon cells (SACs) and periglomerular cells (PGs). All three cell types receive glutamatergic input from the olfactory nerve terminals via the neuropil in the core of a glomerulus structure.

The interglomerular circuit is comprised of local inhibition of ETCs by GABAergic periglomerular cells (Murphy et al., 2005) and by GABA and dopamine co-expressing SACs, whichtune down presynaptic olfactory nerve terminal glutamate release via dopamine receptor D2-dependent inhibition (Ennis et al., 2001; Liu et al., 2013), while forming inhibitory dendro-dendritic contacts with Mitral and external tufted cell dendrites (Cave and Baker, 2009) even between distant glomeruli (Aungst et al., 2003). ETCs also feature a feed-forward excitatory pathway to the Mitral cells (Hayar et al., 2004; De Saint Jan et al., 2009).

1.4.4 Neural stem cells

Neurogenesis during embryonic development is largely based on neural stem cells (NSCs) proliferation and differentiation into the respective cell types. Furthermore, the pool of neuronal and glial cells is constantly replenished also in adult nervous tissue, which is mediated by adult neural stem cells (aNSCs).
The most studied structure during embryonic neurogenesis is the formation of the neopallial cortex by neural stem cells located in the subventricular zone (SVZ) of the lateral ventricle (LV). A part of embryonic neural stem cells of the SVZ leave the repeating cycle of self-renewal app. at embryonic day 10-12 (E10-E12) and start dividing asymmetrically. NSCs begin to change their morphology, extending radial fibers along the newly forming cortex, along which progenitor cells can migrate, therefore the stem cells are also called radial glia (RG). The newly generated neurons form the cortical layers in an inside-out pattern with each new generation of neurons travelling through the existing layers towards the pial surface of the cortex (Ayala et al., 2007). The differentiation of NSCs progresses sequentially through transiently amplifying progenitor cells and intermediate progenitor cells (IPCs) to

neuroblasts and further into immature neurons or glial precursors (Ma et al., 2009; Mamber et al., 2010). Also other neuronal lineages are generated during embryogenesis, such as dopaminergic neurons, which derive from the mesencephalic NSCs or GABAergic neurons, which emerge from the medial and lateral ganglionic eminences (MGE, LGE) (Ayala et al., 2007; Di Cristo, 2007; Faux et al., 2012).

The adult brain still features two niches for adult neural stem cells, which are the remnants of the aforementioned radial glia, one in the SVZ and a second niche in the hippocampal dentate gyrus subgranular zone (SGZ) (Goldman, 1998; Landgren and Curtis, 2011). Adult NSCs, like embryonic NSCs, can generate progenitor cells, even though at a slower rate. These are further able to differentiate into neurons at their final destination. Adult neural stem cells of the SGZ slowly replenish mostly the pool of dentate granular neurons, while aNSCs of the SVZ can form cortical neurons as well as GABAergic neurons of the olfactory bulb (Gage, 2000; Gensert and Goldman, 2001). The progenitor cells that are destined to the olfactory bulb travel long distances through the brain in the rostral migratory stream (RMS) in a state, where mostly migratory and few differentiation processes occur. The final differentiation step of precursor cells migrating along the RMS towards mature neurons is induced in the immediate proximity of the olfactory bulb before the newly arriving neurons can be integrated into the existing olfactory network.

The functionality but also the complexity of neuronal circuits, therefore, also depends on newly generated neuronal and glial cells derived from neural stem cells.

1.4.5 Implication of neuronal systems in neurological diseases

Several neuronal systems, including those described previously, are implicated in various neurological disorders, such as the aforementioned autism spectrum disorder (ASD, see 1.3.4) but also others like epilepsy, mood disorders, Alzheimer´s dementia (AD), Parkinson´s disease (PD), Huntington´s disease (HD) and many more.

The neuropathology of ASD includes forebrain neurons developmental delay, loss of Purkinje cells and age-dependent changes in size and number of neurons in the diagonal band of Broca, the deep cerebellar nuclei and the inferior olive (Kemper and

Bauman, 1998). Some of these changes concern the cerebellar circuits (see 1.4.3.3), which are involved in several processes, such as motor control, attention, language, and fear as well as pleasure responses. Alterations in this system could therefore have an impact in the language deficits and hyperexcitability phenotypes in ASD even though classically cerebellar disturbances are linked to autism, Alzheimer´s dementia and other neurological disorders by the occurrence of ataxia, essential tremors and motor coordination deficits. These effects could originate from alterations in the glutamatergic system, since in postmortem human autistic cerebellar brain tissue genes involved in glutamatergic synaptic transmission were found to be upregulated (EAAT1 and AMPA subunits), which could account for the changes in the excitation/inhibition ratio often associated with ASD (Purcell et al., 2001).

Alterations in neuronal circuitry leading to problems with cognition and motor function are common features of neurological diseases. Parkinson´s disease is characterized by loss of motor function often associated with essential tremors caused by neurodegeneration of dopaminergic neurons especially of the substantia nigra, which are consequently no longer able to innervate the striatal circuits that are fundamental components of the motor control system.

A key observation in Huntington´s disease (HD), in contrast to Parkinson´s disease, is an alteration of the dopaminergic system leading to an increase of dopamine released in the striatum (Chakraborty et al., 2014a; Napolitano et al., 2004; Pandey et al., 2009). HD is a neurodegenerative disorder caused by the mutation of the CAG repeat length in the huntingtin gene (htt, it15). Apart from the impact on the dopaminergic system, Ca^{2+} homeostasis (Hansson et al., 2001; Maciel et al., 2004), mitochondrial dysfunctions (Chakraborty et al., 2014b; Pandey et al., 2008, 2010) and excitotoxicity (Tabrizi et al., 1999) are associated with the pathology of HD. The excitotoxic effect of elevated dopamine release in the striatum via the striatonigral pathway may also lead to the observed loss of dendritic spines (Chakraborty et al., 2014a; Pandey et al., 2009; Tabrizi et al., 1999) and the resulting defects in the direct and indirect pathways ultimately cause motor phenotypes.
The variation of neurotransmitter levels can also cause multiple forms of mood disorders, which are often coincidental with an imbalance not only in the

dopaminergic but also in the serotonergic and noradrenergic systems (Nakatani et al., 2007).

It is also well-established that abnormal cortical and hippocampal circuit activity can cause epilepsy. Epilepsy is mostly due to hyperactivation of hippocampal pyramidal neurons by intrinsic hyperexcitability or due to a disinhibition by GABAergic interneurons (Abrahams and Geschwind, 2008; Alarcón et al., 2008; Cobos et al., 2005; Di Cristo, 2007; Peñagarikano et al., 2011).

An example for a rare neurodegenerative disease is amyotrophic lateral sclerosis (ALS), which is associated with the progressive loss of motor neurons in the corticospinal tract, the brainstem and the anterior horn of the spinal cord (Charcot, 1874; Daoud et al., 2013). This neuron loss results in muscle atrophy, progressive paralysis and ultimately death. Single gene alterations in 13 genes have been identified (including SOD1, TDP-43, FUS, ANG, OPTN and PFN1) accounting for only 10% of ALS cases (Boopathy et al., 2015; Daoud et al., 2013; Figley et al., 2014; Ingre et al., 2013; Kiernan et al., 2011; Smith et al., 2015; Tiloca et al., 2013; Wu et al., 2012). Excitotoxicity induced by hyperactivation of the glutamatergic system and the involvement of astrocytes as well as microglia in dysregulated neurotrophic and neurotoxic factor release have been proposed to cause the loss of motor neurons (Kiernan et al., 2011). Protein aggregates, especially of TDP-43, FUS and mutant form of PFN1, were found in patients with ALS (Boopathy et al., 2015; Figley et al., 2014; Del Poggetto et al., 2015a, 2015b; Tiloca et al., 2013; Wu et al., 2012). Patients suffering from this neurological disease are also showing altered growth cone morphology in motor neurons (Wu et al., 2012) and a change in actin levels (Tiloca et al., 2013), which might be associated with the phosphorylation-dependent interference on actin binding of PFN1 (Ingre et al., 2013).
The only therapy is a treatment targeting the glutamatergic system by use of the glutamate release inhibitor riluzole, but a treatment could be developed by restoring actin dynamics consequently to resolving stress granule protein aggregation produced by certain mutations of PFN1 (Figley et al., 2014; Kiernan et al., 2011).

1.5 The P2-GFP knock-in mouse model

The work for thesis work will take advantage of a novel mouse model generated in the lab expressing a Pfn2-EGFP fusion protein (P2-GFP) in addition to the previously described Pfn2 KO mouse model. The mouse models have been back-crossed into the C57 Bl/6 N background.

To generate the P2-GFP mouse, the CDS of the enhanced green fluorescent protein (EGFP) was fused to the C-terminus of the Pfn2 CDS in exon3 with a 14 aa linker peptide in between (Fig. 13) without any additional alteration of the Pfn2 genomic locus. The targeting construct was transferred to ES cells (129/Sv) by homologous recombination and the cells were injected into blastocysts that were implanted in pseudo-pregnant female mice.

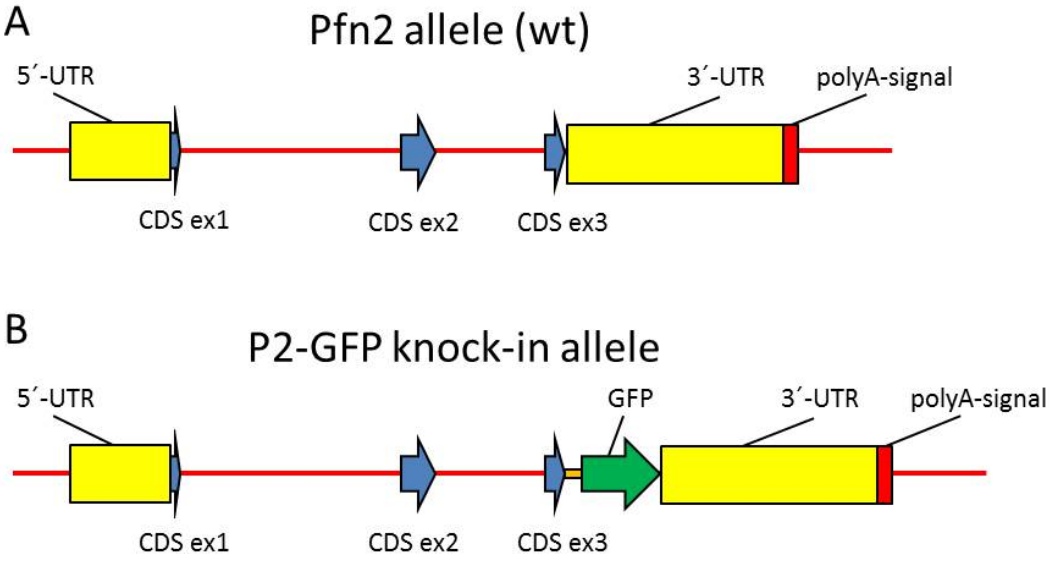

Fig. 13 Pfn2 and P2-GFP alleles
A Pfn2 allele (wt)
B P2-GFP allele with the GFP gene inserted at the C-terminus of Pfn2**.**

P2-GFP expressing mice are viable in homozygosity and show mild behavioral alterations such as jumping phenotype and a low incidence of seizures with rising susceptibility with aging.

1.6 Aim of the thesis

Pfn2 knock-out mice show a complex phenotype including autistic-like behavior and epileptic seizures. This could be of high relevance for the corresponding human disorders. Yet it is still unclear how the Pfn2 knock-out phenotype arises, whether the dysfunction of the glutamatergic system is sufficient or other neurotransmitter systems are involved and are contributing to it as well. The essential problem is that it is still unknown in which cell types of the nervous system Pfn2 is expressed and what functions it might have in different neuronal circuits.

In this thesis the specific expression pattern of Pfn2 in neuronal and non-neuronal cell subtypes of the nervous system in adult as well as embryonic mice is examined using a profilin 2-EGFP fusion protein mouse model. For this purpose, co-immunofluorescence stainings of P2-GFP with marker proteins for subtypes of various neuronal cells, glial cells, neural stem cells, precursor cells and synaptic subcompartments are performed on tissue sections as well as cultured hippocampal neurons from the P2-GFP KI mouse model and imaged using conventional widefield and laser-scanning confocal fluorescence microscopy.

In addition, the expression level of the P2-GFP fusion protein in comparison to wt Pfn2 is studied, evaluating the binding efficiencies of different anti-Pfn2 antibodies using Strep-tagged variants of P2-GFP and Pfn2 and calculating the expression level in tissue extracts of homozygous and heterozygous P2-GFP mutant mice. The biochemical properties of P2-GFP in comparison to Pfn2 are also evaluated by performing binding assays to poly-L-proline beads and by co-immunoprecipitation experiments, in order to validate the P2-GFP mouse model for future *in vivo* studies.

In the last part of the thesis, the roles and functions of Pfn2 employing cultured primary hippocampal neurons derived from both P2-GFP KI and Pfn2 KO animals are studied during neuronal development and its trafficking is visualized following the application of various chemical stimuli.

2. Results

2.1 Analysis of the expression pattern of Pfn2 in the nervous system

The loss of Pfn2 in the brain is responsible for complex phenotypes that phenocopy human autism in most of its aspects (see 1.3.4). The molecular and physiological origin of autism is still very unclear, and it is not known which neurotransmitter system is mainly involved, although genes encoding proteins specific for different neuronal subtypes and neurotransmitter systems have been found mutated or inactivated in patients with ASD (see 1.3.4). From this respect, knowing in which neuronal subtypes Pfn2 is expressed and therefore which circuits could be affected by its removal, could shed light on the physiological origin of ASD.
For this purpose the P2-GFP mouse model (see 1.5) was created and has been used in this study to co-localize P2-GFP expression with specific markers for the different neuronal subtypes and neuronal compartments. Where a co-expression of the marker and the P2-GFP was observed, it was possible to determine that Pfn2 is expressed in the corresponding neuronal subtype.

Extensive attempts in defining classes or subtypes of neurons have been made throughout the decades, but the wealth of cell types with distinct molecular, morphological and electrophysiological features made these attempts extremely difficult and as yet incomplete. Especially GABAergic neurons show an immense variety of cell types with very specific and often not yet well understood functions (Ascoli et al., 2008; Battaglia et al., 2013).
Identification of the different cell types in the brain is largely based on their location, morphology, molecular composition and electrophysiological properties. Using high-resolution microscopy, the first three traits (location, morphology, molecular composition) can be used to identify the cell types under investigation.

In this thesis, whole mouse brains were dissected from P2-GFP knock-in homozygous mice (G/G), Pfn2 KO and wild type controls and sectioned sagittally or coronally using a vibratome with a thickness of 20 µm (see 4.3.2), which corresponds to approximately 2 cell layers. High-resolution confocal laser-scanning microscopy

(see 4.3.5) was applied to visualize neurons and neuronal structures in the brain with the best possible signal-to-noise ratio in order to reach the light-microscopy lateral resolution limit of 250-500 nm.

P2-GFP was additionally labelled with an anti-GFP antibody and a secondary Alexa Fluor 488-coupled antibody, since tissue fixation with formaldehyde markedly reduces the fluorescence efficiency of the GFP moiety. Neuronal subtypes were identified by fluorescently labelling marker proteins with the corresponding specific primary antibodies and secondary antibodies conjugated with Alexa Fluor 555 or CF633 dyes for the respective emission channels. A nuclear DNA staining substance was also applied to aid the identification of certain brain structures (DAPI and Draq5 dyes).
In order to control for non-specific signals in every emission channel, serial scans with all available lasers over the whole visible spectrum ("lambda stacks") using the same settings as for the specifically stained sample were obtained for control slides missing one staining component (primary and/or secondary antibody) from P2-GFP KI, wild type and Pfn2 KO sections.

2.1.1 All excitatory neuronal systems express Pfn2 at varying levels

The most widely used mode of synaptic transmission is mediated by excitatory neurotransmitters such as glutamate, dopamine, noradrenaline, serotonin and acetylcholine (see 2.1.1.1- 2.1.1.5).

The excitatory neuronal systems will be discussed in the order of their expression level of Pfn2 (see Fig. 21 for an overview). In general, all excitatory neuronal systems expressed Pfn2, but interesting observations concerning the expression level and the cell type as well as the subcellular localization of the protein lead to a more distinct and complex picture of the role of Pfn2 in neuronal networks and its potential role in neurological diseases.

2.1.1.1 Glutamatergic neurons display the highest expression of Pfn2

The most common neurotransmitter in the brain is glutamate. Many areas in the brain feature at least some glutamatergic neuron types, but they are mostly enriched in the cortex, the hippocampus and the cerebellum. In the latter especially small, densely packed granule neurons are the most numerous neuronal type, while most glutamatergic neurons in the cortex and the hippocampal CA regions are described as pyramidal or principal neurons based on their common features in terms of morphology and strong excitatory output.

Glutamatergic neurons are included in several neuronal circuits: many cortical pathways, the hippocampal perforant path, mossy fibers and Schaffer collaterals (see 1.4.1.1), as well as olfactory (see 1.4.1.2) and cerebellar (see 1.4.1.3) circuitries.
In order to identify glutamatergic neurons specifically, neurogranin (Nrgn) was used as a marker, a protein exclusively present in the glutamatergic system. Neurogranin is a post-synaptically localized calmodulin-binding protein involved in synaptic plasticity and a known biomarker for glutamatergic neurons, which was also found to be up-regulated in Alzheimer´s disease and mesial temporal lobe epilepsy (MTLE) (Díez-Guerra, 2010; Hoffman et al., 2014; Höglund et al., 2015; Singec et al., 2004; Wu et al., 2015). Nrgn staining is prominent in the cell bodies and dendrites of glutamatergic neurons.

Previous work has already shown Pfn2 to be expressed in certain glutamatergic neurons (Pilo Boyl et al., 2007), but only few neuronal circuits were analyzed leaving most areas and cell types to be investigated.
Pfn2 was found to be expressed in all glutamatergic neurons in varying amounts (see also Fig. 21). The highest expression in the brain was featured by two large neuronal types, the CA2 pyramidal neurons of the hippocampus (Fig. 14A), and the Mitral cells of the olfactory bulb (data not shown).

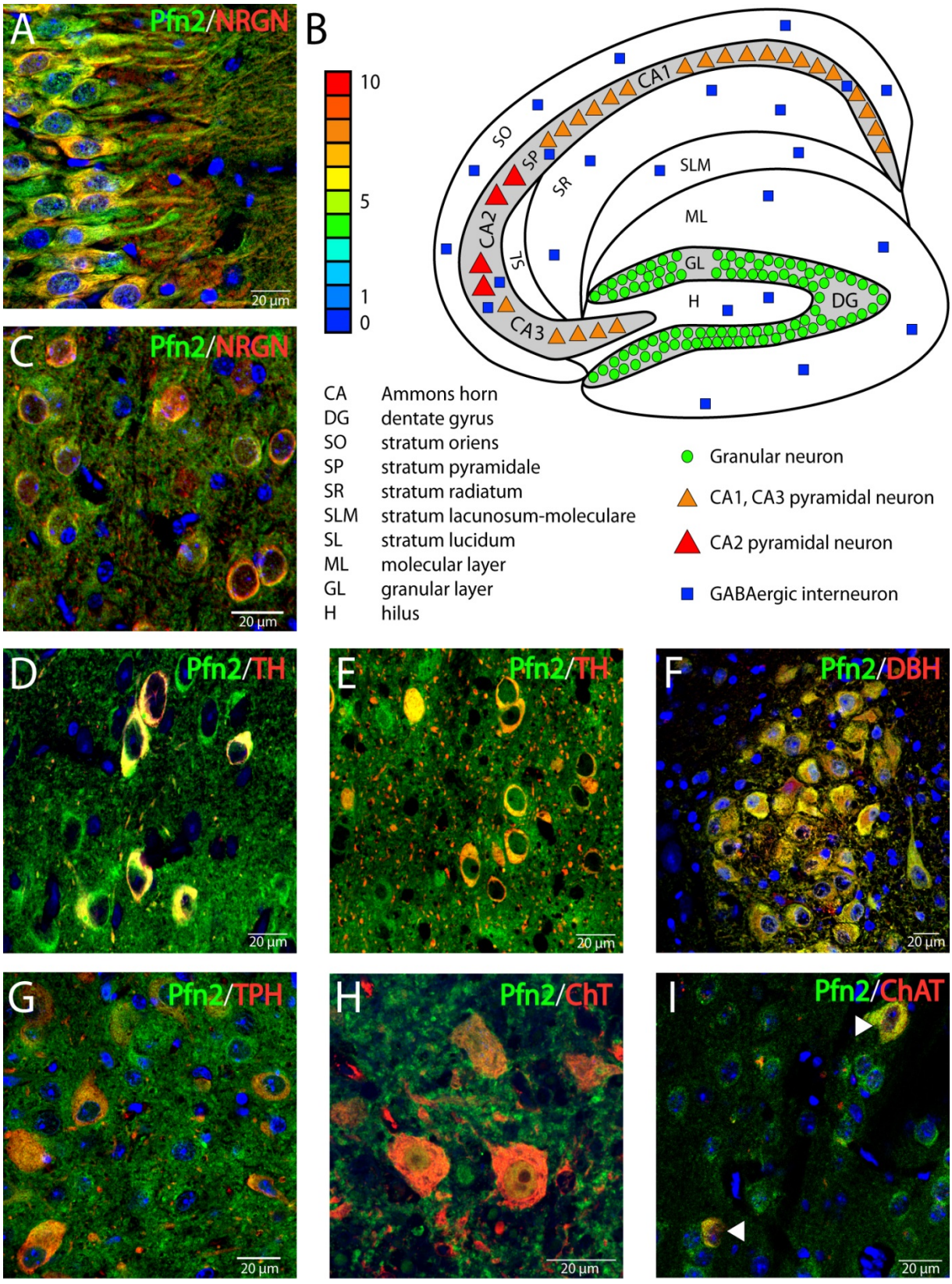
A
Pfn2/NRGN
20 µm
B
10
5
1
0
CA1
SO
SP
SR
SLM
ML
CA2
SL
GL
H
DG
CA3
C
Pfn2/NRGN
20 µm
CA Ammons horn
DG dentate gyrus
SO stratum oriens
SP stratum pyramidale
SR stratum radiatum
SLM stratum lacunosum-moleculare
SL stratum lucidum
ML molecular layer
GL granular layer
H hilus
Granular neuron
CA1, CA3 pyramidal neuron
CA2 pyramidal neuron
GABAergic interneuron
D
Pfn2/TH
20 µm
E
Pfn2/TH
20 µm
F
Pfn2/DBH
20 µm
G
Pfn2/TPH
20 µm
H
Pfn2/ChT
20 µm
I
Pfn2/ChAT
20 µm

High expression of Pfn2 could be observed in pyramidal neurons of the hippocampal formation extending their dendrites towards the stratum radiatum (Fig. 14A, schematized in Fig. 14B). The dentate gyrus granular neurons, on the other hand, show interestingly low expression of Pfn2 in their cell bodies (Fig. 14B) but high expression in their mossy fiber processes (data not shown).

Most neurons of the cortex are glutamatergic featuring an equal expression of Pfn2 throughout the cortical layers (Fig. 14C). A similar distribution was found in the thalamus and the cerebellum.

Pfn2 can also be found in axons, pre-synaptic boutons and spines by co-localization stainings of P2-GFP with pre- and post-synaptic markers (data not shown).

The control stainings of wildtype littermates showed only Nrgn signals (Supp. Fig. 5) and control stainings without incubating with the primary antibodies using only the respective secondary antibodies yielded no specific signal (Supp. Fig. 11).

Fig. 14 All excitatory neuronal systems express Pfn2

All main excitatory systems express Pfn2 at different levels.

(**A**) Highest levels of Pfn2 (green) are present in glutamatergic neurons of the CA2 region of the hippocampus, identified by localization, size and their expression of neurogranin (Nrgn, red). Nuclei are stained with Draq5 (blue). (**B**) Color-code schematic view of Pfn2 expression in the hippocampus showing highest expression levels of Pfn2 in CA1-3 pyramidal neurons and medium levels in granular neurons of the dentate gyrus (DG), while GABAergic neurons are completely devoid of Pfn2 (see chapter 2.1.2 for more details). (**C**) Glutamatergic (Nrgn, red) cortical neurons feature intermediate levels of Pfn2. (**D**) Dopaminergic neurons of the ventral tegmental area (VTA) and (**E**) of the substantia nigra (SN) specifically labelled using an antibody against tyrosine hydroxylase (TH, red) express high levels of Pfn2. (**F**) Adrenergic neurons of the locus coeruleus (LC) in the brainstem identified by dopamine hydroxylase (DBH, red) express medium-high levels of Pfn2. (**G**) Serotonergic neurons of the Raphe nuclei, specifically expressing tryptophan hydroxylase (TPH, red) contain high amounts of Pfn2. (**H**) Cholinergic neurons of the pedunculopontine tegmental nucleus (ppt) labelled by the choline transporter (ChT, red) show low expression of Pfn2. (**I**) Large cholinergic interneurons of the striatum identified by the enzyme choline acetyltransferase (ChAT, red, arrowheads) show high enrichment of Pfn2.

2.1.1.2 Dopaminergic neurons express very high levels of Pfn2

Dopamine is mostly released upon reward mechanisms and therefore associated with motivational responses and addiction, but it is also involved in locomotion, learning and fine motor coordination. Dopamine acts in the striatum on two types of medium spiny neurons (MSNs): on the dopamine D1 receptor (D1R)-positive cells it increases MSN excitability, while on the dopamine D2 receptor (D2R)-expressing cells it decreases MSN excitability due to the properties of the D2 receptor type (Tan et al., 2003).

Dopaminergic neurons can be classified into several groups by their location (Supp. Fig. 1). The most prominent areas containing dopaminergic neurons are the substantia nigra (SN, group A9), the ventral tegmental area (VTA, group A10) with the small associated retrorubral field (RRF, group A8) and the olfactory bulb (OB, group A16) (Smidt and Burbach, 2007). Dopamine is released in three major pathways in the brain (mesolimbic, mesocortical and nigrostriatal pathways), which target different brain areas specifically (Supp Fig. 1). Dopaminergic neurons are regulated by inhibitory signaling from medium spiny neurons of the striatum targeting long dendritic projections originating from the dopaminergic nuclei and additional inhibition by local interneurons in the pars reticulata (Tan et al., 2003).

To specifically identify dopaminergic neurons, the rate-limiting enzyme of dopamine synthesis, tyrosine hydroxylase (TH), was used as marker protein (Gelman et al., 2003; Kumer et al., 1996; Lindgren et al., 2000; De Marchis et al., 2007; Thompson et al., 2005). Tyrosine hydroxylase is majorly involved in the transition of tyrosine to DOPA, which is further processed to dopamine in dopaminergic and noradrenergic neurons.

Pfn2 was found highly expressed in dopaminergic neurons. The highest expression of Pfn2 was in the SN (Fig. 14D) and VTA (Fig. 14E). Less expression was observed in the RRF (data not shown) and a differential expression was found in the olfactory bulb (see 2.1.7). The control stainings from wildtype animals showed only TH signals (Supp. Fig. 5) and control stainings without incubating with the primary antibodies only using the respective secondary antibodies yielded no specific signal (Supp. Fig. 11).

2.1.1.3 The noradrenergic system shows high Pfn2 expression

A source of powerful excitation in the CNS is noradrenaline (norepinephrine) of the catecholamine family of neurotransmitters. Noradrenaline is mainly released upon states of stress, danger, it raises attention, arousal and emotional as well as memory functions, to increase the motivation for the respective task.
Noradrenergic neurons (also addressed as adrenergic neurons) can be found exclusively in the locus coeruleus (LC) of the hindbrain (pons) adjacent to the cerebellar formation (Supp. Fig. 2). Only a very limited number of neurons releasing noradrenaline is present in the mouse brain (app. 30.000), but can still have a large impact in a number of brain areas and cognitive functions (Swanson and Hartman, 1975).

Noradrenaline is produced by an additional step in the dopamine synthesis pathway by dopamine-β-hydroxylase (DBH) mediated catalysis of dopamine. DBH is therefore used to exclusively label noradrenergic neurons (Jin et al., 2004; Swanson and Hartman, 1975).

Noradrenergic neurons were found to express a quite high amount of Pfn2 (Fig. 14F). The low density of noradrenergic neurons in the brain complicates the analysis due to few brain sections actually containing LC neurons. Therefore several serial sections were analyzed to ensure the expression pattern of Pfn2 in the full area of the locus coeruleus (see also Fig. 20, compare Supp. Fig. 12). The control stainings of wildtype slices showed only DBH signals (Supp. Fig. 5) and control stainings using only the respective secondary antibodies yielded no specific signal (Supp. Fig.11).

2.1.1.4 Pfn2 is expressed at quite high levels in serotonergic neurons

The regulation of emotions, sleep, mood, sexuality, appetite and body temperature is strongly mediated by the serotonergic neuronal system (Svenningsson et al., 2004). This neuronal system innervates widely the CNS, eliciting both excitatory and

inhibitory responses from targeted cells, depending on their expression of the respective subtypes of the serotonin receptors (5-HTRs, 14 subtypes). Serotonergic signaling originates exclusively from the Raphe nuclei of the brainstem from where efferents reach nearly all brain regions with varying input intensity (Supp. Fig. 3).

To address the question, if Pfn2 could have a role on signaling originated from neurons releasing the monoamine serotonin (5-hydroxytryptamine, 5-HT), the tryptophan hydroxylase (TPH) enzyme of the serotonin metabolism pathway was used as a marker for the identification of these neurons. The TPH enzyme mediates the final rate-limiting step of serotonin biosynthesis and is also a target in the serotonergic pathway of therapeutic anti-depressant drugs (Andrade, 2011; Chandana et al., 2005; Cohen et al., 1995).

The expression of Pfn2 in the neurons of the Raphe nuclei was pronounced (Fig. 14G) even if not as high as in the glutamatergic or dopaminergic systems (see Fig. 20). Serotonergic neurons were found interspersed with glutamatergic neurons in the Raphe area (see Supp. Fig. 12).
The wildtype control stainings showed only TPH signals (Supp. Fig. 5) and control stainings using only the respective secondary antibodies yielded no specific signal (Supp. Fig. 11).

2.1.1.5 Most cholinergic neurons show minor expression of Pfn2

Neurons releasing the monoamine neurotransmitter acetylcholine (ACh) in the brain are contributing to the responses of cognitive tasks such as attention, learning and memory, reward mechanisms, motor activity and analgesia (Sarter and Parikh, 2005). ACh release can mediate excitatory or inhibitory responses due to the differential effects of the two families of acetylcholine receptors, nicotinic (ionotropic) and muscarinic (metabotropic) respectively, but excitatory stimulation is the prevalent form of signaling from cholinergic innervations.
The major cholinergic regions in the brain are located in the medial septum ventral to the striatum as well as a pontomesencephalic region near the cerebellum (Supp Fig.

4). The medial septal group as well as the pedunculopontine tegmental nucleus (ppt) and laterodorsal tegmental nucleus (ldt) feature dispersed cholinergic neurons of medium size with output projections to virtually the entire brain and spinal cord (Supp Fig. 4) (Woolf, 1991). Apart from the cholinergic neurons in the CNS, cholinergic motor neuron innervations of the PNS also release ACh to stimulate muscle contraction.

In order to produce the neurotransmitter acetylcholine, the enzyme choline acetyltranferase (ChAT) is synthesizing ACh from choline and acetyl coenzyme A (Kreitzer, 2009). After synaptic release, ACh is cleaved to choline and acetate by the enzyme acetylcholinesterase (AChE). The free choline is taken up again by the high-affinity choline transporter (ChT) present on the pre-synaptic cholinergic neuron, which is the rate-limiting step in ACh synthesis (Misawa et al., 2001; Sarter and Parikh, 2005). Therefore, both ChAT and ChT were used to identify cholinergic neurons in this thesis.
Cholinergic neurons express minor amounts of Pfn2 (Fig. 14H) compared to other neuronal systems (see also Fig. 20). These low-expressing neurons can be found in the medial septal group of the forebrain as well as in the ppt and ldt of the midbrain. An exception is the group of large cholinergic interneurons in the striatum, which feature high expression of Pfn2 (Fig. 14I). Also motor neurons of the spinal cord express Pfn2 (data not shown).
The control stainings from wildtype brain sections showed only ChAT or ChT signals respectively (Supp. Fig. 5) and control stainings using only the respective secondary antibodies yielded no specific signal (Supp. Fig. 11).

Summarizing the excitatory neuronal systems, glutamatergic neurons express the highest level of Pfn2 in the brain (see also Fig. 21, compare Supp. Fig. 12). Especially pyramidal neurons of the CA2 subfield as well as Mitral cells of the olfactory bulb show extensive Pfn2 enrichment, while other cells vary greatly in the expression and even subcellular distribution of Pfn2. The dopaminergic system is expressing nearly equally high levels of Pfn2 in the brain (compare Fig. 21). The noradrenergic system also features high amounts of Pfn2 (Fig. 14F, compare Fig. 21), similar to the serotonergic system (Fig. 14G, compare Fig. 21). Most

cholinergic neurons show a moderate expression of Pfn2 with the exception of the large cholinergic interneurons of the striatum (compare Supp. Fig. 12). Therefore, the cholinergic system is the only excitatory neuronal system not enriched in Pfn2.

2.1.2 The GABAergic neuronal systems show a highly cell type-specific expression pattern of Pfn2

The key inhibitory neuronal system uses gamma-aminobutyric acid (GABA) as neurotransmitter (see 1.4.1). GABAergic neurons mediate the hyperpolarization of neurons, decreasing firing probability and as a result, typically, excitatory systems are tuned down by inhibitory GABA signaling to increase the dynamic range of signal transmission and further computing the underlying information. GABAergic neurons are therefore essentially involved in virtually all brain circuitries and hence all brain functions.

These neurons are located in most brain regions featuring the highest diversity of neuronal subtypes. In order to identify GABAergic neurons, co-immunofluorescence stainings with antibodies directed against GABA or GAD67 (GAD1) were performed.

A distinct trait in certain GABAergic cell types is the regulation of Ca^{2+} homeostasis, which is mediated by different Ca^{2+}-buffering proteins in different cell types. Calmodulin (CaM) was first identified as a Ca^{2+}-buffering protein, but is ubiquitously expressed, while other Ca^{2+}-binding proteins, such as calbindin D28 (CB), calretinin (CR) and parvalbumin (PV) are expressed restricted to populations of specific cell types (Celio, 1990; Di Cristo, 2007; Faux et al., 2012; Figueredo-Cardenas et al., 1998; Grateron et al., 2003; Hendry et al., 1989; Lawrence et al., 2010; Matamales et al., 2009; Rudy et al., 2011; Wang et al., 2004; Wierzba-Bobrowicz et al., 2011; Woodruff and Yuste, 2008; Woodruff et al., 2010). Both the Ca^{2+}-binding proteins CB and PV were also used in this work to identify specific subtypes of inhibitory neurons.

The expression pattern of Pfn2 in these neurons was found to be extremely diverse and differed among cell subtypes for each region of the brain.

Therefore, the results of the expression pattern of Pfn2 in GABAergic cell types will be shown in a brain region-specific order. The cortical, hippocampal as well as

cerebellar GABAergic neurons will be described in chapter 2.1.2.1, while the striatum and the olfactory bulb will be shown in separate chapters (2.1.2.2 and 2.1.3).

2.1.2.1 The expression pattern of Pfn2 is extremely restricted in GABAergic neurons of the cortex, hippocampus and cerebellum

The highest variability of cell types not only restricted to GABAergic types, is present in the cerebral cortex, which is involved in nearly all brain functions including cognition, memory and language control (see 1.4) (Grateron et al., 2003; Graus-Porta et al., 2001).
Cortical GABAergic neurons are mostly devoid of Pfn2 with few exceptions (Fig. 15A). PV-positive basket cells are the most numerous cell type (Di Cristo, 2007; Hendry et al., 1989; Méndez and Bacci, 2011; Rudy et al., 2011) and devoid of Pfn2 (Fig. 15B). Among PV-expressing cells, some rarer neurons feature Pfn2 expression, i.e. the Chandelier cells (Fig. 15B), identified by their position and characteristic morphology (Di Cristo, 2007; Hendry et al., 1989; Rudy et al., 2011; Woodruff and Yuste, 2008; Woodruff et al., 2010). Other cortical GABAergic neuron subtypes express calbindin, namely the bitufted neurons and a subset of Martinotti cells (Wang et al., 2004). None of the medium-sized Martinotti cells, but all of the few larger bitufted neurons, which are easily identified by the double dendritic bundle morphology of their projections (Di Cristo, 2007; Hendry et al., 1989; Rudy et al., 2011), were observed to express Pfn2 (Fig. 15C). Two GABAergic neuronal cell types were found in the external layer I of the cortex, the Cajal-Retzius (or horizontal) cells and neurogliaform cells (also called spiderweb cells) (Chandana et al., 2005; Rudy et al., 2011), which both lacked Pfn2 expression (data not shown).
In summary, cortical GABAergic neurons are mostly devoid of Pfn2 with the exception of two rare cell types, the fast-spiking Chandelier cells and the bitufted neurons (see also Fig. 17).

The neuronal circuitry of the hippocampal formation is very well established in terms of the contribution of glutamatergic as well as GABAergic neurons (see 1.4.1.1, Fig. 10). The GABAergic neuronal subpopulations can be distinguished by their

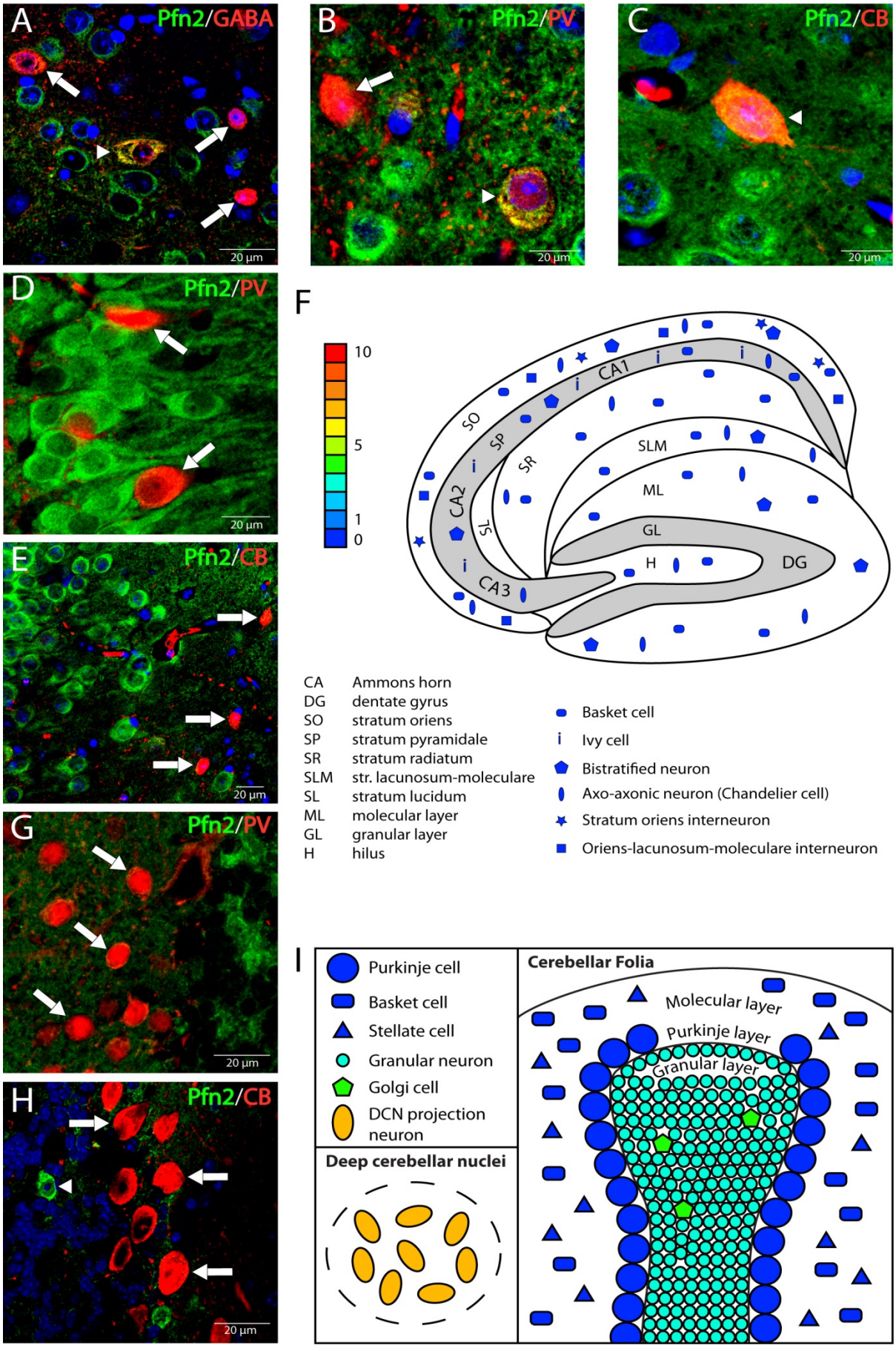
A
Pfn2/GABA
20 µm
B
Pfn2/PV
20 µm
C
Pfn2/CB
20 µm
D
Pfn2/PV
20 µm
E
Pfn2/CB
20 µm
G
Pfn2/PV
20 µm
H
Pfn2/CB
20 µm
F
10
5
1
0
SO
SP
SR
SL
SLM
ML
GL
H
DG
CA1
CA2
CA3
i
CA Ammons horn
DG dentate gyrus
SO stratum oriens
SP stratum pyramidale
SR stratum radiatum
SLM str. lacunosum-moleculare
SL stratum lucidum
ML molecular layer
GL granular layer
H hilus
Basket cell
Ivy cell
Bistratified neuron
Axo-axonic neuron (Chandelier cell)
Stratum oriens interneuron
Oriens-lacunosum-moleculare interneuron
I
Purkinje cell
Basket cell
Stellate cell
Granular neuron
Golgi cell
DCN projection neuron
Deep cerebellar nuclei
Cerebellar Folia
Molecular layer
Purkinje layer
Granular layer

morphology (mostly differences in soma sizes), location and their differential expression of the Ca^{2+}-binding proteins calbindin and parvalbumin (Celio, 1990).
Similarly to the cortex, the most abundant inhibitory cell type are the parvalbumin-positive basket cells, which also in the entire hippocampus is devoid of Pfn2 (Fig. 15D, schematized in Fig. 15F). The most dorsal layer of the hippocampus were the stratum oriens, which is purely inhibitory, since the cell bodies of GABAergic neurons are concentrated in this layer (Lawrence et al., 2010). GABAergic neurons in the stratum oriens are basket cells (PV+), bistratified neurons (PV+), axo-axonic neurons (also called Chandelier cells, PV+) and stratum oriens interneurons (CB+), as well as the exclusively stratum oriens localized oriens-lacunosum-moleculare interneurons (O-LM interneurons, PV+), which all share the absence of Pfn2 expression (Fig. 15E, schematized in Fig. 15F). Most of these cell types can also be found in the remaining strata of the hippocampal formation with varying density but uniformly lack expression of Pfn2. Ivy cells (NPY+) found in the stratum pyramidale in between the array of pyramidal neurons were also devoid of Pfn2 (data not shown, schematized in Fig. 15F).

Fig. 15 The expression of Pfn2 in GABAergic neurons is specific to few cell types in cortex, hippocampus and cerebellum

The very specific expression pattern of Pfn2 in few GABAergic neuron subtypes is depicted for three major brain regions the cortex, the hippocampus and the cerebellum.

(**A**) In the cortex of the mouse brain, only few GABAergic neurons (red) appear to express Pfn2 (green), indicated by an arrowhead, while most GABAergic neurons are devoid of Pfn2 (arrows). (**B**) Parvalbumin-positive basket cells (red) lack Pfn2 (arrow), while large PV-positive Chandelier cells (axo-axonic neurons) (arrowhead) and (**C**) large CB-positive bitufted neurons (arrowhead) express Pfn2. Several types of GABAergic neurons in the hippocampus were specifically labelled for (**D**) parvalbumin (red) or (**E**) calbindin (red) and are completely devoid of Pfn2 (arrows). (**F**) Schematic view of the various hippocampal GABAergic neuron types, color-coded to indicate the expression profile of Pfn2. (**G)** Cerebellar stellate and basket cells (PV+, red) show the absence of Pfn2 (arrows). (**H)** Purkinje cells (CB+, red), do not express Pfn2 (arrows) while GABAergic Golgi cells, identified by their morphology and location among the glutamatergic granular neurons are positive for Pfn2 (arrowhead). (**I**). Color-coded scheme representing the expression level of Pfn2 as described in the cerebellum. To visualize the cell nuclei (blue), the DNA-intercalating dye Draq5 (Biostatus) was used.

In summary, the entire hippocampal formation is devoid of Pfn2 in all populations of GABAergic subtypes (Fig. 17), in clear contrast to the highly Pfn2-positive adjacent neurons of the glutamatergic system (see Fig. 21).

The cerebellum is a structure adjacent to the brainstem mainly involved in motor function but also in language, fear and pleasure responses. The whole cerebellar circuitry (see 1.4.3.3, Fig. 12) is utilizing only two neurotransmitter systems. While the glutamatergic cells show expression of Pfn2 (see 2.1.1), GABAergic neurons of the cerebellum show a similar expression profile of Pfn2 as the cortex, since only one single GABAergic cell type was found to be positive for Pfn2.
GABAergic neurons in the cerebellum can be distinguished based on their location in the three layers of the cerebellar cortex, their morphology (mostly by their soma size and dendritic arborization) and by the differential expression of the Ca^{2+}-binding proteins calbindin and parvalbumin.
In the cerebellum, stellate and basket cells express PV whereas Purkinje cells co-express calbindin and parvalbumin (Bosman et al., 2006; Celio, 1990; Hendry et al., 1989; Sillitoe et al., 2008; Wierzba-Bobrowicz et al., 2011; Woodruff et al., 2010). Pfn2 was not found in any of the PV-expressing neurons, which comprise the majority of GABAergic neurons in the cerebellum with PV-positive basket, stellate and Purkinje cells (Fig. 15G, schematized in Fig. 15I), while among the CB-expressing neurons only Golgi cells were positively recognized to express Pfn2 (Fig. 15H, schematized in Fig. 15I).
These observations are summarized in Fig. 15I, in which it appears that the molecular layer as well as the Purkinje cell layer are devoid of Pfn2, while the rare Golgi cells among the dense glutamatergic granular neurons show the expression of Pfn2 at a medium high level (Fig. 17). The glutamatergic projection neurons of the deep cerebellar nuclei show an intense signal for Pfn2 (see Fig. 21).

Wildtype control stainings showed only GABA, PV or CB signals respectively (Supp. Fig. 6) and control stainings using only the respective secondary antibodies yielded no specific signal (Supp. Fig. 11).

2.1.2.2 Striatal GABAergic neurons express Pfn2 with a subtype- and area-specific pattern

One of the key structures of the basal ganglia is the striatum (see 1.4.3.3, Fig. 11). The striatum is partially responsible for motor function, novelty and exploration as well as motivational behavior (Cuzon Carlson et al., 2011).

The striatum is comprised of app. 98% GABAergic neurons with the vast majority (app. 95%) being medium spiny neurons (MSNs) and the remaining 2-3% aspiny interneurons. Also few (1-2%) cholinergic interneurons are dispersed throughout the striatum (see 2.1.1.5). It can be divided into the dorsal caudate putamen and the ventral nucleus accumbens. Medium spiny neurons are subdivided into dopamine D1 receptor (D1R)-expressing and dopamine D2 receptor (D2R)-expressing neurons, with higher density of D1R-positive MSNs in the dorsal striatum and higher density of D2R-positive MSNs in the ventral striatum (Ennis et al., 2001; Matamales et al., 2009). Since all MSNs receive strong dopaminergic input, these cells express high levels of DARPP32 (dopamine and cAMP-regulated phosphoprotein), while the striatal fast-spiking aspiny interneurons exclusively express parvalbumin (Figueredo-Cardenas et al., 1998; Svenningsson et al., 2004; Zachariou et al., 2005).

Pfn2 was found in a large subset of medium spiny neurons (MSNs) identified by their expression of DARPP32 (Fig. 16A). Few striatal neurons with large somata, identified as the aspiny interneurons, which were not labeled by DARPP32 but by PV (Fig. 16B), as well as the rare cholinergic interneurons (see 2.1.1.5, Fig. 14I), were also positive for Pfn2 (schematized in Fig. 16C). To further elucidate the differences in the expression pattern of Pfn2 in MSNs, these cells were specifically labeled exploiting their differential expression of dopamine receptor subtypes D1R and D2R. All D1R-expressing MSNs were also expressing Pfn2 in the caudate putamen (Fig. 16D, schematized in Fig. 16F) as well as in the nucleus accumbens (Fig. 16E, schematized in Fig. 16F). D2R-positive cells, on the other hand, were lacking Pfn2 in the caudate putamen (Fig. 16G, schematized in Fig. 16I) but expressed low levels of Pfn2 in the nucleus accumbens (Fig. 16H, schematized in Fig. 16I).

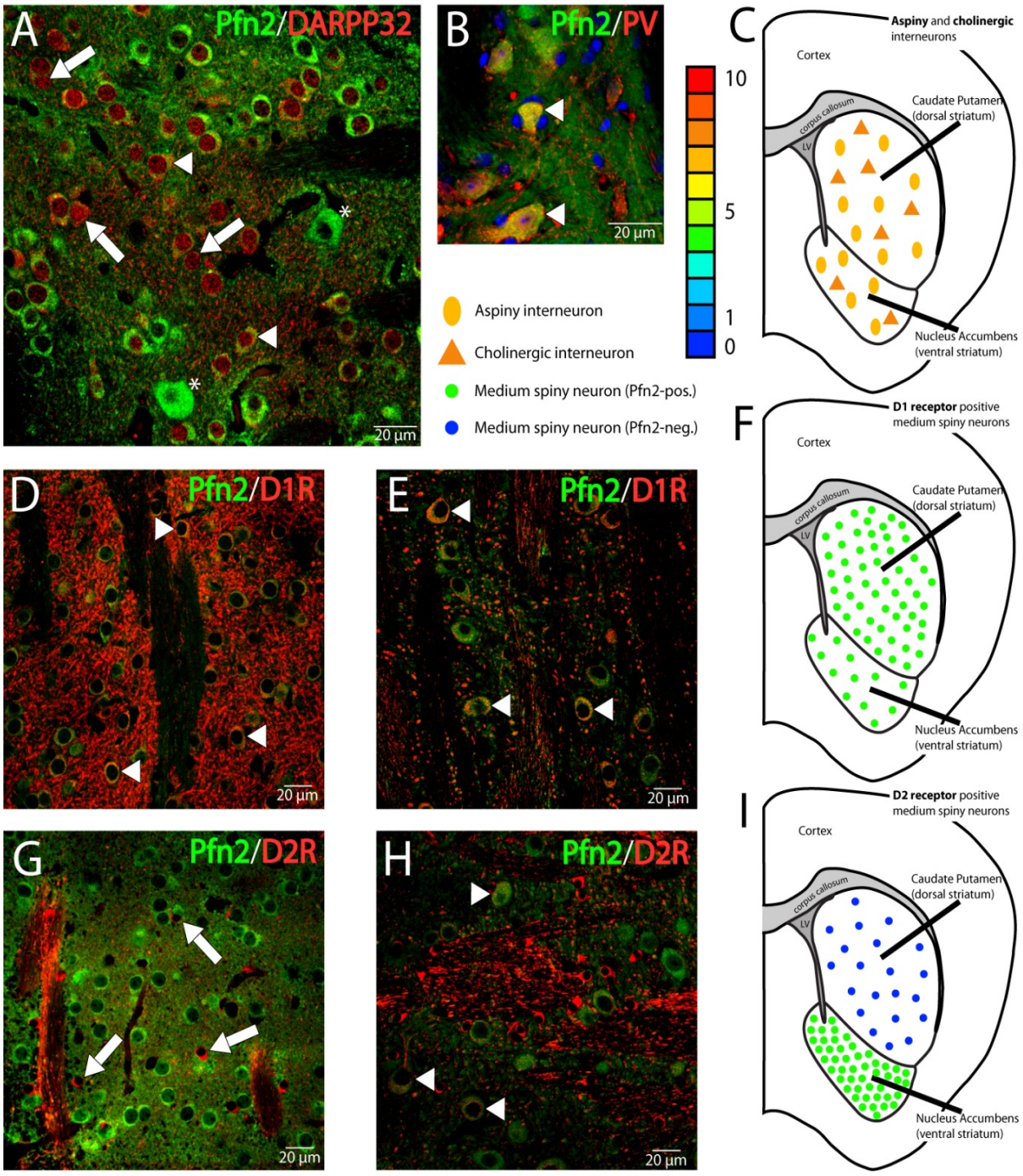
A
Pfn2/DARPP32
20 µm
B
Pfn2/PV
20 µm
Aspiny interneuron
Cholinergic interneuron
Medium spiny neuron (Pfn2-pos.)
Medium spiny neuron (Pfn2-neg.)
10
5
1
0
C
Aspiny and cholinergic interneurons
Cortex
corpus callosum
LV
Caudate Putamen (dorsal striatum)
Nucleus Accumbens (ventral striatum)
D
Pfn2/D1R
20 µm
E
Pfn2/D1R
20 µm
F
D1 receptor positive medium spiny neurons
Cortex
corpus callosum
LV
Caudate Putamen (dorsal striatum)
Nucleus Accumbens (ventral striatum)
G
Pfn2/D2R
20 µm
H
Pfn2/D2R
20 µm
I
D2 receptor positive medium spiny neurons
Cortex
corpus callosum
LV
Caudate Putamen (dorsal striatum)
Nucleus Accumbens (ventral striatum)

In addition, some astrocytes were positive for D2R, which are lacking Pfn2 (the very small cells in Fig. 16H, see 2.1.4 and Fig. 19). The control slices from wildtype animals showed only DARPP32, PV, D1R or D2R signals respectively (Supp. Fig. 7) and control stainings using only the respective secondary antibodies yielded no specific signal (Supp. Fig. 11).

The striatum is the only brain region featuring a high density of Pfn2-positive GABAergic neurons with both medium spiny neurons and aspiny interneurons expressing Pfn2 with the very specific exception of dopamine D2 receptor-positive MSNs in the dorsal striatum (Fig. 17, compare Fig. 21).

Fig. 16 GABAergic neurons of the striatum express Pfn2 depending on subtype and area

(**A**) Pfn2 (green) is expressed in most medium spiny neurons (arrowheads), identified by the expression of DARPP32 (red), but seems to be missing from a certain subpopulation (arrows). Also few large neurons, which are not labelled by DARPP32, express Pfn2 (asterisks). (**B**) GABAergic aspiny interneurons, identified by their expression of parvalbumin (PV, red), show a high Pfn2 expression (arrowheads). (**C**) Color-coded scheme depicting the expression of Pfn2 in aspiny and cholinergic interneurons (see 2.1.1.5, Fig. 14I). $D1R^+$-MSNs (red) in both (**D**) dorsal and (**E**) ventral striatum express medium levels of Pfn2. (**F**) Schematic overview of the D1R-expressing MSNs of the striatum with color-coded expression level of Pfn2. (**G**) $D2R^+$-MSNs (red) of the caudate putamen are negative for Pfn2 (arrows), but (**H**) $D2R^+$-MSNs of the nucleus accumbens show low expression of Pfn2 (arrowheads). (**I**) Schematic representation of the color-coded distribution of Pfn2-positive and -negative $D2R^+$-MSNs in the striatum according to the expression level of Pfn2. To visualize the cell nuclei (blue), the DNA-intercalating dye Draq5 (Biostatus) was used.

Region	Cell type	Marker	Localization
Cortex	Cajal-Retzius cells (GABAergic subtypes)	Reelin	Layer I
	Chandelier cells (axo-axonic neurons)	PV, GAT1	Layer III-V
	Basket cells	PV, Substance P	
	Bitufted neurons (Double Bouquet cells in humans)	CB, CR	Layer II-III (V)
	Neurogliaform cells/ spiderweb cells	NPY, Reelin, 5HT3aR	Layer I
Hippocampus	Chandelier cells (axo-axonic neurons)	PV	Stratum oriens + pyramidale
	Basket cells	PV, Substance P	Stratum oriens + pyramidale
	Bistratified neurons	PV	Stratum oriens + pyramidale
	Ivy cells	NPY, GABA	Stratum pyramidale
	Oriens-lacunosum-moleculare (O-LM) interneurons	PV	Stratum oriens
	Stratum oriens interneurons	CB	Stratum oriens
Cerebellum	Basket cells	PV, (CB)	Molecular layer
	Golgi cells	CB	Granular layer
	Purkinje cells	PV, CB	Purkinje cell layer
	Stellate cells	PV	Molecular layer
Striatum	Aspiny interneurons	PV	
	D1 medium spiny neurons	Dopamine D1 Receptor	
	D2 medium spiny neurons	Dopamine D2 Receptor	Dorsal str. neg.; Ventral str. pos.
Olfactory bulb	Olfactory granular neurons	GABA	Granular layer
	Periglomerular cells	CB	Glomerular layer
	Short axon cells (GABA+/ TH-)	GABA	Glomerular layer
	Short axon cells (GABA+/ TH+)	GABA + TH	Glomerular layer
	Short axon cells (GABA-/ TH+)	TH	Glomerular layer

Fig. 17 Overview of the different subtypes of GABAergic neurons in key regions of the mouse brain

The expression pattern of Pfn2 in GABAergic neurons is restricted to specific cell types. Cell types are identified here by their specific marker proteins as well as their localization within the respective system. Some Pfn2-positive (green) GABAergic cell types were present in these systems, while the majority of cells were found to be Pfn2-negative (red).

2.1.3 Sensory systems show a specific expression profile of Pfn2

Sensory systems in general mediate the transition of stimuli from the environment to synaptic signaling in the brain. One highly organized structure of the brain is the olfactory bulb (OB) (see 1.4.1.2, Fig. 10), which is relaying input from the olfactory receptor neurons located in the nasal epithelium, sending sensory output to the cortex (Cave and Baker, 2009). None of the neurons of the olfactory system are known to have distinctive marker proteins, but can easily be identified by their location in the different layers of the olfactory bulb (see 1.4.1.2, Fig. 10) as well as by their morphology and their differential expression of the neurotransmitters glutamate, dopamine and GABA. Mitral cells and external tufted cells (ETCs) have large cell bodies with extensive and long dendrites directed towards the glomerular layer, while their axons travel out of the OB. These cells are glutamatergic and especially Mitral cells are known to be one of the few neuron types missing the nuclear neuronal protein NeuN. Periglomerular neurons are purely GABAergic, while short axon cells (SACs) co-express dopamine together with GABA, therefore are reactive to the rate-limiting enzyme in the dopamine synthesis machinery, tyrosine hydroxylase (TH, see 2.1.1.2).

Most neurons involved in sensory processing in the OB expressed Pfn2. Especially Mitral cells and external tufted cells showed extremely high levels of Pfn2, and in fact are, together with hippocampal CA2 pyramidal neurons, the highest Pfn2-expressing cells in the brain (Fig. 18A, schematized in Fig. 18B). Also GABAergic granule neurons expressed Pfn2, although at low levels (data not shown, schematized in Fig. 18B). Neurons surrounding the glomeruli differed in their expression of Pfn2. Large external tufted cells were found also in this layer to be very enriched in Pfn2, while medium-sized purely GABAergic periglomerular neurons lacked the expression of Pfn2 (Fig. 18C, schematized in Fig. 18B). The most interesting population of neurons around the glomeruli are the small short axon cells.
SACs seemed to differ in their expression level of Pfn2 depending on the different expression profiles of either dopamine, GABA or the co-expression of both neurotransmitters (Fig. 18C, D, schematized in Fig. 18B). SACs producing predominantly GABA showed low levels of Pfn2 (Fig. 18C, asterisks, schematized in

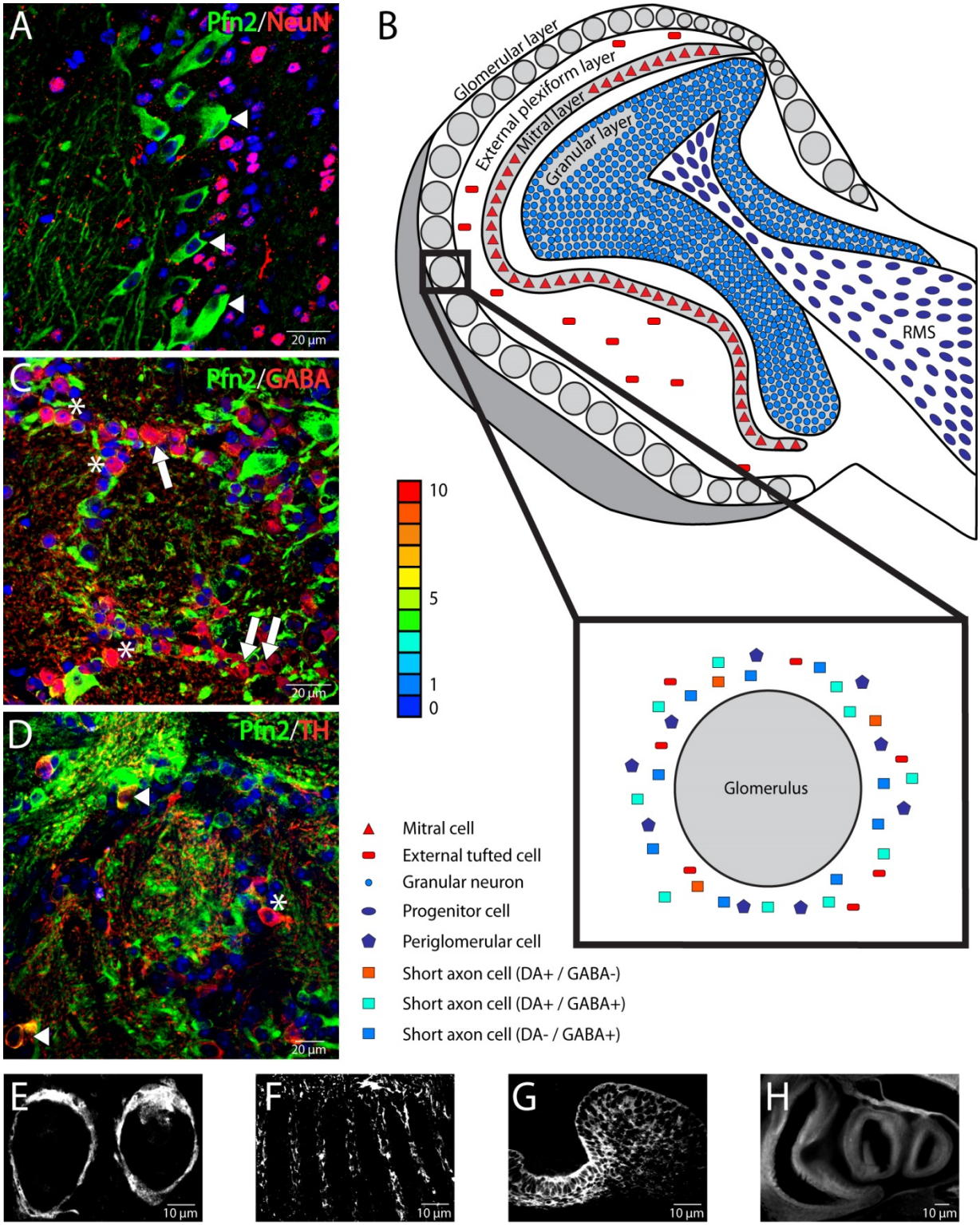
A
Pfn2/NeuN
20 µm
C
Pfn2/GABA
20 µm
D
Pfn2/TH
20 µm
B
Glomerular layer
External plexiform layer
Mitral layer
Granular layer
RMS
10
5
1
0
Glomerulus
Mitral cell
External tufted cell
Granular neuron
Progenitor cell
Periglomerular cell
Short axon cell (DA+ / GABA-)
Short axon cell (DA+ / GABA+)
Short axon cell (DA- / GABA+)
E
10 µm
F
10 µm
G
10 µm
H
10 µm

Fig. 18B), while the expression level of Pfn2 was increased upon co-expression of dopamine in those cells (Fig. 18D, asterisks, schematized in Fig. 18B). Finally, SACs predominantly expressing dopamine were strongly positive for Pfn2 (Fig. 18D, arrowheads, schematized in Fig. 18B).

The olfactory bulb is not the only sensory system, in which Pfn2 plays a certain role. In the developing embryo (E13.5-E19.5) Pfn2 could be found at sensory areas of the whiskers (Fig. 18E), the tongue (Fig. 18F), the teeth (Fig. 18G) and the nasal cavity (Fig. 18H).
The control stainings of wildtype sections showed only NeuN, GABA or TH signals respectively (Supp. Fig. 8) and control stainings using only the respective secondary antibodies yielded no specific signal (Supp. Fig. 11).

Fig. 18 The expression profile of Pfn2 in the olfactory sensory systems of the mouse
Pfn2 is very specifically expressed in the sensory system of the olfactory bulb. (**A**) Mitral cells (devoid of NeuN, red) are highly enriched for Pfn2 (green, arrowheads). (**B**) Schematic overview of the olfactory system with the color-coded expression level of Pfn2 in the various cell types. In the inset, a magnification of a glomerulus and the surrounding neuron types is shown. (**C**) GABAergic periglomerular neurons (red, arrows) are devoid of Pfn2, while short axon cells (SAC, red, asterisks) show low expression of Pfn2. (**D**) GABAergic SACs co-expressing dopamine (TH, red, asterisk) express Pfn2 at moderately higher levels than purely GABAergic SACs. SACs producing mainly dopamine show high levels of Pfn2 (arrowheads). To visualize the cell nuclei (blue), the DNA-intercalating dye Draq5 (Biostatus) was used. Sensory receptor neurons in different regions of the developing embryo (E16.5-E19.5) also show an enrichment of Pfn2, such as (**E**) the whisker pads, (**F**) the tongue, (**G**) the incisor teeth and (**H**) the nasal epithelium.

2.1.4 Glial cells are devoid of Pfn2

Glial cells are the most abundant cell types in the brain and are involved in nearly all higher brain functions and take part in neuronal networks (see 1.4.2, Fig. 8). The CNS of the mouse (and humans) comprises four major types of glial cells. A recent study reported a role for Pfn2 in morphology and spreading of cultured mouse astrocytes (Schweinhuber et al., 2015), furthermore neurological disorders often feature phenotypes associated with a role of glial cells, therefore the expression profile of Pfn2 in these cells was investigated in this thesis.

Astrocytes are the most abundant type of glial cells, responsible for providing neurons with neurotrophic and neuroprotective factors, structural support and also feature neuromodulatory functions (see 1.4.2, Fig. 8) (Hol and Pekny, 2015; Nedergaard and Verkhratsky, 2012; Rossi and Volterra, 2009; Sofroniew and Vinters, 2010; Zeidán-Chuliá et al., 2014). Astrocytes are also invading lesion sites during brain repair forming complex barriers called glial scars.

A common astrocytic marker is glial fibrillary acidic protein (GFAP), an intermediate filament protein involved in cell-cell communication, mitosis and glial scarring (Hol and Pekny, 2015). GFAP is expressed typically in astrocyte precursor cells and in reactive astrocytes e.g. during invasion of a lesion site (15-20% of astrocytes in the healthy adult brain). To be able to localize Pfn2 in all (reactive and dormant) astrocytes, also the Ca^{2+}-binding protein S100β was used as marker protein (Donato et al., 2013; Sofroniew and Vinters, 2010). S100β is involved in Ca^{2+}-homeostasis, especially enhancing migration and proliferation while suppressing apoptosis and differentiation processes (Donato et al., 2013).
Pfn2 was absent from GFAP-positive, reactive astrocytes (Fig. 19A) as well as S100β-positive, reactive and dormant, astrocytes (Fig. 19B) in all brain regions. A morphologically distinct type of astrocytes are the Bergmann glia of the cerebellar Purkinje cell layer, which were also observed to be devoid of Pfn2 (data not shown).

The brain is a fragile system and its blood supply separated from the rest of the body by the blood-brain-barrier, therefore it needs to be protected from infections and toxic material by brain specific immune cells called microglia (see 1.4.2, Fig. 8). Microglia are actively scanning the surrounding tissue for pathogens, cell debris and apoptotic neurons, which are consequently phagocytosed (Beutner et al., 2010; Salter and Beggs, 2014; Zhan et al., 2014).

Microglia get activated upon brain lesions by infections or trauma and migrate to the lesion site, proliferate and remove toxic material. During brain development, these cells are major regulators of synaptic maturation and pruning of excessive synapses (Salter and Beggs, 2014; Zhan et al., 2014). To label specifically microglia, the marker protein Iba1 (ionized Ca^{2+}-binding adaptor molecule 1) was used (Beutner et al., 2010; Zhan et al., 2014). Iba1 is an actin-binding protein upregulated during proliferation and migration of microglia when induced by e.g. brain lesions.
Microglial cells lacked the expression of Pfn2 in the brain (Fig. 19C). In all brain areas these cells showed finely branched processes, which were devoid of Pfn2 as well.

Myelination of axons provided by oligodendrocytes (see 1.4.2, Fig. 8) leads to an immense increase in signal propagation velocity, which is impaired in diseases like multiple sclerosis and schizophrenia (Chen et al., 2007; Pedraza et al., 2008; Saher et al., 2005; Zeidán-Chuliá et al., 2014).
Oligodendrocytes were specifically labelled using the enzyme 2′,3′-cyclic nucleotide 3′-phosphodiesterase (CNPase) and the myelin basic protein (MBP) as markers. The loss of the myelin-sheath associated protein MBP alters the myelin architecture and leads to axonal degeneration, while the loss of the CNPase enzyme has no effect on the ultrastructure of myelin-sheaths but induces axonal pathologies and neurodegeneration (Lappe-Siefke et al., 2003).
Like astrocytes, also oligodendrocytes were found throughout the brain with slightly varying densities for each brain region, but none of these cells could be observed to be expressing Pfn2 in neither the soma (Fig. 19D) nor the myelin-sheaths of their processes (Fig. 19E). Pfn2-positive axons could sometimes be seen at high magnification in close proximity to the myelin-sheath, but Pfn2 was absent from the oligodendrocytic processes.

NG2 cells are a distinct type of glial cells (also called synantocytes, polydendrocytes, GluR or complex cells) present in all brain regions and display an astrocyte-like appearance (see 1.4.2, Fig. 8). These cells are believed to be a type of oligodendrocyte precursor cell (OPC), especially active during re-myelination of brain lesions, but are also responsive for neuronal signaling (Bergles et al., 2010; Nishiyama et al., 2009; Zeidán-Chuliá et al., 2014).

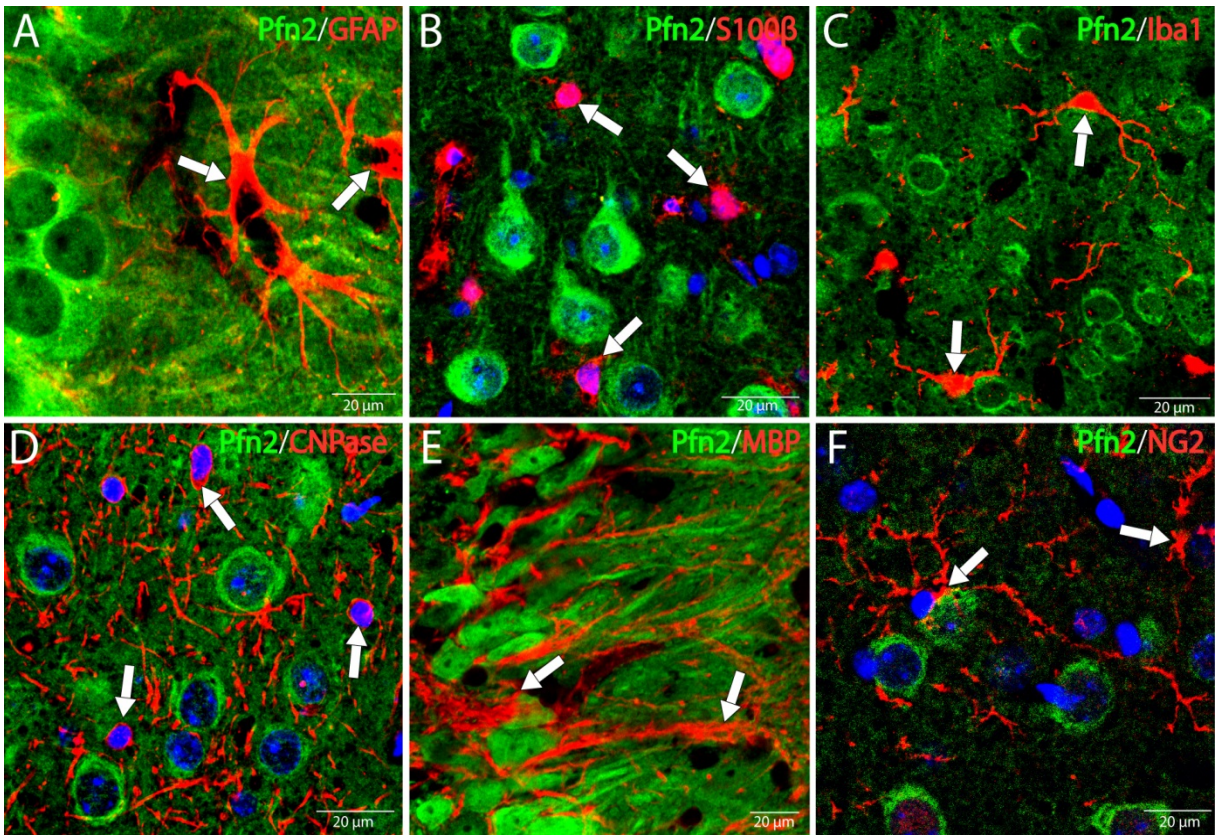

Fig. 19 All glial cell types are devoid of Pfn2

(**A**) GFAP-positive (red, arrows), activated astrocytes as well as (**B**) S100β-positive (red) astrocytes (active and resting cells, arrows) are negative for Pfn2 (green). (**C**) Microglia, specifically expressing the Ca^{2+}-binding protein Iba1 (red, arrows), also lack Pfn2. (**D**) Oligodendrocytes, exclusively producing the enzyme CNPase (red, arrows), lack expression of Pfn2 in both their cell bodies and (**E**) their myelin-sheath processes labelled with MBP (red, arrows). (**F**) NG2 cells, with their still enigmatic role in the brain, could be identified by the exclusive expression of the NG2 surface proteoglycan (red, arrows) and are negative for Pfn2. To visualize the cell nuclei (blue), the DNA-intercalating dye Draq5 (Biostatus) was used.

NG2 cells were identified by their specific expression of the membrane-associated chondroitin sulphate proteoglycan NG2 (Bergles et al., 2010; Nishiyama et al., 2009; Zeidán-Chuliá et al., 2014).
NG2 cells shared the absence of Pfn2 with the other glial cell types mentioned above (Fig. 19F). Numerous but relatively small cell bodies and their fine arborizations were observed at various densities in every brain region, nonetheless could never be colocalized with Pfn2 immunofluorescence.

The control stainings of wildtype littermates brain sections showed only GFAP, S100β, Iba1, CNPase, MBP or NG2 signals respectively (Supp. Fig. 9) and control stainings using only the respective secondary antibodies yielded no specific signal (Supp. Fig. 11).

In conclusion, Pfn2 was found to be absent from all types of glial cells throughout the entire brain structure (compare Supp. Fig. 12).

2.1.5 Differentiation-dependent expression of Pfn2 in neural stem cells

A class of cells in the embryonic and adult brain replenishing different populations of neurons and glial cells are the neural stem cells (see 1.4.4) (Altman, 1965). NSCs mostly proliferate in a state of self-renewal, but are also multipotent and therefore able to differentiate into progenitor cells and further into different types of neurons and glial cells (Sommer and Rao, 2002), after migrating to their final position in the neural networks.

Neurogenesis in general is frequently impaired in neurodegenerative disorders like Alzheimer´s or Parkinson´s disease, while neurogenesis is often increased in consequence to epileptic seizures, trauma or strokes (Di Cristo, 2007; Faux et al., 2012; Gage, 2000). Especially learning and memory formation might be impaired in consequence of gene mutations involving aNSCs (Aimone et al., 2011; Deng et al., 2010; Guo et al., 2011). Since ASD is a neurodevelopmental disorder with complex

phenotypes including epileptic seizures, in consequent to which any cells undergo apoptosis, potential alterations in the process of neuronal development and neurogenesis are a field of interest for investigations of the role of Pfn2 in embryonic and adult neural stem cells.

In order to specifically label neural stem cells in mouse embryonic tissue, selected transcription factors and intermediate filaments have been used as marker proteins, since they are present at very high concentration in this cell population compared to the remaining tissue. Adult neural stem cells (aNSCs) continue to express these transcription factors and intermediate filaments at higher levels compared to other cells. Certain intermediate filament proteins are expressed very specifically at high rates in NSCs, in particular Nestin, Vimentin and glial fibrillary acidic protein (GFAP) (Landgren and Curtis, 2011). Well known transcription factors are required in stem cells to maintain proliferation capacity and multipotency, among them especially Sox2, Oct4, Pax6 and Tbr2 are highly enriched in NSCs and/or in their derived progenitor cells (Beckervordersandforth et al., 2010; Gage, 2000; Ma et al., 2009; Maslov et al., 2004; Ming and Song, 2011; Sommer and Rao, 2002).

The expression pattern of Pfn2 among the neural stem cell populations was not uniform. Pfn2 expression was, in fact, found in NSCs but was missing from progenitor cells, before being expressed again in differentiated neurons (see 2.1.2 and 2.1.3), while all types of glial cells continued to repress Pfn2 after their final differentiation (see 2.1.4).
Radial glia cells (embryonic neural stem cells) expressed Pfn2 during later embryonic development (Fig. 20A) and adult neural stem cells (aNSCs) of the SVZ expressed Pfn2 (Fig. 20B, C, D). On the contrary, in consequence to their initial differentiation, progenitor cells changed their expression pattern and down-regulated Pfn2. Progenitor cells can be identified by the lack of the stem cell marker Nestin, but they continue to express the transcription factor Pax6 (Fig. 20C) (Beckervordersandforth et al., 2010; Ma et al., 2009; Ming and Song, 2011) and acquire the expression of the transcription factor Tbr2 (Fig. 20D).

The progenitor cells migrating along the RMS were also devoid of Pfn2 (Fig. 20E). Following their arrival at their destination, the olfactory bulb, progenitor cells undergo their final differentiation in order to replenish the pool of mature neurons, and at this step they started to re-express increasing amounts of Pfn2 (Fig. 20E, arrowheads). The expression of Pfn2 in aNSCs occured exclusively in the SVZ, whereas aNSCs of the hippocampal SGZ, distinguishable by the presence of Oct4, showed a lack of expression of Pfn2 (Fig. 20F).

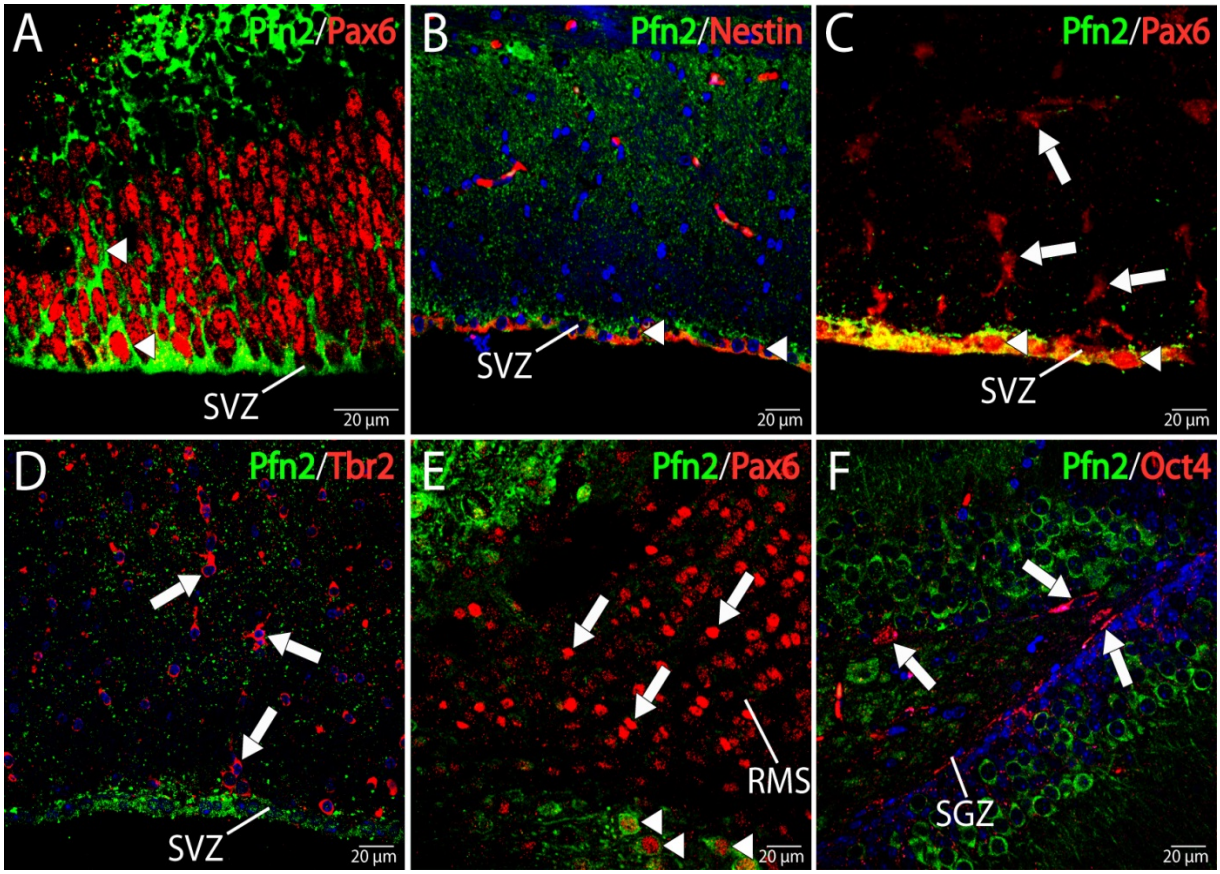

Fig. 20 Neural precursor cells express Pfn2 depending on their differentiation state

(**A**) Pfn2 (green) is present in neural stem cells (NSCs, radial glia) of the embryo (Pax6, red, arrowheads). (**B**) Pfn2 is still expressed in adult NSCs of the subventricular zone (SVZ) identified by the high expression levels of Nestin (red, arrowheads) and (**C**) the transcription factor Pax6 (red, arrowheads). NSC-derived progenitor cells, positive for the transcription factors (**C**) Pax6 and (**D**) Tbr2 (red), do not express Pfn2 (arrows). (**E**) The Pfn2-negative progenitor cells migrate along the rostral migratory stream (RMS, arrows) and up-regulate Pfn2 upon reaching the border of the olfactory bulb and differentiating into neurons (arrowheads). (**F**) Adult NSCs of the subgranular zone (SGZ) located in the hippocampal dentate gyrus, labelled by the transcription factor Oct4 (red), do not show expression of Pfn2 (arrows). To visualize the cell nuclei (blue), the DNA-intercalating dye Draq5 (Biostatus) was used.

The control stainings of wildtype littermates showed only Nestin, Oct4 or Pax6 signals respectively (Supp. Fig. 10) and control stainings using only the respective secondary antibodies yielded no specific signal (Supp. Fig. 11).

In conclusion, the expression of Pfn2 in neural stem cells (NSCs) was found to be dependent on the developmental and differentiation state of the respective cell population (compare Supp. Fig. 12). Pfn2 was expressed in embryonic and adult neural stem cells of the SVZ, but was lacking from progenitor cells, with renewed up-regulation in differentiated neurons (compare Fig. 21). In mature glial cells, instead, Pfn2 continued to be repressed.

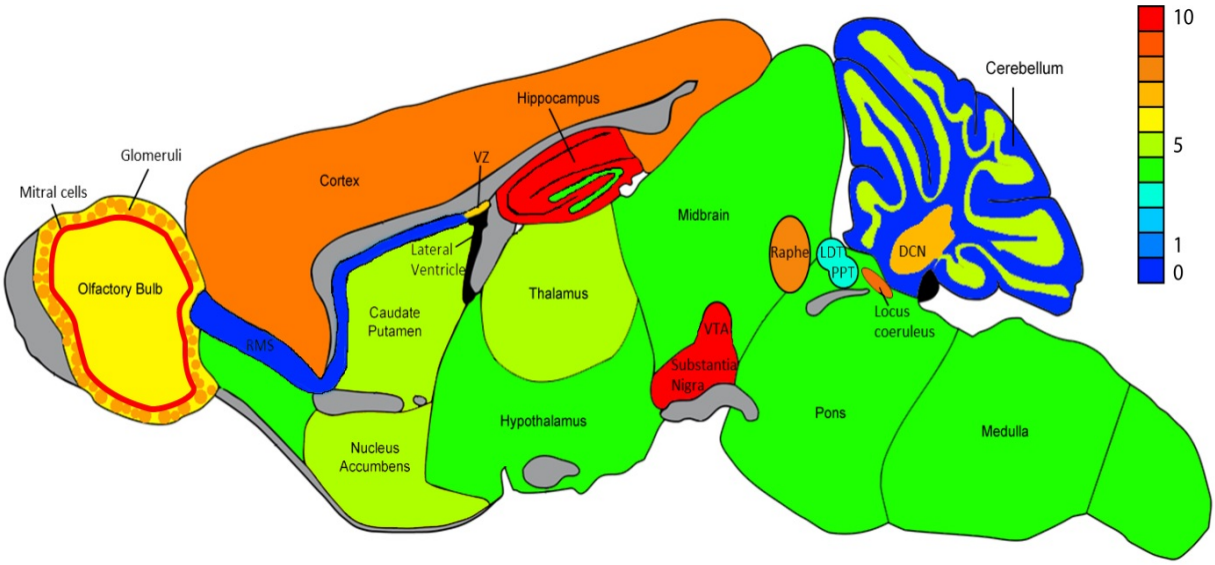

Fig. 21 Schematic overview of the relative expression levels of Pfn2 in the mouse brain

Pfn2 is present in neurons of most regions of the brain with various levels of expression and the exception of progenitor cells along the RMS, Purkinje and many other GABAergic cells of the cerebellar molecular layer and the D2 receptor-positive cells of the caudate putamen.

The regions with the highest expression of Pfn2 are hippocampus, substantia nigra, VTA and the Mitral cell layer of the olfactory bulb. Glial cells lack the expression of Pfn2, therefore they are not included into this schematic representation. A detailed description of each neuronal system with the corresponding regions can be found in the previous chapters (see 2.1.1-2.1.5).

The astonishing specificity of the expression profile of Pfn2 not only across neuronal systems but also, within the same neuronal system, between different brain regions is shown in a color-code corresponding to the relative intensity of the expression level of Pfn2 (Fig. 20). Since glial cells were shown to be devoid of Pfn2 in the adult brain

(see 2.1.4, Fig. 19), only the expression pattern of Pfn2 in neuronal cells is depicted. Hippocampal CA2 pyramidal neurons, olfactory Mitral cells as well as dopaminergic neurons express the highest levels of Pfn2 in the brain (see 2.1.1.1, Fig. 14A, B, D, E and 2.1.3, Fig. 18A, B) and were therefore set as the maximum intensity value (Fig. 21, relative intensity 10/10, shown in red).

2.2 Analysis of the biochemical properties and the expression level of the P2-GFP fusion protein in the knock-in mouse model

The P2-GFP knock-in mouse model besides being useful to study Pfn2 expression patterns, as described in the previous chapters, was designed to be able to follow Pfn2 dynamics and trafficking *in vivo*. Live-cell imaging can be employed to study P2-GFP during *in vitro* neuronal development and in mature neurons following depolarization or neurotransmitter stimulation. In order to employ the mouse model for these purposes, the biochemical properties of the P2-GFP fusion protein needed to be verified as well as the effect of the fusion protein in the mouse itself by behavioral phenotyping.

P2-GFP KI mice are viable in homozygosity and show mild behavioral alterations compared to wildtype mice. Several behavioral paradigms were applied, resulting in moderate impairments, such as minor hyperexcitability and increase in exploration and locomotion in a novel environment. In contrast to the extensively behaviorally impaired Pfn2 KO mouse model, showing autistic-like behavior, P2-GFP KI mice showed no alterations in anxiety or fear as well as unimpaired working memory (Özer, unpublished).

At least two parameters could be the cause of these alterations: the expression level of the recombinant fusion protein could differ substantially from the levels of the endogenous protein, or the biochemical interactions of the fusion protein with its ligands could be impaired by the GFP-tag. These two causes of possible alterations in the P2-GFP KI mouse model due to the insertion of GFP were investigated in detail during this study.

2.2.1 The GFP-tag affects the recognition of P2-GFP by anti-Pfn2 antibodies

The first issue encountered with the P2-GFP mouse model was that the P2-GFP expressed in the homozygous mouse brain could not be quantified directly from tissue lysates using the standard polyclonal anti-Pfn2 antibody routinely employed in our group to study Pfn2, since the P2-GFP fusion protein was not recognized at all (data not shown). The possible reason might be that the GFP moiety fused to the C-terminal of Pfn2 could be hindering (sterically) the C-terminal epitope(s) necessary for antibody recognition. Nevertheless, several different polyclonal and monoclonal anti-Pfn2 antibodies have been produced in the past in our lab, using peptides or truncated versions of Pfn2. Therefore the various anti-Pfn2 antibodies were tested on P2-GFP in order to determine their efficiency in the recognition of P2-GFP compared to the wt protein in Western blot assays to be able to choose the most suitable one for future experiments on the P2-GFP KI mouse model.

The different anti-Pfn2 antibodies (see 5.7 and Supp Fig. 13) were validated to interact with P2-GFP using recombinant versions of the respective profilin isoforms. The cDNAs coding for Pfn2 and P2-GFP, as well as Pfn1 as a control, were inserted in a bacterial expression vector (pMW172-Streptag) in order to obtain the respective proteins fused C-terminally to a Strep-tag (see 4.1.7, 4.2.10-4.2.11, 5.6). The Strep-tag is an eight amino acid long sequence (WSHPQFEK), originally found on biotin, but artificially altered to increase the specificity and affinity towards Streptavidin, a protein found in *Streptomyces avidinii*, or the improved StrepTactin protein. The Strep-tag is small (app. 1 kDa) and with relatively low charge compared to other common tags that can be fused to recombinant proteins (e.g. His-tag, HA-tag, FLAG-tag, myc-tag, GST-tag) therefore we reasoned that it should not interfere substantially with Pfn2 antibody recognition. The elution of purified Strep-tagged proteins from an affinity matrix can be accomplished by the addition of biotin derivates (d-desthiobiotin) without the need for denaturing agents and is therefore ideal to produce functional recombinant proteins.

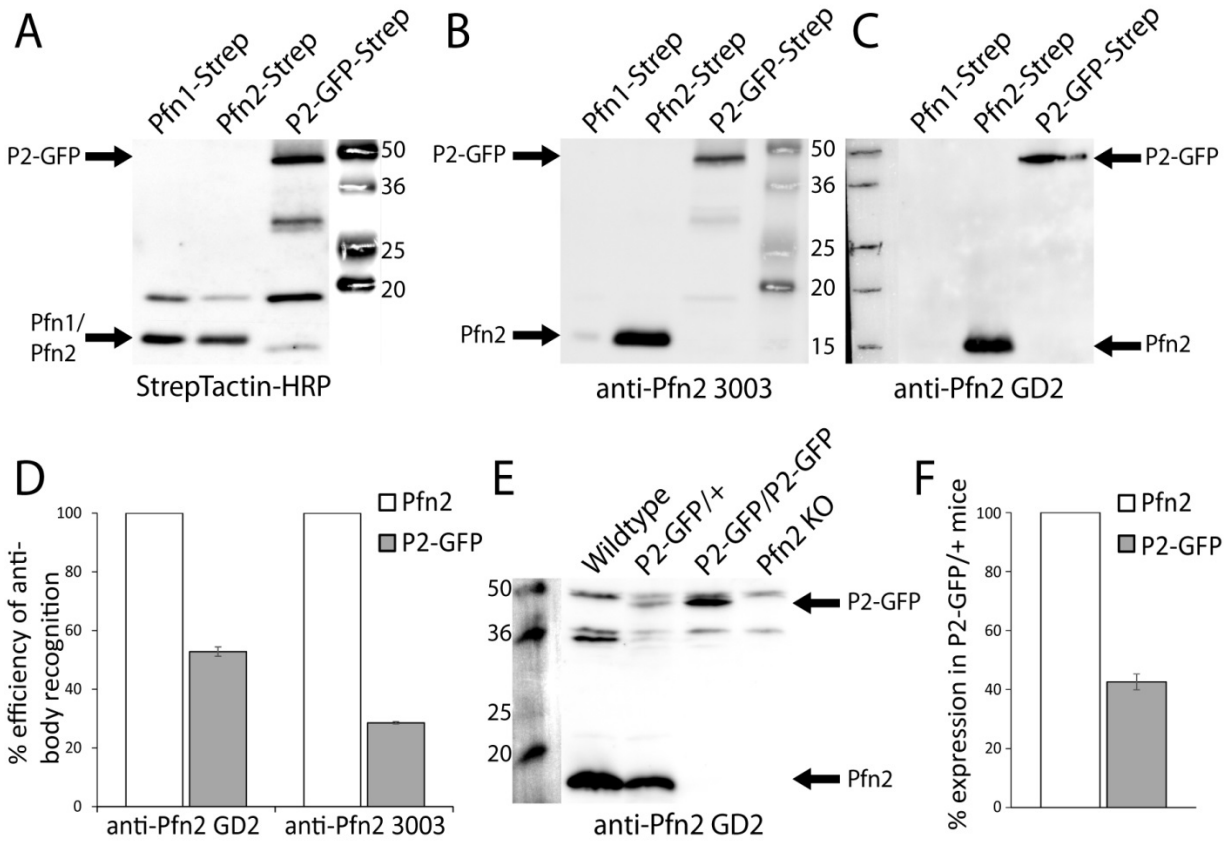

Fig. 22 Antibody recognition assay and expression level of P2-GFP compared to Pfn2

(**A**) Purified Pfn1-Strep, Pfn2-Strep (both app. 15 kDa) and P2-GFP-Strep (app. 42 kDa) were loaded on a Western blot in estimated equal amounts and probed with the StrepTactin-HRP reagent to control for loading errors. The same Western blots were incubated with (**B**) anti-Pfn2 3003 or (**C**) anti-Pfn2 GD2 antibodies to compare the recognition ratios of Pfn2 and P2-GFP. The antibody signals were quantified and calibrated according to the StrepTactin-HRP measured amount of the respective purified protein. (**D**) Binding efficiencies of the anti-Pfn2 antibodies GD2 (53% ± 1.6) and 3003 (29% ± 0.4) towards P2-GFP in comparison to Pfn2. (**E**) Brain tissue extracts from different genotypes were probed with the anti-Pfn2 GD2 antibody to be able to calculate (**F**) the expression level of P2-GFP compared to Pfn2 (43% ± 2.7 in heterozygous P2-GFP KI mice).

Pfn2-Strep and P2-GFP-Strep (as well as Pfn1-Strep as a control) were purified as recombinant fusion proteins from bacterial extracts and estimated equal amounts were loaded onto a polyacrylamide gel for Western blotting (see 4.2.4-4.2.5) (n=3 bacterial clones and purifications). The amount of the Strep-tagged proteins was calibrated using a StrepTactin-HRP conjugated reagent (Fig. 22A).

The signal intensity originated from the StrepTactin-HRP luminescence is directly proportional to the amount of purified protein loaded onto the respective lane. Upon

further incubation with an anti-Pfn2 antibody, the resulting signals could be adjusted for the exact amounts of purified proteins on the membrane.

The specificity and efficiency of binding to P2-GFP was calculated for 4 different anti-Pfn2 antibodies. These antibodies were partially characterized for the specificity towards Pfn2 in contrast to Pfn1 in Western blot and immunoprecipitation (the latter was tested only for certain antibodies) (Gareus et al., 2006). All 4 rabbit-derived antibodies could be shown to recognize specifically Pfn2 in Western blot experiments without also significantly labelling Pfn1.

Of these 4 antibodies produced in rabbit, one serum (anti-Pfn2 DB2) showed high unspecific background signals and was not included in further analysis (data not shown). P2-GFP could be detected with highly various efficiencies using the other three antibodies. In particular, the antibody sera 3003 and GD2 recognized P2-GFP (Fig. 22B, C), although the anti-Pfn2 3003 antibody showed a minor nonspecific recognition of Pfn1 (Fig. 22B). The fourth anti-Pfn2 rabbit serum (T2) did not significantly bind to P2-GFP (data not shown) and was therefore not used further for the analysis of P2-GFP.

The antibody binding efficiency to P2-GFP in comparison to Pfn2 was calculated for the rabbit antisera 3003 and GD2 (Fig. 22D). While the antiserum 3003 recognized P2-GFP with 29% ± 0.4% efficiency compared to Pfn2, the antiserum GD2 was the most efficient, recognizing P2-GFP with 53% ± 1.6% efficiency compared to Pfn2.

2.2.2 The expression of P2-GFP is reduced compared to Pfn2 in heterozygous knock-in mice

An often neglected consequence of mutations in genomic loci, such as the insertion of a GFP-tag in a gene, is a decrease of the expression level of the targeted gene product. The P2-GFP fusion protein expressing mouse model features certain mild behavioral abnormalities (Özer, unpublished), which could be explained by a decrease of the level of the GFP-tagged variant of Pfn2 or by a decreased functionality of the fusion protein. Based on the estimated antibody binding efficiency values (see 2.2.1), the anti-Pfn2 antiserum GD2 was chosen to probe brain tissue

lysates from several heterozygous P2-GFP KI mice by Western blot analysis in order to estimate the relative expression levels of Pfn2 and P2-GFP.
The anti-Pfn2 antibody GD2, as expected, was able to detect Pfn2 as well as P2-GFP on the Western blots (Fig. 22E). The signal intensities of three independent Western blots with different tissue lysates were quantified (Fig. 22F) and calibrated for the anti-Pfn2 GD2 recognition efficiency of P2-GFP. The expression level of P2-GFP was 2.4 times lower (43% ± 2.7%) than that of Pfn2 in heterozygous mice (G/+).

These results implicated a potential reason for the mild behavioral phenotype of homozygous P2-GFP KI mice, based on the reduced expression of the profilin 2 isoform in these mice.
While a reduced expression of the GFP fusion-protein is not ideal for the analysis of this mouse model, it is still highly enriched in nervous tissue. This expression level is higher than could have been expected based on previous experiences with KI mouse models using similar genetic targeting strategies. The P2-GFP KI mouse model can therefore be used further to study the role of Pfn2 in all its various facets.

2.2.3 P2-GFP shows slightly reduced binding affinity to poly-L-proline-stretches and G-actin

The binding properties of Pfn2 are well-defined (see 1.3) and were analyzed for the P2-GFP fusion protein to verify its functionality for future applications. The fusion of the GFP moiety to Pfn2 could potentially alter the binding properties of the P2-GFP fusion protein towards one or more of Pfn2 ligand types. The GFP-tag could interfere with the functionality of P2-GFP due to steric hindrance – the GFP-tag itself is bigger (27 kDa) than the target protein Pfn2 (14 kDa) – or due to the introduction of charged residues into the fusion protein.

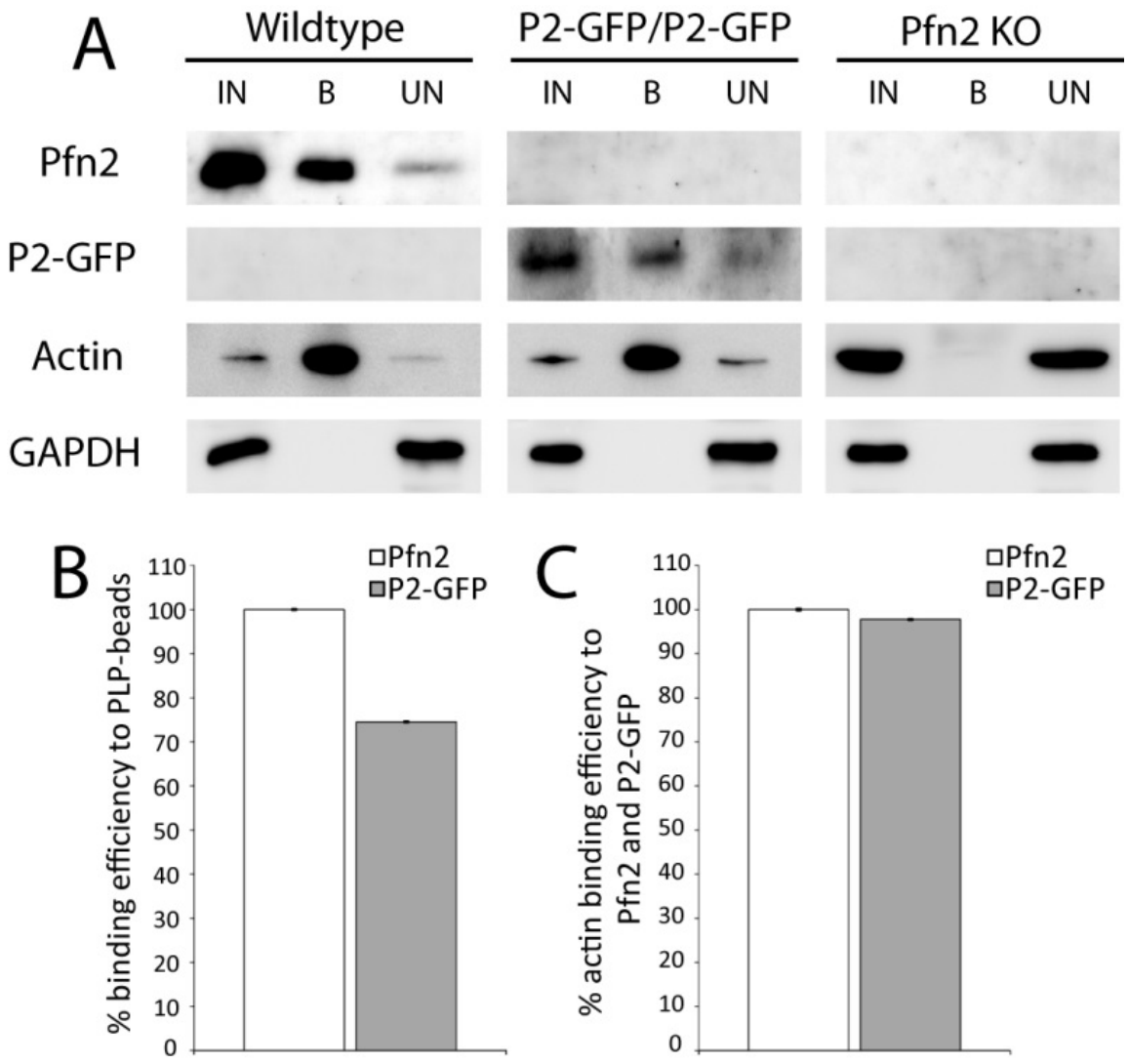

Fig. 23 The binding efficiency of P2-GFP fusion protein to poly-proline stretches but not to G-actin is reduced compared to Pfn2

(**A**) Pfn2 and P2-GFP were efficiently pulled down by PLP-beads from extracts prepared from brains of the respective animal lines, as shown by Western blot analysis (genotype indication on top). The Pfn2 KO control yielded no signals. Profilin-bound G-actin could be equally co-purified with Pfn2 and P2-GFP, but was only barely visible bound to Pfn1 in the Pfn2 KO control. GAPDH signals were used to calibrate the input and unbound fractions on the Western blot. (**B**) Quantification of the binding efficiency of P2-GFP in comparison to Pfn2 to poly-L-proline stretches, obtained by calculating the ratio of unbound/input signals (n=4 for wt, n=5 for G/G, n=3 for Pfn2 KO control) and normalizing it to the Pfn2 ratio. P2-GFP could bind to PLP-beads with an efficiency of 74.56% ± 0.08% compared to Pfn2. (**C**) Quantification of the G-actin binding efficiency calculated accordingly as before (n=6 for wt, n=4 for G/G, n=3 for Pfn2 KO control). The reduced amount of bound P2-GFP to the PLP beads (see in **B**) was taken into consideration in the calculation of the G-actin binding efficiency. G-actin binding was unimpaired (97.81% ± 0.0022%) by the P2-GFP fusion protein.

IN = input fraction, B = bound fraction, UN= unbound fraction. Error bars represent S.E.M.

To quantify the binding properties of P2-GFP in comparison to Pfn2, a pull-down assay using stretches (≥300 residues) of poly-L-proline (PLP) immobilized on sepharose beads (see 4.2.12) was performed on brain lysates of different mouse lines (wt, G/G and Pfn2 KO). This assay is known to precipitate quantitative amounts of Pfn1 and Pfn2 (Janmey, 1991) together with profilin-bound G-actin (see 4.2.13). The brain extracts (input fractions) were incubated with the PLP-beads and both bound and unbound fractions were separated. The purified fractions were analyzed by Western blot to determine the respective ratio of unbound vs. input Pfn2 and P2-GFP to see the depletion efficiency of the respective profilin isoform using the PLP pull-down approach.

The binding efficiency is defined as the unbound/input ratio of the two profilin2 isoforms to PLP. Several independent mouse brain lysates were prepared for each genotype (n=4 for wt, n=5 for G/G and n=3 for Pfn2 KO as a control) and the mean binding efficiency ratios of Pfn2 and P2-GFP to PLP were compared using specific antibodies (anti-Pfn2 GD2).

Pfn2 as well as P2-GFP could be enriched in the PLP pull-down, but with slightly different efficiencies (app. 70% of Pfn2 could be depleted from the input, while the depletion of P2-GFP was 25% less efficient), while the control extracts from Pfn2 KO mice, as expected, yielded no profilin signals (Fig. 23A). The pull-down efficiency of P2-GFP with PLP-stretches was 75% (74.56% ± 0.08%) of Pfn2 (Fig. 23B). The binding capacity of P2-GFP to poly-L-proline stretches *in vitro* is therefore diminished to a certain degree.

Also profilin-bound G-actin was purified with this approach. The amount of G-actin bound to Pfn1, which can be observed in the Pfn2 KO control (Fig. 23A), can be neglected compared to the amount of G-actin bound to the much higher expressed Pfn2 and P2-GFP. The binding efficiency of G-actin to P2-GFP compared to Pfn2 was calculated similarly using a specific antibody (anti-actin, clone C4, Merck Millipore). In contrast to the reduced binding efficiency of P2-GFP to poly-L-proline stretches, co-purified G-actin was found to be equally enriched in P2-GFP complexes compared to Pfn2 complexes (n=6 for wt, n=4 for G/G and n=3 for Pfn2 KO as a control) (Fig. 23A). Comparing the mean unbound/input ratios of G-actin for wt and P2-GFP KI mouse extracts and taking into account the reduced affinity of P2-GFP to

the poly-L-proline beads, a binding efficiency of 98% (97.81% ± 0.0022%) of P2-GFP to G-actin was observed (Fig. 23C).
In order to control for the amount of proteins in the input and unbound fractions, the signals for the "housekeeping" gene GAPDH (glyceraldehyde 3-phosphate dehydrogenase) were used to calibrate the corresponding signals of the input and unbound fractions (Fig. 23A). The presence of Pfn1 and endophilin 1 in the bound fractions of the PLP pull-down was also observed, as expected, verifying the validity of the pull-down approach (data not shown).

Both the expression level (see 2.2.2) and the binding capacity of the P2-GFP fusion protein towards poly-L-proline stretches are reduced. But the interference of the GFP-tag is relatively mild in comparison to other GFP fusion proteins that often completely lack binding capabilities. On the other hand, the GFP-tag is not interfering with the actin-binding capability of P2-GFP. The P2-GFP fusion protein can therefore be used with minor limitations in future *in vivo* studies.

2.2.4 Binding of proline-rich ligands by P2-GFP is not significantly impaired compared to Pfn2

The reduced affinity of P2-GFP for poly-L-proline stretches (see 2.2.3, Fig. 23) could imply a loss of interaction with specific ligands *in vivo*, since Pfn2 is known to bind to a large variety of different proteins involved in a vast array of cellular functions and pathways (Gareus et al., 2006; Witke, 2004; Witke et al., 1998). A loss of binding affinity to specific ligands due to the integration of the GFP moiety in Pfn2 could cause a potential impairment of certain molecular mechanisms in the cells. To unravel the potential impact of the P2-GFP fusion protein on specific Pfn2 functions, the ligand-binding properties of P2-GFP compared to Pfn2 were investigated by an immunoprecipitation (IP) assay (see 4.2.14) on brain tissue extracts.

A common method for the analysis of the composition of protein complexes under physiological conditions is the enrichment of specific ligands of a protein of interest by immunoprecipitation. The co-immunoprecipitated binding partners and their

interaction with either the endogenous Pfn2 or the P2-GFP fusion protein were investigated by Western blot analysis. Specific antibodies against Pfn2 (anti-Pfn2 2T), P2-GFP (anti-GFP-coupled beads; GFP-Trap A, Chromotek) or against both isoforms (anti-Pfn2 GD2; anti-Pfn2 5A7 monoclonal, see also Supp. Fig. 13) were incubated with brain tissue lysates from wildtype and homozygous P2-GFP KI (G/G) animals as well as lysates from Pfn2 KO mice as negative control. Bound protein complexes were precipitated using proteinA- or proteinG-coupled sepharose beads depending on the respective type of immunoglobulin from the host species (see 4.2.14). Each IP that was performed with the same antibodies yielded very similar and comparable results, therefore different IPs for each of the respective genotype are shown compiled together in Fig. 24. Control lysates from Pfn2 KO animals were used to verify the specificity of the antibody as well as the proteinA/G-beads.
Pfn2 is best known for its interaction with G-actin (Carlsson et al., 1977), the components of the WAVE complex (Witke, 2004; Witke et al., 1998), proteins of the formin family (Evangelista et al., 1997; Faix and Grosse, 2006; Imamura et al., 1997) and several proteins involving synaptic function (Gareus et al., 2006; Mammoto et al., 1998; Murk et al., 2012; Witke et al., 1998). Therefore, a selection of these protein ligands of Pfn2 was analyzed by Western blot analyses (Fig. 24).

Pfn2 and P2-GFP could be successfully immunoprecipitated, although with different efficiencies. The P2-GFP IP using the GFP-Trap beads was particularly efficient and yielded highly enriched fractions of P2-GFP complexes (Fig. 24A). Control IPs from Pfn2 KO extracts yielded no unspecific signals, confirming the high specificity of the respective IPs. Both Pfn2 as well as P2-GFP were found to be able to interact with the expected groups of protein ligands with variable affinities.
The most well-known ligand of Pfn2 is G-actin (see 1.3), which could be found enriched in Pfn2 as well as P2-GFP complexes (Fig. 24B). As expected based on the previous observations using PLP-beads in a pull-down assay (see 2.2.3), actin monomers were found in similar amounts in Pfn2- and P2-GFP-bound fractions, relatively to the amount of immunoprecipitated Pfn2 or P2-GFP.

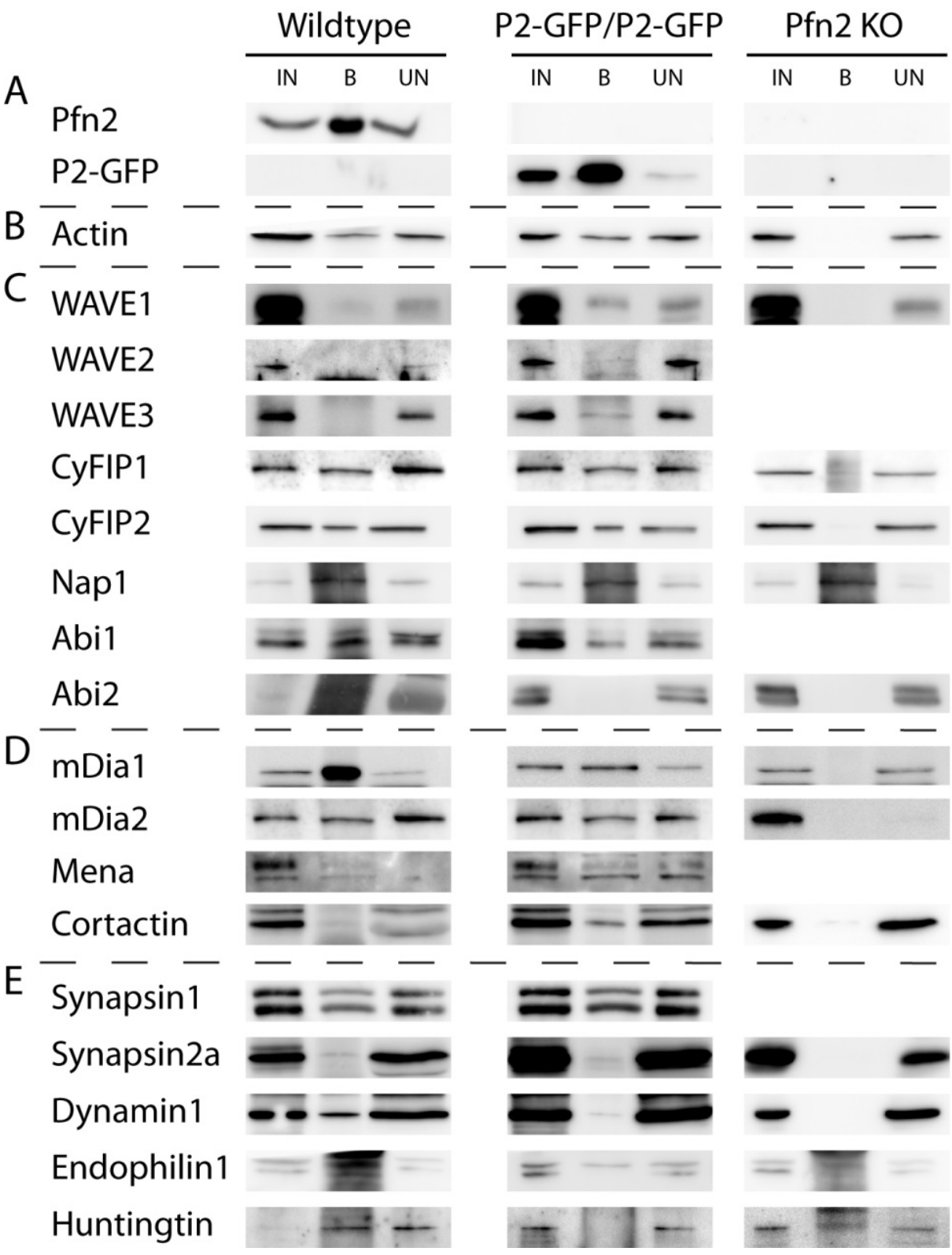
Wildtype
P2-GFP/P2-GFP
Pfn2 KO
IN
B
UN
A
Pfn2
P2-GFP
B
Actin
C
WAVE1
WAVE2
WAVE3
CyFIP1
CyFIP2
Nap1
Abi1
Abi2
D
mDia1
mDia2
Mena
Cortactin
E
Synapsin1
Synapsin2a
Dynamin1
Endophilin1
Huntingtin

A regulator of actin polymerization through its role as a nucleation promoting factor (NPF), acting on the Arp2/3 complex, is the WAVE complex, which is also a well-documented ligand of Pfn2 (see 1.2.1)
(Chen et al., 2014, 2010; Stradal and Scita, 2006; Witke, 2004; Witke et al., 1998). Every analyzed component of the heteropentameric WAVE complex could be found associated with both Pfn2 as well as P2-GFP (Fig. 24C).
While all three isoforms of WAVE (WAVE 1-3) were present in complexes bound to P2-GFP, the corresponding Pfn2 bound fractions appeared less enriched in WAVE proteins, but this is likely due to the lower efficiency of the Pfn2 IP compared to the GFP-Trap IP. Pfn2, in fact, was detected in the corresponding bound fractions of reciprocal IPs of each of the three WAVE isoforms 1-3 (data not shown). Each WAVE protein co-immunoprecipitated Pfn2, whereas a particularly high amount of Pfn2 could be found in WAVE3 complexes.
The interaction of CyFIP1+2 could be shown as well, very efficient with both Pfn2 and P2-GFP (Fig. 24C). CyFIPs (in particular CyFIP1) are believed to feature also actin-independent functions, i.e. in translational regulation for spine development and stabilization associated with the hereditary mental retardation Fragile-X-syndrome (FXS) (Napoli et al., 2008; Pathania et al., 2014). A reciprocal IP of CyFIP1+2 also yielded Pfn2 in the bound fraction both by Western blot analysis and in mass spectrometry (MS) measurements of the co-immunoprecipitated proteins (data not shown).

Fig. 24 Pfn2 ligands bind normally to P2-GFP with few exceptions

(**A**) Pfn2 as well as P2-GFP were successfully immunoprecipitated in wildtype or homozygous P2-GFP KI mice, respectively, without unspecific signals in the Pfn2 KO control. The P2-GFP IP using GFP-Trap beads was more efficient than the Pfn2 IP using the anti-Pfn2 T2 antibody. (**B**) Actin was equally co-precipitated by Pfn2 and P2-GFP. (**C**) The components of the WAVE-complex were present in Pfn2 and P2-GFP complexes with slight variations in binding efficiency. Only the Abi isoforms showed a preference towards Pfn2. (**D**) The actin nucleators investigated here were equally enriched in the Pfn2 and P2-GFP immunoprecipitated fractions, except for mDia1, which was significantly reduced in the P2-GFP bound fraction. Cortactin was identified as a novel interaction partner of Pfn2 and P2-GFP. (**E**) Synaptic proteins were found to interact with Pfn2 as well as P2-GFP. But the binding efficiency of P2-GFP to dynamin1, endophilin1 and huntingtin was reduced.
IN = input fraction, B = bound fraction, UN= unbound fraction

Tightly associated with CyFIP, also the WAVE complex constituent Nap1 could be found in the immunoprecipitated fractions of Pfn2 and P2-GFP, although it was additionally present in the negative control fractions at a comparable rate (Fig. 24C).
The two isoforms of Abi (Abi 1 and 2), were co-precipitated by Pfn2 with enhanced binding affinity compared to P2-GFP (Fig. 24C). Abi isoforms play a role in promoting actin polymerization through the effect of the WAVE complex and are additionally involved in spine maturation and learning and memory processes through other complexes (Grove et al., 2004; Innocenti et al., 2004, 2005; Kunda et al., 2003).

Another family of proteins, majorly involved in the remodeling of the actin cytoskeleton, in particular in filopodia and lamellipodia, are formins. The formin mDia1 (mammalian Diaphanous 1) is able to drive actin polymerization *in vitro* at very fast rates in the presence of Pfn2, implying an efficient interaction, which was indeed observed in Pfn2-associated complexes as a noteworthy enrichment (Fig. 24D).
P2-GFP, on the other hand, could only marginally enrich mDia1, possibly due to a negative influence of the GFP moiety to the specific complex formation of Pfn2 and mDia1. mDia2, in contrast to mDia1, seemed to be equally co-precipitated by Pfn2 and P2-GFP (Fig. 24D), suggesting divergent modes of binding of the two mDia isoforms to Pfn2.

Also the Ena/VASP family of actin nucleators is involved in regulating actin protrusions (see 1.2). A member of this protein family expressed in nervous tissue is Mena (mammalian Ena), which promotes actin polymerization e.g. in specialized cellular protrusions like lamellipodia, filopodia or axonal projections (Gertler et al., 1996; Lanier et al., 1999). The two splice variants of Mena were bound to Pfn2 and P2-GFP. The GFP-tag did therefore not affect the binding capability.
A novel Pfn2 ligand, the actin nucleation promoting factor cortactin (Cttn), was discovered as well in this study (Fig. 24D). Cortactin interacts with F-actin and the Arp2/3 complex, regulating actin polymerization, branching and stabilization. Cttn has been implicated in spinogenesis as well as activity-dependent morphological changes of spines (Ueda et al., 2013). In both Pfn2 and P2-GFP IPs, cortactin could be enriched, but appears stronger in the more efficient P2-GFP IP.

Pfn2 has been shown to have different synaptic functions during both synaptic vesicle exocytosis and endocytosis, and interacting with a variety of pre- and post-synaptic proteins. Synapsins have a role in synaptogenesis and in synaptic transmission, while the loss of these proteins (Syn1 KO, Syn2 KO, Syn1/Syn2 double KO mouse models) lead to behavioral abnormalities consistent with traits of ASD and epileptiform activity (Greco et al., 2013; Murk et al., 2012). The synapsin family, as expected, was found to interact proportionally with Pfn2 and P2-GFP (Fig. 24E).
A direct interaction of Pfn2 with dynamin 1 (Dyn1) has previously been shown and an inhibitory role of Pfn2 in Dyn1-mediated membrane endocytosis was observed (Gareus et al., 2006; Witke et al., 1998). Dynamin 1 was enriched in Pfn2 IPs, but less markedly in P2-GFP IPs, possibly due to the hindrance of the GFP moiety (Fig. 24E). A similar distribution in Pfn2- and P2-GFP-bound fractions could be detected for endophilin 1 (Enph1) (although also small amounts were visible in the Pfn2 KO control) (Fig. 24E). Enph1 is involved in the membrane fission process during endocytosis (Gareus et al., 2006; Schmidt et al., 1999; Sung et al., 2008).
Huntington´s disease, a fatal neurodegenerative movement disorder, is caused by mutations in the huntingtin gene (*HTT*) (Chakraborty et al., 2014b; Zuccato et al., 2010). Huntingtin is interacting with a vast number of proteins, including Pfn2 (Burnett et al., 2008; Witke et al., 1998). Indeed, Htt could be co-precipitated together with Pfn2 but was lost in P2-GFP complexes, indicating a relevant effect of the GFP moiety specifically on this interaction (Fig. 24E).

The analysis of Pfn2- and P2-GFP-complexes indicates a substantially unimpaired ligand-binding ability of P2-GFP to the majority of proteins. Although P2-GFP binds less efficiently to PLP *in vitro* (see 2.2.3), the interaction with proline-rich ligands *in vivo* under physiological conditions does not seem considerably affected. The binding efficiency of P2-GFP towards its ligands is decreased for Abi1, Abi2, mDia1, dynamin1, endophilin1 and huntingtin, which are associated with diverse cellular functions, i.e. actin dynamics and synaptic activity.

2.3 Pfn2 is a regulator of neuronal development *in vitro*

To elucidate the functions of Pfn2 in neurons, primary murine hippocampal neurons were prepared from isolated embryonic hippocampi (embryonic day 17.5 (E17.5), see 4.4.2) of different genotypes (wt, P2-GFP KI and Pfn2 KO). The localization of Pfn2 in cultured neurons was analyzed and morphological changes during neuronal development due to the deletion of Pfn2 as well as Pfn2 trafficking in mature neurons after various chemical stimulations was studied.

The stages of neuronal development *in vitro* are well-documented for defined culture conditions that ensure the presence of fully functional, mature neuronal networks (Bradke and Dotti, 1999; Dotti et al., 1988; Kaech and Banker, 2006). A monolayer of astrocytes in an adjacent co-culture provides the neurons with nutrients and growth factors, which they release into the medium and therefore condition it to support optimal neuronal development and physiology (see 4.4.3). The positive effect of the astrocyte co-cultures can be acknowledged by markedly increased cell survival rates of the cultured neurons (Bradke and Dotti, 2000; Dotti et al., 1988; Kaech and Banker, 2006).

Neuronal cultures are also a useful system to study the role of specific neurotransmitters without the network framing the neuron *in vivo*. Presumptive changes can therefore be observed directly related to the respective substance used for stimulation without the complex and possibly compromising feed-forward or feed-back mechanisms that would otherwise give rise to secondary effects *in vivo*. In particular, primary hippocampal neurons are used, as these neurons are nearly exclusively glutamatergic and can be considered a single cell type compared to highly mixed populations of cortical or striatal neurons that are also used as neuronal model systems.

Adult Pfn2 KO mice show a strong pre-synaptic phenotype (see 1.3.4), but Pfn2 was shown to be expressed already during embryonic development (see 2.1.5, Fig. 20 and additional data not shown) although it is not essential for neuronal survival. In order to understand the complex role of Pfn2 during the different developmental stages, cultured neurons were used as a model system closely related to neurons *in vivo*.

Therefore, possible alterations during neuronal development due to Pfn2 deficiency at key developmental stages, such as neuritogenesis, neuronal polarization and synaptogenesis were examined. The complexity of Pfn2 KO neurons in comparison to wildtype neurons was analyzed by Sholl analysis (see 2.3.1). Cultures from P2-GFP homozygous KI (G/G) neurons were also included in this analysis to further validate the fusion protein mouse model as a tool to understand Pfn2 function *in vivo*. Furthermore, neurons derived from P2-GFP KI mice were used as a validated tool (see 2.2 and 2.3.1) to study the localization of Pfn2 in the major subcellular structures of cultured neurons and astrocytes (see 2.3.2). The localization of Pfn2 in these neuronal compartments indicated a potential role in these structures that was further analyzed by stimulating mature cultured neurons.
Finally, the trafficking of Pfn2 into the aforementioned neuronal substructures upon exposure to stimulatory agents was investigated in cultured neurons derived from P2-GFP KI animals by high-resolution confocal immunofluorescence imaging (see 2.3.3). A function of Pfn2 in a certain neuronal compartment can be assumed with high confidence, if Pfn2 is enriched following a certain stimulation protocol.

2.3.1 Pfn2 KO neurons show accelerated neuronal development

Neurons in culture show very similar maturation stages as neurons during embryonic development *in vivo*. Dissociated neurons in culture form lamellipodia around the cell bodies after the first few hours (stage 1). Then, the cells extend several neurites (stage 2) from the soma before the neurons after app. 24-48h (DIV1-2 (days *in vitro*) polarize and one neurite starts to rapidly elongate (the future axon, stage 3). The minor neurites (future dendrites) also start to elongate (stage 4) at DIV3-4 to subsequently form elaborate networks (stage 5). Dendritic spines can be observed starting app. 2 weeks after plating (DIV14) but undergo further plastic changes until stable synapses and networks are formed at app. DIV21. Eventually the neurons start to gradually undergo apoptosis after 4 weeks in culture (Dotti et al., 1988; Kaech and Banker, 2006).

In order to investigate potential abnormalities of Pfn2 KO neurons during neuronal development, primary hippocampal neurons were cultured (see 4.4.2) and their

complexity was examined at different developmental stages by Sholl analysis (Binley et al., 2014; Longair et al., 2011; Sholl, 1953) (see 4.4.5, Fig. 25). The Sholl analysis is a method to measure the complexity of neuronal extensions *in silico* by applying concentric circles with a defined interval around the neuronal somata (Fig. 25). The number of intersections of the neuronal tree through these circles is then plotted against the distance from the soma in µm. The Sholl analysis therefore requires the labelling of neuronal processes, which was carried out by fluorescently staining MAP2 (microtubule-associated protein 2), a commonly used marker protein localized to neurites and dendritic processes (Bradke and Dotti, 1997, 1999, 2000; Dotti et al., 1988; Kaech and Banker, 2006; da Silva and Dotti, 2002; Witte and Bradke, 2008; Witte et al., 2008). The complexity of neuronal arborizations was measured and analyzed in this way to be able to identify potential alterations in both P2-GFP KI and Pfn2 KO neurons even in specific segments of the intricate dendritic tree throughout neuronal development.

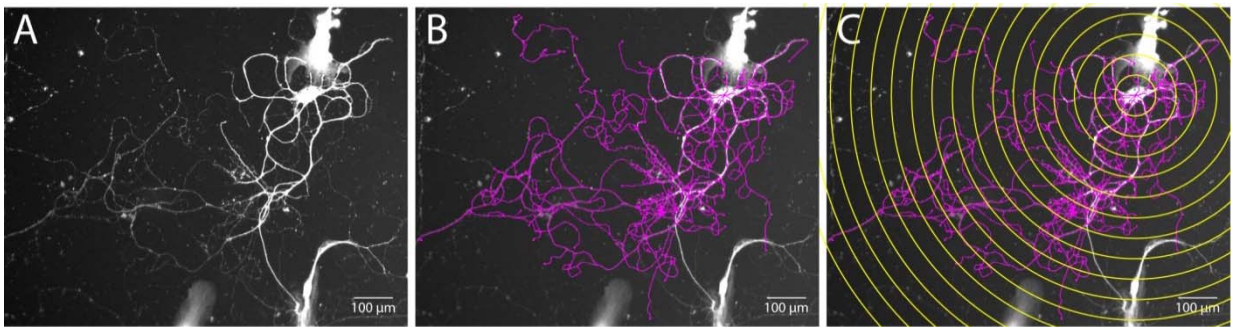

Fig. 25 Sholl analysis of cultured mature hippocampal neurons

(**A**) Representative image of a mature (DIV21) hippocampal neuron in culture. Fluorescent staining of MAP2 is used to visualize the dendritic tree. (**B**) The dendrites of over 100 for less mature stages (DIV1-7) and app. 30 neurons at the mature stages (DIV14-21) are traced manually (pink lines) using the Fiji ImageJ plugin Simple Neurite Tracer (Longair et al., 2011) for each genotype (wt, P2-GFP KI, Pfn2 KO) and each culture (n=3 independent cultures). (**C**) Concentric circles (yellow) of a defined interval (10 µm) are applied *in silico* (shown here are only circles with an interval of 100 µm) extending radially around the soma of the neurons. The intersections of the neurites through these circles are consequently plotted against the distance from the soma (see Fig. 26).

Sholl analyses were carried out averaging between 24 and over 100 neurons (depending on the developmental stage, see Fig.25 and Fig. 26 legend) from three independent cultures of wt, homozygous P2-GFP KI and Pfn2 KO neurons.

Pfn2 KO neurons developed in accordance to the known developmental stages, but they showed an accelerated development (Fig. 26). The number of initial neurites at DIV 1 was higher for Pfn2 KO neurons in comparison to wt neurons (Fig. 26A), but the neurons still formed one major process (the future axon) similarly to the wt neurons. P2-GFP KI neurons developed normally and were indistinguishable from wt neurons at this stage (Fig. 26A).

After 48h of development (DIV 2), Pfn2 KO neurons showed a higher complexity than wt neurons and the major process was growing out longer (app. 50 µm = 25% longer) (Fig. 26B). P2-GFP KI neurons started to show an intermediate phenotype between wt and Pfn2 KO cells. They appeared to have a slightly increased complexity with the leading neurite extending also further than that of wt neurons (Fig. 26B).

At DIV 3 Pfn2 KO neurons started to establish a high degree of neurite branches especially proximal to the soma and still extended the leading process further than wt neurons (app. 70 µm = 25% longer) (Fig. 26C). P2-GFP KI neurons showed an intermediate development with a very slight tendency towards increased proximal branching and an elongated leading process (app. 60 µm = 21% longer) (Fig. 26C).

At DIV 7, neurite extension length was normalized between all genotypes, but the more complex proximal branching in Pfn2 KO neurons was further increased, especially in the first 150 µm adjacent to the soma (Fig. 26D). The intermediate phenotype of P2-GFP KI neurons could still be acknowledged by the low increase in proximal neurite complexity (Fig. 26D).

Over the course of the second week in culture, Pfn2 KO neurons extremely amplified their higher complexity nearly over the full extent of the dendritic tree with only the most distal part at a level comparable to the wt (Fig. 26E). Also P2-GFP KI neurons showed an increased complexity especially in the first 300 µm proximal to the soma (Fig. 26E). Completely developed Pfn2 KO neurons at DIV 21 were similarly complex compared to wt neurons (Fig. 26F). They even started to gradually reduce their dendritic branching at the most distal segments of the neuronal tree (app. the last 250 µm, Fig. 26F).

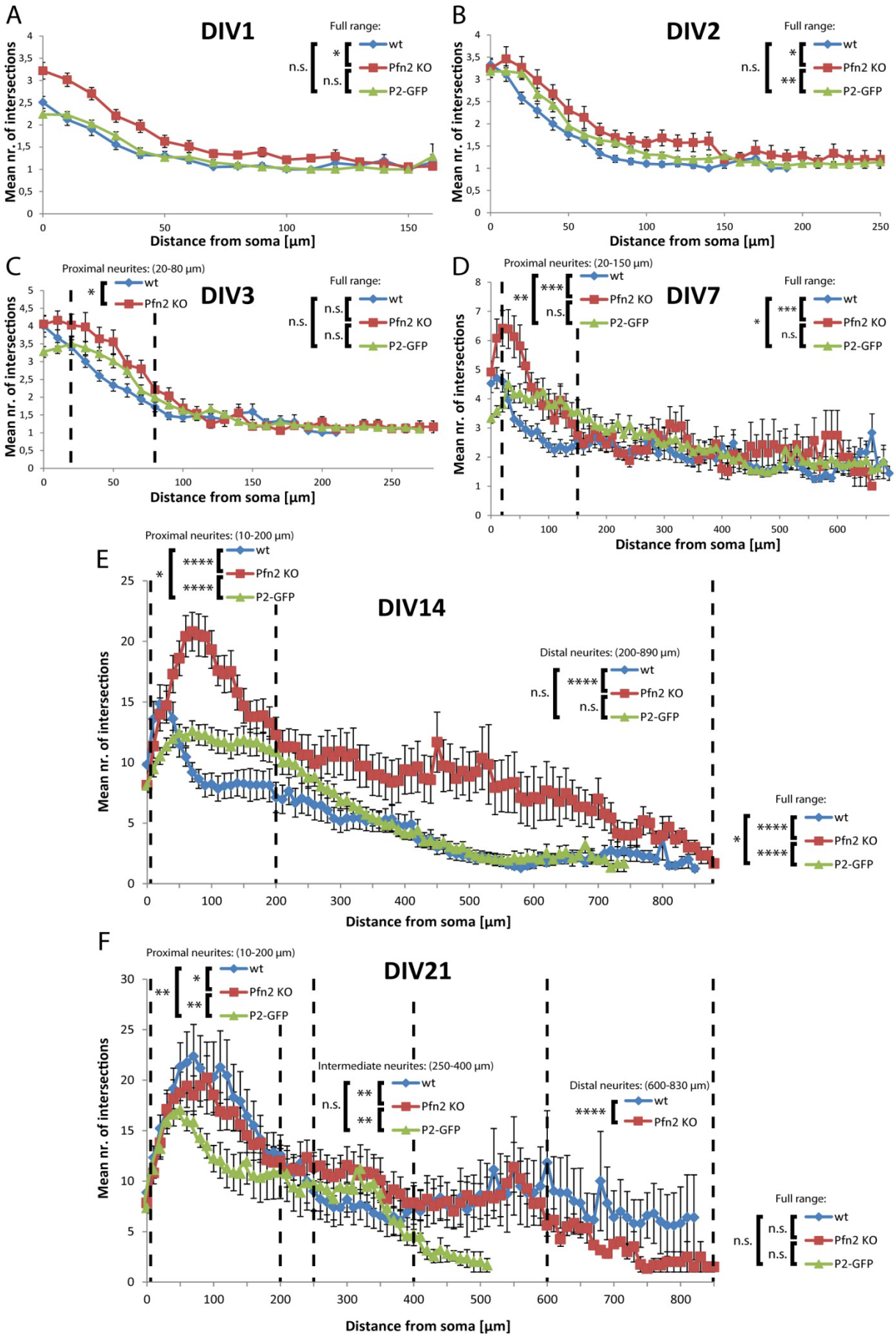
A
DIV1
Full range:
n.s.
*
n.s.
wt
Pfn2 KO
P2-GFP
Mean nr. of intersections
Distance from soma [µm]
B
DIV2
Full range:
n.s.
*
**
wt
Pfn2 KO
P2-GFP
Mean nr. of intersections
Distance from soma [µm]
C
Proximal neurites: (20-80 µm)
*
wt
Pfn2 KO
DIV3
Full range:
n.s.
n.s.
n.s.
wt
Pfn2 KO
P2-GFP
Mean nr. of intersections
Distance from soma [µm]
D
Proximal neurites: (20-150 µm)
**
***
n.s.
wt
Pfn2 KO
P2-GFP
DIV7
Full range:
*
***
n.s.
wt
Pfn2 KO
P2-GFP
Mean nr. of intersections
Distance from soma [µm]
E
Proximal neurites: (10-200 µm)
*
****
****
wt
Pfn2 KO
P2-GFP
DIV14
Distal neurites: (200-890 µm)
n.s.
****
n.s.
wt
Pfn2 KO
P2-GFP
Full range:
*
****
****
wt
Pfn2 KO
P2-GFP
Mean nr. of intersections
Distance from soma [µm]
F
Proximal neurites: (10-200 µm)
**
*
**
wt
Pfn2 KO
P2-GFP
DIV21
Intermediate neurites: (250-400 µm)
n.s.
**
**
wt
Pfn2 KO
P2-GFP
Distal neurites: (600-830 µm)
****
wt
Pfn2 KO
Full range:
n.s.
n.s.
n.s.
wt
Pfn2 KO
P2-GFP
Mean nr. of intersections
Distance from soma [µm]

Pfn2 KO neuronal projections were still slightly more branched in the intermediate range of app. 250-400 µm from the soma. P2-GFP KI neurons were not able to completely develop at DIV 21, but instead shortened most of their dendritic tree (Fig. 26F).

Fig. 26 Sholl analysis revealed a role of Pfn2 in neuronal development

(**A**) Neurons derived from wt, P2-GFP KI and Pfn2 KO animals were analyzed 24h after plating (DIV 1). Pfn2 KO neurons show enhanced initial neurite sprouting, while P2-GFP neurons develop comparably to wt cells. DIV1 wt:KO p= 0.0387, wt:G/G p= 0.08356, G/G:KO p= 0.2143 by Mann-Whitney test, n=67/3 for wt, n=102/3 for G/G and n=64/3 for Pfn2 KO. (**B**) Following 48h in culture (DIV 2), Pfn2 KO and P2-GFP KI neurons show higher complexity than wt neurons and increased neurite elongation. DIV2 wt:KO p= 0.0333, wt:G/G p= 0.843, G/G:KO p= 0.0065 by Mann-Whitney test, n=73/3 for wt, n=90/3 for G/G and n=37/2 for Pfn2 KO. (**C**) Pfn2 KO neurons at DIV 3 increase their proximal complexity in comparison to wt neurons. Both Pfn2 KO and P2-GFP KI neurons develop longer extensions than wt cells. DIV3 full range wt:KO p= 0.4935, wt:G/G p= 0.4636, G/G:KO p= 0.8794, proximal neurites (20-80 µm from soma) wt:KO p= 0.0409 by Mann-Whitney test, n=66/3 for wt, n=73/3 for G/G and n=37/2 for Pfn2 KO. (**D**) The neurite length is similar at DIV 7 between all three genotypes, but the proximal branching of Pfn2 KO neurons remains highly increased. P2-GFP KI neurons show an intermediate phenotype, similar to DIV3. DIV7 full range wt:KO p= 0.001, wt:G/G p= 0.0211, G/G:KO p= 0.4462, proximal neurites (20-150 µm) wt:KO p= 0.0009, wt:G/G p= 0.0047, G/G:KO p= 0.2411 by Mann-Whitney test, n=63/3 for wt, n=53/3 for G/G and n=38/3 for Pfn2 KO. (**E**) After two weeks in culture (DIV14), all genotypes are increasingly complex, but P2-GFP KI and particularly Pfn2 KO neurons show an extreme level of (especially proximal, but at this stage also distal) dendritic complexity. DIV14 full range wt:KO p= 0.00001, wt:G/G p= 0.0345, G/G:KO p= 0.00001, proximal neurites (10-200 µm) wt:KO p= 0.00001, wt:G/G p= 0.0143, G/G:KO p= 0.00001, distal neurites (200-890 µm) wt:KO p= 0.00001, wt:G/G p= 0.0891 by Mann-Whitney test, n=39/3 for wt, n=47/3 for G/G and n=40/3 for Pfn2 KO. (**F**) Wt neurons show a similar complexity to Pfn2 KO neurons at the fully mature stage (DIV21) with the Pfn2 KO neurons starting to gradually reduce their complexity in the distal part of the dendritic tree. P2-GFP KI neurons were not able to reach the completely developed stage. DIV21 full range wt:KO p= 0.5253, wt:G/G p= 0.9261, G/G:KO p= 0.222, proximal neurites (10-200 µm) wt:KO p= 0.0385, wt:G/G p= 0.001 , G/G:KO p= 0.0021, intermediate neurites (250-400 µm) wt:KO p= 0.0011, wt:G/G p= 0.3179, i G/G:KO p= 0.005, distal neurites (600-830 µm) wt:KO p= 0.00001 by Mann-Whitney test, n=24/3 for wt, n=35/3 for G/G and n=36/3 for Pfn2 KO. (**G**) Representative example image of mature (DIV21) neurons in culture. Scale bar 10 µm.

Minitab17 software was used for statistical analysis employing the Mann-Whitney test: $p \geq 0.05$ = n.s., $p \leq 0.05$ = *, $p \leq 0.01$ = **, $p \leq 0.001$ = ***, $p \leq 0.0001$ = **** Error bars represent S.E.M.

In conclusion, comparing wt and Pfn2 KO neurons, the latter appeared to develop a longer leading neurite and to maintain increased arborization complexity. The Pfn2 KO cells therefore developed at a higher velocity, reaching the next developmental stage at an accelerated rate compared to wt neurons. P2-GFP neurons showed an intermediate phenotype between wt and Pfn2 KO cells.

2.3.2 Pfn2 is localized to key structures in neuronal development

Pfn2 KO neurons showed alterations in neuronal development pointing to an accelerated development (see 2.3.1, Fig. 26). Especially specific segments of the dendritic tree were affected by the loss of Pfn2 (proximal branching starting from early stages of development and additionally distal branching at more mature stages). Consequently, a role of Pfn2 in the regulation of dendrite formation and branching (maturation) could be hypothesized. In order to identify the distinct roles of Pfn2 in key structures of neuronal development as well as pre- and post-synaptic compartments, the subcellular localization of Pfn2 was investigated in detail by fluorescent imaging in cultured neurons derived from homozygous P2-GFP KI (G/G) mice.
Several studies used different approaches (mostly based on transfection assays) to visualize Pfn2 in nervous tissue and cultured neurons so far. Nonetheless, the distribution of endogenously expressed Pfn2 in neuronal cells has not been conclusively reported.

Neuronal subcellular compartments were specifically labelled employing common marker proteins for neurites and dendritic shafts (Map2, see 2.3.1), dendritic spines (PSD95) (Chen et al., 2007a; Craig et al., 2006), axonal shafts (Tau1) (Bradke and Dotti, 2000; Kaech and Banker, 2006; Witte et al., 2008) and axonal boutons (VAMP2 (synaptobrevin 2)) (Okawa et al., 2014; Rossi and Volterra, 2009). Fluorescently labelled Phalloidin was used to stain the actin cytoskeleton and cultured astrocytes were identified as GFAP-positive cells (see 2.1.4).

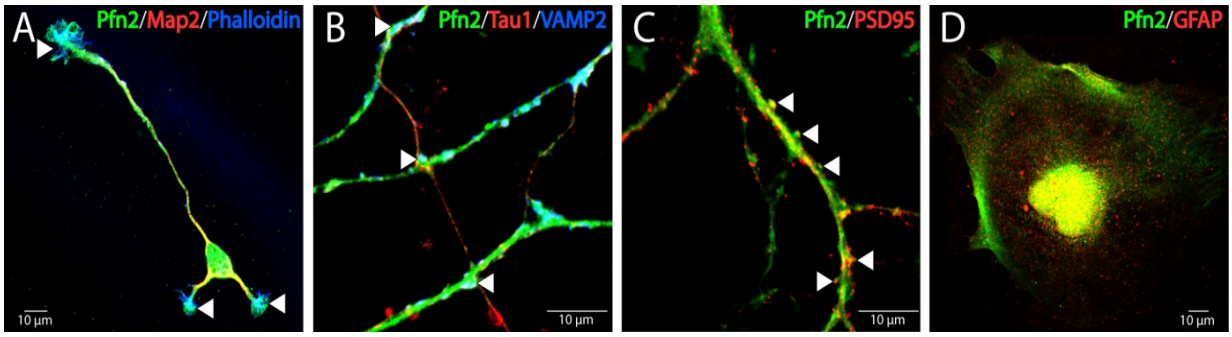

Fig. 27 Localization of Pfn2 in subcellular compartments of cultured neurons and astrocytes
(**A**) Cultured neurons (DIV 2) show Pfn2 (green) enriched in the cell body and neurites (Map2, red, yellow in the merged image). More specifically, Pfn2 is found in future dendrites (shorter processes) as well as in the future axon (longer proces). Actin-rich growth cones (Phalloidin, blue) were enriched in Pfn2 as well (cyan in the merged images, arrowheads). (**B**) Zoomed image of a mature neuron (DIV 21), which localized Pfn2 to dendrites and less markedly to axons (Tau1, red). Pre-synaptic terminals (VAMP2, blue) are, in contrast to the axonal shafts, highly enriched in Pfn2 (cyan in the merged images, arrowheads). (**C**) Post-synaptic spines (PSD95, red) on dendrites of mature neurons (DIV 21) are positive for Pfn2 (yellow in the merged images, arrowheads). (**D**) Cultured astrocytes (GFAP, red) express Pfn2 *in vitro*.

Pfn2 appeared ubiquitously localized in cultured hippocampal neurons (Fig. 27). The initial stages of neuronal development are characterized by neurite extension, growth cone formation and neuron polarization (see 2.3.1). Pfn2 was localized in neurites (Fig. 27A) and more specifically in polarized neurites becoming either the future dendrites (Fig. 27A, shorter processes) or the future axon (Fig. 27A, single longer process). Also growth cones that are essential for neurite outgrowth were strongly enriched in Pfn2 (Fig. 27A, arrowheads). In mature neurons, Pfn2 was mostly localized in dendritic shafts and less to axonal projections (Fig. 27B). Nevertheless, pre-synaptic boutons on axonal projections were prominently labelled by Pfn2 (Fig. 27B, arrowheads). Similarly post-synaptic spines were enriched in Pfn2 (Fig. 27C, arrowheads). The different types of spines, which can be clearly distinguished by their morphology (see 1.4.1), were analyzed as well and showed an equal distribution of Pfn2 among thin/filopodial, stubby and mushroom-shaped spines. Spine necks as well as the PSD-containing tip showed signals for Pfn2, comparable to the known localization of the actin cytoskeleton (data not shown).
In contrast to the observations in the adult brain described previously (see 2.1.4, Fig. 19), Pfn2 was found in cultured astrocytes (Fig. 27D). But these cells were derived

from embryonic GFAP-positive radial glia cells (embryonic stem cells), which were shown to express Pfn2 (see 2.1.6, Fig. 20) and therefore most likely continue to express Pfn2 also under *in vitro* culture conditions.

In summary, Pfn2 is enriched in neurites during neuronal development and localizes to synaptic compartments during maturation. The localization of Pfn2 in cultured neurons emphasizes the importance of this particular profilin isoform for specific processes that need fast and tightly regulated actin dynamics, such as growth cone motility, neurite outgrowth and pre- and post-synaptic compartment physiology.

2.3.3 Stimulation-induced trafficking of Pfn2 into pre- and post-synaptic compartments

A potentially specific function of Pfn2 in neuronal compartments, as mentioned above (see 2.3.2, Fig. 27), was analyzed by differentially stimulating cultured hippocampal neurons and investigating the corresponding trafficking of P2-GFP in response to the stimulus (see 4.4.6). Cultured hippocampal neurons were therefore isolated from P2-GFP KI animals (n=2 independent cultures) and stimulated at developmental maturity (DIV21) (see 4.4.6).

Neurons respond to various neurotransmitters and to changes in specific ion concentrations in the environment (see 1.4.1, Fig. 6 and 7). The application of glutamate activates ionotropic (AMPA and kainate receptors) as well as metabotropic (mGluRs) receptors, which cause sodium influx and depolarization of the cell. A strong depolarization of the membrane potential consequently leads to firing of an action potential. Glutamate binds to NMDA receptors as well, but the co-agonist glycine (or D-serine) is necessary in order to activate the channel. NMDA receptors not only mediate the influx of sodium and efflux of potassium ions, but also induce a high degree of calcium ion entry. Consequently, calcium ions can act as second messenger molecules, activating downstream Ca^{2+}-dependent signaling pathways that include long-term changes in synaptic plasticity (Zito and Scheuss, 2009). The opening of the channel is also voltage-dependent, since a blockage by a magnesium

ion prevents its activation, which can be released by depolarization, e.g. by AMPA or kainate receptor activity. The response of NMDA receptors is therefore not as immediate compared to the AMPA or kainate receptors and has a larger impact on changes in synaptic plasticity. The application of NMDA itself will only open NMDA receptors lacking an effect on the other receptors.
Applying an excess of extracellular potassium leads to a reversal of the membrane potential, allowing potassium entry and the depolarization of the cell. A strong depolarizing effect leads to an increase in the probability of the formation of an action potential.
Changing the ratio of calcium to magnesium ions in the medium to 7:1 has a less strong effect, since extracellular calcium is not able to freely diffuse into the cell, but the probability of synaptic transmission is increased.

GABA stimulation, on the other hand, has the opposing effect of hyperpolarizing the cell, as chloride ion influx is induced by activating GABA receptors, further lowering the membrane potential and decreasing the excitability of the cell.
Finally, LTD is a powerful means to induce synaptic plasticity including decreased synaptic transmission, spine shrinkage, loss of F-actin in spines, protein degradation and decreased local translation (see 1.4.1) (Bellot et al., 2014; Bosch et al., 2014; Chen et al., 2007a; Cingolani and Goda, 2008; Huang et al., 2014; Lee et al., 1998; Li et al., 2007; Oberman and Pascual-Leone, 2013; Shehata et al., 2012). To obtain LTD in cultured neurons, a chemical model of LTD can be applied using a brief application of NMDA at high concentrations (3 min., 25 µm NMDA, see 4.4.6) that is nearly indistinguishable from electrically stimulated LTD in the brain or brain slices (Huang et al., 2014; Lee et al., 1998; Li et al., 2007; Shehata et al., 2012).
The neurons were investigated directly after the stimulations and in addition after washing out the stimulus and incubating the cells in stimulant-free medium for a certain period of time, which allowed the cells to recover from the induced de- or hyper-polarization.

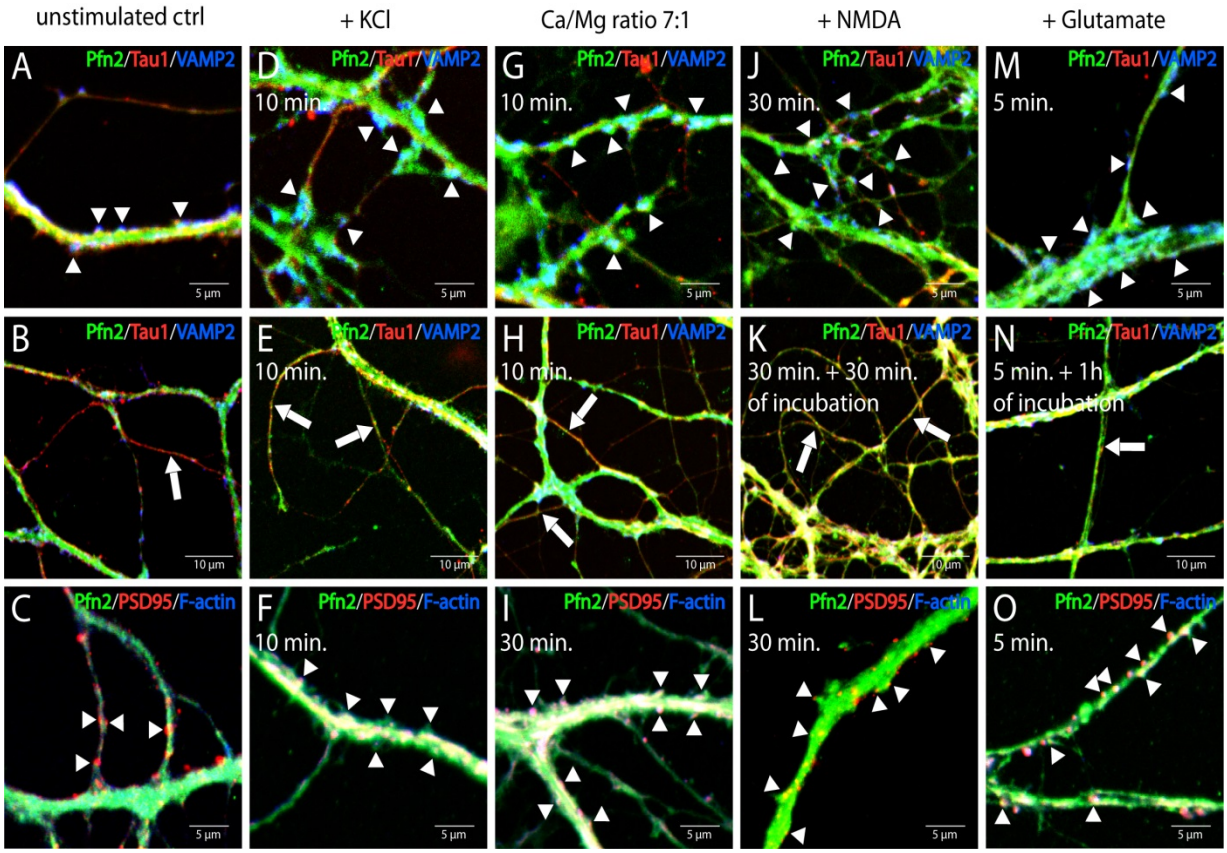

Fig. 28 Pfn2 trafficking into neuronal compartments induced by depolarizing stimulation

Primary hippocampal neurons were stimulated with various depolarizing treatments (indicated at the top) and the trafficking of Pfn2 (P2-GFP, green) in neuronal compartments at specific time points is shown. Fluorescent puncta corresponding in size, shape, density and distribution to either pre-synaptic boutons (identified by labelling VAMP2, blue) or post-synaptic spines (identified by labelling PSD95, red) are visible. Axons are stained using Tau1 (red) as a marker protein.

(**A**) Under normal conditions Pfn2 (green) is present in moderate amounts in pre-synaptic boutons (VAMP2, blue, arrowheads), (**B**) axonal shafts (Tau1, red, arrows) and (**C**) spines (PSD95, red, arrowheads). (**D**) An excess of potassium in the medium (10 min. of exposure) leads to enrichment of Pfn2 in boutons (cyan merge), (**E**) moderately in axons (yellow merge) and (**F**) more pronounced in spines (yellow merge). (**G**) Increasing the Ca^{2+}/Mg^{2+} ratio to 7:1 has similar effects (10-30 min. of exposure) triggering Pfn2 re-localization to boutons, (**H**) slightly to axons and (**I**) to spines. (**J**) Applying NMDA to the cells has a stronger impact. Pfn2 is enriched in pre-synaptic terminals after 5-10 min. of exposure, (**K**) but in axonal shafts most efficiently after 30 min. to 1 h of incubation after washing away NMDA in the medium. (**L**) The application of NMDA induced Pfn2 enrichment into a subset of dendritic spines. (**M**) The strongest effect is observed using glutamate as a stimulatory agent. Pfn2 is re-localized to pre-synaptic boutons after 5 min. of exposure, (**N**) but into axons after 1 h of incubation after removal of glutamate. (**O**) Glutamate stimulation induced Pfn2 re-localization also into post-synaptic spines.

In resting (control) neurons Pfn2 was moderately localized to pre-synaptic boutons, to a minor amount in axonal shafts and also moderately in post-synaptic spines (Fig. 28 and Fig. 29A-C). But Pfn2 showed dynamic responses to the stimulating conditions.

All excitatory stimulation agents (K^+, Ca^{2+}, glutamate (together with glycine) and NMDA) induced similar trafficking of Pfn2 into both pre- and post-synaptic terminals as well as axonal shafts, while enhancing the overall expression level of Pfn2.
Strong depolarization of the cell induced by an excess of potassium in the medium caused a re-localization of Pfn2 into synaptic boutons (Fig. 28D), axonal shafts (Fig. 28E) and dendritic spines (Fig. 28F). The effect of an excess of potassium (KCl, 60 mM, see 4.4.6) in the medium was most pronounced after 5-10 min. of exposure. The re-localization of Pfn2 into pre-synaptic boutons was obvious after 5 min., while an enrichment of Pfn2 in axonal shafts was noticeable after 10 min. of exposure. Dendritic spines showed both an increase in F-actin and Pfn2 after 10 min.
Similarly, but less efficiently, an increased ratio of calcium to magnesium ions in the medium (Ca^{2+}/Mg^{2+} ratio 7:1, see 4.4.6) triggered moderate Pfn2 trafficking to synaptic boutons (Fig. 28G) after 10 min. of exposure, while an enrichment in axons (Fig. 28H) could be observed after 15 min. and dendritic spines (Fig. 28I) were affected after 30 min. The increase in Pfn2, VAMP2 and F-actin levels was also not as obvious as induced by the KCl treatment.
Targeting specifically NMDA receptors (NMDA, 10 µM, see 4.4.6) efficiently induced enrichment of Pfn2 in pre-synaptic terminals (Fig. 28J) and axonal shafts (Fig. 28K), but only a subset of dendritic spines were enriched in Pfn2 (Fig. 28L). The effects were still visible after washing and 30 min. till up to 2h of incubation time after the application of the agonist (data not shown).
The most efficient stimulation was achieved by exposure to glutamate with or without the addition of glycine (glutamate 10 µM, glycine 10 µM, 10 min., see 4.4.6). Activating all types of glutamate receptors induced a prominent enrichment of Pfn2 mostly in pre-synaptic boutons (Fig. 28M), but also in axonal shafts (Fig. 28N) and dendritic spines (Fig. 28O). The changes persisted for 30 min. to at least 2h subsequently to washing the cells.

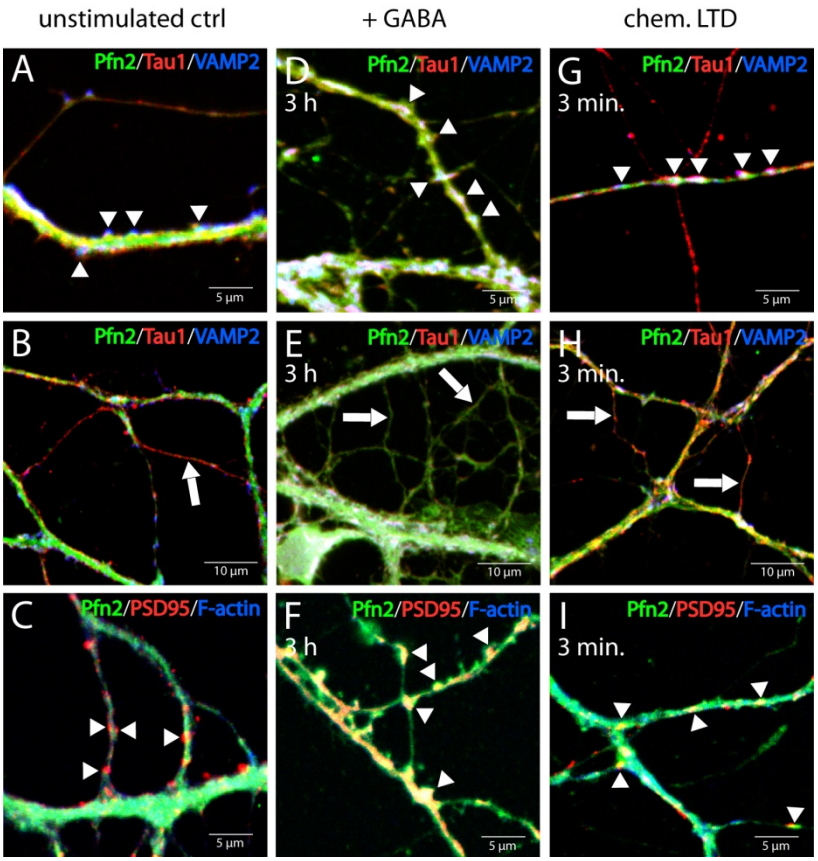

Fig 29 Pfn2 trafficking into neuronal compartments induced by hyperpolarizing stimulation

Primary hippocampal neurons stimulated with hyperpolarizing treatments (indicated at the top) and stained as mentioned above (see Fig. 28) are shown. The trafficking of Pfn2 (P2-GFP, green) into neuronal compartments is shown. Fluorescent puncta corresponding in size, shape, density and distribution to either pre-synaptic boutons (identified by labelling VAMP2, blue) or post-synaptic spines (identified by labelling PSD95, red) are visible. Axons are stained using Tau1 (red) as a marker protein.

(**A**-**C**) The subcellular localization of Pfn2 at resting conditions is shown for specific neuronal compartments (compare Fig. 27). (**D**) The treatment of neurons with GABA (3 h of exposure), on the other hand, has no obvious effect on pre-synaptic boutons, (**E**) but triggers an enrichment of Pfn2 in axons and (**F**) moderately in spines. (**G**) Chemically inducing long term depression using a brief application (3 min.) of a high dosage of NMDA (chem. LTD) also triggers an enrichment of Pfn2 in pre-synaptic terminals, while (**H**) axonal shafts are nearly devoid of Pfn2. (**I**) Post-synaptic spines are moderately enriched in Pfn2 following chemically induced LTD.

An opposite effect on Pfn2 trafficking was observed by hyperpolarization of the cell by GABA treatment and after chemical LTD (Fig. 29). The application of GABA (GABA, 50 µM, see 4.4.6) and a brief, highly concentrated pulse of NMDA as a chemical model of LTD (NMDA, 25 µM, see 4.4.6) and yielded an overall reduction of the fluorescent signals of Pfn2 and VAMP2, but no change in F-actin levels (data not shown, the fluorescent signals were digitally intensified during the acquisition in order to visualize Pfn2 in neuronal compartments).

Even though Pfn2 levels were decreased, GABA-mediated hyperpolarization of the neurons lead to no obvious trafficking of Pfn2 into boutons (Fig. 29D) but interestingly into axons (Fig. 29E) and Pfn2 was found slightly increased in dendritic spines (Fig. 29F).
The chemical LTD protocol still induced an enrichment of Pfn2 in pre-synaptic boutons (Fig. 29G), but was mostly absent from axons (Fig. 29H). The reduction of Pfn2 in axons was only transient, as Pfn2 was present in axons at baseline levels after 1 h of recovery after washing away the NMDA. A slight increase of Pfn2 in post-synaptic spines was also detectable (Fig. 29I).

Pfn2 showed distinctive trafficking following each stimulatory treatment, indicating a role and function in the processes induced by the specific stimulation. Due to the fact that Pfn2 was responding mostly to excitatory stimulation, Pfn2 predominantly responds to depolarization rather than to hyperpolarization of the cell. During and consequent to depolarization, Pfn2 appeared to be needed in both pre- and post-synaptic terminals as well as axonal shafts. In dendrites Pfn2 was stably expressed at high levels.

3. Discussion

3.1 Neuronal systems potentially involved in autism spectrum disorder

Autism spectrum disorder is a neurodevelopmental disease of genetic origin becoming more and more relevant, now with a prevalence of app. 13/10,000 children (Kogan et al., 2009). The key observation in autistic patients is an imbalance in the excitation/ inhibition ratio in the central nervous system. Nevertheless, it is still debated, which neuronal systems are involved or contribute to this imbalance in ASD. The Pfn2 KO mouse model shows autistic-like phenotypes, such as hyperexcitability, social and communication deficits, coordination impairments and epileptic seizures. In order to understand the possible contribution of Pfn2 to these complex phenotypes, its expression profile in the different neuronal systems has been investigated in detail in this thesis taking advantage of a P2-GFP fusion protein knock-in mouse model, by co-localizing the P2-GFP fusion protein with a range of specific markers for neuronal sub-populations.

3.1.1 Excitatory neuronal systems are all potentially involved in ASD and seizures phenotypes of Pfn2 KO mice

Autistic patients show an excess of glutamate in the brain (Hussman, 2001) and many brain functions are modulated by pathways involving glutamatergic signaling, such a majority of behavioral functions, including social behavior, emotion, learning and memory as well as motor functions. Therefore glutamatergic neurons are under growing investigation in autism research (see 1.4.2) (Abrahams and Geschwind, 2008; Alarcón et al., 2008; Bellot et al., 2014; Di Cristo, 2007; Jacob et al., 2011; Peñagarikano et al., 2011; Szatmari et al., 2007).

Previous studies have shown a function of Pfn2 in glutamatergic neurons, in which pre-synaptic vesicle release was increased due to impairments in fast actin-dynamics in pre-synaptic terminals (Pilo Boyl et al., 2007). In this study, Pfn2 was found expressed in all excitatory neuronal systems with varying levels (see 2.1.1). More specifically, glutamatergic neurons express the highest levels, dopaminergic, noradrenergic as well as serotonergic neurons express high levels of Pfn2, while

cholinergic neurons are the exception among excitatory systems producing only low levels of Pfn2 (see 2.1.1.2-2.1.1.5, Fig. 14, Fig. 21, Supp. Fig. 12).

3.1.1.1 The potential role of Pfn2 in increased sensitivity of sensory neurons in ASD

Pfn2 could play a relevant role in the neuronal regulation of sensory information propagation. This work shows a strong expression of Pfn2 in the olfactory system of the mouse, as an example of the various sensory systems (see 2.1.3, Fig. 18, Fig. 21, Supp. Fig. 12). The highest expression level of Pfn2 was indeed observed among all glutamatergic neurons, but in particular in pyramidal neurons of the hippocampal CA2 region and in olfactory Mitral and external tufted cells (see 2.1.1.1, 2.1.3, Fig. 14, 18, 21 and Supp. Fig. 12).

Glutamatergic Mitral cells and external tufted cells (ETCs), which mediate the sole output from the olfactory bulb (De Saint Jan et al., 2009) would become hyperexcitable in the absence of Pfn2. Short axon cells (SACs), on the other hand, are the primary active cells around glomeruli that filter sensory information reaching the glomeruli structures from sensory neurons in the nasal epithelium. These cells can directly modulate Mitral cell and ETC signaling but primarily target neighboring SACs and GABAergic periglomerular neurons, which in turn inhibit Mitral cell and ETC signaling (Cave and Baker, 2009; Ennis et al., 2001; McQuiston and Katz, 2001; Murphy et al., 2005). SACs show increased expression of Pfn2 upon expression of dopamine and is present in minor levels in cells co-expressing GABA and dopamine (see 2.1.3, Fig. 18, Fig. 21, Supp. Fig. 12).
The complexity of this network makes it difficult to decipher the role of Pfn2 in each of these neurons in the olfactory circuitry, but it is conceivable to hypothesize that the hyperactivation of Mitral cells and ETCs is enough to lead to a strong excitatory output transmission from the olfactory bulb in response to environmental stimuli. The excess of excitation could be further potentiated in Pfn2 KO mice, since sensory information might not be filtered as efficiently by feed-back mechanisms in the glomerular network, since also modulatory short axon cells, partially lacking Pfn2,

could be dysregulated as well. This hyperexcitable state of the olfactory circuit leads to a higher probability of sensory information being transferred to the rest of the brain, inducing a hypersensitivity towards sensory stimulation, a trait that is also often observed in autistic patients.

On the same line, although not specifically addressed yet, an increased sensitivity to pain has also been observed in Pfn2 KO mice (Pilo Boyl, unpublished observation). On embryonic tissue, also other sensory compartments, such as the whiskers, teeth and the tongue showed the expression of Pfn2 (see 2.1.3, Fig. 18) and in a previous study, expression of Pfn2 in the retina has been observed (Perlas, unpublished observation). It can therefore be assumed that other, if not all, sensory systems might show similar abnormalities due to the deletion of Pfn2. Thus a dysregulation of the sensory systems could be an initial cause of the shift in the excitation/inhibition balance in the brain that is a key feature in ASD.

Often associated with ASD are epileptic seizures, which most often result from hyperactivity of the hippocampal formation (Gant et al., 2009). Excitatory glutamatergic signaling was already shown to be increased in Pfn2 KO mice (Pilo Boyl et al., 2007). Therefore, the highest Pfn2 levels in glutamatergic hippocampal neurons reported in this study (see 2.1.1.1, Fig. 14 and 21), point to their causative role for the spontaneous epileptic seizures observed in Pfn2 KO mice. Hippocampal GABAergic neurons, on the other hand, were shown to be generally devoid of Pfn2 in the hippocampus and are therefore not directly affected by the deletion of Pfn2 (see 2.1.2.1, Fig. 15, 17 and 21). Hence, even feed-back mechanisms in the hippocampal circuitry that normally regulate excessive signaling might be hyperactivated in Pfn2 KO mice, leading to a potentiation of the excitability that ultimately leads to the observed epileptic seizures.

3.1.1.2 The possible contribution of Pfn2 in other excitatory systems to ASD-related symptoms

Autistic traits such as novelty-dependent hyperactivity and motor coordination deficits could be associated with dysregulation of the dopaminergic system, which also features very high levels of Pfn2 (see 2.1.1.2, Fig. 14, Fig. 21, Supp. Fig. 12). Dopamine is released to medium spiny neurons in the striatum, where it can induce differential behavioral patterns that could be affected by the deletion of Pfn2 (see 3.1.3, Supp. Fig. 1). Stimulating VTA fibers in the Pfn2 KO background yielded an approximately 2-fold increased dopamine release compared to wildtype mice, which leads to elevated dopamine levels in striata of Pfn2 KO mice (Pilo Boyl, unpublished). Especially the deletion of the dopamine transporter (DAT) was shown to lead to excessive dopamine in the striatum due to a lack of neurotransmitter reuptake and behavioral (motor) abnormalities (Giros et al., 1996) similar to the Pfn2 KO mouse phenotype. Pfn2 expression was found in the major dopaminergic regions of the SN and the VTA at high levels, a dysregulation of dopaminergic signaling might therefore contribute to motor abnormalities, such as the novelty-dependent hyperactivity and hyperlocomotion phenotypes of Pfn2 KO mice. The dopaminergic system in humans is affected in neurodegenerative diseases, such as Parkinson´s disease, causing severe phenotypes mostly concomitant with motor deficits (Björklund and Dunnett, 2007; Cave and Baker, 2009; Durieux et al., 2011; Kreitzer, 2009; Miller et al., 2013; Missale et al., 1998; Nakatani et al., 2007; Oades et al., 2005; Santos et al., 2010; Smidt and Burbach, 2007; Svenningsson et al., 2004; Tan et al., 2003).

The noradrenergic signaling from the locus coeruleus is impaired in a number of neurological disorders including Rett syndrome, a closely related variant of autism spectrum disorders, where adrenergic neurons were found to be hyperexcitable (Santos et al., 2010). This hyperexcitability phenotype could also be present in adrenergic neurons of Pfn2 mutant mice, since these neurons are highly Pfn2-positive (see 2.1.1.3, Fig. 14, Fig. 21, Supp. Fig. 12). A potential hyperexcitability of adrenergic neurons in Pfn2 KO mice could contribute to a subset of the autistic traits observed in the mouse model.

Noradrenergic neurons fire minimally in resting conditions and answer by strongly increasing their firing upon relevant stimuli (danger, threat, novelty) to induce the “fight-or-flight” response (Cannon, 1929), not only innervating certain brain areas but also the entire body through receptors at organs and especially neuromuscular junctions (NMJs). Behavioral abnormalities like panic (Pilo Boyl, unpublished), low aggressivity (Di Nardo, unpublished) and increased novelty seeking behavior (Pilo Boyl et al., 2007) of Pfn2 KO mice could in part originate from dysregulation of stimulus-induced activity of adrenergic neuronal signaling due to the lack of Pfn2. Further detailed studies on the activity of adrenergic neurons in Pfn2 KO mice would therefore be important.

The serotonergic system is often associated with ASD and its symptoms both at the genetic and physiological level. Thus a high expression level of Pfn2 in serotonergic neurons (see 2.1.1.4, Fig. 14, Fig. 21, Supp. Fig. 12) could be in line with the autism-like phenotype of Pfn2 KO mice. In fact, early studies on autistic patients already reported elevated serotonin levels in whole blood as well as platelet samples (Anderson et al., 1990; Chandana et al., 2005; Chugani et al., 1997, 1999; Cohen et al., 2003, 1995; Crawley, 2004; Dufour-Rainfray et al., 2010; Makkonen et al., 2008; Schain and Freedman, 1961) and elevated serotonin levels were found in the striatum (especially the nucleus accumbens) in association with neurological disorders like schizophrenia, depression and addiction (Brocco et al., 2002; Svenningsson et al., 2004) as well as with traits of ASD like hyperlocomotion and social interaction impairments. Elevated serotonin levels were also found in hippocampi of Pfn2 KO mice (Pilo Boyl, unpublished) and the high expression level of Pfn2 in serotonergic neurons could support the hypothesis that hyperactivation of the serotonergic system as a consequence to the loss of Pfn2 could participate to the autistic phenotype to some degree. Furthermore serotonin metabolism alterations were evident in some cases of autism linked to mutations in the genes coding for the tryptophan 2,3-oxigenase and monoamine oxidase-A (MAO-A) enzymes required for serotonin synthesis (Chandana et al., 2005; Cohen et al., 2003; Jones et al., 2004; Nabi et al., 2004). Alterations in serotonin synthesis can lead to developmental delay, which is a trait often associated with ASD. Children normally produce high serotonin levels (app. double than adults) until reaching 5 years of age when the levels

gradually decrease to adult levels, while autistic children produce serotonin increasingly more starting from approximately 2 years till 15 years of age with finally app. 1.5 times the average adult levels (Chandana et al., 2005). This phase of high serotonin levels during early childhood is critical for normal brain development and might be affected in ASD patients, furthermore accounting for increased anxiety (leading to learning deficits), obsessive-compulsive disorder symptoms and repetitive behavior. These changes have not been investigated in mouse models of ASD, but Pfn2 is already expressed in nervous tissue during embryonic development (earliest stage investigated was E13.5, see 2.1.5). The absence of Pfn2 could therefore be responsible for sustained serotonergic activation during embryonic and early postnatal development and consequently for developmental alterations similar to human ASD patients. Serotonin reuptake inhibitors are among the few pharmacological treatments, applied to ASD patients, which contribute to alleviate certain symptoms (Kim, 2015). Interestingly, systemic injection of the SSRI fluoxetine (Prozac) completely rescued the novelty-dependent hyperlocomotion phenotype in adult Pfn2 KO mice (Pilo Boyl, unpublished). Further investigations of the serotonergic system in Pfn2 mutant mice during embryonic development and under pharmacological stimulation could shed light on the impact of Pfn2 to the ASD-associated phenotypes.

The ASD-related Rett syndrome is also associated with the loss of (acetyl-) cholinergic neurons (see 1.3.4) and a reduced ChAT activity in the brain (Nag and Berger-Sweeney, 2007; Zimmerman, 2008). The impact of this system in the Pfn2 KO model for autism spectrum disorders could be interesting, as cholinergic innervations have a widespread and powerful influence throughout the CNS (Supp. Fig. 4). Interestingly, Pfn2 is expressed at low levels in the acetylcholinergic system, which is an exception within the excitatory neuronal systems (see 2.1.1.5, Fig. 14, Fig. 21, Supp. Fig. 12). Alterations in the cortical cholinergic input can lead to cognitive impairments often found in Alzheimer´s dementia and schizophrenia patients, shown in human and rodent studies by performing attention tasks and in mouse models with lesions in the cholinergic brain regions (Sarter and Parikh, 2005). The large impact of cholinergic neurons on cognitive functions has been acknowledged as a result of the specific loss of cholinergic neurons at the initial

stages of Alzheimer´s disease. A known trait of Alzheimer´s disease is in fact cholinergic hypofunction early in the disease propagation (Dineley et al., 2015), leading to the most common Alzheimer treatment of increasing the acetylcholine levels in the brain by pharmacologically inhibiting the enzyme acetylcholinesterase, which inactivates ACh under normal conditions. In autistic patients lower binding of ACh to certain acetylcholine receptors as well as a reduction of their expression level was observed (Dineley et al., 2015; Perry et al., 2001), but further studies are necessary to achieve better insight in the role of ACh in ASD in general and the result of the possibly increased ACh signaling due to the loss of Pfn2.
The expression of Pfn2 could be especially important for fine adjustments of synaptic transmission, since rare cholinergic interneurons of the striatum show higher levels of Pfn2. Cholinergic interneurons are tonically active and stop firing only briefly and upon reward-related dopaminergic input. Pfn2 could be needed to fast and precisely control synaptic vesicle release in these neurons.

Excitatory synaptic circuits are enriched in Pfn2 and upon its removal could therefore all be potentially involved in various ASD-related phenotypes. In order to understand the specific roles of Pfn2 in these systems, a conditional deletion of Pfn2 in individual types of neurons would be necessary to be able to grasp the specific impact of each of these systems to the complex autistic symptoms.

3.1.2 The possible role of Pfn2 in the fine-tuning of cortical and cerebellar circuit activity

The implications of the GABAergic system in ASD are various and highly dependent on the respective neuronal circuitry and the impact of the cell type to the network activity. The best described physiological alteration in ASD is the imbalance of the excitation/inhibition ratio in the brain, which is most often shifted towards a hyperexcitable state. Hyperexcitation could be an effect of increased excitatory activity or a loss of inhibitory signaling. It is conceivable that alterations in either excitatory or inhibitory systems or even the summation of several systems working consecutively could lead to the hyperexcitable state most of the times associated with

ASD and other common neurological disorders (Chao et al., 2010; Hussman, 2001; Lawrence et al., 2010). Alterations in GABAergic signaling could contribute to the autism-like behavior of Pfn2 KO mice especially in certain pathways, since the expression pattern of Pfn2 in the GABAergic system is restricted to very specific neurons (see 2.1.2, Fig. 15-18, Fig. 21, Supp. Fig. 12).

Pfn2 is present in only two rare types of GABAergic cortical neurons, namely Chandelier cells and bitufted neurons (see 2.1.2.1, Fig. 15, Fig. 17). Chandelier cells (axo-axonic neurons) are large, fast-spiking neurons, important for feed-forward inhibition in cortical circuits including sensory information processing (Rudy et al., 2011). These cells are active upon high network activity to spatiotemporally fine-tune cortical circuits (Molnár et al., 2008; Szabadics et al., 2006; Woodruff and Yuste, 2008; Woodruff et al., 2010). Pfn2 in Chandelier cells might be necessary to provide a regulation of fast and precise pre-synaptic actin-dynamics and therefore control cortical network activity. GABAergic bitufted neurons (Double-Bouquet cells in humans) form reciprocal connections with pyramidal neurons (Zilberter et al., 1999) but target also other GABAergic neurons in a dense array of hundreds of synapses formed by a single bitufted neuron (Ballesteros Yáñez et al., 2005; Pesold et al., 1999; Sills et al., 2012; Staiger et al., 2009). Therefore bitufted cells are able to locally and comprehensively regulate cortical neuronal firing, a process which in turn Pfn2 could have a role for precisely regulating synaptic signaling.

In contrast to Chandelier and bitufted neurons, GABAergic basket cells, which are responsible mostly for the synchrony of network activity (Méndez and Bacci, 2011), are generally devoid of Pfn2 (see 2.1.2.1, Fig. 15, Fig. 17).

Similarly to the cortex, the only cerebellar GABAergic neuron type that expresses Pfn2 are Golgi cells, which are rare cells located among the granular neurons in charge of additional modulation of mossy and parallel fiber signaling (Sillitoe et al., 2008). Pfn2 therefore could again have a role for fine-tuning of the cerebellar circuitry.

The excitation/inhibition ratio in the brain is shifted towards an excess of excitation in Pfn2 KO mice. Synaptic signaling of most GABAergic neurons is not directly affected by the loss of Pfn2, but Pfn2 is present specifically in the rare GABAergic neurons that are important for fine-tuning of the respective brain circuitry, which could be altered in consequence to the deficiency of Pfn2. If these rare GABAergic neurons

would also be hyperexcitable in Pfn2 deficient mice, their increased local inhibition probably does not significantly alter the global excess of excitation. Therefore these cells cannot counterbalance the ASD-associated imbalance in the excitation/inhibition ratio. The exact function of Pfn2 in GABAergic cells might also be different from excitatory neurons. Further studies using a conditional knock-out mouse model for Pfn2 in GABAergic neurons will be necessary to examine the specific role of Pfn2 in the rare cortical and cerebellar GABAergic neuron types that endogenously express Pfn2.

3.1.3 The potential role of Pfn2 in motor coordination

Pfn2 was shown to be upregulated specifically in striatal medium spiny neurons of a 3-nitropropionic acid (3NP)-induced neurodegeneration model of Huntington´s disease in the rat (Chakraborty et al., 2014b). Striatal neurons show an interesting expression pattern of Pfn2 (see 2.1.2.2, Fig. 16) that could suggest a direct involvement of Pfn2 in MSN-mediated motor functions. MSNs are divided into two groups, expressing either D1 receptors, denser in the caudate putamen (dorsal striatum, CPu) than in the nucleus accumbens (ventral striatum, NAc), or D2 receptors, denser in the NAc than in the CPu. Only the $D2R^+$ MSNs of the CPu are devoid of Pfn2.

The loss of Pfn2 could lead to hyperactivity of MSNs, either due to alterations of intrinsic synaptic properties or due to the increase of dopaminergic input into the striatum. Among MSNs, the balance of $D1R^+$- and $D2R^+$- neuronal activity mediates the regulation of motor functions through the direct and indirect pathways (Kreitzer, 2009; Sano et al., 2003). Striatal efferents of the direct pathway coordinate motor functions via disinhibition of the motor cortex – involving a direct signaling through the internal globus pallidus and the thalamus to the cortex –, while the indirect pathway act via a feed-back loop between the external globus pallidus and the subthalamic nucleus back to the internal globus pallidus, the substantia nigra and the thalamus to inhibit cortical motor circuits. Therefore, immediate motor responses are activated by the direct pathway, such as anxiety, fear and flight responses, while the indirect pathway is mostly involved in tasks like motor learning and activity planning (Ena et al., 2011). As a result of the specific expression pattern of Pfn2 in MSNs, the motor

alterations of Pfn2 KO mice could be linked to the specific pathway, in which the Pfn2-expressing cells are involved. Since Pfn2 is found predominantly in $D1R^+$-MSNs, motor dysfunctions in Pfn2 KO mice are more likely to involve the direct pathway. Hence, the dysfunction of the direct pathway could be partially responsible for behavioral abnormalities of Pfn2 KO mice, such as hyperlocomotion, increased response to novel stimuli and panic behavior.

The association of MSNs with motor functions can also be acknowledged by the various mouse models involving the different dopamine receptors. D1R KO mice show deficits in spatial learning, movement initiation and response to stimuli (Drago et al., 1998a). The targeted ablation of $D1R^+$-MSNs causes severe abnormalities with bradykinesia, dystonia and myoclonic jerks (Drago et al., 1998b). On the contrary, the ablation of $D2R^+$-MSNs in mice induces a hyperactivity phenotype and a reduced sensitivity to dopaminergic stimulation (Sano et al., 2003). Possibly, the deletion of Pfn2 leads to hyperactivity in these MSNs that are normally Pfn2-positive, inducing an opposing effect to the KO of dopamine receptors or ablation of MSNs in mice, resulting in the behavioral phenotypes of Pfn2 KO mice mentioned above.

A type of rare interneuron located throughout the whole striatum is the GABAergic aspiny interneuron, which is fast-spiking and aids to regulate the proper function of MSNs by local inhibition. The loss of Pfn2 in these cells could therefore also lead to a more pronounced dysregulation of the signal propagation in MSNs.

3.1.4 Glial cells are not directly responsible for ASD-associated phenotypes due to the loss of Pfn2

The population of glial cells in general is also a target of autism research, since several behavioral endophenotypes of ASD could be contributed by the various types of glial cells. A role of Pfn2 in glial cells is not directly responsible for with this phenotype, since Pfn2 was found to be completely absent from these cells (see 2.1.4, Fig. 19, Supp. Fig. 12).

Astrocytes are the glial cells responsible for neurotransmitter clearance at the synaptic cleft and part of the so-called tripartite synapse (pre- and post-synaptic sites together with an astrocytic process). A dysfunction of potassium clearance from the extracellular space by astrocytes leads to a rise of extracellular potassium concentrations that can cause epileptic seizures by impairing neuronal repolarization efficiency (Rossi and Volterra, 2009; Schousboe, 2003). Similarly an excess of glutamate resulting from disturbed clearance of the extracellular space by astrocytes can cause excitotoxicity or epileptic seizures. Seizures, in turn, are known to induce astrogliosis (Sofroniew and Vinters, 2010; Zeidán-Chuliá et al., 2014), which was absent in Pfn2 KO mice (data not shown).

Even though a function of Pfn2 was proposed in cultured astrocytes (Schweinhuber et al., 2015), a direct role of Pfn2 in mature astrocytes could be ruled out *in vivo*, since these cells are devoid of Pfn2. Cultured astrocytes are isolated from embryonic brain tissue, in which mature astrocytes that can be found in adult tissue have not developed, yet. Embryonic brains contain radial glia, embryonic stem and precursor cells, which give rise to the astrocytic cultures. Cultured astrocytes are therefore still radial glia-like, which is probably why they express Pfn2 (see 2.3.2, Fig. 26), while mature astrocytes *in vivo* lack its expression (see 2.1.4, Fig. 19).

Synaptic transmission is influenced by many parameters, including maturation of synapses also mediated by microglial pruning (Rossi and Volterra, 2009; Salter and Beggs, 2014; Zeidán-Chuliá et al., 2014; Zhan et al., 2014) and by a mechanism involving myelination provided by oligodendrocytes. Indeed, excessive myelination of a particular brain region (left and right medial frontal cortex) and a loss of myelination of another region (left temporo-parietal junction) was also observed in children diagnosed with autism spectrum disorder (Zeidán-Chuliá et al., 2014). Even NG2 cell differentiation to oligodendrocytes, which re-myelinate neurons at the lesion site, could be important for certain aspects of ASD symptoms, since an increase in NG2 cell number was observed in a mouse model for ASD (Bergles et al., 2010; McFarlane et al., 2008; Nishiyama et al., 2009; Pedraza et al., 2008; Zeidán-Chuliá et al., 2014). But Pfn2 is absent from all these cell types, therefore glial cells have no direct influence on the autistic-like phenotype that arises in consequence of a deficiency of Pfn2. Nevertheless glial cells in other mouse models or in human patients could still feature certain Pfn2-independent roles in ASD-related symptoms.

3.1.6 Neural stem cells as a novel field of research for ASD

An interesting observation was the expression of Pfn2 in neural stem cells both in embryonic (radial glia) and adult (aNSCs) tissue (see 2.1.5, Fig. 20, 21, Supp. Fig. 12). Detailed studies revealed a differentiation state-dependent expression of Pfn2, which is present at moderate levels in NSCs, absent from NSC-derived progenitor cells and upregulated again upon the final differentiation to neurons.

Pfn2 does not necessarily have a decisive role during neuronal or glial cell differentiation, as all major cell types were present in Pfn2 KO mice (data not shown). Pfn2 could be important for the maintenance of the highly proliferative state and/or the differentiation of neural stem cells. An interesting observation was the upregulation of two transcription factors important for multipotency (Sox2 and Oct4) in NSCs of Pfn2 KO mice (see 2.1.5, data not shown).

The loss of Pfn2 in NSCs could have several possible consequences. Pfn2 is normally upregulated upon progenitor differentiation to post-mitotic neurons (see 2.1.5, Fig. 20), possibly in consequence to differentiation-associated cytoskeletal remodeling. Therefore, the KO of Pfn2 could lead to cytoskeletal changes in NSCs accompanied by diminished differentiation, which can be observed by the increase in transcription factors in NSCs necessary for the maintenance of pluripotency. A possible consequence could be a decreased asymmetric cell division (differentiation) of NSCs and therefore the loss of newly generated progenitor cells and neurons.

On the other hand, the upregulation of transcription factors important for the stemness (potential to differentiate into all types of progenitor cells) that was observed in NSCs of Pfn2 KO mice is generally associated with a high proliferation of NSCs. The pool of NSCs at the SVZ could therefore be enlarged in Pfn2 KO mice. These possible outcomes of Pfn2 deletion should be investigated further in more detail.

During the migration phase, progenitor cells travel along the RMS at a speed of up to 0.5-1 mm per day (22.8 µm/h), so that proliferation is nearly absent (Luskin and Boone, 1994). Pfn2 is suppressed during the migration of progenitors, which is in agreement with the proposed inhibitory role of Pfn2 in migration processes involving the invasiveness of epithelial tumor formations (Mouneimne et al., 2012). Migration

processes seem to require Pfn1 rather than Pfn2, as could be shown by neuronal migration deficits in mutant mouse lines of Pfn1 ($Pfn1^{+/-}$ and $Pfn1^{flx/flx;Nes\text{-}Cre}$ mice) (Kullmann et al., 2011, 2012; Pilo Boyl et al., 2007).
At their final destination, progenitor cells upregulate Pfn2 upon differentiating to post-mitotic neurons, indicating a role of Pfn2 in developmental processes like axonal vs. dendritic polarization or synaptogenesis. Pfn2 KO neurons do not show gross morphological abnormalities (2.3.1, data not shown), but Pfn1 could compensate to a certain degree for the loss of Pfn2. In fact, $Pfn2^{-/-}$/ $Pfn1^{flx/flx;Nes\text{-}Cre}$ double KO mice are embryonic lethal (Pilo Boyl, unpublished observation), which suggests at least a compensatory role of Pfn2 in developmental processes.

A potential contribution of Pfn2 in the development of neuronal circuits is in agreement with autism etiology, which is commonly believed to be of neurodevelopmental origin with dysregulation and imbalance of neuronal network activities. Also epileptic seizures often originate from impairments in neuronal network integrity due to developmental alterations, in which neural stem cells are majorly involved (Ma et al., 2009; Ming and Song, 2011).
In conclusion, a novel involvement of NSCs in ASD could be hypothesized with a potential role of Pfn2 in embryonic and adult neurogenesis.

3.2 The P2-GFP fusion protein is a validated tool for further studies on the roles and functions of Pfn2

A part of the thesis project was the characterization of the biochemical properties of the P2-GFP fusion protein. The P2-GFP fusion protein knock-in mouse model was generated mainly in order to visualize Pfn2 either *in vitro* or *in vivo* (see 1.5, Fig. 13), but the fusion of the GFP-tag to the protein of interest often affects the expression level and/or the function of the targeted protein as well as its interaction with potential binding partners due to steric or ionic interference of the GFP moiety. Indeed, homozygous P2-GFP KI mice show mild behavioral abnormalities, in particular a low degree of hyperexcitability and transiently increased exploratory behavior, but no changes in anxiety, fear or working memory (Özer, unpublished). These are only

moderate behavioral alterations in comparison to Pfn2 KO mice that show complex ASD-related phenotypes, pointing to a substantial expression and functionality of the P2-GFP fusion protein. Nevertheless, in order to study Pfn2 using the P2-GFP KI model as a tool, the expression and functionality of the P2-GFP fusion protein was accurately verified (see 2.2, Fig. 22-24).

3.2.1 Sufficient expression levels of the P2-GFP fusion protein

The first problem encountered studying the P2-GFP fusion protein was the limited capability of the anti-Pfn2 antibodies currently used in the lab to recognize it in Western blotting. Therefore, several anti-Pfn2 antibodies were analyzed for their recognition efficiency of P2-GFP in comparison to Pfn2. While most antibodies failed to bind to P2-GFP, two polyclonal antibodies (anti-Pfn2 3003 and anti-Pfn2 GD2) were able to sufficiently recognize P2-GFP, although less efficiently than the wt isoform (see 2.2.1, Fig. 22). The GFP moiety (27 kDa) is fused to the C-terminus of Pfn2 (14 kDa) creating the P2-GFP fusion protein, therefore especially C-terminal antibody-binding epitopes could be shielded and only anti-Pfn2 antibodies targeting farther located epitopes could possibly efficiently bind to P2-GFP.
This phenomenon is not unique for Pfn2. A similar problem was encountered while generating a GFP-actin fusion protein mouse model (Gurniak and Witke, 2007), where some anti-actin antibodies were not able to recognize the fusion protein on Western blots.
Secondly, the expression level of P2-GFP in comparison to Pfn2 was calculated using brain tissue extracts from heterozygous P2-GFP KI mice probed with the antibodies directed against Pfn2 that were previously verified to bind most efficiently also to P2-GFP (see 2.2.1-2.2.2, Fig. 22). The results are very promising, since the GFP moiety is not interfering substantially with the expression of the P2-GFP fusion protein. Heterozygous P2-GFP KI animals still express 43% (± 2.7%) of P2-GFP compared to Pfn2. This level of expression can be considered quite high compared to other GFP fusion protein KI mouse models (Chan et al., 2004; Gurniak and Witke, 2007). Pfn2 was estimated to be present in most cells at very high concentrations (2-10 µM) (Mogilner and Edelstein-Keshet, 2002; Pollard et al., 2000), which means that the P2-GFP mutant mice would still express P2-GFP in quite high amounts that are

sufficient to study its cellular functions. There are indications that homozygous P2-GFP KI mice express P2-GFP at even higher levels than heterozygous P2-GFP KI mice, as homozygous KI mice are only able to produce the fusion protein without possible compensatory expression of Pfn2 (data not shown).

3.2.2 P2-GFP binding to Poly-L-Proline stretches is only slightly impaired

Even though the expression level of P2-GFP is adequate in comparison to Pfn2, the main effect of the GFP moiety (27 kDa) on a smaller protein, such as Pfn2 (14 kDa), could easily be an impairment of its functionality by interfering with interaction partners. One of the best characterized binding domains of profilins is their poly-L-proline interaction site that can be exploited for *in vitro* Pfn2 pull-down experiments using poly-L-proline stretches immobilized on beads. The results shown in this thesis demonstrate that binding efficiency of the fusion protein to poly-L-proline is up to 75% of that of Pfn2 (see 2.2.3, Fig. 23). The poly-L-proline binding domain of Pfn2 is composed of both a C- and an N-terminal helix (see 1.3). Since the GFP-tag is fused to the C-terminus of Pfn2 in the P2-GFP fusion protein, at least three hypotheses are possible to explain the slight reduction of binding efficiency: either the formation of the PLP-binding groove is disturbed or the GFP moiety could sterically hinder the access of the PLP stretches to the domain, or finally, since long proline-rich stretches can accommodate several adjacent profilins in very close proximity, the GFP moiety could increase the spacing between them, thus reducing the pull-down efficiency. From the binding efficiency of P2-GFP to its ligands *in vivo*, as determined by immunoprecipitation (see 2.2.4, Fig. 24) and discussed below, the latter two hypotheses appear more plausible.

The interaction with G-actin, on the other hand, is unimpaired. PLP-beads are known to be able to pull down the profilactin complex with profilin and actin in a 1:1 ratio (Janmey, 1991). Based on this fact, the observed reduction of the signal for actin in the P2-GFP-bound fraction to 73% of the signal of Pfn2-bound actin is due to the decrease in PLP-binding efficiency of P2-GFP rather than actin binding itself. When corrected for the PLP-binding efficiency of P2-GFP, actin binding to P2-GFP shows nearly 100% efficiency. The GFP moiety is therefore not interfering with the actin

binding efficiency of the P2-GFP fusion protein. This outcome was expected, as the actin binding domain on Pfn2 is located on the opposite side of the PLP-binding domain and is therefore not inhibited by the GFP-moiety that is located on the C-Terminus near the PLP-binding site.
The P2-GFP fusion protein is therefore mainly functional *in vitro* and only slightly reduced in its ability to bind to poly-L-proline stretches.

3.2.3 P2-GFP binds only specific proline-rich ligands with reduced affinity

In order to finally characterize P2-GFP properties in more physiological conditions, an immunoprecipitation assay was performed, verifying the binding of P2-GFP to a variety of known interaction partners of Pfn2. P2-GFP is able to bind to various known ligands of Pfn2, but with varying efficiency (see 2.2.4, Fig. 24). In particular, interaction partners with a high molecular weight are the most affected (i.e. huntingtin, mDia1 and dynamin1). The non-proline residues in proximity of the proline-rich domains of the ligands are known to mediate the specificity and binding efficiency to the proline-binding domain of Pfn2 (Kursula et al., 2008, Massimi, unpublished). These interactions could influence the binding strength of P2-GFP with certain ligands to a greater extent than with others, since the GFP-tag could sterically interfere (e.g. on proteins like mDia1, which can accommodate an array of up to 13 Pfn2 proteins in close proximity (Kursula et al., 2008), but also add repulsive charges in the vicinity of the binding domain.

Confirming the results from the pull-down assays (see 2.2.3, Fig. 23), actin interacts equally well with Pfn2 and P2-GFP. The actin-binding domain of P2-GFP is therefore functional in the cell, as expected from its location opposite of the PLP-binding domain and the GFP moiety.
P2-GFP can also co-precipitate all investigated components of the WAVE- complex. It is not yet understood, how Pfn2 is binding to the WAVE- complex. The WAVE and Abi subunits are not accessible to profilins when incorporated in the WAVE-complex (Innocenti et al., 2004), but there are indications by pull-downs using Pfn2-beads that

the interaction occurs either with the CyFIP or the Nap1 subunits. Interestingly, specifically the interaction of Abi1 with P2-GFP was inhibited by the GFP-tag. If the incorporation of Abi1 into the WAVE- complex would be hindered, the proper function of the WAVE- complex in promoting actin polymerization through the Arp2/3-complex could be impaired, resulting in dysfunctional actin dynamics. More likely, the interaction of P2-GFP with free Abi1, that was not incorporated in the WAVE-complex, is diminished, since the remaining components of the WAVE- complex were all unaffected. The potential outcome of the loss of this specific interaction should be investigated in more detail in the future.

An interesting observation was the high loss of mDia1 in the P2-GFP-bound fraction. The formin mDia1 contains an array of 13 proline-rich binding domains for Pfn2 (Kursula et al., 2008), which means, since mDia1 is mostly present *in vivo* in a dimerized form, that 26 Pfn2 molecules could possibly interact with a single mDia1 dimer. The closely localized proline-rich domains of mDia1 imply a steric hindrance of the GFP moiety that decreases the binding efficiency of P2-GFP. On the other hand, the interaction with mDia2 or Mena was undisturbed by the GFP moiety, possibly due to a wider spacing between the proline-rich regions.

During this thesis work, a novel interaction partner of Pfn2 was discovered. The F-actin and Arp2/3- complex interacting protein cortactin was enriched in P2-GFP complexes.

As a consequence of the largely uninhibited interaction of protein ligands involved in actin dynamics with P2-GFP, only minor alterations in cytoskeletal functions would be expected in this fusion protein knock-in mouse model.

The mild behavioral hyperexcitability phenotype of P2-GFP KI mice raises the question if P2-GFP is able to interact with synaptic proteins in a similar way as Pfn2. Especially certain synaptic proteins (dynamin1, endophilin1 and huntingtin) were found to be binding less efficiently to P2-GFP than to Pfn2. This weaker interaction could therefore account for synaptic dysfunctions leading to the minor increase in novelty-induced excitability and locomotion of (homozygous) P2-GFP KI mice. Based on this hypothesis, the complete loss of these interactions could contribute to the stronger behavioral phenotype of Pfn2 KO mice. Nevertheless, an indication of the

functionality of the P2-GFP fusion protein *in vivo* is the unimpaired binding of the synapsin isoforms Syn1 and Syn2a.
Since it has been shown that the GFP-tag of P2-GFP has only a minor effect on the ligand binding properties of the fusion protein, the P2-GFP KI mice can be considered a validated tool for any further investigations regarding Pfn2 trafficking and dynamics *in vivo*. Furthermore, the GFP moiety can be exploited as a target for pull-down or immunoprecipitation experiments. For the analysis of protein complexes associated with Pfn2 this approach could be very beneficial, since no ligand loss would occur due to binding to an epitope by an antibody and it seems that only few and specific ligands are affected by the GFP-tag, while the efficiency of the GFP-Trap IP system is very high.

3.3 Diverging roles of Pfn2 throughout neuronal development

Pfn2 is highly expressed in neuroectodermal embryonic tissue and later in neural stem cells and post-mitotic neurons. A role of Pfn2 in developmental processes could therefore be assumed. Neuronal development can be studied in great detail in primary hippocampal neurons in culture, which during the developmental stages undergo changes considered to be very similar to neurons *in vivo*. These cells are able to reach mature stages including synaptogenesis and form complex neural networks, which makes them a valuable model for the investigation of the different roles that Pfn2 could have throughout the different stages of neuronal development as well as in maturity.

3.3.1 The loss of Pfn2 induces accelerated neuronal development

The loss of Pfn2 causes an accelerated developmental phenotype in cultured neurons, since Pfn2 KO neurons appeared to develop the characteristic features of the respective developmental stages in a shorter time period than wt neurons. Pfn2 KO cells were forming more initial neurites that extended at a higher velocity and showed more complex branching compared to wt neurons during each investigated developmental stage (see 2.3.1, Fig. 26).

The observed increase in initial neurite number upon deletion of Pfn2 is in agreement with previous findings (Pilo Boyl et al., 2007). Neurite sprouting and initial elongation (DIV 1-3) are processes well-known to be dependent on cytoskeletal dynamics (Bellot et al., 2014; Bradke and Dotti, 1999, 2000; Cingolani and Goda, 2008; Coles and Bradke, 2015; Ertürk et al., 2007, 2012; Hellal et al., 2011; Pilo Boyl and Witke, 2014; Schubert and Dotti, 2007; Schubert et al., 2006; da Silva and Dotti, 2002; Witte and Bradke, 2008; Witte et al., 2008). In consequence to the loss of Pfn2, it has been proposed that filamentous actin networks become less stable (Da Silva et al., 2003), possibly facilitating the growth of microtubuli that are the main cytoskeletal component necessary for neurite formation and elongation, resulting in more and longer processes (app. 20-25%, see 2.3.1). In fact, Pfn2 is enriched in the growth cone of wt neurons (see 2.3.2, Fig. 27), therefore the loss of Pfn2 could lead to disturbed growth cone dynamics due to local actin instability and effectively enhance tubulin filament outgrowth.

After one week in culture (DIV 7), the Pfn2 KO cells resemble wt cells that have been cultured for close to two weeks. Pfn2 KO neurites elongate to a maximal distance similar to wt neurites (app. 700 µm), but already form extensive branching, mostly proximal to the soma. The developmental program is therefore undisturbed in Pfn2 KO neurons, but the stages appear to be reached at advanced time points in comparison to wt cells.

Similarly, after two weeks in culture (DIV 14), the Pfn2 KO cells remind of nearly fully mature neurons with complex arborizations over the full range of the dendritic tree, which is characteristic of the third week in culture (DIV 21) in wt neurons. The cells are also able to start synaptogenesis, since synaptic protrusions appear on the projections (data not shown).

Finally after three weeks in culture, Pfn2 KO cells become nearly indistinguishable from fully mature wt neurons, except for the most distal part of the dendrite network. Therefore, Pfn2 KO cells do not extend their dendritic network beyond the usual average range of mature wt neurons, and develop extensions with similar length and complexity as wt neurons. The loss of the most distal branches in Pfn2 KO neurons could originate either from a gradual degradation of their processes beginning at the most distal part, reminding of wt neurons that are past the fourth week in culture, or

from problems establishing complex branches at the most distal dendritic segments (app. the last 250 µm) possibly due to impairments in actin-dynamics.

In this study, the loss of Pfn2 therefore leads to a different phenotype than reported in a previous study, where the knock-down (KD) of Pfn2 in hippocampal CA1 neurons in organotypic slice cultures (to app. 70% of baseline level due to silencing using plasmid for shRNAs delivered by the gene gun approach) induced a mild reduction of dendritic complexity (app. 30%) and spine number (app. 20%) (Michaelsen et al., 2010). The hippocampal slices cultures were prepared at postnatal day 6 (P6) and transfected after 5 more days inducing the KD of Pfn2, when the neuronal projections are mostly developed. Therefore, hippocampal neurons in culture could lead to different results, since Pfn2 is completely deleted already at the beginning of the development and the cells have to newly establish their neurites while Pfn2 is absent. In contrast to partial loss of Pfn2 in organotypic brain slices (Michaelsen et al., 2010), the complete loss of Pfn2 in mice induced no changes in the number of synaptic terminals (Pilo Boyl et al., 2007).

Considering the expression of Pfn2 during development *in vivo* (see 2.1.5, 3.1.6, Fig. 20-21), the loss of Pfn2 could induce an accelerated neuronal development during embryonic development as well. Synaptogenesis could also be affected by the absence of Pfn2, since local actin-polymerization at synaptic terminals, in which Pfn2 is normally enriched (see 2.3.2, Fig. 27), could be dysregulated. It would be interesting to analyze synaptogenesis in detail (i.e. the time point of synapse formation and the number of synaptic protrusions). An earlier onset of synaptogenesis *in vivo* could lead to the observed excess of synaptic activity and hyperexcitability of Pfn2 KO neurons (Pilo Boyl et al., 2007), ultimately resulting in autistic-like behavior in adulthood.

P2-GFP KI neurons were analyzed as well to verify the proper development of the KI mouse model. The cells displayed an intermediate phenotype between wt and Pfn2 KO neurons. They did not develop a higher number of initial neurites, but showed a similar increase in neurite elongation as Pfn2 KO cells. A moderate increase in proximal neurite complexity was visible in P2-GFP KI neurons until the second week in culture. The cells started to degenerate during the third week in culture, possibly due to a technical bias in the culture conditions. The P2-GFP fusion protein is likely to cause impairments in actin-polymerization only to a moderate degree, which is

enough to trigger enhanced neurite elongation and proximal branching, but not severe enough to induce the accelerated development and extensive branching of Pfn2 KO neurons.

3.3.2 Enrichment of Pfn2 in neuronal substructures is mostly dependent on excitatory stimuli and depolarization

Taking advantage of the validation of the P2-GFP KI mouse at the biochemical (see 2.2, 3.2), developmental (2.3, 3.3.1) and behavioral (Özer, unpublished) level, the trafficking of P2-GFP was visualized in mature primary hippocampal neurons following different stimulations.

Under normal culture conditions of primary hippocampal neurons Pfn2 is found mostly in dendritic projections, but also in moderate amounts in pre- and post-synaptic specializations, while axonal shafts show only minor levels of Pfn2 (see 2.3.2-2.3.3, Fig. 27-29). Pfn2 therefore is localized majorly on the post-synaptic compartments of neurons. All the more striking is therefore the quick and efficient trafficking of Pfn2 into axonal shafts and pre-synaptic boutons upon exposure to specific stimulatory agents (see 2.3.3, Fig. 28-29).
Stimulating neurons with glutamate or NMDA causes excitatory post-synaptic potentials (EPSPs), which can lead to action potentials, if the stimulation is provided for an appropriate duration. Action potentials in turn require the activity of axons and pre-synaptic boutons. Prolonged post-synaptic stimulation can therefore have an effect on pre-synaptic compartments as well. The enrichment of Pfn2 not only in post-synaptic sites but also in axons and pre-synaptic terminals can therefore be induced also by post-synaptic stimulation.

A different effectiveness of different excitatory stimulatory agents on neuronal activity can be observed on Pfn2 as well. Post-synaptic stimulation by the application of glutamate (with or without glycine) induced the strongest trafficking of Pfn2 to pre-synaptic boutons, followed by direct pre-synaptic stimulation by increasing the extracellular potassium concentration. Moderately effective results were obtained

from the addition of NMDA and increasing the Ca/Mg ratio to 7:1 in the medium. The differences in the effects of these excitatory stimulations are due to the activation of different pathways in the neurons.

High levels of extracellular potassium lead to inward flow of potassium inducing a strong depolarization and synaptic vesicle release probably by opening pre-synaptic voltage-gated Ca^{2+}- channels (Oltedal et al., 2008). Glutamate activates several kinds of post-synaptic receptors (NMDAR, AMPAR, kainate receptors and metabotropic glutamate receptors (mGluRs)) (see 1.4.1), which mediate a strong depolarization (EPSPs) of the cells, ultimately increasing action potential firing rates and raising F-actin levels (Bellot et al., 2014; Schubert and Dotti, 2007). NMDA is specifically activating NMDARs but not the remaining glutamate receptors. Specific activation of NMDARs induces re-localization of AMPARs, actin polymerization and cytoskeletal reorganization associated with synaptic plasticity changes (Bosch et al., 2014; Zhou et al., 2009). Therefore the strong trafficking of Pfn2 into neuronal compartments induced by glutamate stimulation and the observed moderate effect of NMDA on the trafficking of Pfn2 leads to the conclusion that NMDARs definitely have an influence on Pfn2 trafficking, but is not the only pathway that is contributing to Pfn2 re-localization. The activity of other glutamate receptors is therefore likely to contribute to Pfn2 trafficking as well. Neuronal stimulation of AMPA receptors alone has already been shown to have no significant effect on Pfn2 trafficking (Ackermann and Matus, 2003). It can be hypothesized that a combination of not only the activity of NMDARs, but also the activity of kainate receptors and/or mGluRs are able to efficiently induce Pfn2 re-localization into neuronal substructures.

Increasing the Ca^{2+}/Mg^{2+} ratio to 7:1 in the extracellular space probably induces the removal of the Mg^{2+} blockade of NMDA receptors, leading to a higher excitability of the neurons.

It is noteworthy that Pfn2 is more rapidly enriched in synaptic boutons and spines than in axons by excitatory stimuli, as can be seen e.g. by an excess of Ca^{2+} in the medium, which triggered re-localization of Pfn2 to boutons and spines after 10 min. of the exposure, while axonal shafts could be seen enriched in Pfn2 after a minimum of 30 min. after stopping the stimulation exposure by medium exchange (see 2.3.3, Fig. 28). Even glutamate that triggered the strongest enrichment of Pfn2 in pre-synaptic

sites already after 5 min. of exposure was able to induce the trafficking and/or expression of Pfn2 in axons only after 1 h subsequently to the end of glutamate application by the exchange of the medium. Similar results were obtained by NMDA stimulation that induced enrichment of Pfn2 in axonal shafts after an incubation of 30 min. to 1 h after removal of the stimulus. With increasingly elapsed time, Pfn2 might therefore be transported to axonal shafts either as a reserve for fast trafficking into boutons upon high activity, or to stabilize the axonal projections in consequence to prolonged agonist exposure and increased neuronal activity. The presence of *Pfn2* mRNA in axonal shafts of developing neurons has been reported (Wang et al., 2014). *Pfn2* mRNA is still present in mature neurons, the necessary Pfn2 could also be locally expressed from the mRNA upon stimulation-induced increased neuronal activity.

In excitatory post-synaptic spines, an enrichment of Pfn2 was observed induced by either de- or hyperpolarization of the cells (see 2.3.3, Fig. 28-29). This enrichment of Pfn2 was most pronounced by application of glutamate or an excess of potassium and can still be seen even 1-2 h after the exposure to the stimuli (i.e. glutamate and NMDA). A role of Pfn2 in spines is expected for actin-dependent synaptic plasticity. Pfn2 could either be necessary during the stabilization of the spine structure by enhancing actin polymerization, or Pfn2 could be important for the formation and/or maintenance of spine structure, where it is known to interact with a variety of proteins involved in cytoskeletal dynamics, such as ROCK (Schubert et al., 2006; da Silva and Dotti, 2002), the Arp2/3-complex and formins (Witke, 2004). Also an overexpressed, GFP-tagged version of Pfn2 could be induced in a previous work to localize to dendritic spines by KCl or NMDA treatment as well as by electric LTP and LTD protocols (Ackermann and Matus, 2003). More recently, profilin (isoform not specified as Pfn1 and/or Pfn2) was also re-localized to dendritic spines in an activity-dependent manner (NMDA treatment) (Michaelsen et al., 2010).

In post-synaptic sites it is well established, and was observed following neuronal stimulation in the experiments presented here (2.3.3, Fig. 28-29), that F-actin levels increase in an activity-dependent manner (Bellot et al., 2014; Bosch et al., 2014; Cingolani and Goda, 2008; Pilo Boyl and Witke, 2014; Schubert et al., 2006). Similarly, pre-synaptic terminals are believed to contain an actin meshwork, which is

essential to maintain the separation of the large reserve pool of synaptic vesicles from the smaller readily releasable pool of docked/primed vesicles at the pre-synaptic membrane as well as the tightly regulated flow of synaptic vesicles between these pools and the vesicle reuptake process (see 1.4.1). Consequently following excitatory stimuli, Pfn2 enrichment in spines and in axons and pre-synaptic terminals might be needed in order to contribute to the regulation of actin dynamics following stimulation-induced enhanced neuronal activity. Murk et al. reported a similar re-localization of Pfn2 to pre-synaptic terminals following KCl treatment (Murk et al., 2012), which is compliant with the results of the present study. In pre-synaptic boutons it could be hypothesized that Pfn2 is needed for the regulation of synaptic activity by stabilizing and enhancing the rapid formation of a pre-synaptic actin network between the two synaptic vesicles pools in order to limit excessive vesicle release that would otherwise be triggered by the stimulation. In line with this hypothesis, the loss of Pfn2 *in vivo* showed a complex phenotype of enhanced synaptic vesicle release and lack of F-actin formation upon stimulation of synaptosomes (Pilo Boyl et al., 2007), while loss of Pfn1 had no effect on excitatory synapse morphology and physiology (Görlich et al., 2012). Pfn2 therefore has an inhibitory role on synaptic vesicle exocytosis possibly by enhancing the formation of actin filaments and thereby strengthening the actin network in pre-synaptic terminals. In Pfn2 KO animals the pre-synaptic actin network could be disturbed leading to the observed excessive synaptic vesicle release, which is the cause of the hyperexcitability and autistic-like behavior of the Pfn2 KO mice.

Pre-synaptic vesicle release can be triggered in the millisecond range (Südhof, 2013), while already within 2 min. 85% of post-synaptic actin is exchanged at dendritic spines (Cingolani and Goda, 2008). Therefore these enormously dynamic processes need to be regulated precisely. The proposed role of Pfn2 in the regulation of fast actin dynamics and remodeling (see 3.1.2-3.1.4) could be further emphasized by the observed enrichment of Pfn2 upon stimulated neuronal activity in synaptic terminals, where the regulation of actin dynamics is necessary.

Consequently to the chemical induction of LTD, Pfn2 levels are also increased in pre-synaptic boutons but reduced in axons (see 2.3.3, Fig., 29). Pfn2 could play a role in

the inhibition of vesicle release, as proposed above, by enhancing the restraining actin network in pre-synaptic boutons also in consequence to LTD. In axons, on the other hand, LTD might induce less dynamic changes in actin filament turnover and Pfn2 is not essential at this point. On the post-synaptic site a moderate enrichment of Pfn2 could be observed. Pfn2 could contribute to the cytoskeletal reorganization necessary for LTD-induced shrinkage of post-synaptic spines. Over extended durations, LTD causes a shift of the G/F-actin ratio towards G-actin in spines (Cingolani and Goda, 2008) that needs to be sequestered and recharged by an ADP-ATP exchange, at which point the contribution of Pfn2 could be essential. For example, Pfn2 could also have a possible function in the process of unsilencing of synapses after the immediate effects of LTD.

Neurons also do not show any excitotoxic effects prior to 18 h after the induction of chemical LTD, but protein degradation, the inhibition of local translation and a decrease in synaptic plasticity are immediate consequences of LTD (Shehata et al., 2012). Hence, Pfn2 could also be degraded in neurons, which could be observed by reduced overall levels of Pfn2 (see 2.3.3).

An impairment in LTD in dendritic spines can also cause hyperexcitability (Sano et al., 2003), but the loss of Pfn2 is known to have no effect on LTP or LTD (Pilo Boyl et al., 2007). Hence, the contribution of Pfn2 in pre- rather than post-synaptic sites is mostly responsible for the hyperexcitability phenotype in Pfn2 KO mice.

The application of GABA to neuronal cultures leads to a reduced excitability of the cells and coincided with a diminished expression of Pfn2. The hyperpolarization (IPSP) of the neurons caused by a treatment with GABA had no effect in boutons, but Pfn2 was potently enriched in axons and moderately in post-synaptic terminals (see 2.3.3, Fig. 29). The enrichment of Pfn2 in axons following GABA treatment could be due to a reorganization of actin filaments, but more detailed studies are necessary to understand the specific pathway. Pfn2 could be needed to form new filopodial protrusions that are needed to sample the environment for active neuronal projections and to establish new active synaptic contacts, as existing synaptic connections were silenced by the GABA-induced hyperpolarization.

In conclusion, trafficking of Pfn2 into both pre- and post-synaptic compartments as well as axonal shafts can be observed mostly following excitatory stimuli (both pre- and post-synaptic stimulation) but also to a minor extent using inhibitory stimulation. Therefore, Pfn2 is responsive to neuronal activity.

3.4 Outlook on the future research directions to further understand the various roles of Pfn2 in neuronal circuits and its implication in ASD

Several approaches would shed additional light on the role and function of Pfn2 also with respect to autism and epilepsy. Removal of Pfn2 does not have an evident effect on neuronal survival, since the different neuronal populations investigated in this study are still present in Pfn2 KO mice, but certain neuronal subtypes could still be affected. Either their cell number could be reduced, e.g. in consequence to the excess of excitation and the resulting excitotoxicity or by the effects of epileptic seizures, or the connections of certain pathways are altered. Especially the number and distribution of NSCs should be examined further in Pfn2 KO mice, since this work also yielded indications that NSC number and the level of certain transcription factors (Oct4 and Sox2) might be altered in the KO mouse model. A higher number of NSCs could be expected, if the stem cells are driven to a hyperproliferative state by the loss of Pfn2. If the deletion of Pfn2 has negative effects on differentiation, e.g. due to impaired actin remodeling during asymmetric cell division, the number of progenitor cells in the RMS would be reduced in Pfn2 KO mice.

The Pfn2 KO mouse model is a conventional KO, with deletion of Pfn2 in all cells that express Pfn2 at any time point throughout development. A conditional KO mouse model could be very useful to induce Pfn2 deficiency in specific cell types, populations or brain regions. The resulting changes would affect only certain neuronal circuits that might give rise to only a subset of symptoms. The impact of a specific neuronal system to ASD- or epilepsy-related phenotypes could therefore be unraveled and further studied in greater detail.

Different sensory systems could be investigated in more detail in Pfn2 KO mice as well, e.g. using behavioral tests for pain sensitivity (tail flick or hot plate tests). More specific approaches, such as the buried food test (Greco et al., 2013), could also reveal a potential hypersensitivity of the olfactory system in Pfn2 KO mice. This proposed hypersensitivity phenotype could contribute to autistic behavior, since sensory stimuli could be received differentially (e.g. more intense) or their output signaling from the olfactory bulb could be increased in autistic brains.
In order to address behavioral phenotypes, pharmaceutical therapies could be applied to Pfn2 KO mice targeting the neuronal systems that were investigated in this study. Indeed, dopamine antagonists are among the drugs that are commonly used to treat autistic patients. Haldol is so far the most effective treatment in reducing autistic symptoms by counterbalancing elevated dopamine levels, but it has severe side effects (McDougle and Posey, 2002).

Pfn2 has a function in neuronal development as shown in axonal and dendritic projections (see 2.3.1-2.3.3, 3.3.1-3.3.2, Fig. 25-28). In line with the accelerated developmental phenotype of Pfn2 KO neurons *in vitro*, the loss of Pfn2 could lead to impairments in connectivity or synaptogenesis *in vivo*, where a regulation of the cytoskeletal reorganization is crucial. Histological analyses of dendritic branching and synaptic connections at high resolution (i.e. Golgi-staining or super-resolution fluorescent microscopy) in Pfn2 KO mice would be valuable to investigate these processes. Electrophysiological measurements would reveal differences in the excitability, firing rates and related parameters could be performed on different neuronal populations or pathways connecting different brain areas.

Taking advantage of the validation of the P2-GFP mouse model presented in this work, Pfn2 dynamics could be investigated and visualized in live cells either *in vitro* or *in vivo* (for the latter e.g. using two-photon microscopy). Furthermore, the GFP-tag could be exploited for efficient immunoprecipitation experiments using anti-GFP antibodies that do not interfere with the binding of Pfn2 to its ligands. The interaction of Pfn2 with pre- or post-synaptic proteins could be verified and in addition stimulating conditions could be applied to analyze quantitative changes of ligand binding.

One of the tools developed during this thesis could also be used in a potentially highly beneficial approach to pull down native complexes (e.g. Arp2/3- or the different WAVE- complexes) using Strep-tagged versions of Pfn2 (see 2.2.1), since a mild elution protocol (biotin for competitive binding) can be used that would leave entire complexes intact. Therefore e.g. the composition of the different WAVE- complexes interacting with Pfn2 in certain brain areas, cell types or stimulation conditions could be unraveled, which would help to understand the role of the different complexes and Pfn2 during the initiation of actin polymerization.

4. Methods

4.1 Molecular Biology

4.1.1 Genomic DNA extraction from mouse tails

To extract genomic DNA from mouse tail tips, 200 µl of DNA extraction buffer (see 5.1.1) containing 0.5 mg/ml proteinase K were added to tail biopsies (app. 3-4 mm) and the proteins of the tissues were digested o.n. at 55°C.
After the digestion the solution was mixed briefly and shaken vigorously for 1 min. with ½ Vol. of saturated NaCl solution before spinning it down at 14,000 rpm for 15 min at room temperature (RT). 2.5 Vol. of absolute ethanol were added to 200 µl of the supernatant and the resulting flocculum of genomic DNA was precipitated by spinning down at 14,000 rpm for 3 min. The supernatant was aspirated using a pulled Pasteur pipet and air dried (or at 37°C for 5 min.). The DNA was resuspended in 200 µl of Milli-Q water (aqua bidest.) on a shaker at RT (or at 37°C) for app. 30 min before storing the DNA at 4°C. For a genotyping PCR (see 4.1.2.1), 1 µl of this solution was used.

4.1.2 Polymerase Chain Reaction

Nearly any DNA sequence can be amplified by a PCR (polymerase chain reaction) (Mullis and Faloona, 1987). For this purpose the DNA template (e.g. genomic DNA, see 4.1.1) is first denatured at 94-98°C for 30 sec.-2 min. This treatment separates the leading and lagging strand of the DNA, so that they are both able to function as templates for DNA replication. To these ssDNA (single-stranded DNA) templates can anneal specific oligonucleotides, so called “primers”, at a temperature of app. 55-65°C for 15-90 sec. The primers are chosen in pairs, with one in the 5´-3´ direction (sense or forward primer) and the other in the 3´-5´ direction (antisense or reverse primer) of the DNA template and are 18-25 nt long oligonucleotide sequences. Other features of the primers that help to increase the performance of the reaction should be a relatively high content of GC base pairs (40-60%) and at least two cytosines (C) or guanines (G) at the 3´-terminal of the primer. This yields a strong DNA-primer interaction, which is needed for the binding of an enzyme called the *Taq*-polymerase

(see 5.2.1) to the DNA-primer interaction site. The *Taq*-polymerase is a thermostable enzyme from the archaea bacterium *Thermus aquaticus*. At a temperature of 68-72°C (temperature optimum for the activity of the *Taq*-polymerase) the polymerase catalyzes the incorporation of free deoxynucleotides (dNTPs) (see 5.2.1) at the 3´-OH of the primer, complementary to the template strand of DNA. The enzyme needs divalent ions for its catalytic function, which are supplemented to the reaction in form of magnesium chloride ($MgCl_2$) (see 5.2.1) to work efficiently. This whole process of denaturing, annealing and elongation of the desired DNA template is repeated in 25-35 cycles in which the DNA is amplified exponentially. The reaction finishes with final elongation period of 5 min. to ensure the full length of the newly synthesized DNA.

4.1.2.1 Genotyping PCRs

Determination of mouse genotypes was done by PCR, screening for mutated allele(s).
Genomic DNA from tail biopsies (see 4.1.1) was used as DNA template.

P2-GFP knock-in mice genotyping PCR

To determine the genotype of the P2-GFP knock-in (KI) mice, the corresponding PCR was performed with a primer pair (see 5.5) amplifying a sequence with a length of 273 bp from the Pfn2 wt allele and a primer pair, amplifying a 404 bp fragment of the P2-GFP knock-in allele (Tab. 1). The sense primer was the same in both primer pairs. The resulting DNA samples were loaded on a 1.5% agarose gel (see 4.1.3, 5.1.1).

Tab. 1 P2-GFP genotyping PCR reaction conditions

Degrees	Time	
98°C	2 min.	
96°C 55°C 72°C	30 sec. 1 min. 15 sec. 30 sec.	35 cycles
72°C	5 min.	

Reagent	Concentration	Amount [µl]
H_2O		11.2
Go-Taq Flexi Buffer	5x	4.0
$MgCl_2$	25 mM	1.2
dNTPs	10 mM	0.4
Primer pair Pfn2-for/ Pfn2-rev	20 µM	1.0
Primer pair Pfn2-for/ PGFP-1	20 µM	1.0
Go-*Taq*-polymerase (Promega)	5 u/µl	0.2
Subtotal		19 µl
Genomic DNA		1 µl
Total		20 µl

Pfn2-lacZ (Pfn2 KO) mice genotyping PCR

The genotype of the Pfn2-lacZ (Pfn2 KO) mice was determined by a PCR with a primer pair amplifying a sequence with a length of 273 bp of the Pfn2 wt allele and a primer pair (see 5.5) amplifying a DNA fragment of app. 200 bp of the Pfn2-lacZ allele (Tab. 2). The sense primer was the same in both primer pairs. The resulting DNA samples were loaded on a 2% agarose gel (see 4.1.3, 5.1.1).

Tab. 2 Pfn2-lacZ (Pfn2 KO) genotyping PCR reaction conditions

Degrees	Time	
98°C	2 min.	
96°C 55°C 72°C	30 sec. 1 min. 15 sec. 30 sec.	35 cycles
72°C	5 min.	

Reagent	Concentration	Amount [µl]
H_2O		11.2
Go-Taq Flexi Buffer	5x	4.0
$MgCl_2$	25 mM	1.2
dNTPs	10 mM	0.4
Primer pair Pfn2-for/ Pfn2-rev	20 µM	1.0
Primer pair Pfn2-for/ nestLacZ-rev	20 µM	1.0
Go-*Taq*-polymerase (Promega)	5 u/µl	0.2
Subtotal		19 µl
Genomic DNA		1 µl
Total		20 µl

4.1.3 Gel Electrophoresis

Visualization of nucleic acid samples was performed by loading them on agarose gels (1.5-2% agarose in 1x TAE buffer, see 5.1.1) supplemented with ethidium bromide (app. 7-9 µl from stock (10 mg/ml) in 100 ml agarose in TAE). Nucleic acids are negatively charged due to the phosphate residues of their backbone structure. This feature can be exploited in electrophoresis, since nucleic acids run through the agarose gel towards the cathode (plus pole), when an electric potential difference is applied. The detection of the loaded samples was accomplished by imaging the ethidium bromide incorporated in the nucleic acid, when excited by UV radiation.

4.1.4 Engineering of plasmids for the expression of Streptag-fusion proteins

A plasmid vector for the production of Streptag-fusion proteins (pMW172-Strepag, produced by Julia Hecker) was used to insert the cDNA sequences of mouse Pfn1,

Pfn2 and P2-GFP respectively in order to produce recombinant Streptag-fusion proteins of these profilin isoforms (see 5.6).

The cDNA sequences of Pfn1, Pfn2 and P2-GFP were obtained by PCR amplification (see 4.1.2) from previously engineered plasmids (produced by Pietro Pilo Boyl and Walter Witke). The primer pairs were designed to include unique restriction sites for endonucleases suitable to insert these sequences into the Streptag plasmid vector (see . The PCR was performed using the Phusion polymerase instead of the *Taq*-polymerase (see 4.1.2), a proof-reading polymerase that minimizes the occurrence of sequence errors.

Tab. 3 Restriction digestion

Reagent	Concentration	PCR digestion	Vector digestion
DNA (PCR product)		pellet	
pMW172-Streptag	1 µg/ µl		2 µl
Endonuclease I (*NdeI*)	10 U	1 µl	1 µl
Endonuclease II (*SacI*)	10 U	1 µl	1 µl
Restriction buffer (Buffer 4, NEB)	10x	5 µl	5 µl
H_2O		43 µl	11 µl
Total		50 µl	20 µl

The PCR products were verified on agarose gels and afterwards diluted to 100 µl with H_2O and 1/10 vol. 3 M Na-acetate and precipitated by the 2.5 vol. of absolute EtOH by incubating at -80°C for a few hours. The precipitate was spun down at 14,000 rpm for 5 min. and the pellet was resuspended in the buffer required for the restriction digestion (see Tab.3). The restriction digestion was carried out for 1 h at 37°C. The digested DNA was loaded onto a preparative agarose gel (1.2%) and a current of 120 V was applied. After the electrophoresis, the desired band of the PCR product was cut out of the gel and the DNA was eluted with help of the Fermentas gel extraction kit. Briefly, the agarose was solubilized and the DNA bound to silica-membranes in microspin columns before the DNA was washed and recovered with 10 mM Tris-HCl pH 8.0 (35 µl). The amount of the eluted DNA was verified by loading it on an agarose gel.

The pMW172-Streptag vector (4 µg) was digested with the same restriction enzymes as the inserts (see Tab. 3), producing the same base pair overhangs. The digested, linearized vector was treated with a phosphatase (Antartic phosphatase, 1 µl) for app. 1 h to cleave off the 5´-phosphate-group left on the vector by the restriction digestion in order to prevent relegation of residual single-digested plasmids. The enzyme was inactivated by incubation at 75°C for 10 min. The concentration of the linearized, dephosphorylated vector (2 µl = ~200 ng) was verified on an agarose gel together with 200 ng of the undigested, circular vector as a control. The linear plasmid DNA was precipitated as described above and app. 200 ng were added to a ligation reaction with the respective insert DNA sequence.

The insert and vector sequences were ligated (see Tab. 4) as well as a control reaction exclusively ligating the vector to account for the dephosphorylation efficiency. The connection of the juxtaposed 3´-OH and 5´-phosphate groups was mediated by a T4 DNA ligase catalyzed reaction of the DNAs of the Streptag vector and the insert sequences of the respective profilin isoform (Pfn1, Pfn2, P2-GFP). The reaction was carried out o.n. at 16°C in a water bath.

The ligated vector can be transformed into bacteria as described in 4.1.6.

Tab. 4 Ligation of vector and insert sequences

Substance	**Concentration**	**Pfn1 ligation**	**Pfn2 ligation**	**P2-GFP ligation**	**Empty vector ligation**
Vector DNA	100 ng/µl	2 µl	2 µl	2 µl	2 µl
Pfn1 cDNA (426 bp)	50 ng/µl	1 µl			
Pfn2 cDNA (426 bp)	50 ng/µl		1 µl		
P2-GFP cDNA (1246 bp)	30 ng/µl			5 µl	
T4 Ligase	2000 U/ µl	1 µl	1 µl	1 µl	1 µl
Ligase buffer	10x (NEB)	1.5 µl	1.5 µl	1.5 µl	1.5 µl
H_2O		9.5 µl	9.5 µl	5.5 µl	10.5 µl
Total		15 µl	15 µl	15 µl	15 µl

4.1.5 Alkaline lysis miniprep of bacterial plasmids

Miniprep inoculi were prepared picking single colonies from LB_{Amp} agar plates and transferring them into 2 ml of LB_{Amp} medium. Inoculi were grown o.n. at 37°C in a shaker. The inoculi (1.5 ml) were spun down at 14,000 rpm for 30 sec. and the supernatant was discarded. The bacteria were resuspended in 50 mM glucose/20 mM EDTA/25 mM Tris-HCl pH 7.4 (miniprep solution 1, 100 µl) before adding 0.2 N NaOH/1% SDS (miniprep alkaline solution, 200 µl) to lyse the cells. The alkaline solution was mixed with the bacterial suspension by inversion of the Eppendorf tube and incubated on ice for 3-5 min. for an efficient lysis of the cells. Precipitation of membranes, genomic DNA and other debris was achieved by adding 3 M K-acetate pH 5.2 (miniprep solution 2, 150 µl) and mixing by inversion of the Eppendorf tube. The suspension was kept on ice for 10 min. before it was centrifuged at 14,000 rpm for 15 min. at 4°C. The supernatant (400 µl) was transferred in absolute EtOH (1 ml), mixed and incubated at RT for 5 min to precipitate the plasmid DNA. After spinning down the solution at 14,000 rpm for 10 min. at RT, the supernatant was discarded and the pellet was air dried. The dry pellet was resuspended in 10 mM Tris-HCl pH 7.4 (40 µl) and the RNA was digested with RNAseA (200 ng/µl) for 15 min. at 37°C. The plasmid DNA was stored at -20°C. Positive clones were identified by restriction digestion with the cloning enzymes (NdeI/ SacI, see Tab. 3).

4.1.6 Chemical transformation of competent bacteria

Chemically competent bacteria (100 µl) treated with $CaCl_2$ to achieve the capacity to uptake plasmids were thawed on ice and gently mixed with 5 µl of a ligation reaction for each transformation. The bacteria were incubated on ice for 20 min. with occasional mixing before inducing plasmid uptake with a heatshock of 45 sec. at 42°C. The bacteria were afterwards incubated for 5 min. at RT and transferred to 900 µl of LB_0- medium in glass tubes. The glass tubes were incubated shaking for 30 min. (minimum) at 37°C in a shaker before plating them on LB- agar plates supplemented with the required antibiotics (100 µg/ml ampicillin). The plates were then incubated o.n. at 37°C.

4.1.7 Production of Profilin-Streptag expression glycerol stocks

Competent bacteria from the strain BL21 (DE3) RP were transformed with the respective profilin-Streptag plasmids and plated on LB-agar plates supplemented with ampicillin (100 µg/ml) and chloramphenicol (25 µg/ml). A single colony was picked with a sterile toothpick and inoculated in $LB_{Amp/Cam}$-medium (25 ml). The culture was incubated o.n. at 37°C before addition of 20% glycerol (6 ml) to the culture. The cell suspension was mixed and aliquoted in Eppendorf tubes (1 ml). Each aliquot shock frozen in liquid nitrogen (N_2(l)). The glycerol stocks were stored in at -80°C. Expression of recombinant proteins was obtained starting from the glycerol stocks (see 4.2.10).

4.2 Biochemistry

4.2.1 Total protein lysates from mouse tissues

Mouse tissues were dissected on ice, washed briefly in cold PBS^- (see 5.1.3) to remove the blood and either stored after shock freezing in liquid nitrogen (N_2(l)) at -80°C or used directly for a protein lysate.
To obtain a total protein lysate, the dissected mouse tissue (fresh or frozen) was homogenized in 2x SDS loading buffer (see 5.1.2) with an electric homogenizer sat at 600 rpm in a glass/Teflon douncer. The solution was transferred to an Eppendorf tube and boiled at 99°C for 10 min. vortexing for 15-30 sec. every 2 min. (in total 4-5 times). The lysates were stored at -20°C.

4.2.2 Cytoplasmic protein lysates

Cytoplasmic protein lysates were obtained by homogenizing a mouse tissue (fresh or frozen) in cold TritonX-100 lysis buffer (TLB, see 5.1.2) with a homogenizer set at 600 rpm in a glass/Teflon douncer on ice. The homogenate was incubated for 10 min. on ice to completely solubilize the cell membranes, transferred into Eppendorf tubes and centrifuged for 15 min. at 14,000 rpm at 4°C to remove the nuclei and cell

debris (including the actin cytoskeleton). The supernatant was recovered and, depending on the type of further analysis, ultracentrifuged for 30 min. at 60,000 rpm and 4°C or transferred to a new Eppendorf tube. After a quantification of the protein concentration by Bradford assay (see 4.2.3), the lysate was either denatured by boiling at 99°C for 10 min. 1x SDS loading buffer or the lysate was shock frozen in liquid nitrogen and stored at -80°C.

4.2.3 Protein quantification

Quantification of the protein content in protein lysate samples was carried out by Bradford assays.

The Bradford assay is based on the shift of the absorbance wavelength of the dye Coomassie Brilliant Blue G-250 from 465 nm in an unbound condition to 595 nm, when the dye is in a complex with the proteins in the lysate (Bradford, 1976).

This excitation and emission detection are obtained using a spectrophotometer, which has to be calibrated to the absorption of a serial dilution of a protein solution with defined concentration (usually BSA) and blanked with lysis buffer before the protein sample can be measured. A fraction (4 µl) of the native protein lysate was boiled with 1 µl of 5x SDS-loading buffer in an Eppendorf tube for 2-3 min. at 99°C, cooled on ice and briefly spun down diluting it to 50 µl with H_2O. The same amount of lysis buffer was treated in the same way as a control (blank) sample.

For total protein lysates an aliquot of 5 µl was transferred into an Eppendorf tube and diluted to 50 µl with H_2O. 5 µl of 1x SDS loading buffer were used as a blank.

12.5 µl (cytoplasmic protein lysate) or 10 µl (total protein lysate), corresponding to 1 µl of the original lysate, were then added to 1 ml of a 1:5 dilution of Bradford reagent in a quartz photometer cuvette, mixed and measured after 3 min..

The measured absorbance (A) value was divided by the slope of the calibration curve of defined concentrations of BSA (here 0.048) to calculate the protein concentration of the sample in µg/µl.

4.2.4 Discontinuous SDS-polyacrylamide gel electrophoresis

The SDS-polyacrylamide gel electrophoresis (SDS-PAGE) (Laemmli, 1970) is a common method to separate proteins based on their apparent molecular weight.
To achieve a continuous separation, the proteins are denatured by the hydrophobic interaction with sodium dodecylsulfate (SDS), the reducing reagent β-mercaptoethanol and high temperatures. The denatured proteins remain coated by the negative charge of the sulfate group from the SDS according to their molecular weight, so that their native charge by their amino acid sequences is negligible.
Polyacrylamide gels used for SDS-PAGE consist of two solid phases. The upper phase, called “stacking gel”, contains 4% acrylamide, is app. 2 cm in length and allocates wells to load the protein samples (see 5.1.2). The pH of the stacking gel is slightly acidic at 6.8. The pH of the stacking gel should ensure the concentration of the protein samples to a thin layer. The bottom phase, also referred to as the “resolving gel”, consists of a more variable percentage of acrylamide in the range from 6%-20% with a basic pH of 8.8 for optimal migration towards the anode. The different percentages of acrylamide are chosen to achieve an optimal separation of the protein of interest. In the case of Pfn2, which has a MW of 14 kDa, a polyacrylamide gel with a dense pore size (15%) is optimal to achieve a good separation of the proteins from low molecular weight proteins. The polyacrylamide gels were casted using a homemade casting chamber. To run protein samples through the gels, they were mounted in running chambers, containing running buffer and a current was applied. Electrodes placed on the top and at the bottom of the gels create a current passing through the gel, so that the negatively charged proteins migrate towards the anode (positive pole). A voltage of 80 V was applied to the polyacrylamide gel while the proteins ran through the stacking gel (30 min.). A voltage of 120-150 V was applied to the resolving gel depending on the percentage of acrylamide used.

4.2.5 Western Blotting

Western blot assays are used to transfer proteins from a polyacrylamide gel onto a polyvinylidene difluoride (PVDF) or nitrocellulose membrane (see 5.3.3) (Towbin et al., 1979). This transfer onto membranes is convenient to label proteins with specific antibodies and detect them using an enzymatic reaction that produces a colored or luminous signal.

4.2.5.1 Submerged transfer

The transfer of proteins onto a membrane is most efficient, when the applied current is moderate over a longer period of time. A submerged transfer (wet blot) relies on these features, so especially proteins with a molecular weight over app. 90 kDa, that are sometimes less efficiently transferred using other methods, can be quantitatively fixed onto a membrane.
After a SDS-PAGE has been run, the gel is mounted on two sheets of Whatman paper laid on a sponge pad and covered by a Methanol-activated PVDF membrane, two more sheets of Whatman paper and another sponge pad. This stack is mounted in a chamber filled with Towbin transfer buffer (see 5.1.2) and a current is applied.
The voltage applied to the blotting chamber was 110 V for 1h with a cooling ice piece at RT or at 20 V o.n. at 4°C.

4.2.5.2 Semi-dry transfer

The semi-dry transfer method (semi-dry blot) was used as a fast transfer method, especially for proteins below the a molecular weight of app. 90 kDa.
The treatment of the components and the assembly of the blot stack were similar to the description in 4.2.5.1 for the submerged transfer except for the sponge pads that are not needed.
The components of the blotting stack were put directly between the electrodes of a semi-dry blotting chamber and a fixed amperage of 280 mA per 6x9 cm stack was applied for 30-35 min.

4.2.6 Antibody signal detection via enhanced chemiluminescence

After the transfer, the membranes were washed quickly in 1x NCP (see 5.1.2) and nonspecific binding sites were blocked using 5% nonfat milk/1xNCP for 30 min. at RT.

Then the membranes were incubated with appropriately diluted primary antibodies in 5% nonfat milk/1xNCP (blocking solution) for 2h at RT or o.n. at 4°C depending on the antibody (the latter was normally preferred). Membranes were washed 3 times for 15 min. each with 1x NCP to remove unbound primary antibody. Secondary antibodies, corresponding to the host species of the primary antibody, conjugated to the enzyme horseradish peroxidase (HRP), were diluted 1:5000 in blocking solution and applied to the membranes for 1h at RT. The membranes were washed again 3 times for 10 min. each with 1x NCP at RT and afterwards developed using enhanced chemiluminescence (ECL) reagents as substrates for the HRP.

The ECL reagents were mixed from two stock solutions, which contained luminol (Solution A) and hydrogen peroxide (Solution B) (see 5.1.2), before the incubation on the membranes. The HRP enzyme catalyzes the chemiluminescent reaction, in which the luminol emits light upon its oxidation.

The light signal was captured by exposing x-ray films for a definite time period or digitally using an imager with a CCD-camera (LAS4000 Mini, GE Healthcare).

4.2.7 Western blot quantification

The light emitted by a protein band is proportional to the amount of primary antibody on the membrane, so the light intensity was used to quantify the relative amounts of proteins between the lanes on the same membrane or different membranes using one or more stably expressed marker proteins (housekeeping genes) as controls.

Using the software Multi Gauge V3.0 from Fujifilm Life Science the intensity of detected antibody signals was quantified. The ratios between lanes within the same blot were calculated using Microsoft Office Excel.

4.2.8 Coomassie staining

Visualization of proteins on polyacrylamide gels is often accomplished by a Coomassie Brilliant Blue staining. This staining is widely used to estimate protein concentration and to verify the blotting efficiency after a Western blot transfer. The method can detect proteins starting from a minimal amount of app. 50 ng.
Subsequent to the SDS-PAGE the proteins were fixed in the gel twice for 15 min. each at RT with a fixation solution (40% MeOH/10% AcOH, see 5.1.2) (not necessary for gels after a Western blot, as the proteins were fixed by the methanol of the blotting buffer and the heat produced during the blotting process). The gel was stained with a 0.1% Coomassie Brilliant Blue solution for 30 min. at RT before washing 1-2x for 15 min. with the fixation solution and afterwards 2 times 30 min. each with a washing solution (20% MeOH/10% AcOH, see 5.1.2), to completely remove unbound Coomassie. The gels were scanned and stored in water.

4.2.9 Silver staining

The silver staining technique also helps to visualize proteins by incorporating elementary silver to proteins in polyacrylamide gels. It is about 10x more sensitive then Coomassie staining and is therefore preferred, when low protein concentrations are analyzed on a gel (e.g. IP or pull-down fractions).
After the polyacrylamide gels the proteins were fixed to the gel by a fixation solution of 50% MeOH/12% AcOH/0.5 ml 37% HCOH/l /H_2O (see 5.1.2) and incubated for 2 h to o.n. at RT. Subsequent to the fixation, the gels were washed 3 times with 50% EtOH/H_2O for 10 min. each. The gels were incubated next with a sodium thiosulfate solution (0.2 g/l $Na_2S_2O_3$/H_2O, see 5.1.2) for 1 min., rinsed with tap water 3 times for 20 sec. each and afterwards incubated with a silver nitrate solution (2 g/l $AgNO_3$/0.75 ml 37% HCOH/l H_2O, see 5.1.2) for 20 min. Rinsing of the gels with tap water 2 times for 20 sec. each was followed by a silver precipitation step using a reducing sodium carbonate/ sodium thiosulfate solution (60 g/l $NaCO_3$/0.5 ml 37% HCOH/l /4 mg/l $Na_2S_2O_3$/H_2O) for 5-10min. When the development of the silver staining yielded sufficiently prominent signals, the precipitation of elementary silver was interrupted by

rinsing away the reducing solution with tap water twice and stopping the reaction by adding a solution of 10% EtOH/10% AcOH (see 5.1.2). The stained gels were scanned and stored in water in the dark at 4°C.

4.2.10 Protein expression in bacterial cells

The *E. coli* BL21 (DE3) RP, T7 polymerase expressing, bacterial strain was transformed with the plasmids encoding for the three tagged profilin isoforms (see 4.1.5). After the transformation, they were plated on LB-agar plates supplemented with chloramphenicol (25 µg/ml) and ampicillin (100 µg/ml) and incubated o.n. at 37°C. One colony was picked, inoculated in LB-medium (30 ml) supplemented with the same antibiotics and grown o.n. at RT on a shaker. One aliquot directly from the fresh culture (25 ml) or one frozen aliquot of the bacterial glycerol stocks (see 4.1.7) were inoculated in 2 l of LB-medium supplemented with chloramphenicol (25 µg/ml) and carbenicillin (200 µg/ml) and grown at RT to an OD_{600} of 0.5-0.7. An aliquot of the culture was pelleted and frozen (non-induced sample) and the remaining bacterial culture was induced to produce the desired recombinant protein by addition of 1 mM IPTG for 4h at 37°C or o.n. at 22°C.
In order to purify the protein, the culture was incubated on ice for 15 min. and pelleted at 8,000 rpm for 5 min. at 4°C. The supernatant was discarded and the bacterial pellet was resuspended in 50 ml Streptag-lysis-buffer containing 5 mM EDTA, 0.5% TritonX-100, 10% sucrose, 1x “Complete” protease inhibitor in PBS (see 5.1.2). The lysis-solution was further incubated on ice and treated with ultrasonication 4x 1 min. with 30 sec. intervals at a tip energy of 8 AU. The lysate was homogenized using a tight-fitting glass douncer and afterwards cleared by ultracentrifugation for 30 min. at 35,000g at 4°C. The supernatant was recovered and the soluble proteins were purified as described in 4.2.11.

4.2.11 Protein isolation by Streptag purification

The recombinant Streptag fusion proteins (see 4.2.10) were isolated using an affinity column purification approach.

The column was filled slowly with 2 ml of Streptavidin-coupled sepharose beads 1:1 slurry (GE Healthcare) at 4°C. The beads were washed according to the manufacturer´s specifications and equilibrated with 5 Vol. of Streptag lysis buffer (see 5.1.2).
The cleared bacterial lysate (see 4.2.10) was passed on the Streptavidin-coupled sepharose beads column three times before the unbound sample (flow through fraction, FT) was collected. The column was washed with 16 Vol. of Streptag washing buffer containing 100 mM Tris-HCl pH 8/150 mM NaCl/1 mM EDTA (see 5.1.2) until no further proteins were detected in the washing fraction, which was verified by Bradford assay. The Streptag fusion proteins bound to the beads were eluted using 0.5 Vol. of Streptag elution buffer containing 100 mM Tris-HCl pH 8/150 mM NaCl/1 mM EDTA/2.5 mM D-desthiobiotin (see 5.1.2) by incubating it with the beads on the capped column for 1 min. before collecting the eluate. The eluate was supplemented with 2x SDS loading buffer for Western blot analysis (see 4.2.5) or stored at -80°C.
The beads were regenerated using 15 Vol. of Streptag regeneration buffer containing 100 mM Tris-HCl pH 10.5/150 mM NaCl/1 mM EDTA/1 mM HABA (see 5.1.2) and washed again after the regeneration process with 15 Vol. of Streptag washing buffer. The beads were stored in the capped column with Streptag washing buffer at 4°C for further use.

4.2.12 Coupling of Poly-L-Proline to CNBr-activated sepharose beads

Poly-L-proline (PLP, 500 mg, Sigma) was dissolved in cold 1x coupling buffer for 2 days at 4°C on a rotating wheel. CNBr (cyanobromide)- activated sepharose beads 4 Fast Flow™ (10 g, GE Healthcare) were resuspended in 200 ml of cold 1 mM HCl and afterwards washed 5 times for 3 min. each with 200 ml cold 1 mM HCl. After a centrifugation at 2000 rpm for 5 min. the supernatant was removed carefully with a glass Pasteur pipet. The sepharose beads were washed once with cold distilled water and once with cold 1x coupling buffer before adding the dissolved poly-L-proline in coupling buffer (see 5.1.2). The coupling reaction was carried out o.n. at 4°C on a rotating wheel.

The poly-L-proline-coupled beads were washed three times with 200 ml of cold coupling buffer before unbound PLP was removed by incubation with 0.1 M Tris-HCl pH 8/0.5 M NaCl for 2 hours at RT. The beads were washed four times alternating between the washing solutions of 0.1 M sodium acetate pH 4 /0.5 M NaCl and Tris-HCl pH 8 /0.5 M NaCl each and were finally washed and stored at 4°C in 20 mM Tris-HCl pH 8/5 mM EDTA/100 mM NaCl/0.1% NaN_3/20% EtOH as a 1:1 slurry.

4.2.13 Poly-L-Proline binding assay

An aliquot of 50 µl of PLP beads slurry (see 4.2.12) was packed into a microspin column and equilibrated with TLB lysis buffer. The columns were loaded with 1 mg of protein lysates from wt, Pfn2 KO, homozygous and heterozygous (G/G; G/+) P2-GFP KI mouse cortex lysates. The lysates were incubated by flowing through the columns 3 times to optimize binding efficiency before collecting the unbound (or flow through fraction, FT).

The beads in the columns were washed 3-4 times with TLB (without “Complete” protease inhibitor) and removed from the columns by adding 50 µl of 2x SDS-loading buffer twice and transferring the beads into new Eppendorf tubes to ascertain that the maximal amounts of beads were collected.

The beads were boiled in the SDS loading buffer for 10 min. at 99°C to elute the bound proteins from the beads. After cooling the tubes quickly on ice, the beads were spun down at 14,000 rpm for 1 min. and supernatants (bound fraction) were recovered.

The unbound fractions (FT) and an aliquot of each of the original lysates (input fraction) were diluted to a concentration of 0.5 µg/µl in 1x SDS loading buffer and the proteins were denatured by boiling at 99°C for 10 min. The fractions (input, bound, unbound (FT)) were stored at -20°C. For Western blot analysis equal amounts of input and flow through fractions from each of the different mouse genotypes were loaded together with 1% of the respective bound fractions.

4.2.14 Immunoprecipitation

Profilin2 and P2-GFP were immunoprecipitated with the help of the polyclonal rabbit antibody anti-Pfn2 T2 (Walter Witke), which is known to specifically recognize Pfn2. 1 mg of mouse cortex lysates of wildtype and Pfn2 KO animals in TLB (see 4.2.2, 5.1.2) were incubated with the anti-Pfn2 T2 antibody (15 µl, terminal bleed) o.n. at 4°C on a rotating wheel. The host-species specific Fc (heavy) chain of the anti-Pfn2 antibody was precipitated with a mixture of proteinA- and proteinG-coupled sepharose beads (50 µl beads slurry in a 1:1 ratio of proteinA and proteinG) by incubation for 4 h at 4°C on a rotating wheel. After the incubation period, the tubes were placed on ice to let the beads settle for 5 min. before spinning them down in a cooled (4°C) centrifuge at 1500 rpm for 1 min. The supernatant (unbound or flow through fraction, FT) was recovered and denatured with 1x SDS loading buffer for 10 min. at 99°C. The beads were washed 4 times with 1 ml of cold TLB with intervals of 5 min. on ice to let the beads settle down in the tube between each step, followed by spinning 1 min. at 1,500 rpm. Bound proteins were eluted by denaturation with 100 µl of 2x SDS-loading buffer at 99°C for 10 min. The samples were placed on ice for a few minutes before spinning them down at 14,000 rpm for 1 min. and recovering the supernatant (bound fraction) before Western blot analysis.
P2-GFP complexes were immunoprecipitated using monoclonal llama antibodies (nanobodies) specific for GFP (green fluorescent protein) coupled to agarose beads (GFP-Trap®-A, Chromotek). The GFP-Trap beads were used for immunoprecipitation (20 µl) according to the manufacturer´s instructions.
The input fraction (cortex lysate) and FT fraction from all IPs were boiled at 99°C in 2x SDS loading buffer for 10 min. and adjusted to a final concentration of 0.5 µg/µl.

The proteinA- and proteinG-sepharose beads were treated before the application in the immunoprecipitation assay to block unspecific binding and equilibrate them in the dilution buffer. The beads were stored in a 1:1 slurry in 20% EtOH. To remove the EtOH, 100 µl of beads slurry were spun down at 1,500 rpm for 1 min. at 4°C and the supernatant was aspirated. The beads were washed twice with 1 ml of cold PBS and unspecific binding capacity of the sepharose beads was blocked by incubation with PBS/0.1% BSA for 1 h at 4°C. The beads were spun down at 1,500 rpm for 1 min. at

4°C before discarding the supernatant and washing them twice with 1 ml of cold TLB, preparing a 1:1 slurry in cold TLB (+ Complete protease inhibitors) for the immunoprecipitation reaction.

4.3 Histology

4.3.1 Mouse tissue dissection

Mice were sacrificed by cervical dislocation. Mouse tissues were dissected on ice and fixed in 4% PFA (see 5.1.3) for 24-48 hours at 4°C to crosslink the proteins. Each tissue was washed 2x with cold PBS (see 5.1.3) for at least 30 min. each at 4°C.

4.3.2 Vibratome cutting of mouse brains

Mouse brains were cut sagittally or coronally to sections with a thickness of 20 µm using a Leica Vibratome VT 1200S. A razor blade was cleaned with 70% EtOH (careful not to bend the blade) and inserted into the blade holder at a slightly inclined angle to the object table to achieve the optimal settings. The vibration accuracy was measured using the Leica “VibroCheck” device and tuned to perfectly horizontal levels (0° alteration).

For sagittal slices, the brains were cut with a scalpel near the midline at the height of app. 2/3^{rds} of the brain before the cut surface was glued to the vibratome tray.

In this way, the resulting slices would comprise at least one entire hemisphere. A piece of 2% agarose was glued next to the brain (on the opposite side of the blade) to stabilize it during the cutting procedure.

For coronal slices, the cerebellum was cut off with a scalpel and the brain was glued to the vibratome tray on the cut surface.

An optional step for sectioning of soft tissue (young mice) was embedding of the brain in using 6% low-melting agarose. The agarose was removed after cutting the sections, since it mediates strong autofluorescence.

The vibratome tray was submerged in ice cold 1x PBS supplemented with 0.1% sodium azide (NaN_3) and cooled with ice surrounding the tray. Brain slices were cut

at a speed of 0.16-0.26 mm/s and a vibration amplitude of 1 mm to a thickness of 20-25 µm. The sections were collected with a smoothened glass pipet in 24-well plates containing cold 1x PBS/0.1% sodium azide (NaN_3) and stored at 4°C wrapped in plastic and aluminum foil.

4.3.3 Vibratome cutting of mouse spinal cords

Mouse spinal cords were dissected from adult mice on ice under a binocular microscope. The skin was removed before the muscles were separated from along the spine. The vertebrae were opened dorsally to expose the spinal cord. The spinal roots were removed in order to lift the spinal cord.
The spinal cord was separated in the thoracic, lumbar and sacral segments, embedded in 6% low-melting agarose and cut coronally with a Leica Vibratome VT 1200S. The agarose was removed after obtaining the sections, since it is strongly autofluorescent. The preparation of the instrument and the cutting process was performed as described in 4.3.2. The cutting speed was set at 0.26 mm/s and sections were cut with a thickness of 80 µm.

4.3.4 Vibratome cutting of mouse embryos

Mouse embryos at different embryonic stages were dissected in HBSS under a binocular microscope. Maternal tissue was completely removed and the embryos were fixed 24-40h at 4°C with 4% PFA depending on the age (embryonic day) of the embryo. For embryos of embryonic day 16.5 (E16.5) and later, the head was separated from the body before the fixation to achieve maximal penetration of the PFA in the tissue. After fixation the embryo was washed twice with cold PBS for 30 min. each.
The embryos (or embryo heads) were cut sagittally with a Leica Vibratome VT 1200S. For this procedure, the limbs and skin were removed from one side of the embryo and the sample was glued to the vibratome tray on the exposed surface.
Embryos at early developmental stages (E13.5) were embedded in 6% low-melting agarose. The agarose was removed after obtaining the sections, since it is strongly autofluorescent.

The preparation of the instrument and the cutting process was performed as described in 4.3.2. The cutting speed was set at 0.20-0.26 mm/s and sections were cut with a thickness of 60-80 µm depending on their age.

4.3.5 Immunofluorescence

4.3.5.1 Immunofluorescence staining of vibratome sections

Matched tissue sections from several homozygous P2-GFP KI, wildtype and Pfn2 KO mice as controls were chosen with the help of a stereomicroscope, depending on the area to be investigated.

The sections were transferred to 24-well plates with an aluminium foil lid and autofluorescence was quenched by incubation with 50 mM ammonium chloride (NH_4Cl, see 5.1.3) for 1 h at RT. The slices were washed 10 min. at RT with 1x TBS (see 5.1.3) to adjust the pH after the acidic ammonium chloride treatment. Afterwards nonspecific binding sites for the primary and secondary antibodies were blocked by addition of 300 µl of a blocking solution containing 1x TBS-T/2%-10% NGS and 1%-2% DMSO (see 5.1.3) o.n. at 4°C. The composition of the blocking solution was antibody-, antigen- and section-dependent. Antibodies with relatively high background require a blocking solution with a higher amount of serum proteins (5-10% NGS). Inaccessible target antigens (scaffolding proteins, PSD-associated proteins etc.) or thick sections (embryos, spinal cord) required incubation with a higher concentration of DMSO (2%).

The blocking solution was removed using a glass Pasteur pipet and 200 µl of the respective primary antibody appropriately diluted in blocking solution were added to each brain slice that was incubated o.n. (or 24-48 h) at 4°C or RT. The incubation period and the dilution of the primary antibody (several primary antibodies can be applied together, in the same solution) are dependent on the affinity and the binding kinetics of the antibodies, which need to be tested individually. After the incubation, the primary antibody solution was removed and the slices were washed a minimum of three times with 1 ml of TBS-T (see 5.1.3) for 15 min at RT to remove unbound antibodies.

The sections were incubated with 250 µl of secondary antibodies appropriately diluted in blocking solution (Alexa- or ATTO-dyes 1:1000, CF-dyes 1:500) for 1-2 h at RT. The secondary antibody solution was removed from the sections and they were washed a minimum of three times with 1 ml of TBS-T for 15 min each at RT to remove unbound antibodies. A subsequent washing step was performed o.n. at 4°C.
To visualize the cell nuclei, DNA-intercalating dyes were chosen with regard to their excitation wavelengths. To localize cell nuclei and tissue structures through the oculars by eye, the DNA dye DAPI was added in 300 µl of TBS-T for 15 min. at RT at a concentration of 10 ng/ml (1:100,000 from the stock). Another DNA- binding dye (Draq5, Biostatus, UK), was chosen to visualize the nuclei, which can be excited at 640 nm and has an emission peak at 680 nm. Draq5 was incubated in TBS-T for 15 min. at RT at a concentration of 1 µM (1:5000 from the stock). Maximal efficiency is achieved by incubating with Draq5 solution before incubating with DAPI solution, due to DAPI´s higher affinity and the saturation of binding sites for Draq5. To wash away unbound DNA dyes, an incubation with 1 ml of TBS-T for 15 min. at RT followed. A subsequent washing step with 1 ml of TBS for 10 min. at RT was included to remove the TritonX-100 from the sections.

The staining of the Ca^{2+}-binding proteins calbindin (CB) and parvalbumin (PV) required an additional step of incubation with a calcium-buffer before quenching the autofluorescence with the ammonium chloride solution. These proteins are recognized by the specific antibodies preferably in their Ca^{2+}-bound conformation.

4.3.5.2 Immunofluorescence of cultured hippocampal neurons

Hippocampal neurons were stained in a humid chamber. The paraffin dots were removed from the coverslips and they were washed quickly with TBS by turning the coverslips with the cell side on drops of washing buffer (100 µl). Before lifting the coverslips to transfer them on a drop of the following solution, 100 µl of TBS were added underneath the coverslip, raising it slightly from the parafilm, so no cells were harmed during the transfer. The cells were permeabilized for 1 min. at RT using TBS/0.2% TritonX-100 (TBS-T) and autofluorescence was quenched by incubation with ammonium chloride (NH_4Cl, 50 mM) for 10 min. at RT. The coverslips were

washed by dipping them thrice gently in a beaker with TBS and once with a drop of TBS/0.2% Tween-20 on parafilm. Unspecific binding sites were blocked by incubation with TBS/0.2% Tween-20/10% NGS (see 5.1.3) o.n. at 4°C. The cells were incubated with primary antibodies o.n. at 4°C or RT depending on the antibody in blocking solution. The coverslips were washed again by gently dipping them thrice in TBS and placing them on a drop of TBS/0.2% Tween-20. The secondary antibody was added in blocking solution for 2 h at RT before washing in the same way as described above and washing a fourth time o.n. at 4°C. The cells were incubated, if required with a DNA dye to stain the nuclei. Draq5 (1 µM), propidium iodide (0.5 µg/ml) or DAPI (10 ng/ml) was therefore added in TBS for 10 min. at RT. The coverslips were washed quickly again in TBS/0.2% Tween-20 and quickly in H_2O before mounting them on a glass slide with app. 10 µl of Mowiol mounting medium per 13 mm^2 coverslip (see 5.1.3). They were sealed with nail polish after drying for a few hours at RT.

4.3.5.3 Mounting of vibratome sections

The sections were transferred on glass slides, flattened using a fine brush and the slide was dried around the slices. A mounting medium was warmed (55°C) and was added to the slice with a cut P200 pipet tip (app. 100-120 µl/ brain section or 80 µl/ spinal cord section or 150 µl/ embryo section). The amount of mounting medium also determines the distance of the sample from the glass of the coverslip, which should be minimal to prevent light scattering and absorption by the mounting medium.
To achieve maximal resolution of the resulting images, certain mounting media were prepared dependent on the type of analysis. A new mounting medium was invented with consideration of a high number of publications and articles yielding an increased signal-to-noise ratio (SNR) due to minimal scattering of light.
The “glycerol mounting medium” (see 5.1.3) consists of glycerol, a Tris-based buffering system to keep the basic pH and three kinds of antifadent reagents to scavenger different species of (mostly oxygen) radicals.
Glycerol is a viscous medium that, at a concentration of 90%, has a refractive index of n= ~1.46, which is close to the refractive index of immersion oil (n= 1.518) and the cover glass (n= ~1.5). The Tris-buffer in the medium is needed to keep the pH above 8.5 to achieve an optimal quantum yield efficiency of the fluorophores in absorbing

photons of the desired wavelength and emitting maximal amounts of photons in their respective spectrum. Free radicals in the mounting medium are inevitably produced by the high power of the laser light excitation. These (mostly oxygen) radicals need to be hindered in reacting and therefore permanently inactivating the fluorophores. Different radical species can be scavenged by different antifadent substances such as n-propyl-gallate (NPG), 1,4-diazabicyclo[2.2.2]octane (DABCO) or *p*-phenylendiamine (PPD). These reagents are added to the medium in different concentrations (see 5.1.3), since especially PPD is also partially quenching the fluorescence emission efficiency, if it is too concentrated. PPD also produces a slight yellow color of the medium, which turns brown upon oxidation, which is an indicator for suboptimal storage. An additional step in medium preparation is to de-gas the solution to minimize oxygen in the mounting medium, which can be processed to free oxygen radicals. The antifadents are chemically very active, so, in order to keep them stable, high temperatures (above app. 70°C) and a long light exposure should be avoided. The solution is stored at -80°C to further prevent degradation and oxidation of the antifadents.

The medium is therefore ideal for imaging high-resolution images, since it diminishes light scattering and prevents photodamage of the fluorophores. Due to the high concentration of glycerol, this mounting medium will not get solid, so immediate air-tight sealing with nail polish is required.

The handling of a fluid mounting medium can be difficult especially for round coverslips commonly used in tissue culture conditions.

Another mounting medium was prepared to achieve a better sample stability without diminishing the refractive index too much (see 5.1.3). This medium was Mowiol-based – a polyvinylalcohol (PVA), which solidifies upon oxygen exposure and is otherwise inert in terms of reaction capabilities with the cell or tissue sample. The Mowiol mounting medium has a refractive index of n= 1.45 at 20% in a Tris-based buffering system to keep the pH above 8.5. This refractive index is slightly worse than that of the glycerol mounting medium, but still good enough for high-resolution imaging. Mowiol needed to be mixed in 40mM Tris-HCl pH 8.5 for several hours at ~50°C to solubilize completely. The medium could be de-gassed and the same antifadents at the same concentrations as for the glycerol mounting medium were

added. The solution was stored at -80°C to further prevent degradation and oxidation of the antifadents.

The sections were gently covered with a glass coverslip from one side, so the mounting medium was evenly distributed. These coverslips No. 1.5 (Marienfeld) had a definite thickness of 0.17 mm (+/- 0.005 µm) optimized for the refractive index of the immersion oil (n= 1.518) and for the correction of an oil- immersion objective lens to further reduce light scattering. The samples were sealed air-tight with nail polish to prevent oxygen from reacting with the antifadents of the mounting medium.

4.4 Neuron culture

4.4.1 Preparation of coverslips

Coverslips with a thickness of 0.17 mm and a diameter of 13 mm (No. 1.5 H Marienfeld) were were stacked in porcelain staining racks and incubated with concentrated HNO_3 (≥ 65%) in glass beakers under a fume hood o.n. at RT. The porcelain staining racks were washed 4 times with Milli-Q water and sterilized with dry heat for 6h with rising temperature of 100-220°C. The coverslips were transferred to 6 cm^2 dishes with sterile forceps, so each dish would contain max. 8 coverslips. Paraffin was melted in a waterbath on a heating block for min. 3 h and 3 dots were applied on each coverslip with a glass Pasteur pipet. For enhanced adhesion of neuronal cells, poly-L-lysine in borate buffer (see 5.1.4) was applied to each coverslip two days before a hippocampal neuron culture was planned. A drop of poly-L-lysine was placed on each coverslip (app. 100-200 µl) and incubated for 24 h at RT in a humid chamber. One day before a hippocampal neuron culture was planned, the coverslips were washed with sterile H_2O 3 times before adding MEM-HS or MEM-FCS (see 5.1.4). The coverslips were equilibrated with the medium at 37°C in an incubator for min. 24 h and maximal 2 weeks before neuronal cells were plated on the coverslips.

4.4.2 Hippocampal neuron culture

A pregnant mouse was sacrificed by cervical dislocation and E17.5 embryos were recovered. To obtain the hippocampi of the embryos, they were decapitated, a piece of tail was cut for genotyping and the skull was opened with a fine bend pair of forceps. The skin and skull bones were removed and the entire brains were dissected out of the skull without harming their structure. The brains were transferred to 6 cm^2 cell culture dishes filled with app. 5 ml of HBSS/HEPES (see. 5.1.4) under a stereomicroscope (see 5.4.1). The meninges were removed from the brains with two pairs of fine forceps and the hippocampi were dissected out. The hippocampi were transferred to an Eppendorf tube with app. 1 ml of HBSS/HEPES. The isolated hippocampi were transferred to a 15 ml tube in a laminar flow hood, the HBSS was removed. A Trypsin (0.05%) solution (see 5.1.4) was added (5 ml) and the tissues were incubated in a water bath at 37°C for 15 min. After the incubation, the Trypsin solution was removed and the hippocampi were washed thrice with HBSS/HEPES. The hippocampi were dissociated in 3 ml HBSS/HEPES by pipetting up and down using a glass Pasteur pipet, which had been presoaked with a 5% BSA solution. The cells were further isolated by pipetting up and down with a fire-polished Pasteur pipet with app. half of the normal diameter. The cell density was determined with the help of a hemocytometer and the cells were plated at a density of 150,000 cells/ 6 cm^2 dish containing 8x 13 mm Ø coverslips and an astrocyte co-culture with MEM-FCS medium (see 5.1.4). The MEM-FCS medium was exchanged for N2-medium (see 5.1.4) 24 h after plating and the medium was further changed (2/3) once per week. The coverslips were treated as described in 4.3.1 and astrocytes were grown app. 30-50% confluent in the 6 cm dishes as described in 4.4.3.

4.4.3 Astrocyte culture

Astrocytes were cultured as co- cultures for hippocampal neurons from E19.5 embryos. The brains were dissected as described for culturing hippocampal neurons (see 4.4.2) but the cortices were recovered from the embryos instead of the hippocampi. The cortices were treated in the same way as the hippocampi (see

4.4.2) but the dissociated cell suspension was resuspended in 10 ml of MEM-FCS and plated on 75 cm^2 flasks (app. 5 brains/flask).
The astrocytes in the flasks were grown to 100% confluency and split in 3 new flasks. For that the cells in the flask were washed with HBSS/HEPES and incubated with a Trypsin (0.05%) solution for 10 min. at 37°C before splitting the cell suspension equally into 3 new flasks. Astrocytes could be split maximum 3 times before problems with adhesion and proliferation occurred. One 75 cm^2 flask with 90-100% confluent astrocytes could be spilt onto app. 40x 6 cm^2 dishes as a co-culture for hippocampal neurons. The MEM-FCS medium was changed (2/3) once per week.

4.4.3.1 Astrocyte freezing

An astrocyte co-culture can be established from previously cultured cells, which were stored in a cryo-tank with liquid nitrogen. A 90-100% confluent 75 cm^2 flask was washed with HBSS/HEPES and incubated with 3 ml of a Trypsin (0.05%) solution for 10 min. at 37°C. The trypsinization was stopped by 5 ml of FCS and the cell suspension was transferred to a 15 ml tube. DMSO was added to the cell suspension to a final concentration of 10% (app. 1 ml) and the cells were transferred to 2 ml cryo-tubes. The tubes were incubated first on ice for several minutes and afterwards at -80°C in a stryropor box for 24 h. The cell suspension in the cryo-tubes was permanently stored in liquid nitrogen. The cells were thawed quickly in a water bath at 37°C and plated on 6 cm^2 dishes or 25-75 cm^2 flasks with MEM-FCS.

4.4.4 Cell fixation

Hippocampal neurons and astrocytes were grown in 6 cm^2 dishes with MEM-FCS (astrocytes) or N2-medium (neurons). The dishes were washed once with HBSS/HEPES and fixed afterwards using 4% PFA, 0.25% glutaraldehyde, 2% sucrose in PBS for 20 min. at 37°C (see 5.1.4). After the fixation period, a small amount of the fixation solution was left and the dishes were filled to 5 ml with HBSS/HEPES. The dishes were stored in the dark at 4°C wrapped with parafilm.

4.4.5 Sholl analysis

Hippocampal neurons of different mouse lines were fixed (see 4.3.4) at different time points (days *in vitro*, DIV) and their complexity was compared applying Sholl analysis. Sholl analysis is based on the intersections of dendritic projections through circles of a defined diameter *in silico*.

Hippocampal neurons (see 4.3.2) originating from wildtype, homozygous P2-GFP KI, and Pfn2 KO mice were fixed at different developmental stages (DIV 1, 2, 3, 7, 14 and 21). The cells were immuno-stained using the early neurite/dendrite specific antigen Map2 (see 4.3.5.2) and imaged using a widefield fluorescence microscope (Keyence Biorevo BZ-9000). The images were stitched together (Adobe Photoshop), if necessary, due to large dendritic arborizations exceeding the field of view of the 20x objective. The projections were semi-automatically traced (Simple Neurite Tracer plugin in Fiji ImageJ) and traced neurites were implemented in the Sholl analysis plugin in Fiji ImageJ. The intersections of neurites at rings of 10 µm intervals surrounding the neuronal somata were counted for each time point and genotype (high number of neurons were analyzed for n=3 individual neuronal cultures for each genotype). The mean number of intersections for each DIV and genotype was calculated and Sholl plots were generated to compare differences in the complexity of the neuronal arborizations.

4.4.6 Neuron Stimulation

The hippocampal neurons were cultured from homozygous P2-GFP (G/G) embryos (E17.5) for 21 days (DIV 21) and subsequently stimulated. The cells were washed with ACSF (see 5.1.5) once and equilibrated in ACSF for 15 min. at 37°C before a stimulating solution or drug was added.

General pre- (and post-) synaptic stimulation was accomplished by exchanging the ACSF with ACSF containing 90 mM KCl (see 5.1.5) or ACSF with an increased Ca/Mg ratio of 7:1 (see 5.1.5) (the sodium concentration was adjusted accordingly to keep the osmolality stable) and incubating the cells for varying time periods (1 min., 5 min., 10 min.).

Specific receptor agonists were applied directly into the ACSF (see 5.1.5).

- Glutamate (10 µM final concentration) or a solution containing both glutamate (10 µM final concentration) and glycine (10 µM final concentration) were added to target the different types of glutamate receptors for varying time periods (5 min., 15 min., 30 min.).
- NMDA was supplied to the hippocampal neurons for 30 min. at a final concentration of 10 µM
  OR for 3 min. at a final concentration of 25 µM to chemically induce long-term depression (chem. LTD) of the neurons.
- GABA (50 µM final concentration) was applied to hippocampal neurons in ACSF for 3 h.

The cells were fixed (see 4.3.4) directly after stimulation or after washing away the respective stimulatory agent with ACSF and an incubation period of 30 min., 1 h or 2 h in fresh ACSF medium.

5. Material

5.1 Solutions and buffers

5.1.1 Solutions for the analysis of nucleic acids

Name	Substance	concentration
DNA extraction buffer	Tris-HCl pH 7.4	50 mM
	NaCl	100 mM
	SDS	1%
	EDTA	5 mM
	Proteinase K	0.5 µg/ µl
DNA loading buffer (100 ml)	Sucrose	40%
	SDS	0.5%
	Bromphenole blue	0.25%
	TE buffer	to 100 ml
Proteinase K (stock in H_2O)	Proteinase K	10 µg/ µl
TAE-buffer 50x pH 8.3	Tris base	2 M (242.2 g)
	Acetic acid (glacial)	57.1 ml
	EDTA 0.5 M (pH 8,0)	0,05 M (100 ml)
TE buffer	Tris-HCl pH 8.0	100 mM
	EDTA	1 mM

5.1.2 Solutions for biochemical analysis

Name	Substance	concentration
Coomassie gel destain (fixation solution)	Methanol Acetic acid	40% 10%
Coomassie gel staining solution	Methanol Acetic acid Coomassie Brilliant Blue G-250	50% 10% 0.1% filtrated
Coomassie gel destain (washing solution)	Methanol Acetic acid	20% 10%
Sepharose-resin Coupling buffer	$NaCO_3$ pH 8.3 NaCl	0.1 M 0.5 M
ECL solution A (200 ml)	Tris-HCl pH 8.6 Luminol stock p-hydroxy-coumarin stock	0.1 M 4 ml 0.1 ml
ECL solution B (200 ml)	Tris-HCl pH 8.6 H_2O_2 (30%)	0.1 M 0.2 ml
Luminol stock solution (10 ml)	Luminol in DMSO	0.44 g
NCP 10x pH 8-8.2	NaCl Tris base Tween-20 HCl 6 M	1.47 M 0.4 M 0.5% app. 40-45 ml

p-hydroxy-coumarin stock	p-hydroxy-coumarin in DMSO	150 mg
PLP-Sepharose beads acidic washing solution	Na-acetate pH 4.0 NaCl	0.1 M 0.5 M
PLP-Sepharose beads basic washing solution	Tris-HCl pH 8.0 NaCl	0.1 M 0.5 M
PLP-Sepharose beads storage solution	Tris-HCl pH 8.0 EDTA NaCl NaN_3 EtOH	20 mM 5 mM 100 mM 0.1% 20%
Polyacrylamide resolving gel 8% (50 ml for 7 gels)	H_2O Acrylamide (30%) Tris-HCl 2 M pH 8.8 SDS (20%) APS (10%) TEMED	26.7 ml 13.3 ml 9.5 ml 250 µl 320 µl 25 µl
Polyacrylamide resolving gel 15% (50 ml for 7 gels)	H_2O Acrylamide (30%) Tris-HCl 2 M pH 8.8 SDS (20%) APS (10%) TEMED	15 ml 25 ml 9.5 ml 250 µl 320 µl 25 µl
Polyacrylamide stacking gel 4% (30 ml for 7 gels)	H_2O Acrylamide (30%) Tris-HCl 0.5 M pH 6.8 SDS (20%) APS (10%) TEMED	18.3 ml 3.9 ml 7.5 ml 150 µl 180 µl 14 µl
SDS-loading buffer 5x (SDS-sample buffer 5x)	Tris-HCl pH 6.8 Glycerol SDS β-mercaptoethanol Bromphenole blue	110 mM 20% 3.8% 8% ad libitum
SDS-running buffer 10x	Tris base Glycine SDS (20%)	0.25 M 1.92 M 1%
Sepharose beads blocking solution for IP	PBS BSA (1 mg/ml)	1x 0.1%
Sepharose beads deblocking solution	HCl 37%	1 mM
Silver stain $AgNO_3$ solution	$AgNO_3$ Formaldehyde 37%	2 g/l 0.75 ml/l
Silver stain fixation solution	Methanol Acetic acid (glacial) Formaldehyde 37%	50% 12% 0.5 ml/l
Silver stain Na_2CO_3 solution	Na_2CO_3 Formaldehyde 37% $Na_2S_2O_3$	2 g/l 0.5 ml/l 4 mg/l
Silver stain $Na_2S_2O_3$ solution	$Na_2S_2O_3$	0.2 g/l
Silver stain stopping solution	Ethanol absolute	10%

	Acetic acid (glacial)	10%
Streptag lysis buffer	EDTA	5 mM
	Triton-X 100	0.5%
	sucrose	10%
	Complete protease inhibitor, EDTA-free, Roche	1x
Streptag washing buffer	Tris-HCl pH 8	100 mM
	EDTA	1 mM
	NaCl	150 mM
Streptag elution buffer	Tris-HCl pH 8	100 mM
	EDTA	1 mM
	NaCl	150 mM
	D-Desthiobiotin	2.5 mM
Streptag regeneration buffer	Tris-HCl pH 10.5	100 mM
	EDTA	1 mM
	NaCl	150 mM
	HABA	1 mM
Triton lysis buffer (TLB)	NaCl	150 mM
	Tris-HCl pH 7.4- 8	50 mM
	TritonX-100	1%
	Complete protease inhibitor, EDTA-free, Roche	1x
Towbin transfer buffer 1x	Tris base	25 mM
	Glycine	192 mM
	methanol	20%

5.1.3 Solutions for histological analysis

Name	**Substance**	**concentration**
IF blocking solution for vibratome sections	TBS-T	1x
	NGS	2-10%
	DMSO	1-2%
IF blocking solution for cultured neurons	TBS	1x
	NGS	10%
	Tween-20	0.2%
Paraformaldehyde (PFA) 4% (pH 7.2, 100 ml)	PBS 1x	60 ml
	PFA	4 g
		dissolve at 65 ºC
	PBS 1x	adjust volume to 100 ml
		sterile filtrate
PBS (10x) pH 7.4	NaCl	1.5 M
	Na_2HPO_4	162 mM
	NaH_2PO_4	38 mM
TBS 10x	Tris-HCl pH 7.4	400 mM
	NaCl	1.5 M
TBS-T	TBS	1x
	TritonX-100	0.2%
Autofluorescence quenching solution	Ammoniumchloride (NH_4Cl)	50 mM
Glycerol mounting medium	Glycerol	90%
	Tris-HCl pH 8.5	40 mM

	n-propyl-gallate (NPG)	5%
	1,4-diazabicyclo[2.2.2]octane (DABCO)	2.5%
	p-phenyl-endiamine (PPD)	0.25%
Mowiol mounting medium	Mowiol	20%
	Tris-HCl pH 8.5	40 mM
	n-propyl-gallate (NPG)	5%
	1,4-diazabicyclo[2.2.2]octane (DABCO)	2.5%
	p-phenyl-endiamine (PPD)	0.25%

5.1.4 Solutions for neuron culture

Solution	Substance	Amount
N2-medium	Neuropan2	5 ml
	Pyruvic acid	5 ml
	Glucose (20%)	15 ml
	$NaHCO_3$ (5,5%)	20 ml
	MEM (10x)	50 ml
	H_2O	to 400 ml
		adjust pH to 7.3
		fill up to 500 ml
		filter sterile
MEM-HS/FCS	MEM (10x)	50 ml
	Glucose (20%)	15 ml
	$NaHCO_3$ (5,5%)	20 ml
	L-glutamine (200 mM)	5 ml
	MEM essential amino acids (50x)	10 ml
	MEM non-essential amino acids (100x)	10 ml
	Horse serum (HS)/fetal calf serum (FCS), heat-inactivated	50 ml
	H_2O	to 400 ml
		adjust pH to 7.3
		fill up to 500 ml
		filter sterile
HBSS/HEPES	HBSS	500 ml
	HEPES 1 M pH 7.25	3.5 ml
Trypsin	Trypsin/EDTA (0.05%)	100 ml
	HEPES 1 M pH 7.25	700 µl
Fixative for neurons	PFA	4%
	Glutaraldehyde	0.25%
	Sucrose	2%
AraC (200x)	AraC	12 mg
	H_2O	50 ml
Borate buffer	Boric acid	1.24 g
	Borax	1.90 g
	H_2O	to 400 ml
		to pH 8.5
		filter sterile
Poly-L-lysine	Poly-L-lysine hydrobromide	100 mg
	Borate buffer	100 ml

5.1.5 Solutions for neuron stimulation

Solution	Substance	Concentration
ACSF	NaCl	124 mM
	KCl	2.5 mM
	NaH_2PO_4	1.2 mM
	$NaHCO_3$	24 mM
	HEPES	5 mM
	Glucose	12.5 mM
	$MgSO_4$	2 mM
	$CaCl_2$	2 mM
ACSF for KCl stimulation	NaCl	36.5 mM
	KCl	90 mM
	NaH_2PO_4	1.2 mM
	$NaHCO_3$	24 mM
	HEPES	5 mM
	Glucose	12.5 mM
	$MgSO_4$	2 mM
	$CaCl_2$	2 mM
ACSF for pre-synaptic stimulation increasing the Ca^{2+}/Mg^{2+} ratio to 7:1	NaCl	124 mM
	KCl	2.5 mM
	NaH_2PO_4	1.2 mM
	$NaHCO_3$	24 mM
	HEPES	5 mM
	Glucose	12.5 mM
	$MgSO_4$	0.5 mM
	$CaCl_2$	3.5 mM

5.1.5.1 Receptor agonist solutions for neuron stimulation

Receptor agonist	Substance	Concentration
NMDA	ACSF	1x
	NMDA	10 µM
NMDA for chemical LTD	ACSF	1x
	NMDA	25 µM
Glutamate	ACSF	1x
	Glutamate	10 µM
Glutamate/glycine	ACSF	1x
	Glutamate	10 µM
	Glycine	10 µM
GABA	ACSF	1x
	GABA	50 µM

5.2 Commercial solutions, chemicals and reagents

5.2.1 Commercial solutions for nucleic acid analysis

Name	Manufacturer
dNTPs	Promega
DTT 0.1 M	Invitrogen
First strand buffer 5x	Invitrogen
Go-*taq*-polymerase	Promega
$MgCl_2$	Invitrogen
$MgCl_2$	Promega
PCR-flexi-buffer (5x)	Promega

5.2.2 Commercial solutions for protein analysis

Name	Manufacturer
Bradford reagent (5x)	Bio-Rad
Broad Range marker	Bio-Rad
Clean-blot™ IP Detection Reagent (HRP)	Thermo Scientific
SeeBlue Plus2 Prestained marker	Invitrogen

5.2.3 Liquid chemicals

Name	Manufacturer
1 kb Plus DNA Ladder	Invitrogen
Acidic acid glacial	Merck
Acrylamide (30%)	Bio-Rad
β-Mercaptoethanol	Sigma
Bovine serum albumin (BSA), (10 mg/ml)	New England Biolabs
Broad Range marker	BioRad
Chloroform	Merck
Dimethyl sulfoxide (DMSO)	Merck
Ethanol (technical)	Merck
Ethanol for analysis	Merck
Ethidiumbromide (1%)	Bio-Rad
Formaldehyde 37%	Sigma
Formamide	Sigma
Glycerol	Sigma
Hydrochloric acid (HCL) (fuming, 37%)	Merck
Hydrogen peroxide (30%)	Merck
Isopropanol	Merck
Methanol	VWR
Mowiol 4-88	Roth
Normal goat serum (NGS)	Vector Laboratories
Nitrogen (liquid)	German-Cryo
Nonidet P-40	Sigma
Phenol	Merck
Protein A sepharose 4 Fast Flow	GE Healthcare

Protein G sepharose 4 Fast Flow	GE Healthcare
SeaBlue Plus2 Pre-Stained Standard	Invitrogen
TEMED	Sigma
Triton-X 100	Roche
Tween-20	Sigma

5.2.4 Solid chemicals

Name	**Manufacturer**
Agarose	Sigma
APS	Fisher Scientific
Borax	Merck
Boric acid	Merck
Bovine serum albumin (BSA)	Merck
Bromphenol blue	Bio-Rad
Coomassie Brilliant Blue	Bio-Rad
CNBr-activated sepharose beads 4 Fast Flow	GE Healthcare
DTT	Sigma
EDTA	Sigma
GABA	Sigma
Glucose	Merck
Glutamate	Sigma
Glycine	Applichem
Luminol	Sigma
Magnesium chloride ($MgCl_2$)	Sigma
Milk powder (non-fat)	Roth
MOPS	Serva
NaH_2PO_4	Sigma
Na_2HPO_4	Sigma
NMDA	Sigma
NaOH pellets	Sigma
Paraffin, low-melting	Merck
PBS^-	Sigma
p-hydroxy-Coumarin	Sigma
Poly-L-proline MW > 40,000	Sigma
Propyl gallate	Sigma
Protease inhibitor cocktail tablets, Complete, EDTA-free	Roche
Proteinase K	Sigma
Silvernitrate	Applichem
Sodium acetate	Merck
Sodium azide (NaN_3)	Merck
Sodium carbonate ($NaCO_3$)	Merck
Sodium chloride (NaCl)	Merck
Sodium deoxycholate	Merck
Sodium dodecylsulfate (SDS)	Merck
Sodium thiosulfate (NaS_2O_3)	Sigma
Tris Base Ultra Pure Quality	Roth

5.3 Laboratory material

5.3.1 Plastic ware

5.3.1.1 Plastic ware

Name	Manufacturer
Eppendorf tubes (0.5 ml, 1.5 ml, 2 ml)	Eppendorf
Tubes (15 ml, 50 ml, 150 ml)	Sarstedt
PCR tubes	Bioplastics
Pipettes (5 ml, 10 ml, 25 ml, 50 ml)	BD Falcon
Pipette tips (plugged)	ART
Pipette tips (20 µl, 200 µl, 1000 µl)	Sarstedt
24-well plates	Corning
Micro Bio-spin chromatography columns	Bio-Rad
Chromatography columns (2 ml/ 15 ml/ 50 ml)	Bio-Rad

5.3.1.2 Plastic ware for tissue culture

Name	Manufacturer
24-well-plates	Corning
Eppendorf tubes (1.5 ml, 2 ml)	Eppendorf
Tubes (15 ml)	Corning
Pipettes (5 ml, 10 ml, 25 ml, 50 ml)	BD Falcon
Dishes (3 cm Ø, 6 cm Ø)	Nunc
Flask (T-25, T-75)	Nunc

5.3.2 Glass ware

Name	Manufacturer
Glass bottles (50 ml, 100 ml, 250 ml, 500 ml, 1000 ml, 2000 ml)	Schott
Glass pipettes	Brand
Pasteur pipettes	Brand

5.3.3 Further material

Name	Manufacturer
PVDF transfer membrane Immobilon-P	Millipore
Bio Max XAR Film	Kodak

5.4 Technical equipment

5.4.1 General technical equipment

Name	Manufacturer
Accu-Jet/Pipet boy	Brand
Agarose gel electrophoresis running chamber	European Molecular Biology Laboratory
Centrifuge 5415 D	Eppendorf
Centrifuge 5417 R	Eppendorf
Centrifuge J2-HS	Beckman
Centrifuge J2-MC	Beckman
Cover slips No. 1.5H	Marienfeld
ECL-Imager LAS Mini	GE Healthcare
Film developer Curix 60	AGFA
Freezer (-80 °C)	Thermo Scientific
Gel documentation machine UV	Herolab
Polyacrylamide gel electrophoresis running chamber	Hoefer
Glass-Teflon tissue grinders	Kimbel Kontes
Heating block	Grant/QBT
Homogenizer	Bosch
Magnetic stirring plate	Heidolph
Microscope slides super premium	VWR
PCR machine PTC-200 Peltier thermal cycler	MJ Research
pH-meter, pH Level 2	InoLab
Pipettes	Gilson
Power supply (for agarose gels)	Pharmacia
Power supply Power PAC 200/ 300	Bio-Rad
Razor blades for vibratome cutting	Gilette
Rocker	Heidolph
Scale	Sartorius
Scale (analytic)	Kern & Sohn
SDS gel apparatus SE250	Pharmacia Biotech
Semi-dry blotting chamber	Bio-Rad
Shaker	New Brunswick Scientific
Spectrophotometer UV-DU 640	Beckmann
Ultracentrifuge Optima™ TL	Beckmann
UV-Table	Bachofer
Vibratome VT 1200S	Leica
Vortex-Genie 2	Scientific Industries
Water purifier	Millipore

5.4.2 Microscope

Name	Manufacturer
Axioplan 2	Carl Zeiss
Zeiss Meta detector PMT	Carl Zeiss
Zeiss LSM 510 laser set	Carl Zeiss
Argon/2 laser 488 nm/458 nm/477 nm/514 nm	25 mW
HeNe laser 543 nm	1 mW
HeNe laser 633 nm	10 mW
Zeiss LSM 510 Meta filter set	Carl Zeiss

- LP 505
- BP 475-525
- BP 500/20
- BP 505-530
- BP 530-600
- BP 560-615

Immersol™ 518 F Immersion Oil	Carl Zeiss

5.5 Oligonucleotides

The oligonucleotides were produces by Eurofins MWG Operon.

Oligo	Sequence (5´-3´ direction)
Pfn2-for (s) (229)	GTC TTG GTC TTT GTA ATG GGA AAA G
Pfn2-rev (as) (268)	GGA GTA CAC AAG GAA AC
PGFP-1 (as) (593)	TTG AAG AAG TCG TGC TG
PPI-1 (s) (614)	TTT CGT CAA TGG GCT GAC AC
PPI-9 (as) (616)	AAG CTC AAA GCA AGA AGG GAC
PPII-28 (s) (615)	AGT CAA GGT GGG GAG CCA AC
PPI-3 (as)	AGC CCA TGT GGT TTT GGC AGC
PPI-2 (as)	GGAAGG GAC AGA TGA GG
PPII-2 (s)	AAA TAC GTC TGG GCA GCC AC
CPII-1as (as)	TGTGCCTGCGTGGACACC
CPII-2as (as)	ATAAAGGTTGGTTACAGACC

5.6 Newly generated bacterial expression constructs

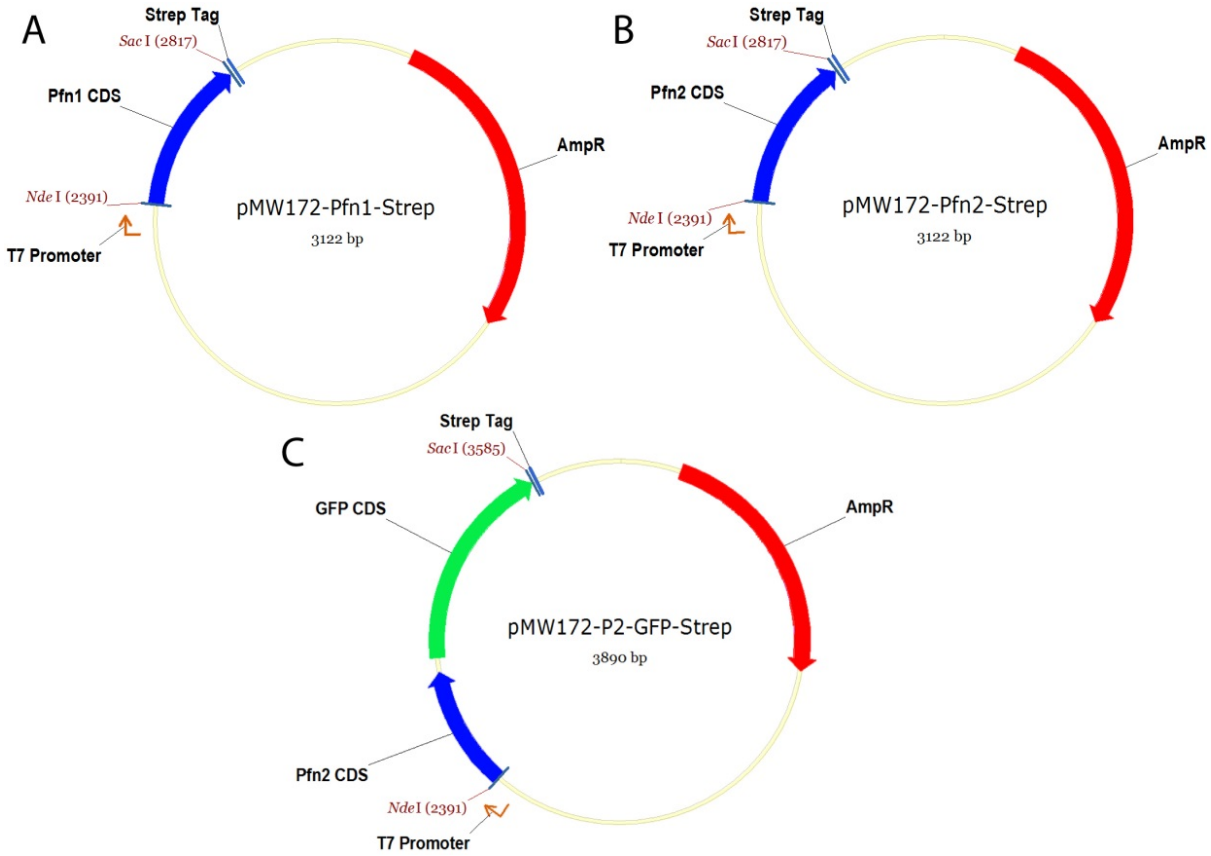

Fig. 28 Bacterial expression vectors for Pfn1-, Pfn2- and P2-GFP-Streptag fusion proteins
The cDNA of mouse Pfn1, Pfn2a or P2-GFP was generated from isolated brain tissue RNA. The respective gene was integrated in the pMW172-Strepag expression vector (kindly provided by Julia Hecker) by *SacI* and *NdeI* mediated insertion. PMW172-Streptag vectors with the inserted gene of Pfn1 (**A**, Witke archive Nr. 574), Pfn2 (**B**, Witke archive Nr. 571) and P2-GFP (**C**, Witke archive Nr. 573) were obtained from bacteria and the corresponding fusion proteins were purified from bacterial extracts.

5.7 Antibodies

5.7.1 Primary antibodies

Antigen	Host species	Company	Dilutions	Conditions
Abi1	Rb poly	Sigma	WB 1:2000	2 h, RT
Abi2	Ms mono	Sigma	WB 1:200	o.n., 4°C
Actin (clone C4)	Ms mono	ImmunO	WB 1:2000	2 h, RT
Arp3	Rb poly	Anika Steffens	WB 1:1800	2 h, RT
DBH	Sh poly	Cell signaling	IF 1:500	o.n., 4°C
Calbindin	Ms mono	Sigma	IF 1:400	o.n., 4°C
ChAT	Rb poly	Abcam	IF 1:200	24 h, RT
ChT	Ms mono	SYSY	IF 1:500	o.n., RT
Cleaved-caspase3	Rb poly	Millipore/ Chemicon	IF 1:100	o.n., 4°C

Cleaved-caspase3-Alexa488	Rb poly	Cell signaling	IF 1:100	o.n., 4°C
CNPase	Ms mono	Millipore	IF 1:100	o.n., 4°C
Cortactin	Ms mono	Anika Steffens	WB 1:1000	1 h, RT
CyFIP1	Rb poly	Upstate cell signaling	WB 1:500	o.n., 4°C
CyFIP2 (5C9)	Ms mono	Walter Witke	WB 1:2	o.n., 4°C
CyFIP2 (5C9)-affinity purified	Ms mono	Walter Witke	IF 1:100	o.n., 4°C
DARPP32	Rb poly	Cell signaling	IF 1:100	o.n., 4°C
Dopamine D1 receptor	Rb poly	Alomone	IF 1:50	o.n., 4°C
Dopamine D2 receptor	Rb poly	Alomone	IF 1:50	o.n., 4°C
Iba1	Rb poly	WAKO Chemicals	IF 1:750	o.n., 4°C
Dynamin1	Ms mono	Upstate cell signaling	WB 1:1000	o.n., 4°C
Endophilin1	Rb poly	Walter Witke	WB 1:500	o.n., 4°C
GABA	Rb poly	Sigma	IF 1:1000	o.n., 4°C
$GABA_B$-receptor	Gp poly	Sigma	IF 1:1000	o.n., 4°C
Gad1	Rb poly	SYSY	IF 1:200	o.n., 4°C
Gephyrin	Ms mono	SYSY	IF 1:200	o.n., 4°C
GFAP	Rb poly	Sigma	IF 1:150	o.n., 4°C
			WB 1:100	o.n., 4°C
GFAP	Ms mono	Millipore	WB 1:500	o.n., 4°C
			IF 1:500	o.n., 4°C
GFP	Chk poly	Abcam	WB 1:2000	o.n., 4°C
			IF 1:1000	o.n., 4°C
GFP	Chk poly	Acris	WB 1:500	o.n., 4°C
			IF 1:500	o.n., 4°C or RT
GFP-Atto488	Llama mono	Chromotek	IF 1:100	o.n., 4°C
GFP-Trap-A	Llama mono	Chromotek	IP	
GluR1	Rb poly	Upstate cell signaling	IF 1:500	o.n., 4°C
Grip	Rb poly	SYSY	IF 1:100	24 h, RT
Huntingtin	Ms mono	Chemicon	WB 1:1000	o.n., 4°C
Map2	Rb poly	Millipore	IF 1:500	o.n., 4°C
Map2	Ms mono	Transduct. Labs.	IF 1:1000	o.n., 4°C
MBP	Rb poly	Abcam	IF 1:100	o.n., RT
mDia1	Ms mono	BD Transduct. Labs.	WB 1:500	o.n., 4°C
mDia2	Rb poly	Anika Steffens	WB 1:1000	o.n., 4°C
Mena	Rb poly	Walter Witke	WB 1:500	o.n., 4°C
Nap1	Rb poly	Upstate cell signaling	WB 1:1000	o.n., 4°C
Nestin	Ms mono	Millipore	IF 1:100	o.n., 4°C
NeuN (clone A60)	Ms mono	Millipore	IF 1:100	o.n., 4°C
Neurofilament 200 (clone RT97)	Ms mono	Böhringer Mannheim	IF 1:500	o.n., 4°C
Neurofilament 200	Rb poly	Sigma	IF 1:500	o.n., 4°C
NG2	Rb poly	Millipore	IF 1:100	o.n., RT
NRGN	Rb poly	ProteinTech	IF 1:500	o.n., 4°C
Oct4a	Rb poly	Cell Signaling	IF 1:200	o.n., 4°C
Parvalbumin	Ms mono	Sigma	IF 1:500	o.n., 4°C
Pax6	Rb poly	Covance	IF 1:100	o.n., 4°C
Pfn1 T	Rb poly	Walter Witke	WB 1:1000	o.n., 4°C
			IF 1:100	o.n., 4°C
Pfn2 T2	Rb poly	Walter Witke	WB 1:2000	2h, RT - o.n., 4°C

			IF 1:100	o.n., RT
Pfn2 3003	Rb poly	Walter Witke	WB 1:1000	o.n., 4°C
			IF 1:100	o.n., 4°C
Pfn2 5A7	Ms mono	Walter Witke	IP 1:100	
Pfn2 DB2	Rb poly	Walter Witke	WB 1:100	o.n., 4°C
			IF 1:100	o.n., 4°C
Pfn2 GD2	Rb poly	Walter Witke	WB 1:1000	o.n., 4°C
			IF 1:100	o.n., 4°C
PSD95	Rb poly	SYSY	IF 1:100	o.n., 4°C
PSD95	Ms mono	Upstate cell signaling	IF 1:200	o.n., RT
Rac1	Ms mono	Anika Steffens	WB 1:2000	o.n., 4°C
Reelin	Ms mono	Millipore	WB 1:1000	o.n., 4°C
			IF 1:100	o.n., 4°C
S100β	Rb poly	Abcam	WB 1:1000	o.n., 4°C
			IF 1:1000	o.n., 4°C
Snap25	Rb poly	Sigma	IF 1:500	o.n., 4°C
Sox2	Rb poly	Cell signaling	IF 1:200	o.n., 4°C
Sox2	Ms mono	Cell signaling	IF 1:200	o.n., 4°C
Synapsin 1	Ms mono	Chemicon	IF 1:200	2 h, RT
Synapsin 2a	Ms mono	Transduct. Labs.	IF 1:2000	2 h, RT - o.n., 4°C
Synaptophysin	Ms mono	Sigma	IF 1:400	o.n., 4°C
Synaptotagmin1	Rb poly	SYSY	IF 1:100	o.n., 4°C
Tau1 (clone PC1C6)	Ms mono	Millipore	IF 1:1000	o.n., 4°C
Tbr1	Rb poly	Millipore	IF 1:200	o.n., 4°C
Tbr2	Rb poly	Millipore	IF 1:200	o.n., 4°C
TH (clone TH-2)	Ms mono	Sigma	IF 1:150	o.n., 4°C
TH	Gp poly	SYSY	IF 1:500	o.n., 4°C
TPH	Ms mono	Sigma	IF 1:200	o.n., 4°C
β3-tubulin	Ms mono	Promega	IF 1:1000	o.n., 4°C
γ-tubulin	Ms mono	Sigma	WB 1:500	o.n., 4°C
VAMP2	Rb poly	SYSY	IF 1:1000	o.n., 4°C
VASP	Rb poly	Anika Steffens	WB 1:1000	o.n., 4°C
VIAAT	Rb poly	Bruno Grasnier	IF 1:500	o.n., 4°C
VGluT1	Gp poly	Millipore	IF 1:500	o.n., RT
VGluT2	Gp poly	SYSY	IF 1:500	o.n., 4°C
Vimentin	Rb poly	Abcam	IF 1:1000	o.n., 4°C
Wave1	Ms mono	BD Transduct. Labs.	WB 1:1000	2 h, RT
Wave2	Rb poly	Upstate cell signaling	WB 1:500	o.n., 4°C
Wave3	Goat poly	Santa Cruz	WB 1:500	o.n., 4°C
Wave3	Rb poly	Abcam	WB 1:1000	o.n., 4°C

5.7.2 Secondary antibodies

Antigen species	**Conjugate**	**Host species**	**Company**	**dilution**
Chicken	Alexa 488	Goat	Life Technologies	1:1000
Chicken	Alexa 488	Goat	Abcam	1:500
Chicken	Atto 488	Alpaca	Creative Diagnostics	1:100

Chicken	HRP	Goat	Dianova	1:5000
Goat	HRP	Donkey	Dianova	1:5000
Guinea Pig	CF 543	Donkey	Biotium	1:1000
Guinea pig	Alexa 594	Goat	Life Technologies (Molecular Probes)	1:500
Guinea pig	HRP	Rabbit	Sigma	1:5000
Mouse	Alexa 488	Goat	Life Technologies (Molecular Probes)	1:1000
Mouse	Alexa 555	Goat	Life Technologies	1:1000
Mouse	Alexa 594	Goat	Life Technologies (Molecular Probes)	1:1000
Mouse	Alexa 647	Goat	Life Technologies (Invitrogen)	1:500
Mouse	CF 633	Donkey	Biotium	1:500
Mouse	HRP	Goat	Dianova	1:5000
Rabbit	Alexa 488	Goat	Life Technologies	1:1000
Rabbit	Alexa 555	Goat	Life Technologies	1:1000
Rabbit	Alexa 594	Goat	Life Technologies (Molecular Probes)	1:1000
Rabbit	Alexa 647	Goat	Life Technologies (Invitrogen)	1:500
Rabbit	CF 633	Donkey	Biotium	1:500
Rabbit	HRP	Goat	Dianova	1:5000
Sheep	Alexa 555	Donkey	Life Technologies	1:1000

5.8 Dyes and staining reagents

Dye type	Conjugate	Company
DAPI		Sigma
Draq5		Biostatus
Phalloidin	Alexa 488	Life Technologies
Phalloidin	Alexa 594	Life Technologies
Phalloidin	Alexa 680	Life Technologies
Phalloidin	Atto 488	AttoTec
Phalloidin	CF 542	Biotium
Propidium iodide		Sigma
Streptactin	HRP	Bio-Rad

5.9 Animal lines

Line	Reference
Pfn2-lacZ (Pfn2 KO)	Walter Witke
P2-GFP	Pietro Pilo Boyl
wt	Charles River

6. References

Abrahams, B.S., and Geschwind, D.H. (2008). Advances in autism genetics: on the threshold of a new neurobiology. Nat. Rev. Genet. *9*, 341–355.

Ackermann, M., and Matus, A. (2003). Activity-induced targeting of profilin and stabilization of dendritic spine morphology. Nat. Neurosci. *6*, 1194–1200.

Ahuja, R., Pinyol, R., Reichenbach, N., Custer, L., Klingensmith, J., Kessels, M.M., and Qualmann, B. (2007). Cordon-Bleu Is an Actin Nucleation Factor and Controls Neuronal Morphology. Cell *131*, 337–350.

Aimone, J.B., Deng, W., and Gage, F.H. (2011). Resolving New Memories: A Critical Look at the Dentate Gyrus, Adult Neurogenesis, and Pattern Separation. Neuron *70*, 589–596.

Alarcón, M., Abrahams, B.S., Stone, J.L., Duvall, J. a., Perederiy, J. V., Bomar, J.M., Sebat, J., Wigler, M., Martin, C.L., Ledbetter, D.H., et al. (2008). Linkage, Association, and Gene-Expression Analyses Identify CNTNAP2 as an Autism-Susceptibility Gene. Am. J. Hum. Genet. *82*, 150–159.

Anderson, G.M., Horne, W.C., Chatterjee, D., and Cohen, D.J. (1990). The hyperserotonemia of autism. Ann. N. Y. Acad. Sci. *600*, 331–340; discussion 341–342.

Anderson, G.R., Galfin, T., Xu, W., Aoto, J., Malenka, R.C., and Sudhof, T.C. (2012). Candidate autism gene screen identifies critical role for cell-adhesion molecule CASPR2 in dendritic arborization and spine development. Proc. Natl. Acad. Sci. *109*, 18120–18125.

Andrade, R. (2011). Serotonergic regulation of neuronal excitability in the prefrontal cortex. Neuropharmacology *61*, 382–386.

Ascoli, G.A., Alonso-Nanclares, L., Anderson, S.A., Barrionuevo, G., Benavides-Piccione, R., Burkhalter, A., Buzsáki, G., Cauli, B., Defelipe, J., Fairén, A., et al. (2008). Petilla terminology: nomenclature of features of GABAergic interneurons of the cerebral cortex. Nat. Rev. Neurosci. *9*, 557–568.

Aumeier, C., Polinski, E., and Menzel, D. (2015). Actin, actin-related proteins and profilin in diatoms: A comparative genomic analysis. Mar. Genomics.

Aungst, J.L., Heyward, P.M., Puche, a C., Karnup, S. V, Hayar, A., Szabo, G., and Shipley, M.T. (2003). Centre-surround inhibition among olfactory bulb glomeruli. Nature *426*, 623–629.

Ayala, R., Shu, T., and Tsai, L.-H. (2007). Trekking across the brain: the journey of neuronal migration. Cell *128*, 29–43.

Ballesteros Yáñez, I., Muñoz, A., Contreras, J., Gonzalez, J., Rodriguez-Veiga, E., and DeFelipe, J. (2005). Double bouquet cell in the human cerebral cortex and a comparison with other mammals. J. Comp. Neurol. *486*, 344–360.

Bang, M.L., and Owczarek, S. (2013). A matter of balance: Role of neurexin and neuroligin at the synapse. Neurochem. Res. *38*, 1174–1189.

Battaglia, D., Karagiannis, A., Gallopin, T., Gutch, H.W., and Cauli, B. (2013). Beyond the frontiers of neuronal types. Front. Neural Circuits *7*, 13.

Beckervordersandforth, R., Tripathi, P., Ninkovic, J., Bayam, E., Lepier, A., Stempfhuber, B., Kirchhoff, F., Hirrlinger, J., Haslinger, A., Lie, D.C., et al. (2010). In vivo fate mapping and expression analysis reveals molecular hallmarks of prospectively isolated adult neural stem cells. Cell Stem Cell *7*, 744–758.

Behnen, M., Murk, K., Kursula, P., Cappallo-Obermann, H., Rothkegel, M., Kierszenbaum, A.L., and Kirchhoff, C. (2009). Testis-expressed profilins 3 and 4 show distinct functional characteristics and localize in the acroplaxome-manchette complex in spermatids. BMC Cell Biol. *10*, 34.

Bellot, A., Guivernau, B., Tajes, M., Bosch-Morató, M., Valls-Comamala, V., and Muñoz, F.J. (2014). The structure and function of actin cytoskeleton in mature glutamatergic dendritic spines. Brain Res. *1573*, 1–16.

Bergles, D.E., Jabs, R., and Steinhäuser, C. (2010). Neuron-glia synapses in the brain. Brain Res. Rev. *63*, 130–137.

Beutner, C., Roy, K., Linnartz, B., Napoli, I., and Neumann, H. (2010). Generation of microglial cells from mouse embryonic stem cells. Nat. Protoc. *5*, 1481–1494.

Biggin, P.C. (2002). Glutamate receptors: Desensitizing dimers. Curr. Biol. *12*, 631–632.

Binley, K.E., Ng, W.S., Tribble, J.R., Song, B., and Morgan, J.E. (2014). Sholl analysis: A quantitative comparison of semi-automated methods. J. Neurosci. Methods *225*, 65–70.

Birbach, A., Verkuyl, J.M., and Matus, A. (2006). Reversible, activity-dependent targeting of profilin to neuronal nuclei. Exp. Cell Res. *312*, 2279–2287.

Björklund, A., and Dunnett, S.B. (2007). Dopamine neuron systems in the brain: an update. Trends Neurosci. *30*, 194–202.

Blasco, R., Cole, N.B., and Moss, B. (1991). Sequence analysis, expression, and deletion of a vaccinia virus gene encoding a homolog of profilin, a eukaryotic actin-binding protein. J. Virol. *65*, 4598–4608.

Boopathy, S., Silvas, T. V., Tischbein, M., Jansen, S., Shandilya, S.M., Zitzewitz, J. a., Landers, J.E., Goode, B.L., Schiffer, C. a., and Bosco, D. a. (2015). Structural basis for mutation-induced destabilization of profilin 1 in ALS. Proc. Natl. Acad. Sci. 201424108.

Bosch, M., Castro, J., Saneyoshi, T., Matsuno, H., Sur, M., and Hayashi, Y. (2014). Structural and molecular remodeling of dendritic spine substructures during long-term potentiation. Neuron *82*, 444–459.

Bosman, L.W.J., Hartmann, J., Barski, J.J., Lepier, A., Noll-Hussong, M., Reichardt, L.F., and Konnerth, A. (2006). Requirement of TrkB for synapse elimination in developing cerebellar Purkinje cells. Brain Cell Biol. *35*, 87–101.

Bradke, F., and Dotti, C.G. (1997). Neuronal polarity: Vectorial cytoplasmic flow precedes axon formation. Neuron *19*, 1175–1186.

Bradke, F., and Dotti, C.G. (1999). The role of local actin instability in axon formation. Science *283*, 1931–1934.

Bradke, F., and Dotti, C.G. (2000). Establishment of neuronal polarity: Lessons from cultured hippocampal neurons. Curr. Opin. Neurobiol. *10*, 574–581.

Brocco, M., Dekeyne, A., Veiga, S., Girardon, S., and Millan, M.J. (2002). Induction of hyperlocomotion in mice exposed to a novel environment by inhibition of serotonin reuptake. Pharmacol. Biochem. Behav. *71*, 667–680.

Burnett, B.G., Andrews, J., Ranganathan, S., Fischbeck, K.H., and Di Prospero, N. a. (2008). Expression of expanded polyglutamine targets profilin for degradation and alters actin dynamics. Neurobiol. Dis. *30*, 365–374.

Butler-Cole, C., Wagner, M.J., Da Silva, M., Brown, G.D., Burke, R.D., and Upton, C. (2007). An ectromelia virus profilin homolog interacts with cellular tropomyosin and viral A-type inclusion protein. Virol. J. *4*, 76.

Calabresi, P., Picconi, B., Tozzi, A., Ghiglieri, V., and Di Filippo, M. (2014). Direct and indirect pathways of basal ganglia: a critical reappraisal. Nat. Neurosci. *17*, 1022–1030.

Campellone, K.G., and Welch, M.D. (2010). A nucleator arms race: cellular control of actin assembly. Nat. Rev. Mol. Cell Biol. *11*, 237–251.

Cannon, W.B. (1929). Organization for Physiological Homeostasis. Physiol Rev *IX*, 399–431.

Carlsson, L., Nyström, L.E., Sundkvist, I., Markey, F., and Lindberg, U. (1977). Actin polymerizability is influenced by profilin, a low molecular weight protein in non-muscle cells. J. Mol. Biol. *115*, 465–483.

Cave, and Baker (2009). Dopamine systems in the forebrain. Adv Exp Med Biol 15–35.

Celio, M. (1990). Calbindin D-28k and parvalbumin nervous system. Neuroscience *35*, 375–475.

Chakrabarti, S., and Fombonne, E. (2005). Pervasive developmental disorders in preschool children: confirmation of high prevalence. Am. J. Psychiatry *162*, 1133–1141.

Chakraborty, J., Nthenge-Ngumbau, D.N., Rajamma, U., and Mohanakumar, K.P. (2014a). Melatonin protects against behavioural dysfunctions and dendritic spine damage in 3-nitropropionic acid-induced rat model of Huntington's disease. Behav. Brain Res. *264*, 91–104.

Chakraborty, J., Pandey, M., Navneet, a K., Appukuttan, T. a, Varghese, M., Sreetama, S.C., Rajamma, U., and Mohanakumar, K.P. (2014b). Profilin-2 increased expression and its altered interaction with β-actin in the striatum of 3-nitropropionic acid-induced Huntington's disease in rats. Neuroscience.

Chan, F., Bradley, A., Wensel, T.G., and Wilson, J.H. (2004). Knock-in human rhodopsin-GFP fusions as mouse models for human disease and targets for gene therapy. Proc. Natl. Acad. Sci. *101*, 9109–9114.

Chandana, S.R., Behen, M.E., Juhász, C., Muzik, O., Rothermel, R.D., Mangner, T.J., Chakraborty, P.K., Chugani, H.T., and Chugani, D.C. (2005). Significance of abnormalities in developmental trajectory and asymmetry of cortical serotonin synthesis in autism. Int. J. Dev. Neurosci. *23*, 171–182.

Chao, H., Chen, H., Samaco, R.C., Xue, M., Chahrour, M., Yoo, J., Neul, J.L., Gong, S., Lu, H., Heintz, N., et al. (2010). Dysfunction in GABA signalling mediates autism-like stereotypies and Rett syndrome phenotypes. Nature *468*, 263–269.

Chen, B., Brinkmann, K., Chen, Z., Pak, C.W., Liao, Y., Shi, S., Henry, L., Grishin, N. V., Bogdan, S., and Rosen, M.K. (2014). The WAVE regulatory complex links diverse receptors to the actin cytoskeleton. Cell *156*, 195–207.

Chen, L.Y., Rex, C.S., Casale, M.S., Gall, C.M., and Lynch, G. (2007a). Changes in synaptic morphology accompany actin signaling during LTP. J. Neurosci. *27*, 5363–5372.

Chen, Y., Balasubramaniyan, V., Peng, J., Hurlock, E.C., Tallquist, M., Li, J., and Lu, Q.R. (2007b). Isolation and culture of rat and mouse oligodendrocyte precursor cells. Nat. Protoc. *2*, 1044–1051.

Chen, Z., Borek, D., Padrick, S.B., Gomez, T.S., Metlagel, Z., Ismail, A.M., Umetani, J., Billadeau, D.D., Otwinowski, Z., and Rosen, M.K. (2010). Structure and control of the actin regulatory WAVE complex. Nature *468*, 533–538.

Chesarone, M. a., and Goode, B.L. (2009). Actin nucleation and elongation factors: mechanisms and interplay. Curr. Opin. Cell Biol. *21*, 28–37.

Chugani, D.C., Muzik, O., Rothermel, R., Behen, M., Chakraborty, P., Mangner, T., Da Silva, E.A., and Chugani, H.T. (1997). Altered serotonin synthesis in the dentatothalamocortical pathway in autistic boys. Ann. Neurol. *42*, 666–669.

Chugani, D.C., Muzik, O., Behen, M., Rothermel, R., Janisse, J.J., Lee, J., and Chugani, H.T. (1999). Developmental changes in brain serotonin synthesis capacity in autistic and nonautistic children. Ann. Neurol. *45*, 287–295.

Cingolani, L. a, and Goda, Y. (2008). Actin in action: the interplay between the actin cytoskeleton and synaptic efficacy. Nat. Rev. Neurosci. *9*, 344–356.

Cobos, I., Calcagnotto, M.E., Vilaythong, A.J., Thwin, M.T., Noebels, J.L., Baraban, S.C., and Rubenstein, J.L.R. (2005). Mice lacking Dlx1 show subtype-specific loss of interneurons, reduced inhibition and epilepsy. Nat. Neurosci. *8*, 1059–1068.

Cohen, I.L., Liu, X., Schutz, C., White, B.N., Jenkins, E.C., Brown, W.T., and Holden, J.J. a (2003). Association of autism severity with a monoamine oxidase A functional polymorphism. Clin. Genet. *64*, 190–197.

Cohen, Z., Ehret, M., Maître, M., and Hamel, E. (1995). Ultrastructural analysis of tryptophan hydroxylase immunoreactive nerve terminals in the rat cerebral cortex and hippocampus: their associations with local blood vessels. Neuroscience *66*, 555–569.

Coles, C.H., and Bradke, F. (2015). Coordinating Neuronal Actin – Microtubule Dynamics. Curr. Biol. *25*, R677–R691.

Cooley, L., Verheyen, E., and Ayers, K. (1992). chickadee encodes a profilin required for intercellular cytoplasm transport during Drosophila oogenesis. Cell *69*, 173–184.

Craig, A.M., Graf, E.R., and Linhoff, M.W. (2006). How to build a central synapse: Clues from cell culture. Trends Neurosci. *29*, 8–20.

Crawley, J.N. (2004). Designing mouse behavioral tasks relevant to autistic-like behaviors. Ment. Retard. Dev. Disabil. Res. Rev. *10*, 248–258.

Di Cristo, G. (2007). Development of cortical GABAergic circuits and its implications for neurodevelopmental disorders. Clin. Genet. *72*, 1–8.

Cuzon Carlson, V.C., Mathur, B.N., Davis, M.I., and Lovinger, D.M. (2011). Subsets of Spiny Striosomal Striatal Neurons Revealed in the Gad1-GFP BAC Transgenic Mouse. Basal Ganglia *1*, 201–211.

D'Angelo, E., and Casali, S. (2012). Seeking a unified framework for cerebellar function and

dysfunction: from circuit operations to cognition. Front. Neural Circuits *6*, 116.

Daoud, H., Dobrzeniecka, S., Camu, W., Meininger, V., Dupré, N., Dion, P. a, and Rouleau, G. a (2013). Mutation analysis of PFN1 in familial amyotrophic lateral sclerosis patients. Neurobiol. Aging *34*, 1311.e1–e2.

Debanne, D., Campanac, E., Bialowas, A., Carlier, E., and Alcaraz, G. (2011). Axon physiology. Physiol. Rev. *91*, 555–602.

Deng, W., Aimone, J.B., and Gage, F.H. (2010). New neurons and new memories: how does adult hippocampal neurogenesis affect learning and memory? Nat. Rev. Neurosci. *11*, 339–350.

Díez-Guerra, F.J. (2010). Neurogranin, a link between calcium/calmodulin and protein kinase C signaling in synaptic plasticity. IUBMB Life *62*, 597–606.

Dineley, K.T., Pandya, A.A., and Yakel, J.L. (2015). Nicotinic ACh receptors as therapeutic targets in CNS disorders. Trends Pharmacol. Sci. 1–13.

Donato, R., Cannon, B.R., Sorci, G., Riuzzi, F., Hsu, K., Weber, D.J., and Geczy, C.L. (2013). Functions of S100 proteins. Curr. Mol. Med. *13*, 24–57.

Dotti, C.G., Sullivan, C., and Banker, G. (1988). The Establishment of Polarity by Hippocampal Neurons in Culture. J. Neurosci. *8(4)*, 1454–1468.

Drago, J., Padungchaichot, P., Accili, D., and Fuchs, S. (1998a). Dopamine receptors and dopamine transporter in brain function and addictive behaviors: insights from targeted mouse mutants. Dev. Neurosci. *20*, 188–203.

Drago, J., Padungchaichot, P., Wong, J.Y., Lawrence, a J., McManus, J.F., Sumarsono, S.H., Natoli, a L., Lakso, M., Wreford, N., Westphal, H., et al. (1998b). Targeted expression of a toxin gene to D1 dopamine receptor neurons by cre-mediated site-specific recombination. J. Neurosci. *18*, 9845–9857.

Dufour-Rainfray, D., Vourc'h, P., Le Guisquet, A.-M., Garreau, L., Ternant, D., Bodard, S., Jaumain, E., Gulhan, Z., Belzung, C., Andres, C.R., et al. (2010). Behavior and serotonergic disorders in rats exposed prenatally to valproate: A model for autism. Neurosci. Lett. *470*, 55–59.

Durieux, P.F., Schiffmann, S.N., and de Kerchove d'Exaerde, A. (2011). Targeting neuronal populations of the striatum. Front. Neuroanat. *5*, 40.

Dutta, S., Das, S., Guhathakurta, S., Sen, B., Sinha, S., Chatterjee, A., Ghosh, S., Ahmed, S., Ghosh, S., and Usha, R. (2007). Glutamate receptor 6 gene (GluR6 or GRIK2) polymorphisms in the Indian population: A genetic association study on autism spectrum disorder. In Cellular and Molecular Neurobiology, pp. 1035–1047.

Eden, S., Rohatgi, R., Podtelejnikov, A. V, Mann, M., and Kirschner, M.W. (2002). Mechanism of regulation of WAVE1-induced actin nucleation by Rac1 and Nck. Nature *418*, 790–793.

Egile, C., Rouiller, I., Xu, X.P., Volkmann, N., Li, R., and Hanein, D. (2005). Mechanism of filament nucleation and branch stability revealed by the structure of the Arp2/3 complex at actin branch junctions. PLoS Biol. *3*, 1902–1909.

Ena, S., de Kerchove d'Exaerde, A., and Schiffmann, S.N. (2011). Unraveling the differential functions and regulation of striatal neuron sub-populations in motor control, reward, and motivational processes. Front. Behav. Neurosci. *5*, 47.

Ennis, M., Zhou, F.M., Ciombor, K.J., Aroniadou-Anderjaska, V., Hayar, A., Borrelli, E., Zimmer, L.A., Margolis, F., and Shipley, M.T. (2001). Dopamine D2 receptor-mediated presynaptic inhibition of olfactory nerve terminals. J. Neurophysiol. *86*, 2986–2997.

Ertürk, A., Hellal, F., Enes, J., and Bradke, F. (2007). Disorganized microtubules underlie the formation of retraction bulbs and the failure of axonal regeneration. J. Neurosci. *27*, 9169–9180.

Ertürk, A., Mauch, C.P., Hellal, F., Förstner, F., Keck, T., Becker, K., Jährling, N., Steffens, H., Richter, M., Hübener, M., et al. (2012). Three-dimensional imaging of the unsectioned adult spinal cord to assess axon regeneration and glial responses after injury. Nat. Med. *18*, 166–171.

Evangelista, M., Blundell, K., Longtine, M.S., Chow, C.J., Adames, N., Pringle, J.R., Peter, M., and Boone, C. (1997). Bni1p, a yeast formin linking cdc42p and the actin cytoskeleton during polarized morphogenesis. Science *276*, 118–122.

Faix, J., and Grosse, R. (2006). Staying in shape with formins. Dev. Cell *10*, 693–706.

Faux, C., Rakic, S., Andrews, W., and Britto, J.M. (2012). Neurons on the move: migration and lamination of cortical interneurons. Neurosignals. *20*, 168–189.

Figley, M.D., Bieri, G., Kolaitis, R.-M., Taylor, J.P., and Gitler, A.D. (2014). Profilin 1 associates with stress granules and ALS-linked mutations alter stress granule dynamics. J. Neurosci. *34*, 8083–8097.

Figueredo-Cardenas, G., Harris, C.L., Anderson, K.D., and Reiner, A. (1998). Relative Resistance of Striatal Neurons Containing Calbindin or Parvalbumin to Quinolinic Acid-Mediated Excitotoxicity Compared to Other Striatal Neuron Types. Exp. Neurol. *149*, 356–372.

Folstein, S.E., and Rosen-Sheidley, B. (2001). Genetics of autism: complex aetiology for a heterogeneous disorder. Nat. Rev. Genet. *2*, 943–955.

Fombonne, E. (2003). The prevalence of autism. JAMA *289*, 87–89.

Fombonne, E. (2008). Is autism getting commoner? Br. J. Psychiatry *193*, 59.

Gage, F.H. (2000). Mammalian Neural Stem Cells. Science (80-.). *287*, 1433–1438.

Galvan, A., Devergnas, A., and Wichmann, T. (2015). Alterations in neuronal activity in basal ganglia-thalamocortical circuits in the parkinsonian state. Front. Neuroanat. *9*, 1–21.

Gant, J.C., Thibault, O., Blalock, E.M., Yang, J., Bachstetter, A., Kotick, J., Schauwecker, P.E., Hauser, K.F., Smith, G.M., Mervis, R., et al. (2009). Decreased number of interneurons and increased seizures in neuropilin 2 deficient mice: Implications for autism and epilepsy. Epilepsia *50*, 629–645.

Gareus, R., Di Nardo, A., Rybin, V., and Witke, W. (2006). Mouse profilin 2 regulates endocytosis and competes with SH3 ligand binding to dynamin 1. J. Biol. Chem. *281*, 2803–2811.

Geese, M., Schlüter, K., Rothkegel, M., Jockusch, B.M., Wehland, J., and Sechi, A.S. (2000). Accumulation of profilin II at the surface of Listeria is concomitant with the onset of motility and correlates with bacterial speed. *1426*, 1415–1426.

Gelman, D.M., Noaín, D., Avale, M.E., Otero, V., Low, M.J., and Rubinstein, M. (2003). Transgenic mice engineered to target Cre/LoxP-mediated DNA recombination into catecholaminergic neurons. Genesis *36*, 196–202.

Gensert, J.M., and Goldman, J.E. (2001). Heterogeneity of cycling glial progenitors in the adult mammalian cortex and white matter. J. Neurobiol. *48*, 75–86.

Gertler, F.B., Niebuhr, K., Reinhard, M., Wehland, J., and Soriano, P. (1996). Mena, a relative of VASP and Drosophila enabled, is implicated in the control of microfilament dynamics. Cell *87*, 227–239.

Gieselmann, R., Kwiatkowski, D.J., Janmey, P. a, and Witke, W. (1995). Distinct biochemical characteristics of the two human profilin isoforms. Eur. J. Biochem. *229*, 621–628.

Gillberg, C. (2000). Typical neuroleptics in child and adolescent psychiatry. Eur. Child Adolesc. Psychiatry *9*.

Giros, B., Jaber, M., Jones, S.R., Wightman, R.M., and Caron, M.G. (1996). Hyperlocomotion and indifference to cocaine and amphetamine in mice lacking the dopamine transporter. Nature *379*, 606–612.

Goldman, S.A. (1998). Adult neurogenesis: from canaries to the clinic. J. Neurobiol. *36*, 267–286.

Goldschmidt-Clermont, P.J., Furman, M.I., Wachsstock, D., Safer, D., Nachmias, V.T., and Pollard, T.D. (1992). The control of actin nucleotide exchange by thymosin beta 4 and profilin. A potential regulatory mechanism for actin polymerization in cells. Mol. Biol. Cell *3*, 1015–1024.

Goley, E.D., and Welch, M.D. (2006). The ARP2/3 complex: an actin nucleator comes of age. Nat. Rev. Mol. Cell Biol. *7*, 713–726.

Görlich, A., Zimmermann, A.-M., Schober, D., Böttcher, R.T., Sassoè-Pognetto, M., Friauf, E., Witke, W., and Rust, M.B. (2012). Preserved morphology and physiology of excitatory synapses in profilin1-deficient mice. PLoS One *7*, e30068.

Grateron, L., Cebada-Sanchez, S., Marcos, P., Mohedano-Moriano, A., Insausti, A.M., Muñoz, M., Arroyo-Jimenez, M.M., Martinez-Marcos, A., Artacho-Perula, E., Blaizot, X., et al. (2003). Postnatal development of calcium-binding proteins immunoreactivity (parvalbumin, calbindin, calretinin) in the human entorhinal cortex. J. Chem. Neuroanat. *26*, 311–316.

Graus-Porta, D., Blaess, S., Senften, M., Littlewood-Evans, A., Damsky, C., Huang, Z., Orban, P.,

Klein, R., Schittny, J.C., and Müller, U. (2001). β1-Class integrins regulate the development of laminae and folia in the cerebral and cerebellar cortex. Neuron *31*, 367–379.

Greco, B., Managò, F., Tucci, V., Kao, H.-T., Valtorta, F., and Benfenati, F. (2013). Autism-related behavioral abnormalities in synapsin knockout mice. Behav. Brain Res. *251*, 65–74.

Greengard, P., Allen, P.B., and Nairn, A.C. (1999). Beyond the Dopamine Receptor. Neuron *23*, 435–447.

Grove, M., Grove, M., Demyanenko, G., Demyanenko, G., Echarri, A., Echarri, A., Zipfel, P. a, Zipfel, P. a, Quiroz, M.E., Quiroz, M.E., et al. (2004). Abi2-De cient Mice Exhibit Defective Cell Migration, Aberrant Dendritic Spine Morphogenesis, and De cits in Learning and Memory. Society *24*, 10905–10922.

Guljamow, A., Jenke-Kodama, H., Saumweber, H., Quillardet, P., Frangeul, L., Castets, A.M., Bouchier, C., Tandeau de Marsac, N., and Dittmann, E. (2007). Horizontal gene transfer of two cytoskeletal elements from a eukaryote to a cyanobacterium. Curr. Biol. *17*, 757–759.

Guo, W., Allan, A.M., Zong, R., Zhang, L., Johnson, E.B., Schaller, E.G., Murthy, A.C., Goggin, S.L., Eisch, A.J., Oostra, B.A., et al. (2011). Ablation of Fmrp in adult neural stem cells disrupts hippocampus-dependent learning. Nat. Med. *17*, 559–565.

Gurniak, C.B., and Witke, W. (2007). HuGE, a novel GFP-actin-expressing mouse line for studying cytoskeletal dynamics. Eur. J. Cell Biol. *86*, 3–12.

Hansson, O., Guatteo, E., Mercuri, N.B., Bernardi, G., Li, X.J., Castilho, R.F., and Brundin, P. (2001). Resistance to NMDA toxicity correlates with appearance of nuclear inclusions, behavioural deficits and changes in calcium homeostasis in mice transgenic for exon 1 of the huntington gene. Eur. J. Neurosci. *14*, 1492–1504.

Haugwitz, M., Noegel, A. a., Karakesisoglou, J., and Schleicher, M. (1994). Dictyostelium amoebae that lack G-actin-sequestering profilins show defects in F-actin content, cytokinesis, and development. Cell *79*, 303–314.

Hayar, A., Karnup, S., Ennis, M., and Shipley, M.T. (2004). External tufted cells: a major excitatory element that coordinates glomerular activity. J. Neurosci. *24*, 6676–6685.

Hellal, F., Hurtado, A., Ruschel, J., Flynn, K.C., Laskowski, C.J., Umlauf, M., Kapitein, L.C., Strikis, D., Lemmon, V., Bixby, J., et al. (2011). Microtubule stabilization reduces scarring and causes axon regeneration after spinal cord injury. Science *331*, 928–931.

Hendry, Jones, Emson, Lawson, Heizmann, and Streit (1989). Two classes of cortical GABA neurons defined by differential calcium binding immunoreactivities. Exp. Brain Res. 467–472.

Hering, H., and Sheng, M. (2001). Dendritic spines: structure, dynamics and regulation. Nat. Rev. Neurosci. *2*, 880–888.

Hoffman, L., Chandrasekar, A., Wang, X., Putkey, J.A., and Waxham, M.N. (2014). Neurogranin alters the structure and calcium binding properties of calmodulin. J. Biol. Chem. *289*, 14644–14655.

Höglund, K., Fourier, A., Perret-Liaudet, A., Zetterberg, H., Blennow, K., and Portelius, E. (2015). Alzheimer's disease — Recent biomarker developments in relation to updated diagnostic criteria. Clin. Chim. Acta.

Hol, E.M., and Pekny, M. (2015). Glial fibrillary acidic protein (GFAP) and the astrocyte intermediate filament system in diseases of the central nervous system. Curr. Opin. Cell Biol. *32*, 121–130.

Hu, E., Chen, Z., Fredrickson, T., and Zhu, Y. (2001). Molecular cloning and characterization of profilin-3: a novel cytoskeleton-associated gene expressed in rat kidney and testes. Exp. Nephrol. *9*, 265–274.

Huang, W.-H., Chao, H., Tsai, L., Chung, M., and Huang, Y. (2014). Elevated activation of CaMKIIa in the CPEB3-knockout hippocampus impairs a specific form of NMDAR-dependent synaptic depotentiation. Front. Cell. Neurosci. *8*, 1–12.

Hussman, J.P. (2001). Suppressed gabaergic inhibition as a common factor in suspected etiologies of autism. J. Autism Dev. Disord. *31*, 247–248.

Imamura, H., Tanaka, K., Hihara, T., Umikawa, M., Kamei, T., Takahashi, K., Sasaki, T., and Takai, Y. (1997). Bni1p and Bnr1p: Downstream targets of the Rho family small G-proteins which interact with profilin and regulate actin cytoskeleton in Saccharomyces cerevisiae. EMBO J. *16*, 2745–2755.

Ingre, C., Landers, J.E., Rizik, N., Volk, A.E., Akimoto, C., Birve, A., Hübers, A., Keagle, P.J., Piotrowska, K., Press, R., et al. (2013). A novel phosphorylation site mutation in profilin 1 revealed in a large screen of US, Nordic, and German amyotrophic lateral sclerosis/frontotemporal dementia cohorts. Neurobiol. Aging *34*, 1708.e1–e6.

Innocenti, M., Zucconi, A., Disanza, A., Frittoli, E., Areces, L.B., Steffen, A., Stradal, T.E.B., Di Fiore, P.P., Carlier, M.-F., and Scita, G. (2004). Abi1 is essential for the formation and activation of a WAVE2 signalling complex. Nat. Cell Biol. *6*, 319–327.

Innocenti, M., Gerboth, S., Rottner, K., Lai, F.P.L., Hertzog, M., Stradal, T.E.B., Frittoli, E., Didry, D., Polo, S., Disanza, A., et al. (2005). Abi1 regulates the activity of N-WASP and WAVE in distinct actin-based processes. Nat. Cell Biol. *7*, 969–976.

Jacob, S., Brune, C.W., Badner, J. a., Ernstrom, K., Courchesne, E., Lord, C., Leventhal, B.L., Cook, E.H., and Kim, S.-J. (2011). Family-based association testing of glutamate transporter genes in autism. Psychiatr. Genet. *21*, 212–213.

Janet Dubinsky (1993). Intracellular Calcium Levels during the Period of Delayed Excitotoxicity. J. Neurosci. *13*, 623–631.

Janmey, P.A. (1991). Polyproline affinity method for purification of platelet profilin and modification with pyrene-maleimide. Methods Enzymol. *196*, 92–99.

Jin, S.-H., Kim, H.J.T., Harris, D.C., and Thomas, S. a. (2004). Postnatal development of the cerebellum and the CNS adrenergic system is independent of norepinephrine and epinephrine. J. Comp. Neurol. *477*, 300–309.

Jones, M.B., Palmour, R.M., Zwaigenbaum, L., and Szatmari, P. (2004). Modifier effects in autism at the MAO-A and DBH loci. Am. J. Med. Genet. B. Neuropsychiatr. Genet. *126B*, 58–65.

Kaech, S., and Banker, G. (2006). Culturing hippocampal neurons. Nat. Protoc. *1*, 2406–2415.

Kandel, E.R., Schwartz, J.H., and Jessell, T.M. (2000). Principles of neural science (New York).

Kanner, L. (1943). Autistic disturbances of affective contact. Pathology 217–250.

Kemper, T.L., and Bauman, M. (1998). Neuropathology of infantile autism. J. Neuropathol. Exp. Neurol. *57*, 645–652.

Khadka, D.K., Liu, W., and Habas, R. (2009). Non-redundant roles for Profilin2 and Profilin1 during vertebrate gastrulation. Dev. Biol. *332*, 396–406.

Kiernan, M.C., Vucic, S., Cheah, B.C., Turner, M.R., Eisen, A., Hardiman, O., Burrell, J.R., and Zoing, M.C. (2011). Amyotrophic lateral sclerosis. Lancet *377*, 942–955.

Kim, S.K. (2015). Recent update of autism spectrum disorders. Korean JPediatr *58*, 8–14.

Kim, C.H., and Lisman, J.E. (1999). A role of actin filament in synaptic transmission and long-term potentiation. J. Neurosci. *19*, 4314–4324.

Kogan, M.D., Blumberg, S.J., Schieve, L. a, Boyle, C. a, Perrin, J.M., Ghandour, R.M., Singh, G.K., Strickland, B.B., Trevathan, E., and van Dyck, P.C. (2009). Prevalence of parent-reported diagnosis of autism spectrum disorder among children in the US, 2007. Pediatrics *124*, 1395–1403.

Kreitzer, A.C. (2009). Physiology and pharmacology of striatal neurons. Annu. Rev. Neurosci. *32*, 127–147.

Kron, S.J., Drubin, D.G., Botstein, D., and Spudich, J. a (1992). Yeast actin filaments display ATP-dependent sliding movement over surfaces coated with rabbit muscle myosin. Proc. Natl. Acad. Sci. U. S. A. *89*, 4466–4470.

Krucker, T., Siggins, G.R., and Halpain, S. (2000). Dynamic actin filaments are required for stable long-term potentiation (LTP) in area CA1 of the hippocampus. Proc. Natl. Acad. Sci. U. S. A. *97*, 6856–6861.

Kullmann, J. a, Neumeyer, A., Gurniak, C.B., Friauf, E., Witke, W., and Rust, M.B. (2011). Profilin1 is required for glial cell adhesion and radial migration of cerebellar granule neurons. EMBO Rep. *13*, 75–82.

Kullmann, J. a, Neumeyer, a, Wickertsheim, I., Böttcher, R.T., Costell, M., Deitmer, J.W., Witke, W., Friauf, E., and Rust, M.B. (2012). Purkinje cell loss and motor coordination defects in profilin1 mutant mice. Neuroscience *223*, 355–364.

Kumer, S.C., Kumer, S.C., Vrana, K.E., and Vrana, K.E. (1996). Intricate regulation of tyrosine hydroxylase activity and gene expression. J. Neurochem. *67*, 443–462.

Kunda, P., Craig, G., Dominguez, V., and Baum, B. (2003). Abi, Sra1, and Kette Control the Stability and Localization of SCAR/WAVE to Regulate the Formation of Actin-Based Protrusions. Curr. Biol. *13*, 1867–1875.

Kursula, P., Kursula, I., Massimi, M., Song, Y.-H., Downer, J., Stanley, W. a, Witke, W., and Wilmanns, M. (2008). High-resolution structural analysis of mammalian profilin 2a complex formation with two physiological ligands: the formin homology 1 domain of mDia1 and the proline-rich domain of VASP. J. Mol. Biol. *375*, 270–290.

Lai, S.L., Chan, T.H., Lin, M.J., Huang, W.P., Lou, S.W., and Lee, S.J. (2008). Diaphanous-related formin 2 and profilin I are required for gastrulation cell movements. PLoS One *3*, 1–16.

Lambrechts, A., Verschelde, J.L., Jonckheere, V., Goethals, M., Vandekerckhove, J., and Ampe, C. (1997). The mammalian profilin isoforms display complementary affinities for PIP2 and proline-rich sequences. EMBO J. *16*, 484–494.

Lambrechts, A., Braun, A., Jonckheere, V., Aszodi, A., Vandekerckhove, L., Lanier, L.M., Robbens, J., Colen, I.V.A.N., Ssler, R.F.A., Ampe, C., et al. (2000). Profilin II Is Alternatively Spliced , Resulting in Profilin Isoforms That Are Differentially Expressed and Have Distinct Biochemical Properties. *20*, 8209–8219.

Landgren, H., and Curtis, M. a (2011). Locating and labeling neural stem cells in the brain. J. Cell. Physiol. *226*, 1–7.

Lanier, L.M., Gates, M. a, Witke, W., Menzies, a S., Wehman, a M., Macklis, J.D., Kwiatkowski, D., Soriano, P., and Gertler, F.B. (1999). Mena is required for neurulation and commissure formation. Neuron *22*, 313–325.

Lappe-Siefke, C., Goebbels, S., Gravel, M., Nicksch, E., Lee, J., Braun, P.E., Griffiths, I.R., and Nave, K.-A. (2003). Disruption of Cnp1 uncouples oligodendroglial functions in axonal support and myelination. Nat. Genet. *33*, 366–374.

Lassing, I., and Lindberg, U. (1985). Specific interaction between phosphatidylinositol 4,5-bisphosphate and profilactin. Nature *314*, 472–474.

Laurent, V., Loisel, T.P., Harbeck, B., Wehman, A., Gröbe, L., Jockusch, B.M., Wehland, J., Gertler, F.B., and Carlier, M.F. (1999). Role of proteins of the Ena/VASP family in actin-based motility of Listeria monocytogenes. J. Cell Biol. *144*, 1245–1258.

Lawrence, Y. a, Kemper, T.L., Bauman, M.L., and Blatt, G.J. (2010). Parvalbumin-, calbindin-, and calretinin-immunoreactive hippocampal interneuron density in autism. Acta Neurol. Scand. *121*, 99–108.

Lederer, M., Jockusch, B.M., and Rothkegel, M. (2005). Profilin regulates the activity of p42POP, a novel Myb-related transcription factor. J. Cell Sci. *118*, 331–341.

Lee, H.K., Kameyama, K., Huganir, R.L., and Bear, M.F. (1998). NMDA induces long-term synaptic depression and dephosphorylation of the GluR1 subunit of AMPA receptors in hippocampus. Neuron *21*, 1151–1162.

Leto, K., and Rossi, F. (2011). Specification and Differentiation of Cerebellar GABAergic Neurons. The Cerebellum *11*, 434–435.

Levey, A.I., Hersch, S.M., Rye, D.B., Sunahara, R.K., Niznik, H.B., Kitt, C.A., Price, D.L., Maggio, R., Brann, M.R., and Ciliax, B.J. (1993). Localization of D1 and D2 dopamine receptors in brain with subtype-specific antibodies. Proc. Natl. Acad. Sci. U. S. A. *90*, 8861–8865.

Lévi, S., Logan, S.M., Tovar, K.R., and Craig, A.M. (2004). Gephyrin is critical for glycine receptor clustering but not for the formation of functional GABAergic synapses in hippocampal neurons. J. Neurosci. *24*, 207–217.

Li, R., Huang, F., Abbas, A., and Wigström, H. (2007). Role of NMDA receptor subtypes in different forms of NMDA-dependent synaptic plasticity. BMC Neurosci. *8*, 55.

Lindgren, N., Xu, Z.Q., Lindskog, M., Herrera-Marschitz, M., Goiny, M., Haycock, J., Goldstein, M., Hökfelt, T., and Fisone, G. (2000). Regulation of tyrosine hydroxylase activity and phosphorylation at Ser(19) and Ser(40) via activation of glutamate NMDA receptors in rat striatum. J. Neurochem. *74*, 2470–2477.

Liu, S., Plachez, C., Shao, Z., Puche, A., and Shipley, M.T. (2013). Olfactory bulb short axon cell release of GABA and dopamine produces a temporally biphasic inhibition-excitation response in external tufted cells. J. Neurosci. *33*, 2916–2926.

Longair, M.H., Baker, D.A., and Armstrong, J.D. (2011). Simple neurite tracer: Open source software for reconstruction, visualization and analysis of neuronal processes. Bioinformatics *27*, 2453–2454.

Lu, J., and Pollard, T.D. (2001). Profilin binding to poly-L-proline and actin monomers along with ability to catalyze actin nucleotide exchange is required for viability of fission yeast. Mol. Biol. Cell *12*, 1161–1175.

Luskin, M.B., and Boone, M.S. (1994). Rate and pattern of migration of lineally-related olfactory bulb interneurons generated postnatally in the subventricular zone of the rat. Chem. Senses *19*, 695–714.

Ma, D.K., Bonaguidi, M. a, Ming, G.-L., and Song, H. (2009). Adult neural stem cells in the mammalian central nervous system. Cell Res. *19*, 672–682.

Machesky, L.M., Atkinson, S.J., Ampe, C., Vandekerckhove, J., and Pollard, T.D. (1994). Purification of a Cortical Complex Containing 2 Unconventional Actins from Acanthamoeba by Affinity-Chromatography on Profilin-Agarose. J. Cell Biol. *127*, 107–115.

Maciel, E.N., Kowaltowski, A.J., Schwalm, F.D., Rodrigues, J.M., Souza, D.O., Vercesi, A.E., Wajner, M., and Castilho, R.F. (2004). Mitochondrial permeability transition in neuronal damage promoted by Ca2+ and respiratory chain complex II inhibition. J. Neurochem. *90*, 1025–1035.

Mahoney, N.M., Rozwarski, D.A., Fedorov, E., Fedorov, A.A., and Almo, S.C. (1999). Profilin binds proline-rich ligands in two distinct amide backbone orientations. Nat. Struct. Biol. *6*, 666–671.

Makkonen, I., Riikonen, R., Kokki, H., Airaksinen, M.M., and Kuikka, J.T. (2008). Serotonin and dopamine transporter binding in children with autism determined by SPECT. Dev. Med. Child Neurol. *50*, 593–597.

Mamber, C., Verhaagen, J., and Hol, E.M. (2010). In vivo targeting of subventricular zone astrocytes. Prog. Neurobiol. *92*, 19–32.

Mammoto, a, Sasaki, T., Asakura, T., Hotta, I., Imamura, H., Takahashi, K., Matsuura, Y., Shirao, T., and Takai, Y. (1998). Interactions of drebrin and gephyrin with profilin. Biochem. Biophys. Res. Commun. *243*, 86–89.

De Marchis, S., Bovetti, S., Carletti, B., Hsieh, Y.-C., Garzotto, D., Peretto, P., Fasolo, A., Puche, A.C., and Rossi, F. (2007). Generation of distinct types of periglomerular olfactory bulb interneurons during development and in adult mice: implication for intrinsic properties of the subventricular zone progenitor population. J. Neurosci. *27*, 657–664.

Maslov, A.Y., Barone, T. a, Plunkett, R.J., and Pruitt, S.C. (2004). Neural stem cell detection, characterization, and age-related changes in the subventricular zone of mice. J. Neurosci. *24*, 1726–1733.

Matamales, M., Bertran-Gonzalez, J., Salomon, L., Degos, B., Deniau, J.-M., Valjent, E., Hervé, D., and Girault, J.-A. (2009). Striatal Medium-Sized Spiny Neurons: Identification by Nuclear Staining and Study of Neuronal Subpopulations in BAC Transgenic Mice. PLoS One *4*, e4770.

McFarlane, H.G., Kusek, G.K., Yang, M., Phoenix, J.L., Bolivar, V.J., and Crawley, J.N. (2008). Autism-like behavioral phenotypes in BTBR T+tf/J mice. Genes, Brain Behav. *7*, 152–163.

McQuiston, A.R., and Katz, L.C. (2001). Electrophysiology of interneurons in the glomerular layer of the rat olfactory bulb. J. Neurophysiol. *86*, 1899–1907.

Méndez, P., and Bacci, A. (2011). Assortment of GABAergic Plasticity in the Cortical Interneuron Melting Pot. Neural Plast. *2011*, 1–14.

Michaelsen, K., Murk, K., Zagrebelsky, M., Dreznjak, A., Jockusch, B.M., Rothkegel, M., and Korte, M. (2010). Fine-tuning of neuronal architecture requires two profilin isoforms. Proc. Natl. Acad. Sci. *107*, 15780–15785.

Miller, E.M., Thomas, T.C., Gerhardt, G. a, and Glaser, P.E. a (2013). Dopamine and Glutamate Interactions in ADHD : Implications for the Future Neuropharmacology of ADHD. Atten. Deficit Hyperact. Disord. Child. Adolesc.

Ming, G.-L., and Song, H. (2011). Adult neurogenesis in the mammalian brain: significant answers and significant questions. Neuron *70*, 687–702.

Misawa, H., Nakata, K., Matsuura, J., Nagao, M., Okuda, T., and Haga, T. (2001). Distribution of the high-affinity choline transporter in the central nervous system of the rat. Neuroscience *105*, 87–98.

Missale, C., Nash, S.R., Robinson, S.W., Jaber, M., and Caron, M.G. (1998). Dopamine receptors: from structure to function. Physiol. Rev. *78*, 189–225.

Mogilner, A., and Edelstein-Keshet, L. (2002). Regulation of actin dynamics in rapidly moving cells: a quantitative analysis. Biophys. J. *83*, 1237–1258.

Molnár, G., Oláh, S., Komlósi, G., Füle, M., Szabadics, J., Varga, C., Barzó, P., and Tamás, G. (2008). Complex events initiated by individual spikes in the human cerebral cortex. PLoS Biol. *6*, 1842–1849.

Mondin, M., Carta, M., Normand, E., Mulle, C., and Coussen, F. (2010). Profilin II regulates the exocytosis of kainate glutamate receptors. J. Biol. Chem. *285*, 40060–40071.

Mouneimne, G., Hansen, S.D., Selfors, L.M., Petrak, L., Hickey, M.M., Gallegos, L.L., Simpson, K.J., Lim, J., Gertler, F.B., Hartwig, J.H., et al. (2012). Differential remodeling of actin cytoskeleton architecture by profilin isoforms leads to distinct effects on cell migration and invasion. Cancer Cell *22*, 615–630.

Mullins, R.D., Stafford, W.F., and Pollard, T.D. (1997). Structure, subunit topology, and actin-binding activity of the Arp2/3 complex from Acanthamoeba. J. Cell Biol. *136*, 331–343.

Murk, K., Buchmeier, S., Jockusch, B.M., and Rothkegel, M. (2009). In birds, profilin-2a is ubiquitously expressed and contributes to actin-based motility. J. Cell Sci. *122*, 957–964.

Murk, K., Wittenmayer, N., Michaelsen-Preusse, K., Dresbach, T., Schoenenberger, C.-A., Korte, M., Jockusch, B.M., and Rothkegel, M. (2012). Neuronal profilin isoforms are addressed by different signalling pathways. PLoS One *7*, e34167.

Murphy, G.J., Darcy, D.P., and Isaacson, J.S. (2005). Intraglomerular inhibition: signaling mechanisms of an olfactory microcircuit. Nat. Neurosci. *8*, 354–364.

Nabi, R., Serajee, F.J., Chugani, D.C., Zhong, H., and Huq, a H.M.M. (2004). Association of tryptophan 2,3 dioxygenase gene polymorphism with autism. Am. J. Med. Genet. B. Neuropsychiatr. Genet. *125B*, 63–68.

Nag, N., and Berger-Sweeney, J.E. (2007). Postnatal dietary choline supplementation alters behavior in a mouse model of Rett syndrome. Neurobiol. Dis. *26*, 473–480.

Nakatani, N., Ohnishi, T., Iwamoto, K., Watanabe, A., Iwayama, Y., Yamashita, S., Ishitsuka, Y., Moriyama, K., Nakajima, M., Tatebayashi, Y., et al. (2007). Expression analysis of actin-related genes as an underlying mechanism for mood disorders. Biochem. Biophys. Res. Commun. *352*, 780–786.

Napoli, I., Mercaldo, V., Boyl, P.P., Eleuteri, B., Zalfa, F., De Rubeis, S., Di Marino, D., Mohr, E., Massimi, M., Falconi, M., et al. (2008). The Fragile X Syndrome Protein Represses Activity-Dependent Translation through CYFIP1, a New 4E-BP. Cell *134*, 1042–1054.

Napolitano, M., Centonze, D., Gubellini, P., Rossi, S., Spiezia, S., Bernardi, G., Gulino, A., and Calabresi, P. (2004). Inhibition of mitochondrial complex II alters striatal expression of genes involved in glutamatergic and dopaminergic signaling: Possible implications for Huntington's disease. Neurobiol. Dis. *15*, 407–414.

Nardo, A. Di, Gareus, R., Kwiatkowski, D., and Witke, W. (2000). Alternative splicing of the mouse profilin II gene generates functionally different profilin isoforms. *3803*, 3795–3803.

Nedergaard, M., and Verkhratsky, A. (2012). Artifact versus reality-How astrocytes contribute to synaptic events. Glia *60*, 1013–1023.

Nefsky, B., and Bretscher, a. (1992). Yeast actin is relatively well behaved. Eur. J. Biochem. *206*, 949–955.

Nishiyama, A., Komitova, M., Suzuki, R., and Zhu, X. (2009). Polydendrocytes (NG2 cells): multifunctional cells with lineage plasticity. Nat. Rev. Neurosci. *10*, 9–22.

Oades, R.D., Sadile, A.G., Sagvolden, T., Viggiano, D., Zuddas, A., Devoto, P., Aase, H., Johansen, E.B., Ruocco, L. a., and Russell, V. a. (2005). The control of responsiveness in ADHD by catecholamines: Evidence for dopaminergic, noradrenergic and interactive roles. Dev. Sci. *8*, 122–131.

Oberman, L., and Pascual-Leone, A. (2013). Changes in plasticity across the lifespan: Cause of disease and target for intervention. Prog. Brain Res. *207*, 91–120.

Obermann, H., Raabe, I., Balvers, M., Brunswig, B., Schulze, W., and Kirchhoff, C. (2005). Novel testis-expressed profilin IV associated with acrosome biogenesis and spermatid elongation. Mol. Hum. Reprod. *11*, 53–64.

Okawa, H., Hoon, M., Yoshimatsu, T., Santina, L. Della, and Wong, R.O.L. (2014). Perspective Illuminating the Multifaceted Roles of Neurotransmission in Shaping Neuronal Circuitry. Neuron *83*, 1303–1318.

Oltedal, L., Haglerød, C., Furmanek, T., and Davanger, S. (2008). Vesicular release of glutamate from hippocampal neurons in culture: an immunocytochemical assay. Exp. Brain Res. *184*, 479–492.

Özer, I.D. (2015). Characterizing excitability and anxiety-like behaviors in Profilin2-GFP mice. Lab Rep.

Pandey, M., Varghese, M., Sindhu, K.M., Sreetama, S., Navneet, a. K., Mohanakumar, K.P., and Usha, R. (2008). Mitochondrial NAD+-linked State 3 respiration and complex-I activity are compromised in the cerebral cortex of 3-nitropropionic acid-induced rat model of Huntington's disease. J. Neurochem. *104*, 420–434.

Pandey, M., Borah, A., Varghese, M., Barman, P.K., Mohanakumar, K.P., and Usha, R. (2009). Striatal dopamine level contributes to hydroxyl radical generation and subsequent neurodegeneration in the striatum in 3-nitropropionic acid-induced Huntington's disease in rats. Neurochem. Int. *55*, 431–437.

Pandey, M., Mohanakumar, K.P., and Usha, R. (2010). Mitochondrial functional alterations in relation to pathophysiology of Huntington's disease. J. Bioenerg. Biomembr. *42*, 217–226.

Pathania, M., Davenport, E.C., Muir, J., Sheehan, D.F., López-Doménech, G., and Kittler, J.T. (2014). The autism and schizophrenia associated gene CYFIP1 is critical for the maintenance of dendritic complexity and the stabilization of mature spines. Transl. Psychiatry *4*, e374.

Paul, A.S., and Pollard, T.D. (2008). The role of the FH1 domain and profilin in formin-mediated actin-filament elongation and nucleation. Curr. Biol. *18*, 9–19.

Pedraza, C.E., Monk, R., Lei, J., Hao, Q., and Macklin, W.B. (2008). Production, characterization, and efficient transfection of highly pure oligodendrocyte precursor cultures from mouse embryonic neural progenitors. Glia *56*, 1339–1352.

Peñagarikano, O., Abrahams, B.S., Herman, E.I., Winden, K.D., Gdalyahu, A., Dong, H., Sonnenblick, L.I., Gruver, R., Almajano, J., Bragin, A., et al. (2011). Absence of CNTNAP2 leads to epilepsy, neuronal migration abnormalities, and core autism-related deficits. Cell *147*, 235–246.

Perreault, M.L., Hasbi, a., Alijaniaram, M., Fan, T., Varghese, G., Fletcher, P.J., Seeman, P., O'Dowd, B.F., and George, S.R. (2010). The Dopamine D1-D2 Receptor Heteromer Localizes in Dynorphin/Enkephalin Neurons: INCREASED HIGH AFFINITY STATE FOLLOWING AMPHETAMINE AND IN SCHIZOPHRENIA. J. Biol. Chem. *285*, 36625–36634.

Perreault, M.L., Hasbi, A., O'Dowd, B.F., and George, S.R. (2011). The dopamine d1-d2 receptor heteromer in striatal medium spiny neurons: evidence for a third distinct neuronal pathway in Basal Ganglia. Front. Neuroanat. *5*, 31.

Perrin, B.J., and Ervasti, J.M. (2010). The actin gene family: Function follows isoform. Cytoskeleton *67*, 630–634.

Perry, E.K., Lee, M.L.W., Martin-Ruiz, C.M., Court, J.A., Volsen, S.G., Merrit, J., Folly, E., Iversen, P.E., Bauman, M.L., Perry, R.H., et al. (2001). Cholinergic activity in autism: Abnormalities in the cerebral cortex and basal forebrain. Am. J. Psychiatry *158*, 1058–1066.

Pesold, C., Liu, W.S., Guidotti, a, Costa, E., and Caruncho, H.J. (1999). Cortical bitufted, horizontal, and Martinotti cells preferentially express and secrete reelin into perineuronal nets, nonsynaptically modulating gene expression. Proc. Natl. Acad. Sci. U. S. A. *96*, 3217–3222.

Pilo Boyl, P., and Witke, W. (2014). Small, smaller . . . dendritic spine. EMBO J. *33*, 2737–2739.

Pilo Boyl, P., Di Nardo, A., Mulle, C., Sassoè-Pognetto, M., Panzanelli, P., Mele, A., Kneussel, M., Costantini, V., Perlas, E., Massimi, M., et al. (2007). Profilin2 contributes to synaptic vesicle exocytosis, neuronal excitability, and novelty-seeking behavior. EMBO J. *26*, 2991–3002.

Pinto, D., Pagnamenta, A., Klei, L., and Anney, R. (2010). Functional impact of global rare copy number variation in autism spectrum disorders. Nature *466*, 368–372.

Del Poggetto, E., Chiti, F., and Bemporad, F. (2015a). The Folding process of Human Profilin-1, a novel protein associated with familial amyotrophic lateral sclerosis. Sci. Rep. *5*, 12332.

Del Poggetto, E., Bemporad, F., Tatini, F., and Chiti, F. (2015b). Mutations of profilin-1 associated with amyotrophic lateral sclerosis promote aggregation due to structural changes of the native states. ACS Chem. Biol. 150730140612009.

Pollard, T.D., Almo, S., Quirk, S., Vinson, V., and Lattman, E.E. (1994). Structure of actin binding proteins: insights about function at atomic resolution. Annu. Rev. Cell Biol. *10*, 207–249.

Pollard, T.D., Blanchoin, L., and Mullins, R.D. (2000). Molecular mechanisms controlling actin filament dynamics in nonmuscle cells. Annu. Rev. Biophys. Biomol. Struct. *29*, 545–576.

Prescott, T.J., Gurney, K., and Redgrave, P. (2003). Basal Ganglia. Handb. Brain Theory Neural Networks (2nd Ed. 147–151.

Purcell, A.E., Jeon, O.H., Zimmerman, A.W., Blue, M.E., and Pevsner, J. (2001). Postmortem brain abnormalities of the glutamate neurotransmitter system in autism. Neurology *57*, 1618–1628.

Quinlan, M.E., Heuser, J.E., Kerkhoff, E., and Mullins, R.D. (2005). Drosophila Spire is an actin nucleation factor. Nature *433*, 382–388.

Rossi, D., and Volterra, A. (2009). Astrocytic dysfunction: Insights on the role in neurodegeneration. Brain Res. Bull. *80*, 224–232.

Rubenstein, J.L.R., and Merzenich, M.M. (2003). Model of autism: increased ratio of excitation/inhibition in key neural systems. Genes. Brain. Behav. *2*, 255–267.

Rudy, B., Fishell, G., Lee, S., and Hjerling-Leffler, J. (2011). Three groups of interneurons account for nearly 100% of neocortical GABAergic neurons. Dev. Neurobiol. *71*, 45–61.

Ruiz-García, M., García Del Potro, M., Fernández-Nieto, M., Barber, D., Jimeno-Nogales, L., and Sastre, J. (2011). Profilin: a relevant aeroallergen? J. Allergy Clin. Immunol. *128*, 416–418.

Russo, S., and Nestler, E. (2013). The brain reward circuitry in mood disorders. Nat. Rev. Neurosci. *29*, 609–625.

Rutter, M. (1978). Diagnosis and definition of childhood autism. J. Autism Child. Schizophr. *8*, 139–161.

Rutter, M., and Schopler, E. (1987). Autism and pervasive developmental disorders: concepts and diagnostic issues. J. Autism Dev. Disord. *17*, 159–186.

Safer, D., and Nachmias, V.T. (1994). Beta thymosins as actin binding peptides. Bioessays *16*, 473–479.

Saher, G., Brügger, B., Lappe-Siefke, C., Möbius, W., Tozawa, R., Wehr, M.C., Wieland, F., Ishibashi, S., and Nave, K.-A. (2005). High cholesterol level is essential for myelin membrane growth. Nat. Neurosci. *8*, 468–475.

De Saint Jan, D., Hirnet, D., Westbrook, G.L., and Charpak, S. (2009). External tufted cells drive the output of olfactory bulb glomeruli. J. Neurosci. *29*, 2043–2052.

Salter, M.W., and Beggs, S. (2014). Sublime microglia: Expanding roles for the guardians of the CNS. Cell *158*, 15–24.

Sano, H., Yasoshima, Y., Matsushita, N., Kaneko, T., Kohno, K., Pastan, I., and Kobayashi, K. (2003). Conditional ablation of striatal neuronal types containing dopamine D2 receptor disturbs coordination of basal ganglia function. J. Neurosci. *23*, 9078–9088.

Santos, A., and Van Ree, R. (2011). Profilins: mimickers of allergy or relevant allergens? Int. Arch. Allergy Immunol. *155*, 191–204.

Santos, M., Summavielle, T., Teixeira-Castro, A., Silva-Fernandes, A., Duarte-Silva, S., Marques, F., Martins, L., Dierssen, M., Oliveira, P., Sousa, N., et al. (2010). Monoamine deficits in the brain of methyl-CpG binding protein 2 null mice suggest the involvement of the cerebral cortex in early stages of Rett syndrome. Neuroscience *170*, 453–467.

Sarter, M., and Parikh, V. (2005). Choline transporters, cholinergic transmission and cognition. Nat. Rev. Neurosci. *6*, 48–56.

Schain, R.J., and Freedman, D.X. (1961). Studies on 5-hydroxyindole metabolism in autistic and other mentally retarded children. J. Pediatr. *58*, 315–320.

Schmidt, A., Wolde, M., Thiele, C., Fest, W., Kratzin, H., Podtelejnikov, A. V, Witke, W., Huttner, W.B., and Söling, H.D. (1999). Endophilin I mediates synaptic vesicle formation by transfer of arachidonate to lysophosphatidic acid. Nature *401*, 133–141.

Schousboe, A. (2003). Role of Astrocytes in the Maintenance and Modulation of Glutamatergic and GABAergic Neurotransmission. Neurochem. Res. *28*, 347–352.

Schubert, V., and Dotti, C.G. (2007). Transmitting on actin: synaptic control of dendritic architecture. J. Cell Sci. *120*, 205–212.

Schubert, V., Da Silva, J.S., and Dotti, C.G. (2006). Localized recruitment and activation of RhoA underlies dendritic spine morphology in a glutamate receptor-dependent manner. J. Cell Biol. *172*, 453–467.

Schweinhuber, S.K., Meßerschmidt, T., Hänsch, R., Korte, M., and Rothkegel, M. (2015). Profilin Isoforms Modulate Astrocytic Morphology and the Motility of Astrocytic Processes. PLoS One *10*, e0117244.

Shehata, M., Matsumura, H., Okubo-Suzuki, R., Ohkawa, N., and Inokuchi, K. (2012). Neuronal stimulation induces autophagy in hippocampal neurons that is involved in AMPA receptor degradation after chemical long-term depression. J. Neurosci. *32*, 10413–10422.

Sholl, D. a. (1953). Dendritic organization in the neurons of the visual and motor cortices of the cat. J. Anat. *87*, 387–406.1.

Sillitoe, R. V, Chung, S.-H., Fritschy, J.-M., Hoy, M., and Hawkes, R. (2008). Golgi cell dendrites are restricted by Purkinje cell stripe boundaries in the adult mouse cerebellar cortex. J. Neurosci. *28*, 2820–2826.

Sills, J.B., Connors, B.W., and Burwell, R.D. (2012). Electrophysiological and morphological properties of neurons in layer 5 of the rat postrhinal cortex. Hippocampus *22*, 1912–1922.

da Silva, J.S., and Dotti, C.G. (2002). Breaking the neuronal sphere: regulation of the actin cytoskeleton in neuritogenesis. Nat. Rev. Neurosci. *3*, 694–704.

Da Silva, J.S., Medina, M., Zuliani, C., Di Nardo, A., Witke, W., and Dotti, C.G. (2003). RhoA/ROCK regulation of neuritogenesis via profilin IIa-mediated control of actin stability. J. Cell Biol. *162*, 1267–1279.

Singec, I., Knoth, R., Ditter, M., Volk, B., and Frotscher, M. (2004). Neurogranin is expressed by principal cells but not interneurons in the rodent and monkey neocortex and hippocampus. J. Comp. Neurol. *479*, 30–42.

Smidt, M.P., and Burbach, J.P.H. (2007). How to make a mesodiencephalic dopaminergic neuron. Nat. Rev. Neurosci. *8*, 21–32.

Smith, E.F. (2002). Plant profilin isovariants are distinctly regulated in vegetative and reproductive tissues. Cell Motil. Cytoskeleton *52*, 22–32.

Smith, B.N., Vance, C., Scotter, E.L., Troakes, C., Wong, C.H., Topp, S., Maekawa, S., King, A., Mitchell, J.C., Lund, K., et al. (2015). Novel mutations support a role for Profilin 1 in the pathogenesis of ALS. Neurobiol. Aging *36*, 1602.e17–e1602.e27.

Sofroniew, M. V., and Vinters, H. V. (2010). Astrocytes: Biology and pathology. Acta Neuropathol. *119*, 7–35.

Sommer, L., and Rao, M. (2002). Neural stem cells and regulation of cell number. Prog. Neurobiol. *66*, 1–18.

Song, C., and Leonard, B.E. (2005). The olfactory bulbectomised rat as a model of depression. Neurosci. Biobehav. Rev. *29*, 627–647.

Staiger, J.F., Zuschratter, W., Luhmann, H.J., and Schubert, D. (2009). Local circuits targeting parvalbumin-containing interneurons in layer IV of rat barrel cortex. Brain Struct. Funct. *214*, 1–13.

Steffen, A., Rottner, K., Ehinger, J., Innocenti, M., Scita, G., Wehland, J., and Stradal, T.E.B. (2004). Sra-1 and Nap1 link Rac to actin assembly driving lamellipodia formation. EMBO J. *23*, 749–759.

Stiess, M., and Bradke, F. (2010). Neuronal polarization: The cytoskeleton leads the way. Dev Neurobiol *71*, 430–444.

Stradal, T.E.B., and Scita, G. (2006). Protein complexes regulating Arp2/3-mediated actin assembly.

Curr. Opin. Cell Biol. *18*, 4–10.

Stüven, T., Hartmann, E., and Görlich, D. (2003). Exportin 6: A novel nuclear export receptor that is specific for profilin-actin complexes. EMBO J. *22*, 5928–5940.

Südhof, T.C. (2013). Neurotransmitter release: The last millisecond in the life of a synaptic vesicle. Neuron *80*, 675–690.

Sung, J.Y., Engmann, O., Teylan, M. a, Nairn, A.C., Greengard, P., and Kim, Y. (2008). WAVE1 controls neuronal activity-induced mitochondrial distribution in dendritic spines. Proc. Natl. Acad. Sci. U. S. A. *105*, 3112–3116.

Svenningsson, P., Nishi, A., Fisone, G., Girault, J.-A., Nairn, A.C., and Greengard, P. (2004). DARPP-32: an integrator of neurotransmission. Annu. Rev. Pharmacol. Toxicol. *44*, 269–296.

Swanson, L.W., and Hartman, B.K. (1975). The central adrenergic system. An immunofluorescence study of the location of cell bodies and their efferent connections in the rat utilizing dopamine-beta-hydroxylase as a marker. J. Comp. Neurol. *163*, 467–505.

Swanson, C.J., Bures, M., Johnson, M.P., Linden, A.-M., Monn, J. a, and Schoepp, D.D. (2005). Metabotropic glutamate receptors as novel targets for anxiety and stress disorders. Nat. Rev. Drug Discov. *4*, 131–144.

Szabadics, J., Varga, C., Molnár, G., Oláh, S., Barzó, P., and Tamás, G. (2006). Excitatory effect of GABAergic axo-axonic cells in cortical microcircuits. Science *311*, 233–235.

Szatmari, P., Paterson, A.D., Zwaigenbaum, L., Roberts, W., Brian, J., Liu, X.-Q., Vincent, J.B., Skaug, J.L., Thompson, A.P., Senman, L., et al. (2007). Mapping autism risk loci using genetic linkage and chromosomal rearrangements. Nat. Genet. *39*, 319–328.

Tabrizi, S.J., Cleeter, M.W.J., Xuereb, J., Taanman, J.W., Cooper, J.M., and Schapira, A.H. V (1999). Biochemical abnormalities and excitotoxicity in Huntington's disease brain. Ann. Neurol. *45*, 25–32.

Tabuchi, K., Blundell, J., Etherton, M.R., Hammer, R.E., Liu, X., Powell, C.M., and Südhof, T.C. (2007). A neuroligin-3 mutation implicated in autism increases inhibitory synaptic transmission in mice. Science *318*, 71–76.

Tahirovic, S., and Bradke, F. (2009). Neuronal polarity. Cold Spring Harb. Perspect. Biol. *1*, 1–17.

Takenawa, T., and Miki, H. (2001). WASP and WAVE family proteins: key molecules for rapid rearrangement of cortical actin filaments and cell movement. J. Cell Sci. *114*, 1801–1809.

Tan, S., Hermann, B., and Borrelli, E. (2003). Dopaminergic mouse mutants: Investigating the roles of the different dopamine receptor subtypes and the dopamine transporter. Int. Rev. Neurobiol. *54*, 145–197.

Theriot, J. a., Rosenblatt, J., Portnoy, D. a., Goldschmidt-Clermont, P.J., and Mitchisont, T.J. (1994). Involvement of profilin in the actin-based motility of L. monocytogenes in cells and in cell-free extracts. Cell *76*, 505–517.

Thompson, L., Barraud, P., Andersson, E., Kirik, D., and Björklund, A. (2005). Identification of dopaminergic neurons of nigral and ventral tegmental area subtypes in grafts of fetal ventral mesencephalon based on cell morphology, protein expression, and efferent projections. J. Neurosci. *25*, 6467–6477.

Tiloca, C., Ticozzi, N., Pensato, V., Corrado, L., Del Bo, R., Bertolin, C., Fenoglio, C., Gagliardi, S., Calini, D., Lauria, G., et al. (2013). Screening of the PFN1 gene in sporadic amyotrophic lateral sclerosis and in frontotemporal dementia. Neurobiol. Aging *34*, 1517.e9–e10.

Treutlein, B., Gokce, O., Quake, S.R., and Südhof, T.C. (2014). Cartography of neurexin alternative splicing mapped by single-molecule long-read mRNA sequencing. Proc. Natl. Acad. Sci. U. S. A. *111*, E1291–E1299.

Tsai, L.Y. (1999). Psychopharmacology in autism. Psychosom. Med. *61*, 651–665.

Ueda, S., Negishi, M., and Katoh, H. (2013). Rac GEF Dock4 interacts with cortactin to regulate dendritic spine formation. Mol. Biol. Cell *24*, 1602–1613.

Uusisaari, M.Y., and Knöpfel, T. (2012). Diversity of neuronal elements and circuitry in the cerebellar nuclei. Cerebellum *11*, 420–421.

Valenta, R., Duchene, M., Vrtala, S., Birkner, T., Ebner, C., Hirschwehr, R., Breitenbach, M., Rumpold,

H., Scheiner, O., and Kraft, D. (1991). Recombinant allergens for immunoblot diagnosis of tree-pollen allergy. J. Allergy Clin. Immunol. *88*, 889–894.

Veenstra-VanderWeele, J., Kim, S.J., Lord, C., Courchesne, R., Akshoomoff, N., Leventhal, B.L., Courchesne, E., and Cook, E.H. (2002). Transmission disequilibrium studies of the serotonin 5-HT2A receptor gene (HTR2A) in autism. Am. J. Med. Genet. - Neuropsychiatr. Genet. *114*, 277–283.

Verheyen, E.M., and Cooley, L. (1994). Profilin mutations disrupt multiple actin-dependent processes during Drosophila development. Development *120*, 717–728.

Wang, Y., Toledo-Rodriguez, M., Gupta, A., Wu, C., Silberberg, G., Luo, J., and Markram, H. (2004). Anatomical, physiological and molecular properties of Martinotti cells in the somatosensory cortex of the juvenile rat. J. Physiol. *561*, 65–90.

Wang, Y.-Y., Wu, H.-I., Hsu, W.-L., Chung, H.-W., Yang, P.-H., Chang, Y.-C., and Chow, W.-Y. (2014). In vitro growth conditions and development affect differential distributions of RNA in axonal growth cones and shafts of cultured rat hippocampal neurons. Mol. Cell. Neurosci. *61*, 141–151.

Welch, M.D., Iwamatsu, a, and Mitchison, T.J. (1997). Actin polymerization is induced by Arp2/3 protein complex at the surface of Listeria monocytogenes. Nature *385*, 265–269.

Wierzba-Bobrowicz, T., Lewandowska, E., Stępień, T., and Szpak, G.M. (2011). Differential expression of calbindin D28k, calretinin and parvalbumin in the cerebellum of pups of ethanol-treated female rats. Folia Neuropathol. *49*, 47–55.

Winder, S.J. (2005). Actin-binding proteins. J. Cell Sci. *118*, 651–654.

Winters, B.D., and Bussey, T.J. (2005). Glutamate receptors in perirhinal cortex mediate encoding, retrieval, and consolidation of object recognition memory. J. Neurosci. *25*, 4243–4251.

Witke, W. (2004). The role of profilin complexes in cell motility and other cellular processes. Trends Cell Biol. *14*, 461–469.

Witke, W., Podtelejnikov, A. V, Di Nardo, A., Sutherland, J.D., Gurniak, C.B., Dotti, C., and Mann, M. (1998). In mouse brain profilin I and profilin II associate with regulators of the endocytic pathway and actin assembly. EMBO J. *17*, 967–976.

Witke, W., Sutherland, J.D., Sharpe, a, Arai, M., and Kwiatkowski, D.J. (2001). Profilin I is essential for cell survival and cell division in early mouse development. Proc. Natl. Acad. Sci. U. S. A. *98*, 3832–3836.

Witte, H., and Bradke, F. (2008). The role of the cytoskeleton during neuronal polarization. Curr. Opin. Neurobiol. *18*, 479–487.

Witte, H., Neukirchen, D., and Bradke, F. (2008). Microtubule stabilization specifies initial neuronal polarization. J. Cell Biol. *180*, 619–632.

Woodruff, A., and Yuste, R. (2008). Of Mice and Men, and Chandeliers. PLoS Biol. *6*, e243.

Woodruff, A.R., Anderson, S. a., and Yuste, R. (2010). The Enigmatic Function of Chandelier Cells. Front. Neurosci. *4*, 1–11.

Woolf, N. (1991). Cholinergic systems in mammalian brain and spinal cord. Prog. Neurobiol. *37*, 475–524.

Wu, C.-H., Fallini, C., Ticozzi, N., Keagle, P.J., Sapp, P.C., Piotrowska, K., Lowe, P., Koppers, M., McKenna-Yasek, D., Baron, D.M., et al. (2012). Mutations in the profilin 1 gene cause familial amyotrophic lateral sclerosis. Nature *488*, 499–503.

Wu, L., Zhang, C., and Yin, F. (2015). Dynamic changes in the proteomic profile of mesial temporal lobe epilepsy at different disease stages in an immature rat model. Protein Pept. Lett. *22*, 180–192.

Xiao, C., Zhou, C., Li, K., and Ye, J.-H. (2007). Presynaptic GABAA receptors facilitate GABAergic transmission to dopaminergic neurons in the ventral tegmental area of young rats. J. Physiol. *580*, 731–743.

Yu, D.-M., Tang, W.-C., Wu, P., Deng, T.-X., Liu, B., Li, M.-S., and Deng, J.-B. (2010). The synaptic remodeling between regenerated perforant pathway and granule cells in slice culture. Cell. Mol. Neurobiol. *30*, 309–316.

Zachariou, V., Sgambato-Faure, V., Sasaki, T., Svenningsson, P., Berton, O., Fienberg, A. a, Nairn, A.C., Greengard, P., and Nestler, E.J. (2005). Phosphorylation of DARPP-32 at Threonine-34 is

Required for Cocaine Action. Neuropsychopharmacology *31*, 555–562.

Zafeiriou, D.I., Ververi, A., and Vargiami, E. (2007). Childhood autism and associated comorbidities. Brain Dev. *29*, 257–272.

Zeidán-Chuliá, F., Salmina, A.B., Malinovskaya, N. a, Noda, M., Verkhratsky, A., and Moreira, J.C.F. (2014). The glial perspective of autism spectrum disorders. Neurosci. Biobehav. Rev. *38*, 160–172.

Zhan, Y., Paolicelli, R.C., Sforazzini, F., Weinhard, L., Bolasco, G., Pagani, F., Vyssotski, A.L., Bifone, A., Gozzi, A., Ragozzino, D., et al. (2014). Deficient neuron-microglia signaling results in impaired functional brain connectivity and social behavior. Nat. Neurosci. *17*, 400–406.

Zhou, X., Moon, C., Zheng, F., Luo, Y., Soellner, D., Nuñez, J.L., and Wang, H. (2009). N-methyl-D-aspartate-stimulated ERK1/2 signaling and the transcriptional up-regulation of plasticity-related genes are developmentally regulated following in vitro neuronal maturation. J. Neurosci. Res. *87*, 2632–2644.

Zilberter, Y., Kaiser, K.M., and Sakmann, B. (1999). Dendritic GABA release depresses excitatory transmission between layer 2/3 pyramidal and bitufted neurons in rat neocortex. Neuron *24*, 979–988.

Zimmerman, A. (2008). Autism: Current theories and evidence (Current Clinical Neurology).

Zito, K., and Scheuss, V. (2009). NMDA Receptor Function and Physiological Modulation. In: Encyclopedia of Neuroscience.

Zuccato, C., Valenza, M., and Cattaneo, E. (2010). Molecular Mechanisms and Potential Therapeutical Targets in Huntington ' s Disease. Physiol Rev *90*, 905–981.

7. Supplementary

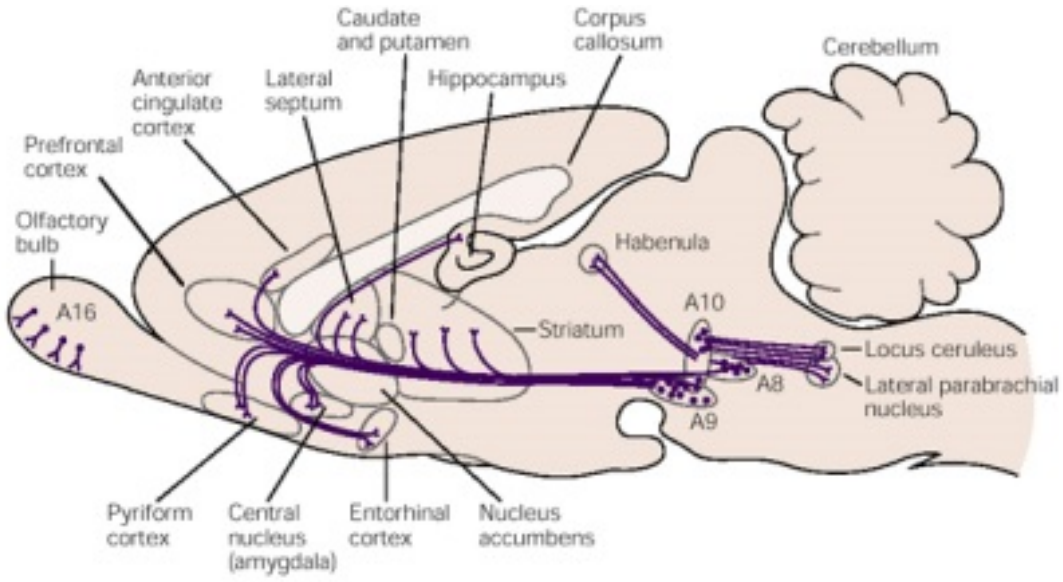

Supplementary Fig. 1 Schematic view of the projections originating from dopaminergic neurons Dopaminergic neurons can be found manly in regions of the mouse brain that can be further subdivided into several neuron groups. The depicted major dopaminergic groups comprise the substantia nigra (SN, group A9) and ventral tegmental area (VTA, group A10), the retrorubral field (RRF, group A8) and the olfactory bulb (group A16). These regions innervate various brain areas, as can be appreciated by the emerging projections that are shown here in purple (modified from Kandel et al., 2000).

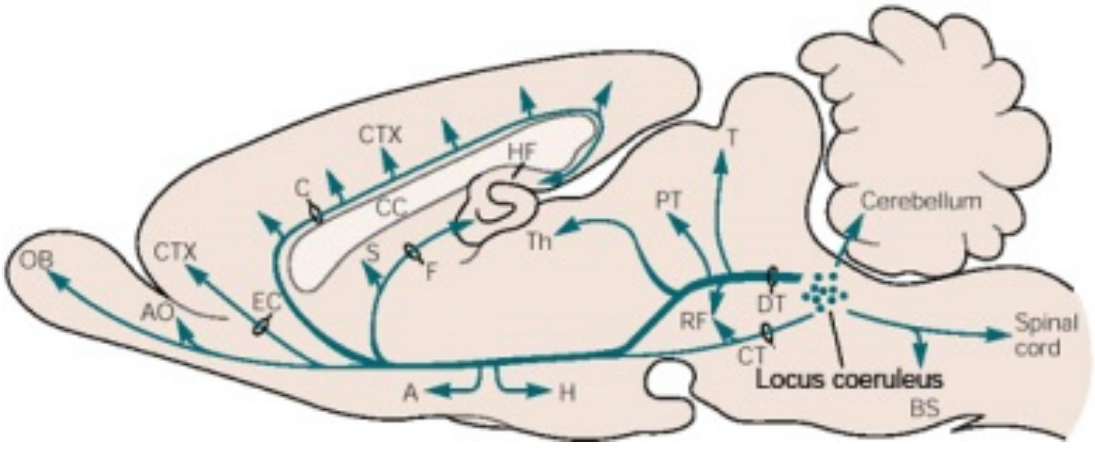

Supplementary Fig. 2 Schematic overview of the innervations originating from noradrenergic neurons of the locus coeruleus

The noradrenergic system has widespread innervations throughout the entire brain, exclusively originating from the locus coeruleus (LC) of the brainstem. Although only small numbers of noradrenergic neurons exist in the mouse brain, they have a pronounced modulatory effect on nearly every neuronal pathway and brain region (modified from Kandel et al., 2000).

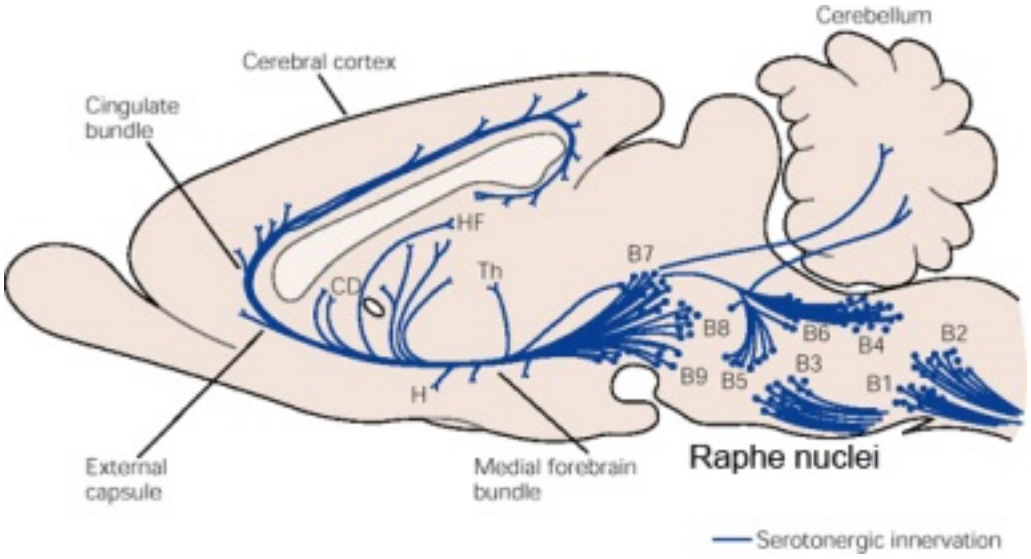

Supplementary Fig. 3 Schematic overview of serotonergic projections of the Raphe nuclei

Serotonergic neurons are located dispersed throughout the Raphe nuclei of the brainstem. They innervate several regions of the basal ganglia (striatum and thalamus), the hippocampus, the cerebellum and cortical areas. Serotonin has a dual role, since it can modulate synaptic transmission through both excitation and inhibition depending on the expression of the different serotonin receptor subtypes (modified from Kandel et al., 2000).

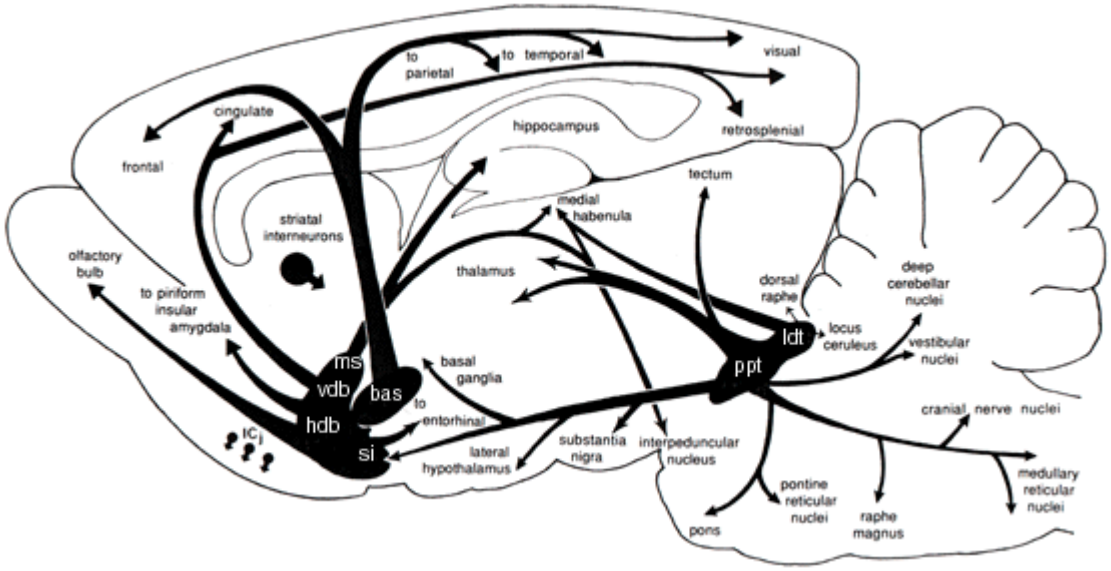

Supplementary Fig. 4 Schematic overview of cholinergic neurons and their projections in the mouse brain

Cholinergic neurons are localized to three groups in the mouse brain. The biggest and most dispersed group is located in the medial septum and a slightly smaller group in the pontomesencephalic region near the cerebellum comprised of the ppt (pedunculopontine tegmental nucleus) and ldt (laterodorsal tegmental nucleus). These neurons send their axons to nearly all brain regions. In addition large cholinergic interneurons can be found isolated in the striatum (modified from Woolf, 1991).

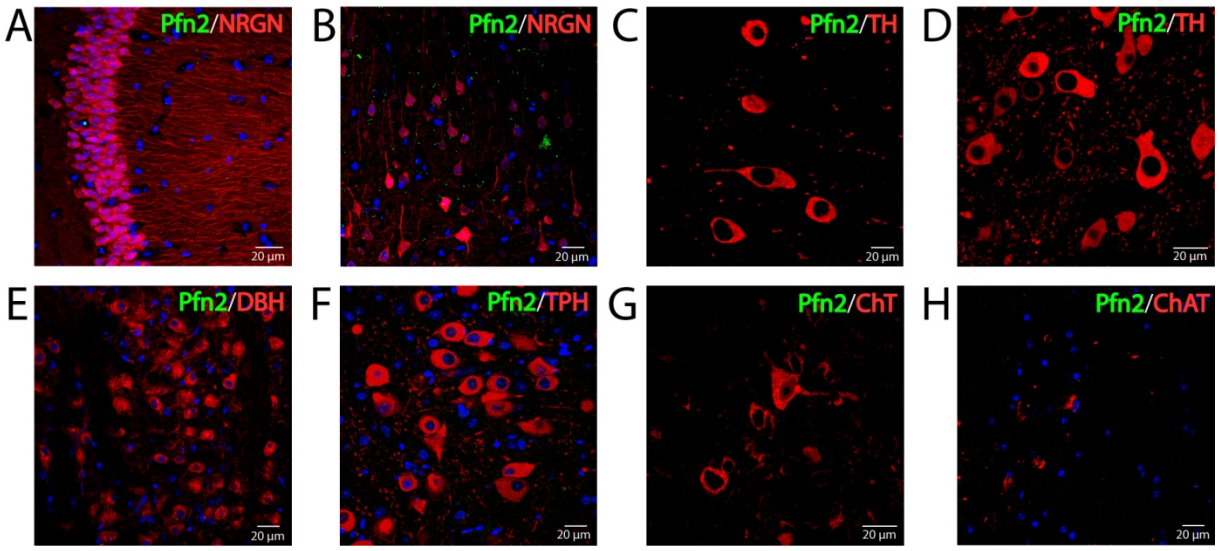

Supplementary Fig. 5 Excitatory neuronal systems immunofluorescence control stainings of wildtype brain sections

Co-Immunofluorescence studies were verified by several control stainings, including the control for the specificity of the P2-GFP signal using wildtype (wt) sections. Wt mice should not express the GFP protein and should therefore show no signal, if they were processed in the same way as the homozygous P2-GFP knock-in animals (G/G) were treated.

A signal for GFP (green) could not be detected using the same settings for image acquisition and processing, confirming the specificity of the P2-GFP labelling approach. The respective controls for the brain regions and neuronal systems were chosen according to the regions of the excitatory neuronal systems that were shown in Fig. 14. (**A**) Glutamatergic neurons were specifically identified using neurogranin (NRGN, red) as a marker protein in the hippocampus and (**B**) the cortex. (**C**) Dopaminergic neurons of the substantia nigra (SN) and (**D**) the ventral tegmental area (VTA) were labelled with an antibody recognizing a specific antigen for TH (red). (**E**) Neurons positive for noradrenaline were analyzed in the locus coeruleus (LC) using DBH (red) as a marker. (**F**) Serotonergic neurons of the Raphe nuclei were stained with an anti-TPH (red) antibody and (**G**) cholinergic neurons were identified by their specific expression of the choline transporter (ChT, red) in the pedunculopontine tegmental nucleus (ppt) or (**H**) by their expression of choline acetyltransferase (ChAT, red) in the striatum. To visualize the cell nuclei (blue), the DNA-intercalating dye Draq5 (Biostatus) was used.

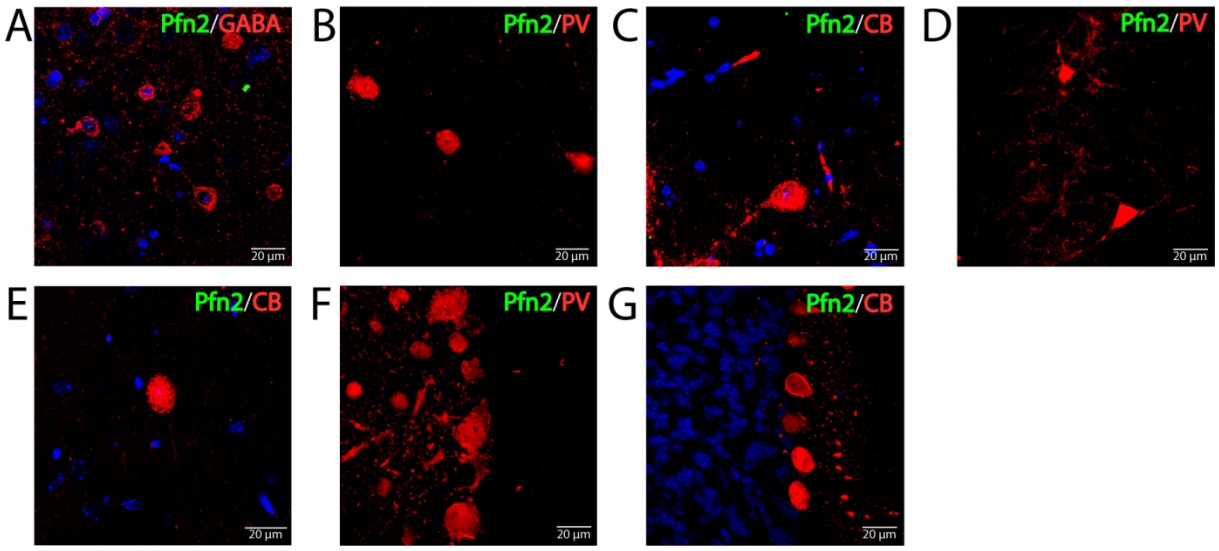

Supplementary Fig. 6 GABAergic neuronal systems immunofluorescence control stainings of wildtype brain sections

Co-Immunofluorescence studies were verified by several control stainings, including the control for the specificity of the P2-GFP signal using wildtype (wt) sections. Wt mice should not express the GFP protein and should therefore show no signal, if they were processed in the same way as the homozygous P2-GFP knock-in animals (G/G) were treated.

A signal for GFP (green) could not be detected using the same settings for image acquisition and processing, confirming the specificity of the P2-GFP labelling approach.

The respective controls for the GABAergic neurons in the mouse brain were chosen according to the regions of the GABAergic neuronal systems that were shown in Fig. 15. GABAergic neuronal subtypes were specifically identified using GABA (red) or the Ca^{2+}-binding proteins parvalbumin (PV, red) and calbindin (CB, red) as markers. (**A**) Few GABAergic neurons co-express Pfn2, which are distributed throughout the cortex and can moreover be subcategorized using (**B**) PV and (**C**) CB to identify specific cell types of GABAergic neurons. The distribution of these marker proteins and therefore of the corresponding GABAergic neuronal subtypes were further studied (**D**, **E**) in the hippocampus and (**F**, **G**) the cerebellum. To visualize the cell nuclei (blue), the DNA-intercalating dye Draq5 (Biostatus) was used.

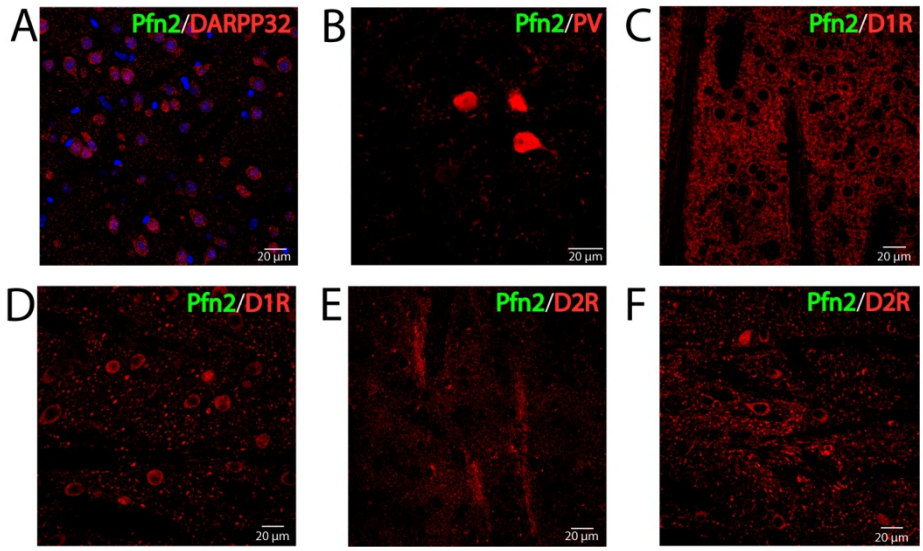

Supplementary Fig. 7 Striatal system immunofluorescence control stainings of wildtype brain sections

Co-Immunofluorescence studies were verified by several control stainings, including the control for the specificity of the P2-GFP signal using wildtype (wt) sections. Wt mice should not express the GFP protein and should therefore show no signal, if they were processed in the same way as the homozygous P2-GFP knock-in animals (G/G) were treated.

A signal for GFP (green) could not be detected using the same settings for image acquisition and processing, confirming the specificity of the P2-GFP labelling approach.

The respective controls for the neurons in the mouse striatum were chosen according to the images that were shown in Fig. 16. (**A**) GABAergic medium spiny neuron (MSN) subtypes were specifically identified using DARPP32 (red). (**B**) Aspiny interneurons were stained with the Ca^{2+}-binding protein parvalbumin (PV, red). MSNs were further subdivided into either dopamine D1 receptor-expressing cells (D1R, red) for the (**C**) dorsal and (**D**) ventral striatum or dopamine D2 receptor-expressing (D2R, red) cells in the (**E**) dorsal and (**F**) ventral striatum. To visualize the cell nuclei (blue), the DNA-intercalating dye Draq5 (Biostatus) was used.

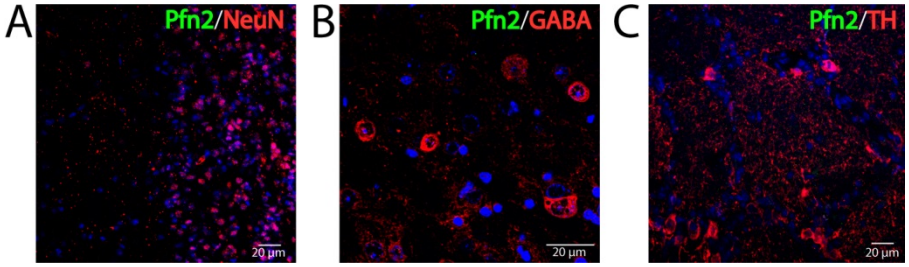

Supplementary Fig. 8 Sensory systems immunofluorescence control stainings of wildtype brain sections

Co-Immunofluorescence studies were verified by several control stainings, including the control for the specificity of the P2-GFP signal using wildtype (wt) sections. Wt mice should not express the GFP protein and should therefore show no signal, if they were processed in the same way as the homozygous P2-GFP knock-in animals (G/G) were treated.

A signal for GFP (green) could not be detected using the same settings for image acquisition and processing, confirming the specificity of the P2-GFP labelling approach.

The respective controls for the neurons in the mouse olfactory bulb were chosen according to the images that were shown in Fig. 18. (**A**) Olfactory granule cells (NeuN, red) next to Mitral cells (NeuN-neg., unlabelled) (**B**) GABAergic periglomerular neurons and short axon cells around a glomerulus (GABA, red) (**C**) Dopaminergic short axon cells around a glomerulus (TH, red).

To visualize the cell nuclei (blue), the DNA-intercalating dye Draq5 (Biostatus) was used.

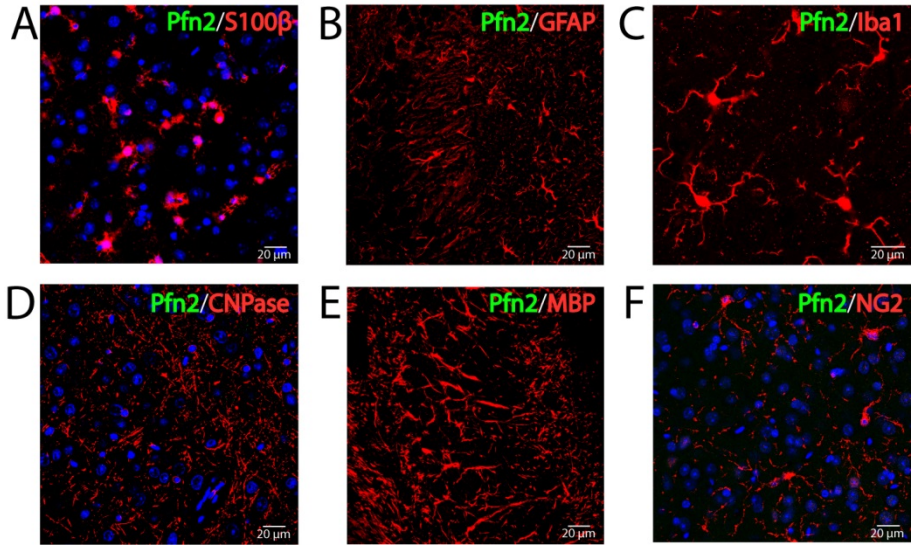

Supplementary Fig. 9 Glial cells immunofluorescence control stainings of wildtype brain sections

Co-Immunofluorescence studies were verified by several control stainings, including the control for the specificity of the P2-GFP signal using wildtype (wt) sections. Wt mice should not express the GFP protein and should therefore show no signal, if they were processed in the same way as the homozygous P2-GFP knock-in animals (G/G) were treated.

A signal for GFP (green) could not be detected using the same settings for image acquisition and processing, confirming the specificity of the P2-GFP labelling approach.

The respective controls for the glial cells were chosen according to the brain regions that were shown in Fig. 20.

The four major types of glial cells in the brain were analyzed. Astrocytes can be in a dormant or a reactive state and express corresponding molecular markers. (**A**) Both types of astrocytes express S100β but (**B**) only reactive astrocytes express GFAP at high levels. (**C**) Also microglia can switch from an inactive to an active state, both states expressing Iba1 as a marker protein for microglia. (**D**) Oligodendrocytes express the enzyme CNPase mostly in their cell bodies, whereas (**E**) the myelin basic protein (MBP) is preferentially localized to myelin-sheaths of their processes. (**F**) The fourth type of glial cells are the NG2 cells, which exclusively produce the NG2 proteoglycan and transport it to their cell membranes. To visualize the cell nuclei (blue), the DNA-intercalating dye Draq5 (Biostatus) was used.

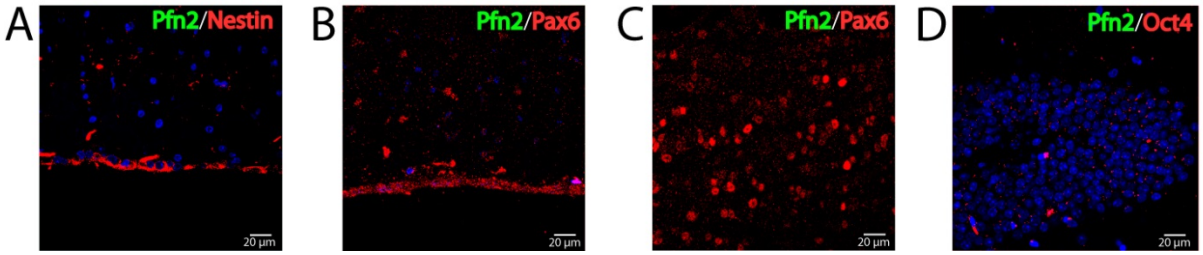

Supplementary Fig. 10 Adult neural stem cell and progenitor cell immunofluorescence control stainings of wildtype brain sections

Co-Immunofluorescence studies were verified by several control stainings, including the control for the specificity of the P2-GFP signal using wildtype (wt) sections. Wt mice should not express the GFP protein and should therefore show no signal, if they were processed in the same way as the homozygous P2-GFP knock-in animals (G/G) were treated.

A signal for GFP (green) could not be detected using the same settings for image acquisition and processing, confirming the specificity of the P2-GFP labelling approach.

The respective controls for adult neural stem cells (aNSCs) and progenitor cells were chosen according to the brain regions that were shown in Fig. 21. (**A**) aNSCs are mainly localized to the subventricular zone (SVZ), where they express high levels of the intermediate filament nestin (red) and (**B**) the transcription factor Pax6 (red), which can also be found in aNSC-derived progenitor cells. (**C**) The progenitor cells remain Pax6-positive (red), while migrating from the SVZ towards the olfactory bulb through the rostral migratory stream (RMS). (**D**) Adult NSCs of the hippocampal dentate gyrus are located in the so-called subgranular zone (SGZ) and are enriched in the transcription factor Oct4 (red). To visualize the cell nuclei (blue), the DNA-intercalating dye Draq5 (Biostatus) was used.

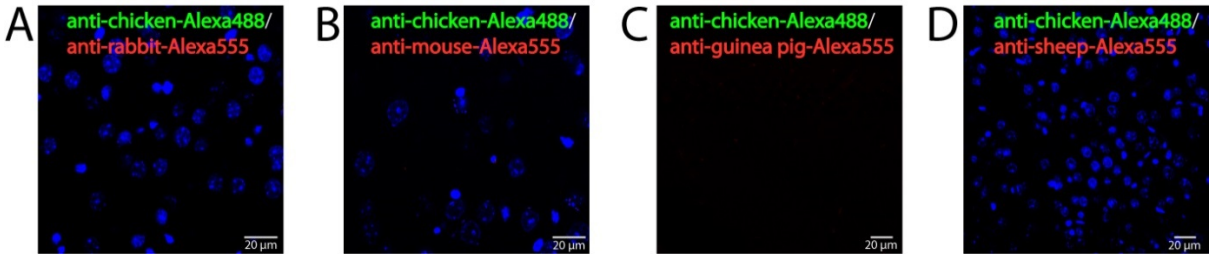

Supplementary Fig. 11 Immunofluorescence control stainings of wildtype brain sections for the specificity of the applied fluorescently-conjugated secondary antibodies

Co-Immunofluorescence studies were verified by several control stainings, including the control for the specificity of the fluorescently-conjugated (Alexa488 or Alexa555) secondary antibody towards preferably the host species of the used primary antibodies.

A signal for secondary antibody conjugated to a fluorescent dye without a corresponding primary antibody could not be detected. The same settings for image acquisition and processing were applied, confirming the specificity of the immunofluorescence approach.

P2-GFP fluorescence was enhanced by an anti-GFP antibody derived from chicken yolk that was labelled by secondary anti-chicken antibodies conjugated to Alexa488 dye molecules (green). In addition several other primary antibodies against specific marker proteins were added, which were labelled with the corresponding secondary antibodies for the respective host species conjugated to the Alexa555 dye. Many primary antibodies are specifically raised in (**A**) rabbits or (**B**) mice as host species as well as other species, which are less frequently used, such as (**C**) guinea pig and (**D**) sheep. To visualize the cell nuclei (blue), the DNA-intercalating dye Draq5 (Biostatus) was used.

Neuronal System/ Cell type	P2 expression	
Glutamatergic neurons	positive	+++
Dopaminergic neurons	positive	+++
Serotonergic neurons	positive	++
Noradrenergic neurons	positive	++
Cholinergic neurons	positive	+
GABAergic neurons	mixed	(++)
Sensory neurons (e.g. Mitral cells)	positive	+++
Adult neural stem cells (aNSCs)	positive	++
Progenitor cells	negative	-
Astrocytes	negative	-
Oligodendrocytes	negative	-
Microglia	negative	-
NG2 cells	negative	-

Supplementary Fig. 12 Neuronal systems expressing Pfn2 in summary

Most neuronal systems express Pfn2, nonetheless with varying levels. Among the excitatory neuronal systems, the glutamatergic and dopaminergic neurons express the highest levels of Pfn2 in the brain. Serotonergic and noradrenergic neurons are also highly positive for Pfn2, while cholinergic neurons merely produce moderate levels of Pfn2. GABAergic neurons express Pfn2 in specific cell types only but most GABAergic neurons are devoid of Pfn2. Sensory neurons are enriched in Pfn2 as well with the glutamatergic Mitral cells being one of the highest Pfn2-expressing cells in the brain. Pfn2 can also be found in adult neural stem cells of the SVZ, but is missing from aNSC-derived progenitor cells. Glial cells in general also lack the expression of Pfn2 in any of the investigated cell populations.

Anti-Pfn2 antibody	Host species	Applications			
		WB	IF	IP	P2-GFP recognition
Anti-Pfn2 2T	Rabbit	x	x	x	-
Anti-Pfn2 GD2	Rabbit	x	(x)	x	53%
Anti-Pfn2 3003	Rabbit	x	-	-	29%
Anti-Pfn2 DB2	Rabbit	(x)	-	-	-
Anti-Pfn2 5A7	Mouse	-	-	x	-

Supplementary Fig. 13 Applications tested for the different anti-Pfn2 antibodies

Different anti-Pfn2 antibodies (2T, GD2, 3003, DB2, 5A7) were raised in rabbits and mice before analyzing their efficiency in certain experimental applications. The anti-Pfn2 2T antibody could be used for all tested purposes, but failed to label also P2-GFP efficiently in Western blot assays. The anti-Pfn2 antibody GD2 could be verified to bind most efficiently to P2-GFP in addition to Pfn2 (53% P2-GFP is labelled compared to Pfn2), but it is only of limited use in IF experiments. P2-GFP was also recognized in WB experiments by the anti-Pfn2 3003 antibody at a rate of 29% of the efficiency it labels Pfn2. This antibody was not operational in the other tested applications. The least effective antibody was anti-Pfn2 DB2, which only showed signals for Pfn2 in Western blots among a high aspecific background. The monoclonal anti-Pfn2 antibody produced by mouse hybridoma cells of the clone 5A7 was only operative in IP. WB= Western blot; IF= Immunofluorescence; IP= Immunoprecipitation